

**Biogeochemistry, Contaminant Transport, and Atmospheric Exchange
In Glacial Cryoconite Meltwater of the McMurdo Dry Valleys, Antarctica**

by

Alex Quinn Mass

B.S., Bucknell University, 2007

M.S., University of Georgia, 2010

M.S., University of Colorado, 2014

A thesis submitted to the Faculty of the Graduate School of the University of Colorado

in partial fulfillment of the requirements for the degree of

Doctor of Philosophy

Department of Civil, Environmental, and Architectural Engineering

2018

This thesis entitled:
Biogeochemistry, Contaminant Transport, and Atmospheric Exchange
In Glacial Cryoconite Meltwater of the McMurdo Dry Valleys, Antarctica
written by Alex Q. Mass has been approved for the
Department of Civil, Environmental, and Architectural Engineering

Dr. Diane McKnight

Dr. Rita Klees

Dr. Richard Kuchenrither

Dr. Karl Linden

Dr. Shelly Miller

Date: _____

The final copy of this thesis has been examined by the signatories, and we find that both the content and the form meet acceptable presentation standards of scholarly work in the above-mentioned discipline.

Abstract

Polar regions serve as a global sink for many forms of semi-volatile pollution emitted from low- or midlatitudes of the populated world. This study examined the long-range atmospheric transport, fate, and phase partitioning of semi-volatile organic contaminants from air masses into meltwater and aeolian sediment on six glaciers in the McMurdo Dry Valleys of Antarctica. A novel low-cost, field-portable instrument was developed for the in-situ solid-phase extraction of trace contaminants in extreme environmental conditions without access to electricity or traditional laboratory facilities. Beyond polar research, this equipment is applicable for rapid field extraction and stabilization of samples assessing air and water quality after natural disasters. This is the first published study to identify the presence of anthropogenic perfluorinated compounds in the Transantarctic Mountain region and indicates a longer range of poleward contaminant transport than prior estimates in the Southern Hemisphere. Additional research examined the biochemistry and climatic variability of open and sealed cryoconite holes on glacial surfaces throughout the initial melt, equilibrium, and refreezing periods in 2013- 2015. High solute concentrations relative to glacial ice indicate that the pools can remain isolated from hydrologic connectivity for more than a decade. Microbial carbon cycling in pools enclosed by ice led to atmospheric disequilibrium and extreme pH. Analysis of unique air, liquid, and ice stratification in cryoconite holes revealed vertical patterns representing a highly accurate, multi-year record of past weather conditions sensitive enough to identify individual dates. This research identifies fluctuations in atmospheric contaminant transport, specific timeframes for deposition events, and may be used in back-trajectory models to help identify the source and variability of semi-volatile emissions in the Southern hemisphere.

Mass, Alex Quinn (PhD., Civil & Environmental Engineering)

Biogeochemistry, Contaminant Transport, and Atmospheric Exchange In Glacial Cryoconite Meltwater of the McMurdo Dry Valleys, Antarctica

Thesis directed by Dr. Diane McKnight

Dedication

To Bob Heath, Mike Denton, and Perry Andersen, who embodied the curiosity and pioneering spirit that lures so many of us to work on the Ice.

I'd like to dedicate my small piece of Antarctica to you.

Acknowledgements

First and foremost I want to thank my advisor, Diane McKnight, for encouraging me to apply to the Civil & Environmental Engineering program at the University of Colorado. She has given me incredible freedom to pursue multiple projects and collaborate with outside teams during my time at CU, including a season at Concordia Station, Antarctica, two field seasons in the McMurdo Dry Valleys, and educational outreach programs travelling through Colorado and New Zealand. The independence to direct my own field research program in the Dry Valleys was an incredible experience and I'm extremely grateful for the faith and opportunity.

I'd like to thank Tarun Anumol for his collaboration on this project and the significant time he has taken out of his schedule to show me multiple analytical methods beyond the technological capabilities of traditional fieldwork settings. Diana Hughes, Christiane Hoppe-Jones, Shane Snyder, Craig Marvin, and the Environmental Method Development team at Agilent Technologies have all been extremely welcoming and instrumental to my research.

The contractors in the United States Antarctic Program are a central part of all fieldwork operations and were incredibly friendly and supportive in the field. In particular, I want to thank Renée Noffke for her cheerful demeanor and amazing oreo snack bars at the Lake Hoare fieldcamp, John Loomis and the field mountaineers for accompanying me on glacial trips, the Helo-Ops pilots who let me do fieldwork on untouched glaciers, get a birds-eye view of the Transantarctics, and hitch-hike onto spare flights for extra sample collection

throughout the season simply because I baked them a batch of cheesy biscuits to thank them early on, and the McMurdo Fire Department medics who welcomed me like family during my time on station and hoarded their limited “freshies” allowance to send me apples in the field.

What I have learned from all of this is that we are all easily bribed with food.

Table of Contents

Chapter 1 Literature Review- Implications of Preferential Deposition of Semivolatile Organic Contaminants in the Cryosphere.....	1
1.1 Semivolatile Organic Contaminants (SVOCs)	1
1.2 Poleward Transport of SVOCs: The Grasshopper Effect.....	2
1.3 Environmental Characterization of the Cryosphere	4
1.4 Antarctic Contamination in a Global Context	6
1.5 Identifying Relevant Media in Antarctic Environments	9
1.6 Study Purpose	18
Chapter 2 Physical Characteristics of Cryoconite Holes On Glaciers of the McMurdo Dry Valleys, Antarctica	20
2.1 Introduction.....	20
2.2 Site Description	22
<i>2.2a Glacier characteristics.....</i>	<i>26</i>
2.3 Methods	32
<i>2.3a Field sampling</i>	<i>32</i>
<i>2.3b Sample categorization.....</i>	<i>33</i>
<i>2.3c Measurement and adjustment for surface elevation</i>	<i>34</i>
2.4 Results and Discussion	36
<i>2.4a Melt initiation in austral summer.....</i>	<i>36</i>
<i>2.4b Profiles of vertical stratification in cryoconite holes and melt pools</i>	<i>41</i>
<i>2.4c The development of ice lids and weathered crusts</i>	<i>44</i>
<i>2.4d Static subsurface channels.....</i>	<i>49</i>
<i>2.4e Headspace and the categorization of melt pools</i>	<i>51</i>

2.4f Sediment thickness.....	54
2.4g Total depth	58
2.4h Diameter.....	65
2.4i Circularity.....	67
2.4j Ice lid thickness.....	69
2.4k Cryoconite lid stratification as an indicator of seasonal melt patterns.....	73
2.4l Variation in glacial melt features across sampled glaciers.....	78
2.5 Conclusions.....	83
2.6 Supporting Data.....	85
2.6a Identification of “extreme subsurface crystal melt” on Joyce Glacier.....	85
2.6b Supporting data tables and figures.....	89
Chapter 3 Multi-annual Variability in Cryoconite Hole Distribution on Glaciers in Taylor Valley, Antarctica.....	100
3.1 Introduction.....	100
3.2 Methods	101
3.3 Results.....	106
3.3a Meteorological influences on sampling sites	106
3.3b Variations in diameter across glaciers and physical states.....	114
3.3c Model-based determination of multiannual cryoconite holes.....	118
3.3d Spatial distribution and net surface change on Canada Glacier.....	121
3.3e Spatial distribution and net surface change on Commonwealth Glacier	124
3.3f Glacial surface budget	127
3.4 Conclusions.....	130

Chapter 4 Variations in Meltwater Composition and Nutrient Cycling Between Ice-Lidded and Open System Cryoconite Holes.....	132
4.1 Introduction.....	132
4.2 Methods	134
<i>4.2a Sampling sites.....</i>	<i>134</i>
<i>4.2b Guidelines for the categorization of melt features.....</i>	<i>137</i>
<i>4.2c Field methods.....</i>	<i>141</i>
<i>4.2d Laboratory methods.....</i>	<i>145</i>
<i>4.2e Critique of current methodology used to estimate isolation age</i>	<i>146</i>
4.3 Results and Discussion	151
<i>4.3a Estimates of cryoconite hole isolation age.....</i>	<i>151</i>
<i>4.3b Major ions.....</i>	<i>158</i>
<i>4.3c The impact of surface elevation on meltwater composition</i>	<i>162</i>
<i>4.3d Solute enrichment during ionic pulse melt.....</i>	<i>164</i>
<i>4.3e Sea-salt adjusted ion concentrations.....</i>	<i>165</i>
<i>4.3f Sulfate</i>	<i>166</i>
<i>4.3g Dissolved Organic Carbon</i>	<i>167</i>
4.4 Conclusions	167
4.5 Supporting Data.....	168
Chapter 5 Physical Considerations for the Deposition and Environmental Partitioning of SVOCs in Glacial Meltwater	176
5.1 Introduction.....	176
5.2 Methods	179
<i>5.2a Defining cryoconite hole characteristics.....</i>	<i>179</i>
<i>5.2b Model for diffusive gas-liquid transfer.....</i>	<i>181</i>

5.2c <i>Modification of temperature-dependent calculations for near-freezing conditions</i>	182
5.3 Results and Discussion	186
5.4 Conclusions.....	191
Chapter 6 Experimental Methods for the Identification of Semivolatile Organic Contaminants in Antarctic Cryoconite Meltwater and Sediment.....	194
6.1 Introduction.....	194
6.2 Field Methods.....	196
6.2a <i>Sample collection</i>	196
6.2b <i>Field sampling controls</i>	201
6.2c <i>Analytical strategies</i>	201
6.3 Cryoconite Water Extractions.....	203
6.3a <i>Solid-phase extractions after Season 1</i>	203
6.3b <i>Solid-phase extractions after Season 2</i>	205
6.4 Sediment Extractions	205
6.5 Liquid Chromatography	208
6.6 Results.....	208
References.....	219

Tables

Chapter 1

Table 1.1 - Spectrum of surface albedos measured in polar environments	13
--	----

Chapter 2

Table 2.1- Geographic and meteorological summary of study glaciers.....	32
Table 2.2- Characteristics of meltholes sampled	53
Table 2.3- Intraglacial averages of surface diameter	89
Table 2.4- Intraglacial averages of circularity	90
Table 2.5- Intraglacial averages of eccentricity	91
Table 2.6- Intraglacial averages of total depth.....	93
Table 2.7- Intraglacial averages of liquid depth.....	94
Table 2.8- Intraglacial averages of headspace.....	95
Table 2.9- Intraglacial averages of sediment depth.....	96
Table 2.10- Intraglacial averages of lid thickness	97
Table 2.11- Intraglacial averages of elevation	99

Chapter 3

Table 3.1- Distribution of cryoconite holes on study glaciers.....	107
Table 3.2- Diameter of cryoconite holes in each physical state on sampling sites.....	116
Table 3.3- Surface balance of cryoconite hole coverage on Canada Glacier	128
Table 3.4- Surface balance of cryoconite hole coverage on Commonwealth Glacier	128

Chapter 4

Table 4.1- Isolation age calculated by new methods in Equation 4.....	153
Table 4.2- Isolation age calculated using the method of Fountain <i>et. al.</i> 2004.....	155

Table 4.3- Cl ⁻ content of subsurface glacial melt.....	163
Table 4.4- Mean proportion of each major ion derived from non-marine sources.....	166
Table 4.5- Cl ⁻ content of subsurface glacial melt.....	168
Table 4.6- Sulfate content of subsurface glacial melt.....	169
Table 4.7- Proportion of non-sesalt sulfate	170
Table 4.8- *Ca ²⁺ content of subsurface glacial melt.....	171
Table 4.9- Proportion of non-sesalt sulfate	173
Table 4.10- Cl ⁻ concentrations in glacial ice in the McMurdo Dry Valleys.....	174

Chapter 5

Table 5.1- SVOCs reported in literature	177
Table 5.2- Parameters of a model unlidded cryoconite hole in the Dry Valleys.....	180
Table 5.3- Contaminants in ambient Antarctic air reported by prior studies	181
Table 5.4- Data for two-film interfacial air: water diffusive transfer model and final summer concentrations	187
Table 5.5- Variation in Henry's Law constants	188
Table 5.6- Model estimates using low-temperature Henry's Law constants reported in literature	190

Chapter 6

Table 6.1- Isotopically labeled PFCs used as internal standards	204
Table 6.2- PFC standards.....	207
Table 6.3- Method detection limits and reporting limits for soil/ PFC extraction	217

Figures

Chapter 1

Figure 1.1- Illustration of the poleward Grasshopper Effect sequestering semivolatile contaminants in glacial regions.....	3
Figure 1.2- Global population distribution in 2000.....	7
Figure 1.3- Antarctic map identifying the McMurdo Dry Valleys.....	10
Figure 1.4- Satellite image encompassing the Greater McMurdo Dry Valleys.....	11
Figure 1.5- Schematic showing (a) the development and (b) the internal structure of a cryoconite hole.....	12
Figure 1.6- A lidded cryoconite hole (45 cm wide) on the surface of Commonwealth Glacier.....	13
Figure 1.7- Accumulation, ablation, and mass balance on Canada Glacier.....	14
Figure 1.8- Energy balance in a lidded cryoconite hole.....	15
Figure 1.9- A lidded cryoconite hole with subsurface hydrologic connectivity.....	16
Figure 1.10- Near-surface channelized melt flowing through Canada Glacier, Antarctica.....	17

Chapter 2

Figure 2.1- Schematic showing (a) the development and (b) the internal structure of a cryoconite hole.....	20
Figure 2.2- Annual remelting (internal melting) of a multiannual lidded cryoconite hole.....	21
Figure 2.3- Antarctic map identifying the McMurdo Dry Valleys.....	23
Figure 2.4- Satellite image encompassing the Greater McMurdo Dry Valleys.....	24
Figure 2.5- Accumulation, ablation, and mass balance on Canada Glacier.....	25
Figure 2.6- Glacier locations in the McMurdo Dry Valleys.....	27
Figure 2.7- Vertical terracing on Wright Lower Glacier.....	29
Figure 2.8- Scalloped basins on Canada Glacier.....	30

Figure 2.9- Cryolake on Canada Glacier.	31
Figure 2.10- Digital Globe Satellite Imagery of Joyce Glacier and Upper Garwood Valley.....	35
Figure 2.11- Total daily discharge from Anderson Creek during each melt season.....	37
Figure 2.12- Surface ice of Canada Glacier in mid-December.....	38
Figure 2.13- Evolution of Canada Glacier over summer 2014-15.....	40
Figure 2.14- Vertical profiles of cryoconite holes and melt pools sampled in 2013-14.....	42
Figure 2.15- Vertical profiles of cryoconite holes and melt pools sampled in 2014-15.....	43
Figure 2.16- An open cryoconite hole on Canada Glacier.....	45
Figure 2.17- A lidded cryoconite hole on Commonwealth Glacier.....	46
Figure 2.18- A portion of the ice lid from a cryoconite hole.....	47
Figure 2.19- A weathered ice lid above a cryoconite hole.....	48
Figure 2.20- A segmented subsurface melt channel on Taylor Glacier.....	50
Figure 2.21- Liquid saturation through low-density surface layers in a stagnant melt channel.	51
Figure 2.22- Sediment and total depth of meltholes sampled.....	55
Figure 2.23- Sediment depth of cryoconite holes and melt pools sampled.	57
Figure 2.24- Total depth of cryoconite holes and melt pools sampled.	59
Figure 2.25- Deep, narrow drainage channel on Canada Glacier.....	61
Figure 2.26- Shallow surface drainage channel on Canada Glacier.	61
Figure 2.27- Liquid and total depth of cryoconite holes and melt pools sampled.....	63
Figure 2.28- Total depth and diameter of cryoconites and melt pools sampled.....	65
Figure 2.29- Diameter of cryoconite holes and melt pools sampled.....	66
Figure 2.30- Diametric circularity of cryoconite holes and melt pools.....	68
Figure 2.31- Diametric circularity and diameter of melt samples.....	69
Figure 2.32- A flat, disk-like lid on a cryoconite hole.....	70

Figure 2.33- Thicker ice towards the center of a large cryoconite hole.	71
Figure 2.34- Vertical profiles of cryoconite holes from Season 2.	74
Figure 2.35- Average daily incoming shortwave radiation in summer 2014-15.	76
Figure 2.36- Distribution of melt features on the ablation zone of each glacier.	78
Figure 2.37- The ablation zone of Wright Upper Glacier.	80
Figure 2.38- Surface and sampling zones on Taylor Glacier.	80
Figure 2.39- Surface and sampling zones on Canada Glacier.	81
Figure 2.40- Surface and sampling zones on Commonwealth Glacier.	82
Figure 2.41- Surface and sampling zones on Adams Glacier.	83
Figure 2.42- Englacial tunnel in Joyce Glacier.	86
Figure 2.43- Eccentricity and diameter of melt samples.	92
Figure 2.44- Vertical profile for the mean depth of features in each melthole type.	98

Chapter 3

Figure 3.1- Taylor Valley, Antarctica.	101
Figure 3.2- Ablation stake on Canada Glacier.	103
Figure 3.3- Circular transects for cryoconite hole distribution.	104
Figure 3.4- Measurements of cryoconite holes along a transect line.	105
Figure 3.5- Stream discharge derived from glacial melt over two austral summers.	108
Figure 3.6- Daily average incoming shortwave radiation on glacier surfaces.	109
Figure 3.7- Canada Glacier surface temperature.	111
Figure 3.8- Commonwealth Glacier surface temperature.	112
Figure 3.9- Diameter of cryoconite holes measured.	117
Figure 3.10- Visual representation of drift for matched cryoconite holes.	120
Figure 3.11- Distribution of cryoconite holes on Canada Glacier.	122

Figure 3.12- Distribution of cryoconite holes on Canada Glacier.....	123
Figure 3.13- Distribution of cryoconite holes on Commonwealth Glacier.....	125
Figure 3.14- Distribution of cryoconite holes on Commonwealth Glacier.....	126

Chapter 4

Figure 4.1- Annual melting in a multiannual lidded cryoconite hole.....	133
Figure 4.2- Glacier locations in the McMurdo Dry Valleys.....	135
Figure 4.3- Scalloped basins on lower Canada Glacier.....	137
Figure 4.4- Open and Lidded Cryoconite Holes in Taylor Valley.....	139
Figure 4.5- Glacial waterfalls in Taylor Valley.....	143
Figure 4.6- Cryoconite hole isolation age.....	152
Figure 4.7- Charge balance of subsurface glacial melt in Taylor and Wright valleys.....	159
Figure 4.8- Charge balance of subsurface glacial melt in the southern Dry Valleys.....	160
Figure 4.9- Charge balance of subsurface glacial melt in the southern Dry Valleys.....	161
Figure 4.10- Sulfate in subsurface glacial melt.....	167

Chapter 5

Figure 5.1- Two-film model for interfacial gas-liquid transfer across intermediate boundaries into bulk concentrations.....	182
Figure 5.2- The temperature dependence of Henry's Law constants for several halogenated VOCs.....	184

Chapter 6

Figure 6.1- Schematic showing (a) the development and (b) the internal structure of a cryoconite hole.....	195
Figure 6.2- Glacier locations in the McMurdo Dry Valleys.....	197
Figure 6.3- Open and lidded cryoconite holes in Taylor Valley.....	198
Figure 6.4- Total ion chromatograms for Canada Glacier cryoconite hole 36.....	210

Figure 6.5- PFCs in sediment before correcting for field, method, and target controls,
part 1.....212

Figure 6.6- PFCs in sediment after correcting for field, target, and method controls,
part 1.....213

Figure 6.7- PFCs in sediment before correcting for field, method, and target controls,
part 2.....214

Figure 6.8- PFCs in sediment after correcting for field, method, and target controls,
part 2.....215

Chapter 1

Literature Review- Implications of Preferential Deposition of Semivolatile Organic Contaminants in the Cryosphere

1.1 Semivolatile Organic Contaminants (SVOCs)

Persistent organic pollutants (POPs) are compounds with relatively long environmental lifespans, far-reaching geographic transport/distribution, and detrimental bioaccumulative effects across ecosystems and human populations. All of the 30 compound groups ratified or proposed for inclusion in the Stockholm Convention's list of banned or restricted POPs are halogenated organic contaminants. The vast majority of these chemicals were used as pesticides or flame retardants.¹ Organohalogens tend to be lipophilic, which leads to high bioaccumulation in the fatty tissues of organisms. These compounds are also more persistent in the environment due to the stability of carbon-halogen bonds resistant to hydrolysis and photolytic degradation.² While the particular compounds identified as POPs are outlined by the United Nations Environment Programme, the main inclusion criteria of high mobility, resistance to degradation, and toxicity apply to additional contaminants that pose environmental threats but are not currently included on those regulatory lists. (The classification of 'persistent bioaccumulative toxic substances' used by the US EPA³ identifies a similar but not identical list.) As such, the inclusive term 'semi-volatile organic contaminants' (SVOCs) is used in this thesis to encompass additional pollutants of concern that exhibit 'POP-like' behavior. The International Agency for Research on Cancer has defined many SVOCs as known or probable human carcinogens.⁴ Additional toxicological effects include endocrine

disruption, teratogenic and developmental effects, and reproductive, immune, and nervous system damage.¹ Implementation of Stockholm Convention guidelines in 2004 led to decreases in the environmental concentrations of polychlorinated biphenyls (PCBs), polybrominated diphenylethers (PBDEs), hexachlorohexane (HCH), and further reduction of dichlorodiphenyltrichloroethane (DDT).^{2,5} Many persistent organic chemicals including PCBs and organochlorine pesticides preferentially deposit and accumulate in cold regions.⁶ High levels of hydrophobic organic contaminants found in Arctic marine life led researchers to investigate the transport and fate of organic contaminants in polar regions⁷, while the discovery of DDT-related compounds in Antarctic biota in the 1960s led to the first investigations of anthropogenic contaminants in Antarctica.⁸ The presence of anthropogenic contaminants far away from emission sources indicates the magnitude and complexity of global contaminant transport.

1.2 Poleward Transport of SVOCs: The Grasshopper Effect

The atmosphere is a major pathway for chemical transport to polar regions.⁶ High concentrations of SVOCs at high latitudes are the result of temperature-dependent partitioning of compounds based on their respective vapor pressure/ volatility. After emission into the atmosphere, the distance a contaminant travels before condensing is dependent on half-life and temperature, causing a pattern of 'global fractionation' for the deposition of gaseous compounds along latitudinal gradients.⁶ This causes polar regions to serve as a global sink for many forms of semivolatile pollution emitted from low- or mid-latitudes of the populated world.⁸ Semivolatile organic contaminants can reach polar regions through long-range atmospheric transport (LRAT), which can be characterized by a

timescale of less than one week for a single deposition event.² Polar deposition does not always occur as a singular deposition and the “grasshopper effect” describes the movement of compounds through multiple step-wise condensation/revolatilization events. SVOCs produced in warmer regions travel in a predominantly gaseous state. The atmospheric circulation of air masses and diffusivity of gases can cause compounds to travel to cold yet seasonally-variable climates such as the annual snowpack of a temperate alpine region. SVOCs that condense in these regions during the winter may re-volatilize during warmer temperatures in the spring. This causes global atmospheric transport in a series of condensation/revolatilization cycles toward colder climates until compounds deposit in regions too cold for revolatilization. The intermittent nature of grasshopper transport (Figure 1.1) extends the transport time for compounds to reach polar regions compared to 1-step LRAT deposition, and both processes contribute to SVOC accumulation at the poles.

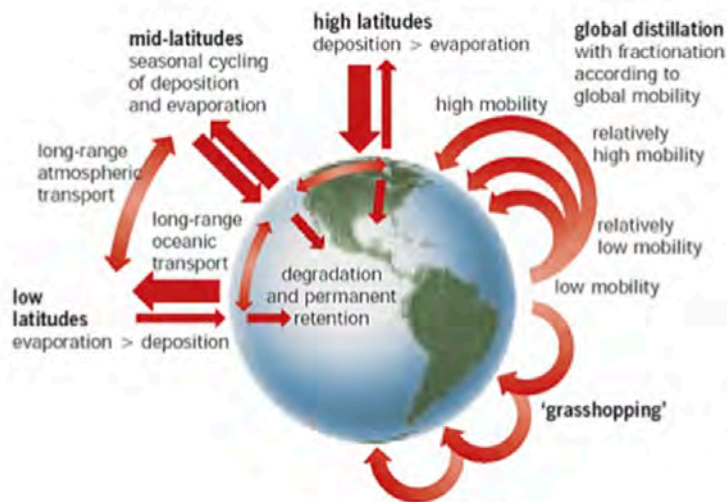


Figure 1.1- Illustration of the poleward Grasshopper Effect sequestering semivolatile contaminants in glacial regions. *Reprinted from UNEP.⁹*

The particular transport time for a poleward SVOC will depend on characteristics including its volatility, location of origin, route of transport, and chemical reactivity. Persistent contaminants that are either volatile and water-soluble or semivolatile and hydrophobic are most likely to accumulate in polar ecosystems due to their phase-partitioning characteristics.^{10,11} These compounds preferentially deposit on glacial surfaces because of cooler air above terrestrial glaciers and snow. The Arctic Monitoring and Assessment Programme (AMAP) declared cryospheric POP levels a 'priority issue' in their 2009 report¹² due to high levels of accumulation far from anthropogenic sources. VOCs have been monitored in the Arctic for more than two decades, but no comparable programs exist for contaminant detection in Antarctica. Both the temperature dependence of global distillation and the rise/poleward flow of air in the equatorial region of Haley cells cause the transport of semivolatile compounds to be hemispherically divided. An extensive review by Kallenborn and Berg¹³ determined that no long-term atmospheric monitoring projects have been conducted in Antarctica thusfar other than select analyses of ozone and aerosols. The first multi-year study of Antarctic contaminants began in 2007,¹⁴ but this data is limited to ship-based and coastal station studies of air and seawater. Little data has been collected from more remote locations, and there are presently no known studies examining anthropogenic contaminants in liquid water in Antarctica.

1.3 Environmental Characterization of the Cryosphere

The cryosphere constitutes the areas of Earth covered by frozen water, including sea, lake, and river ice; snow, glaciers, ice sheets, and permafrost. These frozen areas tend to be in high latitude or high altitude areas and maintain the temperature gradient driving

wind and ocean currents. The high albedo of ice/snow reflects up to 97% of incident solar radiation,¹⁵ and sea ice helps to insulate ocean surfaces and prevent heat loss from the ocean to the atmosphere. Thus melting in the cryosphere results in a positive feedback cycle when open ocean or terrestrial surfaces become exposed beneath melted ice, increasing both the amount of radiation absorbed on each surface. Since glaciated areas contain roughly $\frac{3}{4}$ of the world's fresh water,¹⁶ changes in the mass balance of the cryosphere will have direct consequences on human accessibility to fresh water sources. Antarctica is significantly the largest reservoir for fresh water on Earth. The East and West Antarctic Ice Sheets contain 70% of the world's freshwater stored as ice¹⁶, and the continent is therefore extremely sensitive to climatic changes that could affect this storage.

Glaciers, ice sheets, sea ice, and snowpacks can serve as reservoirs for contaminants on a scale ranging from days to centuries.² Pollutant transport and fate in glaciated regions is controlled by a variety of physical and chemical properties for each compound and can be highly temperature dependent. For a number of semi-volatile contaminants, not enough environmentally relevant temperature-dependent physical and chemical properties have been published in literature in order to derive chemical behavior at temperatures relevant to the cryosphere. The nonlinearity of temperature-dependent gas/liquid partitioning (Henry's Law coefficients) at near-freezing temperatures requires the addition of compound-specific correction factors to calculate phase partitioning.¹⁷ While many chemical properties are not reported below 0°C freezing temperatures, others are undefined below peak water density at 4°C. Many atmospheric transport models lack adequate consideration for the physical behavior of compounds in subfreezing

environments, and estimating global deposition in the face of anthropogenic warming and the sheer variation across climate change models is a difficult task. This makes site-based measurements of contaminants all the more important in order to apply measured concentrations to global transport models, develop baselines for the global signal of pollution,⁸ use back-trajectories to determine the site of emission sources, and characterize glacial deposition in order to identify risks to water security in populated glacial regions.

1.4 Antarctic Contamination in a Global Context

While the predominant anthropogenic contaminants found in the Arctic include polychlorinated biphenyls (PCBs) and isomers of hexachlorohexane (HCH), profiles at Antarctic sites are dominated by hexachlorobenzene (HCB) and organochlorine pesticides including dichlorodiphenyltrichloroethane (DDT), cyclodienes and toxaphene¹⁸. The vast majority of global population (88%; Figure 1.2) and landmass (68%) exists in the Northern hemisphere,¹⁹ thus it is reasonable that a hemispherically-divided transport process would lead to lower concentrations and a different composition of predominant compounds in Antarctica. However, the mean concentration of low-molecular weight PCBs (PCB-28, 31, 52, etc.) was found to be equal between each polar region,²⁰ and relative proportions of Arctic : Antarctic concentrations are shifting due to the phase-out of many pesticides in the Northern hemisphere that are still in use in the south.

The World's Population in 2000, by Latitude



(horizontal axis shows the sum of all population at each degree of latitude)

Figure 1.2- Global population distribution in 2000. *Reprinted from Rankin.¹⁹*

South America has historically been the heaviest user of DDT, toxaphene, and lindane, while South Africa reintroduced DDT in 2000 to curb reemerging malarial outbreaks.²¹ Identification of DDT/DDE ratios in Antarctica may shed light on hemispheric deposition from both the historical and current use of DDT, applying mass balance models to assess the environmental impact of DDT's resurgence for malarial control.^{18,22-24} Fluctuation in the direction of air masses near Antarctica influence the concentration of individual compounds over relatively short timeframes. Kallenborn et al.²⁰ identified 10-fold changes in the ambient air concentration of γ -HCH, PCB-28, and chlordane in Antarctica over the course of a single week due to shifts in the origin of air masses passing over the sampling area. Concentrations of these compounds peaked when air masses originated from South America. Furthermore, shifting concentrations of individual

compounds in the same relative atmospheric transport pathway can help to indicate more specific source regions within a large air mass. Pesticides such as γ -HCH are good indicators of agricultural point-sources, while PCB-28 concentrations are higher in highly populated and industrialized areas. These results emphasize the importance of back-trajectory models to identify the source of LRAT and help to explain the wide variation of concentrations measured in individual studies.

Grannas *et al.*² stressed the importance of examining the cryosphere's role in global contaminant cycling, the change in contaminant interactions due to climate change, and the implications of contaminant fate during snowmelt on populations that rely on meltwater for drinking water. The onset, frequency, and extent of ice/snow melting directly influences the release of snow-bound contaminants into the marine and terrestrial environment.²⁵ Wania *et al.*²⁵ addressed higher exposure risks within the specific time period during the initial stages of seasonal glacial melt when solutes and other compounds are preferentially eluted from ice crystals (known as the 'ionic pulse' in snow/ice melt). This process causes a disproportionately elevated concentration of low- and mid- water soluble compounds in ice and snow to flush into spring melt water and can cause dramatic peaks in meltwater SVOCs initially deposited by snow. Organisms in temperate regions may experience chronic low levels of SVOCs from steady exposure to contaminated water, but alpine and polar regions are particular areas of concern due to accumulation of SVOCs on frozen surfaces and subsequent abrupt seasonal release during pulse melt. This can cause sudden, rapid exposure to higher concentrations of SVOCs and may have more severe health effects for populations in cold regions. SVOC accumulation in the cryosphere is a particular concern for glacial regions such as the Himalayas where more than 1.3 billion people rely on ice and

snow melt as a source of drinking water.²⁶ The rate of long-range atmospheric contaminant transport and degradation is often difficult to tease out from the contribution of local sources in those regions, and thus measurement of atmospheric contaminants in remote glacial areas is necessary in order to examine global deposition gradients independent from localized point-source releases.

1.5 Identifying Relevant Media in Antarctic Environments

The previous sections of this chapter addressed the role of the cryosphere as a global sink for SVOCs and the importance of sampling in remote regions in order to describe the magnitude of hemispheric contaminant transport. SVOCs can be measured from a variety of different environmental media, and prior studies have analyzed contaminant levels in seawater, marine sediments, and ambient coastal air.⁸ Glacial meltwater is particularly relevant from a human health perspective in order to examine the role of glaciers as contaminant reservoirs and the likelihood of SVOCs residing in meltwater runoff rather than partitioning into other media in melting ice. However, no previous research has examined contaminants in glacial melt for one of two reasons; many papers suggest that LRAT deposition does not extend beyond the Southern Ocean due to temperature/volatility gradients surrounding the continent, while other studies may be limited by the sheer lack of liquid water available on the frozen continent.

The majority of Antarctica is covered by ice sheets, and the McMurdo Dry Valleys of Antarctica (MDVs; 77°30'S, 162°00'E; Figure 1.3 and Figure 1.4) represent the largest portion of Antarctica's 0.18% ice-free landmass.²⁷ This region is subject to a narrow 10-

week season of glacial melt each summer which serves as the primary source of liquid water in the valleys.²⁸

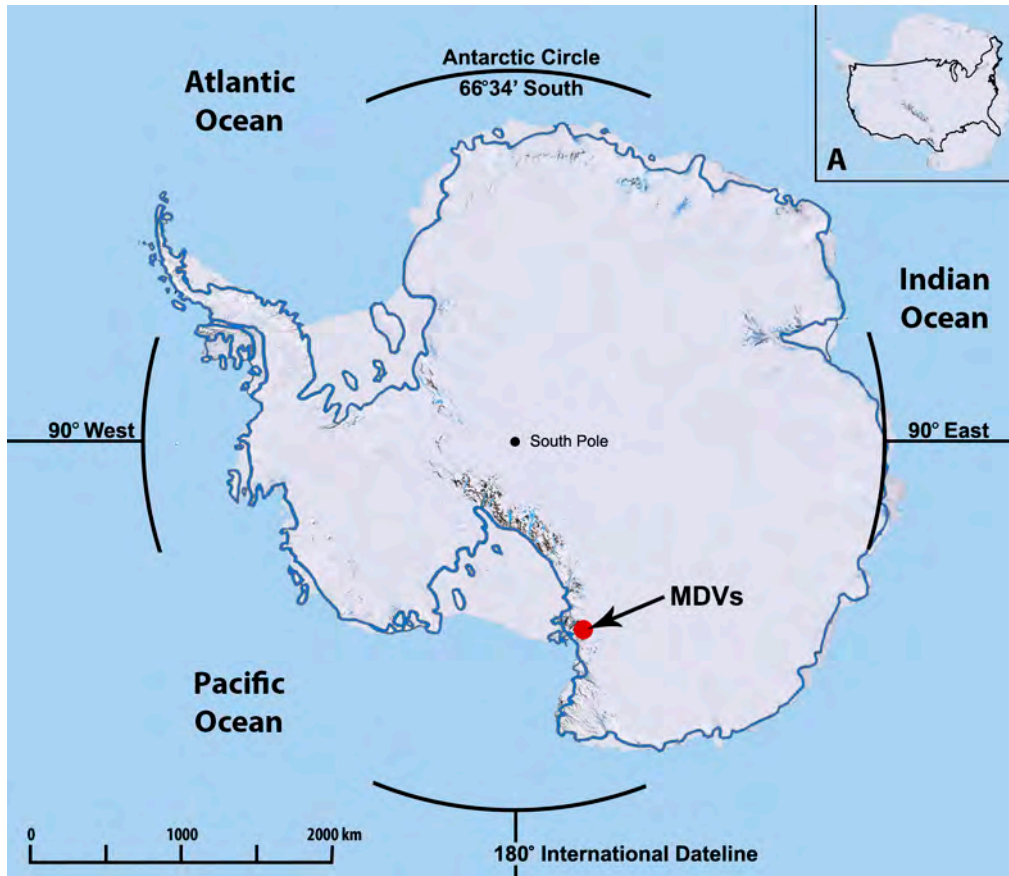


Figure 1.3- Antarctic map identifying the McMurdo Dry Valleys. *Inset image A contrasts Antarctica against the continental United States for scale. Map created by A.Q. Mass using satellite data from USGS 2008.²⁹ Continental borders were drawn to differentiate landmass from marine ice shelves, and both layers were isolated from open ocean/ sea ice extent in order to define the perennial boundaries. The ice-covered area can double in winter during maximum sea ice extent.*

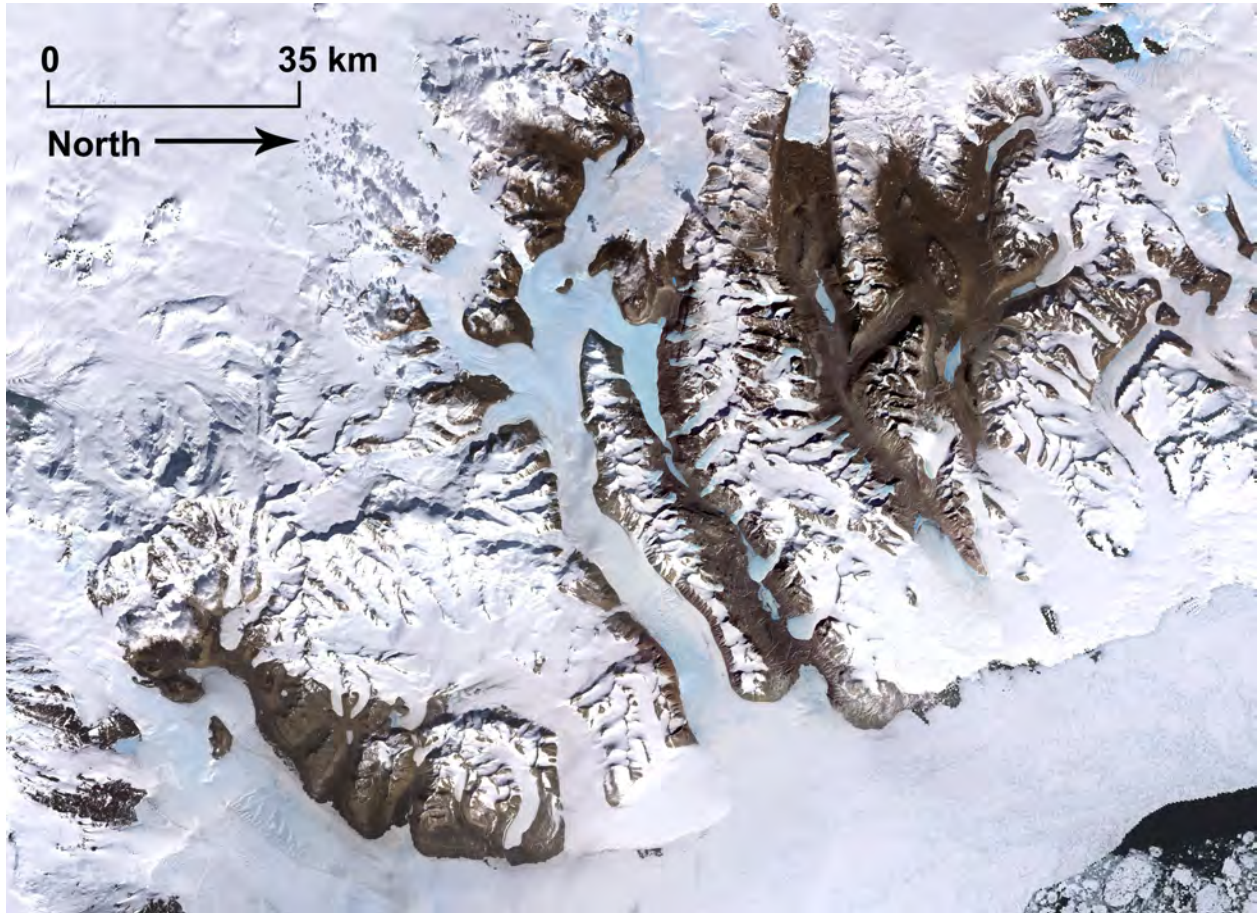


Figure 1.4- Satellite image encompassing the Greater McMurdo Dry Valleys.

Composited by A.Q. Mass using several USGS LANDSAT images.^{29,30}

Meltwater flows from glaciers into lakes covered by a perennial ice layer. Higher contaminant levels found in lake sediment compared to soil samples in Antarctica and the Arctic are suggested to originate from the contribution of glacial melt rich in atmospheric particulate matter trapped within the ice matrix.³¹ SVOCs in the seasonal outflow of water into these lakes has not been studied. Melt on the glacial surface is inhibited by a mean summer air temperature below freezing (apprx. -4°C) and perpetual winds averaging ~ 4 m/s. Seasonally continuous solar radiation into the ice produces warmer temperatures in a layer 5-20 cm beneath the glacial surface. This causes internal melt of the near-surface layer and hydrologic connectivity through subsurface drainage channels routes meltwater

off the glacier.³² Small pockets of liquid melt do exist on the glacial surface in the form of cryoconite holes. These features (Figure 1.5) are small melt pools created by the accumulation of wind-transported sediment known as cryoconite (“frozen dust”) into grooves on the textured surface of glaciers.

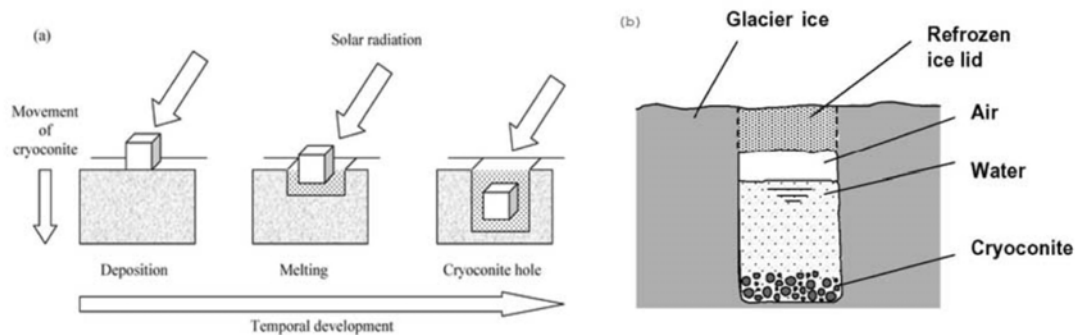


Figure 1.5- Schematic showing (a) the development and (b) the internal structure of a cryoconite hole. Reprinted from (a) Cowan and Tow³³ and (b) Fountain et al.³⁴

Cryoconite sediment deposits have a low albedo ($\alpha \cong 0.09$; Table 1.1) and absorb more solar radiation than the surrounding glacial ice ($\alpha \cong 0.65$)¹⁵, preferentially melting the ice below to create a cylindrical water-filled hole (Figure 1.6).

Table 1.1- Spectrum of surface albedos measured in polar environments

Albedo (α)	Surface
0.97	New snow as measured in Antarctica ¹⁵
0.95	New snow; general ⁹
0.82	Dry snow ⁹
0.73	Wet snow ⁹
0.65	Bare glacial ice ⁹
0.65	Canada Glacier ablation surface ice adjacent to cryoconite holes ¹⁵
0.53	Canada Glacier Cryoconite ice lid ¹⁵
0.50	Bare sea ice ³⁶
0.39	New (shallow) melt pond ^{9,37}
0.20	Mature melt pond ⁹
0.13	Dry cryoconite material; ranged 0.08 ³⁸ – 0.13 ³⁵
0.09	Damp cryoconite material on Greenland Ice Sheet ³⁵
0.06	Open ocean ³⁷



Figure 1.6- A lidded cryoconite hole (45 cm wide) on the surface of Commonwealth Glacier.

These holes eventually reach an equilibrium depth when the radiation absorbed by the bottom sediment equals the heat loss to surrounding ice.³⁹ Cryoconite holes have been found on glaciers around the world including regions of the Arctic,⁴⁰ Antarctic,^{41,42} and mid-latitudes.^{43,44} Their presence is limited to regions with sufficient energy to melt ice and is restricted by the 'equilibrium line' of a glacier; they can be found on the ice-exposed ablation zone lower on a glacial surface but are not found on higher, snow-covered accumulation zones (Figure 1.7).

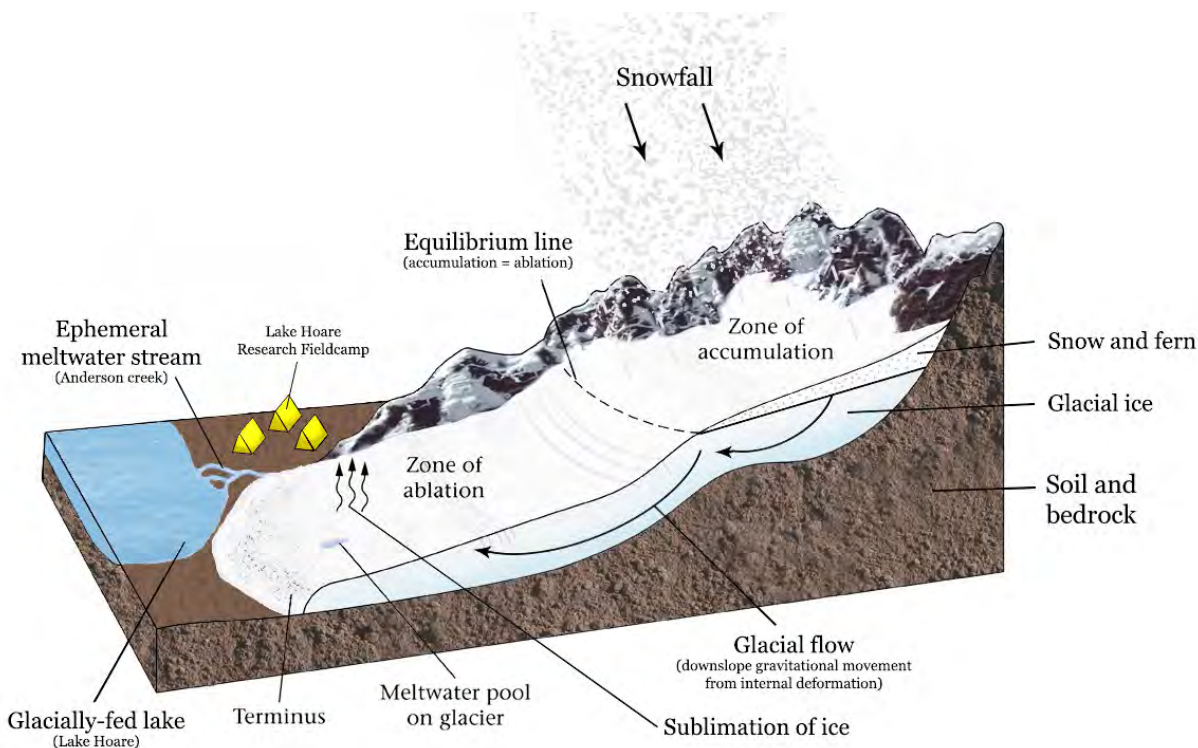


Figure 1.7- Accumulation, ablation, and mass balance on Canada Glacier. *This cross-section of Canada Glacier and the Lake Hoare fieldcamp in the McMurdo Dry Valleys exhibits the water gains and losses that affect glacial mass balance. Snow accumulates at higher elevations and compacts into firn; granular crystals that are ultimately compressed into glacial ice. The glacier itself will flow downslope due to internal deformation. Cryoconite holes form below the equilibrium line in the ablation zone, and during freeze/thaw events may drain into near-surface channels that route meltwater off the glacier. Diagram by A.Q. Mass includes alpine imagery from Marshak 2005.⁴⁵*

Unlike typical cryoconites that form as pools of water open to the surrounding atmosphere, cryoconites in the MDVs are capable of forming 'lids' of condensed blue ice on the pools' surface due to advection from cold winds. Lid formation is unique to the Dry Valleys due to the energy balance of this region—while cold temperatures and near-constant winds keep most glacial surfaces frozen, the consistent 24-hr daylight of Antarctic summer enables cryoconite sediment to absorb and maintain heat long enough to cause internal melting. Lidded cryoconites are thus isolated from atmospheric exchange while maintaining subsurface melt in a 'solid state greenhouse' (Figure 1.8).

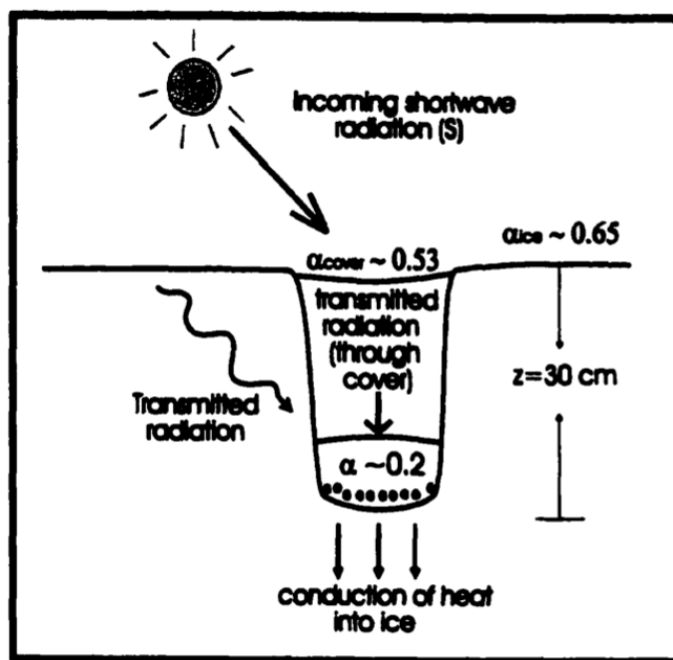


Figure 1.8- Energy balance in a lidded cryoconite hole. Reprinted from Lewis 2001.¹⁵

Glaciers in other world regions are either warm enough that lids do not form, or are cold enough but prevented from adequate sediment warming due to traditional diurnal cycles that disrupt incoming solar radiation at night. Lidded cryoconite holes cover approximately 4.5% of the surface area of glacial ablation zones in Taylor Valley³⁴, absorb

20% more solar radiation than the surrounding whiter glacial ice,¹⁵ and contribute approximately 15% of surface runoff from Canada Glacier.⁴²

Cryoconite holes and transitory melting are generally the only sources of liquid water on glacial ice in the Dry Valleys. Variations in surface ablation, freeze/ thaw cycles, and subsurface hydrologic connectivity all affect the development and duration of these pools, and cryoconites can be isolated from surrounding water movement on a span ranging from days to decades.³⁴ Holes can become connected to subsurface melt channels during freeze or thaw events that shift, expand/crack, or melt the walls of the pool and either drain the hole or enable channelized water to flow through the perforated cryoconite column (Figure 1.9). These “flushing” events lead to the routing of meltwater off glaciers during the summer and serve as part of the larger hydrologic cycle in glacial regions⁴⁶ (Figure 1.10).

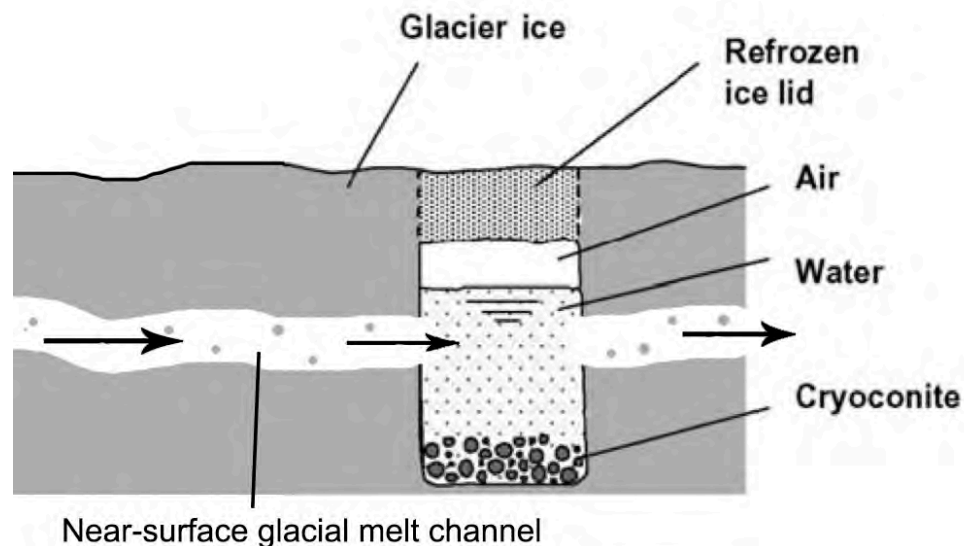


Figure 1.9- A lidded cryoconite hole with subsurface hydrologic connectivity. Modified from a schematic of an isolated cryoconite in Fountain et al..³⁴



Figure 1.10- Near-surface channelized melt flowing through Canada Glacier, Antarctica.

The degree of hydrologic isolation in these pools is interesting in the context of contaminant transport. Various methods^{34,47,48} have been used to estimate the ‘age’ of liquid in a cryoconite hole, and these formations provide a fascinating environment to examine contaminant partitioning into the melt water over time. The presence of ice lids is an intriguing scenario to compare biochemical properties between meltwater capable of gas exchange with ambient air and isolated pools that may become disequibrated from the atmosphere. Since ice lid formation is unique to the Dry Valleys, prior research has focused on microbial activity,⁴⁷ carbon cycling,⁴⁹ and isolation age³⁴ in lidded holes, and little attention has been paid to the characteristics of unlidded pools. No known studies have examined the physical and chemical parameters differentiating open and lidded cryoconite holes, which is essential to establish before making broader assumptions about

atmospheric exchange. The majority of cryoconite hole research has been limited to a single glacier in the Dry Valleys (Canada Glacier) and a more thorough spatial distribution of data is necessary to understand the hydrologic significance of these holes.

1.6 Study Purpose

The following chapters characterize the unique physical and biochemical characteristics of open- and lidded cryoconite holes in order to examine their hydrologic significance in the Dry Valleys ecosystem and potential role as indicators of SVOC deposition in Antarctica.

Chapter 2 examines the physical characteristics of both lidded and unlidded cryoconite holes across six glaciers of the McMurdo Dry Valleys over two summer seasons in order to gain a better understanding of the formation, fluctuation, and variability of supraglacial liquid in limited contact with the atmosphere. Inclusion of both open- and lidded holes examined the parameters governing the existence of both, and vertical profiles were created to describe the downward melt processes responsible for ~15% of glacial surface runoff³⁴ in the Dry Valleys.

Chapter 3 measured the spatial distribution of cryoconite holes on Commonwealth and Canada Glaciers over two seasons in order to obtain an estimate of the glacial surface area populated by cryoconite holes and develop a sense of the scale for the impact these features may have on glacial hydrology. A matrix-based analysis of cryoconite hole distribution across each summer was used to estimate the number of cryoconite holes gained, lost, and present on a multi-annual scale.

Chapter 4 examines the biogeochemistry and nutrient cycling of cryoconite holes across multiple glaciers in the Dry Valleys and proposes new methods for the estimate of hydrologic isolation age in these pools. Spatial gradients in meltwater composition were used to examine the role of microbial communities and regional topography on water chemistry, and chemical indications of atmospheric disequilibrium in lidded cryoconite holes are described.

Chapter 5 discusses the model assumptions used to calculate air:water partitioning of atmospheric contaminants in 0°C air. The limited liquid content within cryoconite holes presents an analytical challenge to identify low contaminant levels from small sample volumes. The degree of equilibrium for various semi-volatile contaminants was estimated in a model cryoconite hole system in order to assess the feasibility of detecting various contaminants in these unique environmental conditions.

Chapter 6 describes the solid-phase extraction of cryoconite meltwater and sediment along with subsequent analysis of contaminants by liquid chromatography. Two analytical methods were used to identify compound classes in each medium and the results of each method are discussed. Analysis of these samples provides reference data for contaminant levels in a unique environmental medium in Antarctica, and contributes to the database of contaminant studies available to model semivolatile distillation in the Southern hemisphere.

Chapter 2

Physical Characteristics of Cryoconite Holes On Glaciers of the McMurdo Dry Valleys, Antarctica

2.1 Introduction

Cryoconite holes are small columns of meltwater created by the accumulation of wind-transported sediment (known as cryoconite) into grooves on the textured surface of a glacier's ablation zone. This sediment has a low albedo and absorbs more solar radiation than the surrounding glacial surface, preferentially melting the ice below to create a cylindrical water-filled hole (Figure 2.1).

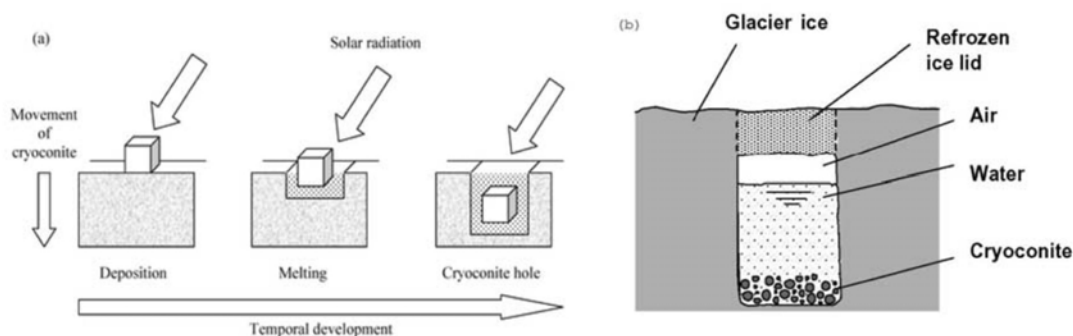


Figure 2.1- Schematic showing (a) the development and (b) the internal structure of a cryoconite hole. Reprinted from (a) Cowan and Tow³³ and (b) Fountain et al..³⁴

These holes eventually reach an equilibrium depth when the radiation absorbed by the bottom sediment equals the heat loss to surrounding ice. Holes can become connected to subsurface melt channels during freeze or thaw events that shift, expand/crack, or melt the walls of the cylinder and either drain the hole or enable channelized water to flow through the cryoconite column. These “flushing” events lead to the routing of meltwater off glaciers during the summer and serve as part of the larger hydrologic cycle in glacial regions.⁴⁶

Cryoconite holes have been found on glaciers around the world including regions of the Arctic,⁴⁰ Antarctic,^{41,42} and mid-latitudes.^{43,44}

Unlike typical cryoconite holes that form as pools of water open to the surrounding atmosphere, cryoconites in the McMurdo Dry Valleys of Antarctica are capable of forming 'lids' of condensed blue ice due to advection from cold winds on the top surface of the liquid pool (Figure 2.2). Lid formation is unique to the Dry Valleys due to the energy balance of this region—while cold temperatures and near-constant winds keep most glacial surfaces frozen, the consistent 24-hr daylight of Antarctic summer enables cryoconite sediment to absorb and maintain heat long enough to cause internal melting.

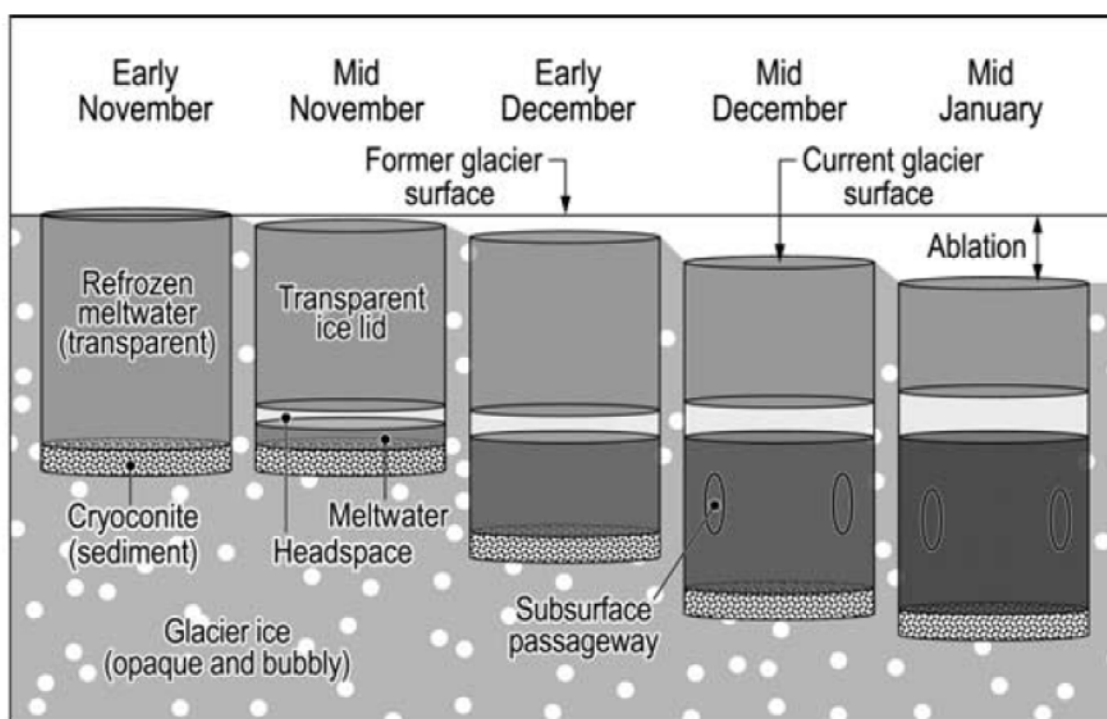


Figure 2.2- Annual remelting (internal melting) of a multiannual lidded cryoconite hole. Reprinted from Fountain et al.,⁴² The cryoconite hole melts in a bottom-up fashion as sediment warmed by insolation melts the overlying ice. Preferential melt of solutes in the ice column enriches the solute concentration in the liquid. An equilibrium depth is reached when the rate of melt-deepening in the hole matches the ablation rate of the glacial surface.

The liquid refreezes in the absence of solar radiation during the winter, and melting in subsequent summers occurs below the ice lid to continue melt-deepening the hole. Lidded cryoconites can therefore be isolated from atmospheric exchange while maintaining subsurface melt in a 'solid state greenhouse'.¹⁵ Flushing events can drain liquid water from the holes or introduce fresh water originating from subsurface drainage channels, while other lidded cryoconites can remain hydrologically isolated for decades.⁴⁹

Lidded cryoconite holes provide a unique scenario to study closed system processes (including nutrient cycling, microbial activity, and subsurface energy balance), but few studies have observed the development and variation of natural cryoconites *in-situ* over the austral summer on glacial surfaces that support the formation of both lidded and unlidded holes. This study measured the physical characteristics of both lidded and unlidded cryoconite holes across six glaciers of the McMurdo Dry Valleys over two summer seasons in order to gain a better understanding of the formation, fluctuation, and variability of supraglacial liquid in limited contact with the atmosphere. Inclusion of both open- and lidded holes examines the parameters governing the existence of both, and vertical profiles were created to classify a melt system responsible for up to 15% of glacial surface runoff³⁴ in the Dry Valleys.

2.2 Site Description

The McMurdo Dry Valleys of Antarctica (MDVs; 77°30'S, 162°00'E; Figure 1.3 and Figure 1.4) are a snow-free region of Southern Victoria Land near McMurdo Sound that comprise the coldest and driest desert on Earth.

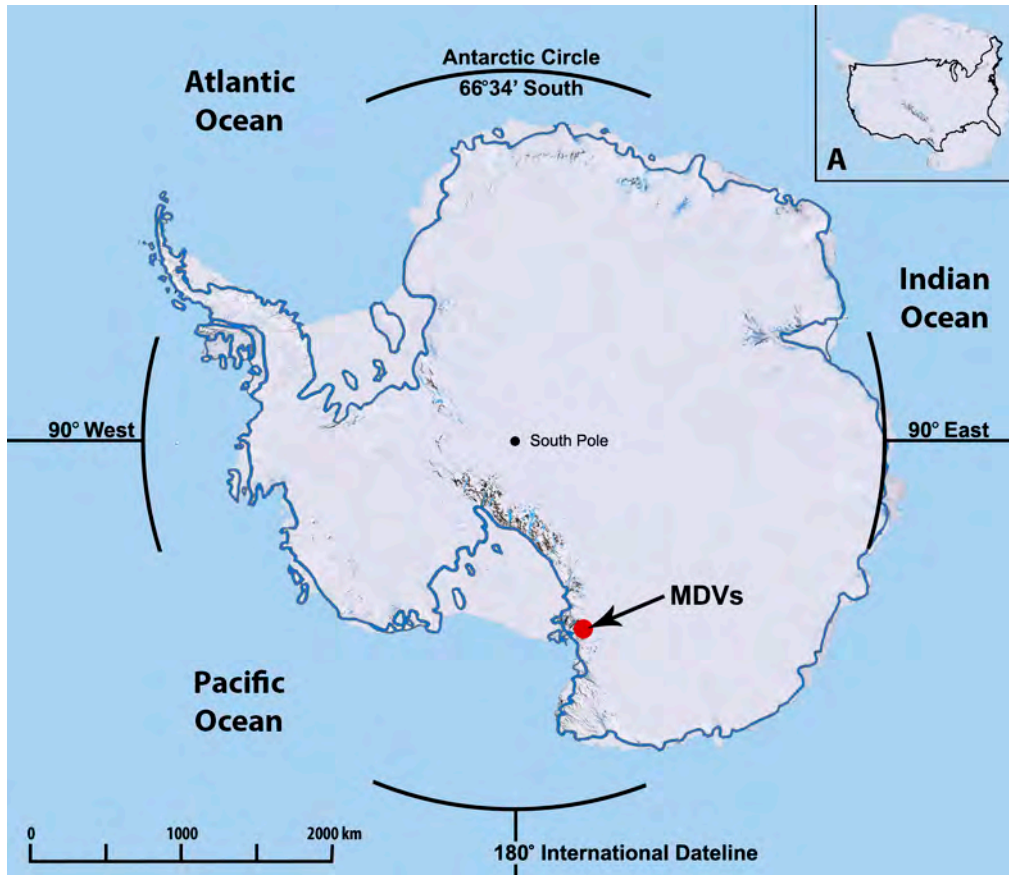


Figure 2.3- Antarctic map identifying the McMurdo Dry Valleys. *Inset image A contrasts Antarctica against the continental United States for scale. Map created by A.Q. Mass using satellite data from USGS 2008.²⁹ Continental borders were drawn to differentiate landmass from marine ice shelves, and both layers were isolated from open ocean/ sea ice extent in order to define the perennial boundaries.. The ice-covered area can double in winter during maximum sea ice extent.*

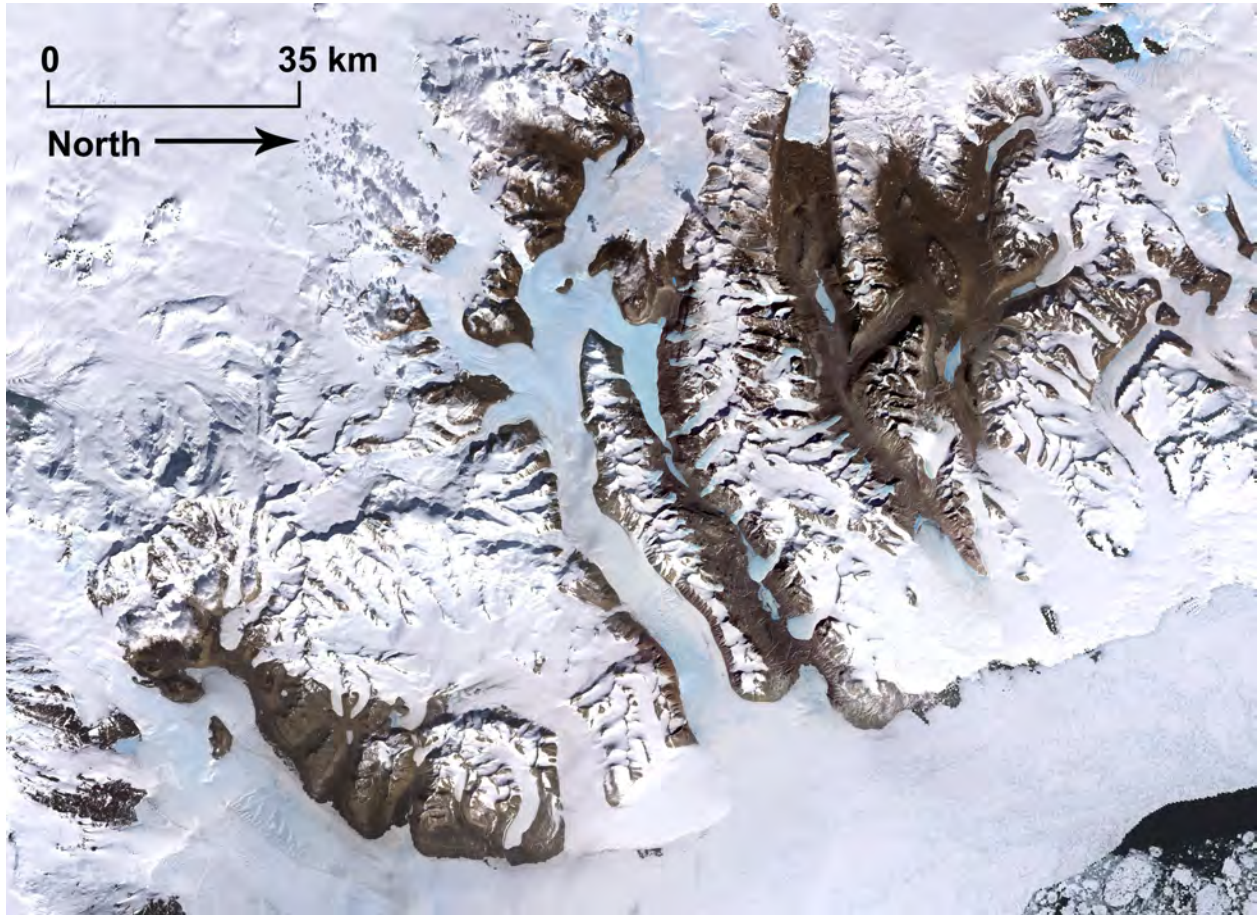


Figure 2.4- Satellite image encompassing the Greater McMurdo Dry Valleys.

Composited by A.Q. Mass using several USGS LANDSAT images.^{29,30}

Extremely low temperatures, precipitation, humidity, organic matter, as well as high salinity, strong katabatic winds, and extreme variation of solar energy collectively cause the area to be one of the least hospitable climates for life³³. The Transantarctic Mountains act as both a precipitation shadow⁵⁰ as well as a physical barrier to prevent the East Antarctic Ice Sheet (EAIS) from flowing into the valleys. The greater Dry Valleys region has a total area of 22,700 km² and an ice-free area of 4,500 km².⁵¹ Exposed rock and soil in the Dry Valleys is the largest contributor to Antarctica's 0.18% ice-free landmass.²⁷

Glaciers in the McMurdo Dry Valleys are unique in that they are “cold-based”; frozen to the ground and driven by their weight to spread down from the East Antarctic Ice Sheet.

These glaciers have smoother surfaces and cause less erosion than the rest of the world's "wet-based" glaciers which move debris along their edges as moraines.⁵⁰ Frigid basal temperatures prevent the formation of sub-glacial or deep englacial melt channels. Summer ablation is due to both sublimation (70%) and melt (~30%), and this glacial mass loss is roughly equal in magnitude to ablation over the remaining 9.5 months from February- November, which occurs via sublimation only. Total annual ablation is ~10 cm/yr. Overall, the mass balance of glaciers in the MDVs is in relative equilibrium because mass loss from ablation is offset by snow accumulation above the equilibrium line (Figure 2.5).

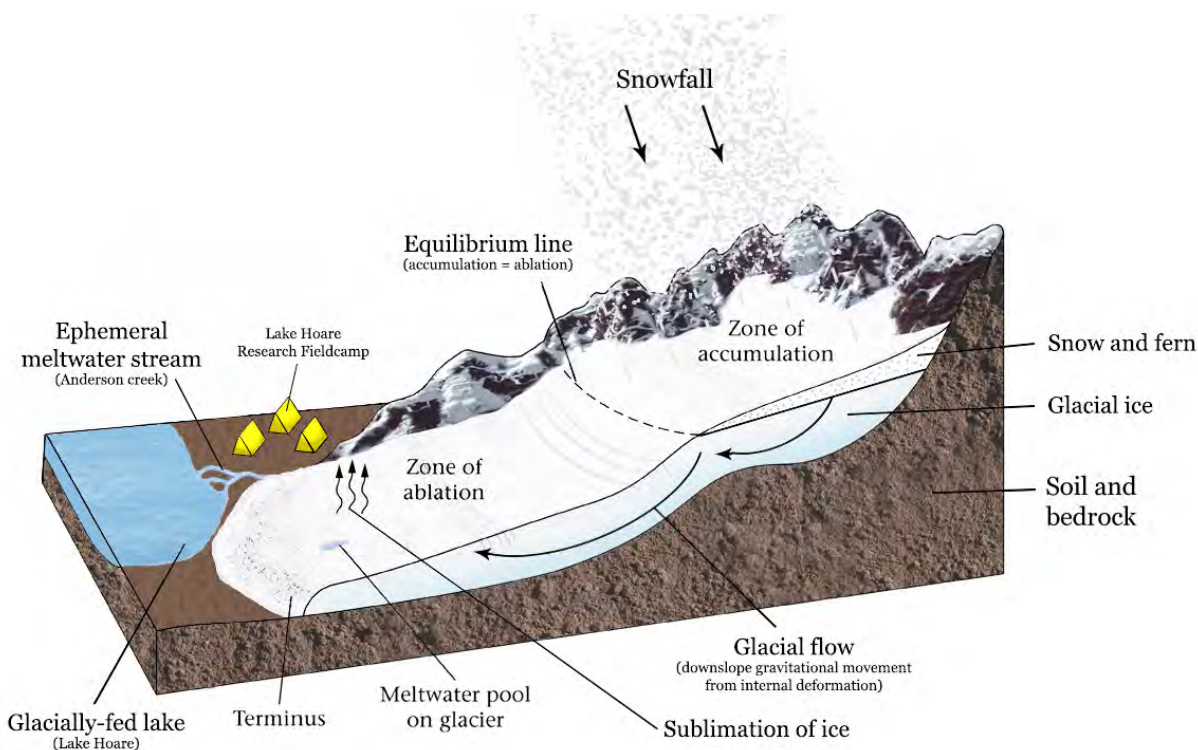


Figure 2.5- Accumulation, ablation, and mass balance on Canada Glacier. This cross-section of Canada Glacier and the Lake Hoare fieldcamp in the McMurdo Dry Valleys illustrates the accumulation and loss of ice contributing to the overall glacial mass balance. Snow accumulates at higher elevations and compacts into firn; granular crystals that are ultimately compressed into glacial ice. The glacier itself will flow downslope due to

internal deformation. Cryoconites and melt pools form below the equilibrium line in the ablation zone, and during freeze/thaw events may drain into near-surface channels that route meltwater off the glacier in waterfalls and streams. (Diagram by A.Q. Mass includes imagery from Marshak 2005.⁴⁵)

Precipitation falls as snow with a water-equivalence of 6-10 cm/yr^{42,52} and sublimates quickly due to low humidity and high winds,⁵³ leaving less than 2.5cm/year available as meltwater.⁵⁴ This leads to a unique environment in which a narrow 10-week season of glacial melt in November-January is the primary source of liquid water in the valleys.²⁸ Melt on the glacial surface is inhibited by a mean summer air temperature below freezing (apprx. -4°C) and perpetual winds averaging ~4 m/s. Seasonally continuous solar radiation transmitted into the ice produces warmer temperatures in a layer 5-20 cm beneath the glacial surface. This causes internal melt of the near-surface layer, and hydrologic connectivity through subsurface drainage channels routes meltwater off the glacier.³²

2.2a Glacier characteristics

Extensions of the EAIS form the basis for the large outlet glaciers at the head of Taylor and Wright Valleys. A series of mountains divide the region and produce small alpine glaciers descending into the valleys (Figure 2.6). The summer wind regime is dominated by coastal westward winds which can carry moist air into the region and yield precipitation as snow. This causes a precipitation gradient with less snow towards the inland side of each valley. Density-driven katabatic winds travelling down-valley are stronger but less frequent during the summer.⁵⁵



Figure 2.6- Glacier locations in the McMurdo Dry Valleys. *Commonwealth (1) and Canada (2) Glaciers both reside in Taylor valley, in which the larger Taylor Glacier (3) extends from the East Antarctic Ice Sheet. Taylor Glacier's northeastern tongue faces coastal McMurdo Sound. Joyce Glacier (4) in Garwood Valley and Adams Glacier (5) in Miers Valley are both fed by the larger Blue Glacier. Wright Valley is bookended by Wright Lower Glacier (6) towards the coast and Wright Upper Glacier (7) further inland. Image rendered from multiple composites using USGS³⁰ source data.*

While Taylor valley has a low elevation gradient with an open outlet to the coast, the Wilson Piedmont Glacier blocks the coastal edge of Wright Valley and flows in a relatively unconfined direction both into the valley and towards the ocean. This blocks the majority of coastal winds in Wright Valley and acts as a precipitation shadow. Total precipitation is therefore greater in Taylor Valley than Wright Valley,⁵² and annual precipitation at Lake Brownworth at the base of Wright Lower Glacier (Wright LG) is one of the lowest recorded in the McMurdo Dry Valleys.⁵⁶ Solar radiation increases with distance from the coast⁵⁷ and increases ablation on glacial surfaces. The opposing gradients for precipitation and

radiation both lead to a significant increase in the equilibrium line altitude (ELA) of glaciers further from the coast. Glacial ELA rises approximately 1100 m over the 40 km distance from the coast to the western boundary of the valleys.⁵⁸

Wright LG descends from the coastal Wilson Piedmont Glacier into Wright Valley. Both glaciers block most of the coastal winds from flowing into the valley and Wright LG receives the full force of eastward winds head-on. Solar radiation onto Wright LG is highest when the sun is on the western side of Wright Valley because the glacier is shaded by the Wilson Piedmont Glacier to the east and mountains on both its northern and southern sides. Since sublimation and melt are both enhanced on vertical ice surfaces,⁵⁹ sunlight limited to a relatively uniform (eastward) direction increases the rate of melt *into* the western slope of Wright LG. Over time this process transformed the diagonal slope of Wright LG into a series of vertical ice terraces escalating up the glacier (Figure 2.7). Above these terraces, the top of the glacier is a relatively flat field of ice ultimately connecting to the Wilson Piedmont Glacier on the coast.



Figure 2.7- Vertical terracing on Wright Lower Glacier. *These 'staircase' formations on the surface of Wright Lower Glacier are perpendicular to both the slope of the glacier and the orientation of Wright Valley. The majority of terrace walls ranged from 0.5-2.5m tall.*

Limited insolation on shaded sections of Canada and Joyce Glacier lead to a small degree of terracing on each glacier although the effect is most prominent on Wright LG. Insolation on Canada Glacier is strongest when the sun is oriented towards the south, but a lesser degree of radiation is still received from both the east and western sides. This dampens the unidirectional effect of terracing and creates scalloped basins on the glacier's surface (Figure 2.8).



Figure 2.8- Scalloped basins on Canada Glacier.

Increased sediment deposition into these features can lead to the formation of 'cryolakes'.¹⁵

These formations can be tens of meters wide with a thick underlying sediment layer that insulates the ice and traps runoff from uphill drainage into the pool (Figure 2.9).



Figure 2.9- Cryolake on Canada Glacier. *The sediment-lined bottom of this cryolake has a diameter roughly 8 m wide, with a frozen layer of runoff melt enclosed in the basin. This cryolake is an example of both terraced ice (left) and scalloped topography (right) around the perimeter of the basin.*

A summary of data for each of the glaciers sampled in this study is provided in Table 2.1 below.

Table 2.1- Geographic and meteorological summary of study glaciers

Glacier	Commonwealth	Canada	Taylor	Adams	Joyce	Wright Lower
Valley	Taylor	Taylor	Taylor	Miers	Garwood	Wright
Glacier type	Alpine- sourced from Asgard mountain range	Alpine- sourced from Asgard mountain range	Outlet- sourced from the East Antarctic Ice Sheet	Alpine- sourced from Blue Glacier	Alpine- sourced from Blue Glacier	Piedmont- sourced from the Wilson- Piedmont Glacier
Distance from sampling zone, and (terminus) to coast	6 km (4km)	15 km (12km)	37 km (36km)	10 km direct, 15 km following valley.	15 km direct, 18 km following valley.	21 km
Average equilibrium line altitude above sea level	384m ± 83m ^{60,61}	350 ⁵⁹ - 380m ⁵⁸	2080m, as part of the EAIS ^a	~575m ^b	~600m ^b	400 ⁵⁸
Directional flow	Southeast	South- Southeast	East- Northeast	East	Southeast	West- Southwest

^aTaylor Glacier is an outlet of the East Antarctic Ice Sheet where it spills into Taylor Valley. The equilibrium line altitude is 65 km further inland on the ice sheet at roughly 2080 m a.s.l.,⁽⁶²⁾ and thus Taylor Glacier itself is entirely within the ablation zone.

^bElevations based on the method described in Fountain⁵⁸ using USGS data.^{63,64}

2.3 Methods

2.3a Field sampling

Physical characteristics including depth, diameter, liquid and sediment content were measured from cryoconite holes and other glacial features in November-January of 2013-14 (Season 1) and 2014-15 (Season 2). The duration of each summer was spent on-site at fieldcamps in Taylor Valley. Certain data, such as identification of glacial waterfalls from the valley floor and helicopter-based observation of glacial surface conditions, could be collected throughout the field season. Measurements of individual cryoconite hole

characteristics were conducted over a series of sampling trips onto the ablation surface of each glacier. Season 1 served as a pilot year in which multiple sampling trips were conducted on three glaciers (Canada, Commonwealth, and Taylor) during the peak of the melt season in mid-January. Field sampling was expanded to six glaciers (adding Joyce, Adams, and Wright Lower) over the full summer in Season 2. Glaciers were chosen based on the observed presence of liquid-filled cryoconite holes, representation of four different dry valleys, and feasible accessibility from the Lake Hoare research fieldcamp at the base of Canada Glacier. Wright Upper Glacier was included in helicopter-based observations, but no melt features could be identified on the surface ice and thus no samples were collected from the glacier. Canada Glacier was sampled more frequently due to its proximity to the main camp and the ability to reach the ablation surface by crossing the Asgard mountains on foot.

2.3b Sample categorization

For the purposes of field sampling, “cryoconite holes” were broadly defined as melt holes in glacial surface ice with a contained shape and no visibly apparent connectivity to surface or subsurface melt channels. Samples needed to exhibit a relatively consistent depth profile; melting downward in a cylindrical shape with perpendicular ice walls and a frozen, level bottom. Additional requirements included a minimum column depth of 6cm, a diameter less than ~2-3m meters, and a layer of underlying sediment in holes containing meltwater. The presence of sediment was not a requirement for the inclusion of hollow column (dry) cryoconite holes, and both wet and dry cryoconite columns were measured.

The results of this study identified a unique subset of liquid-filled samples adhering to the guidelines described above which appeared to have lost the ability to melt-deepen

irrespective of surface ablation rates. These samples were classified as “melpools” and are addressed in subsequent discussion. Sampling guidelines for cryoconite holes and melpools created a distinct boundary to exclude the measurement of cryolakes, which accumulate sediment but lack distinct liquid boundaries in an ice-walled column. Sample selection prioritized cryoconites containing at least 1.5 L of liquid (for meltwater collection discussed in later chapters) but was randomized beyond these initial parameters.

A few similarities between cryoconite holes and near-surface drainage channels were observed during the course of field sampling. In order to examine these characteristics, the physical properties of both surface and subsurface meltwater channels were measured as time permitted during a given glacial trip.

2.3c Measurement and adjustment for surface elevation

The accuracy of handheld GPS devices on Antarctic glaciers has been erratic in previous studies although improvements in satellite coverage and resolution have corrected many of the discrepancies. Elevation measured by handheld GPS (Garmin GPS-map 76) in the field was therefore cross-verified using coordinates in Digital Globe/ Google Earth data³⁰ and topographic maps from the US Geological Survey⁶³ for confirmation. The elevation determined by handheld GPS was consistent with USGS topographic maps and Digital Globe/Google Earth satellite data for all sites except Joyce Glacier. Field measurements on Joyce were consistent with USGS maps⁶³ but 90-150 m lower than elevation determined by Google Earth³⁰. Garmin’s degree coordinates were reported with an accuracy ranging from 4-15 meters and Digital Globe imagery of these coordinates appear to accurately represent the locations and geologic features of individual sampling

sites. However, further investigation revealed significant errors in elevation determined by Digital Globe satellite data throughout upper Garwood Valley (Figure 2.10).



Figure 2.10- Digital Globe Satellite Imagery of Joyce Glacier and Upper Garwood Valley. *Sampling locations on the glacier were close to the terminal cliff edge in the region indicated by the arrow. Resolution was high enough to recognize subtle glacial features (including channels and cryolakes) surrounding individual sampling sites. This wider view in Google Earth³⁰ is shown in order to illustrate the steep topography surrounding upper Garwood Valley.*

Overestimates of low-lying topography including the valley floor, terrestrial lakes, and the majority of Joyce’s ablation zone are contrasted to underestimation of higher topographic features including Péwé Peak, which causes Joyce Glacier’s distinctive east → southward downslope curvature. The higher alpine topography surrounding Garwood valley is reported with greater accuracy but may shade or limit the resolution of topographic detail below the peaks. Thus the initial field-based GPS determination of elevation supported by USGS topographic maps is reported here.

2.4 Results and Discussion

2.4a Melt initiation in austral summer

Waterfalls of melt from near-surface drainage channels began pouring off the terminal face of Canada Glacier on December 10 during Season 1 and December 9 in Season 2. This onset coincided with the early rise in pulse glacial melt into Anderson Creek during both seasons (Figure 2.11). Melt at the base of terminal cliffs on the valley floor began roughly one week prior (December 1st and 5th, respectively). Terminal cliff melt begins earlier in summer due to the ice's proximity to the warmer terrestrial surface, and because the low angle of incident light enhances the radiation received by vertical surfaces.⁵⁹

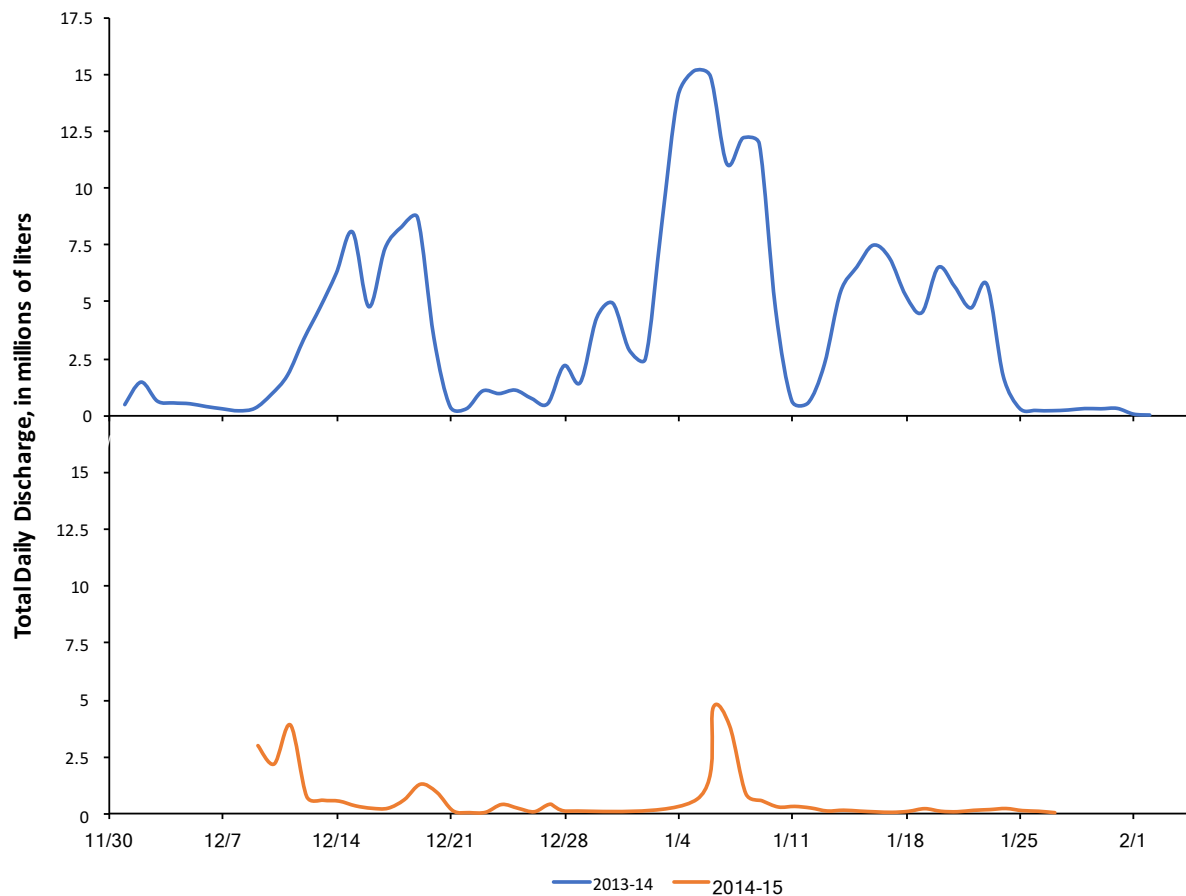


Figure 2.11- Total daily discharge from Anderson Creek during each melt season. Anderson creek is an ephemeral stream of glacial melt draining from the west side of Canada Glacier. Discharge data was not available before December 8 during Season 2 due to sporadic, low-flow measurements.

Canada's glacial surface was still relatively dense and no surface melt channels were identifiable during this initial melt, but fully-frozen cryoconite hole columns were observed (Figure 2.12). The presence of liquid water was evident in cryoconite holes on December 27 in Season 1 and December 28 in Season 2; roughly 2.5 weeks after subsurface melt began draining from the glacier. However, it should be noted that the visible identification of <3 cm meltwater is limited beneath >15 cm of ice in a frozen cryoconite hole. Gradual melt initiation from cryoconite sediment may have begun sooner, but the transformation of predominantly ice-filled columns into substantial liquid-filled pools in the majority of holes

occurred suddenly in this December 27-28 timeframe. The visible transformation of frozen columns into liquid-filled pools occurred simultaneously and was evident on Commonwealth, Canada, Seuss, and Taylor Glaciers within 36 hours of initial identification. The synchronicity of rapid re-melting of cryoconite holes across Taylor Valley during both seasons suggests that the recurrence of liquid in multiannual cryoconite holes is primarily driven by the consistency of solar radiation over a few cloud-free days in late December.

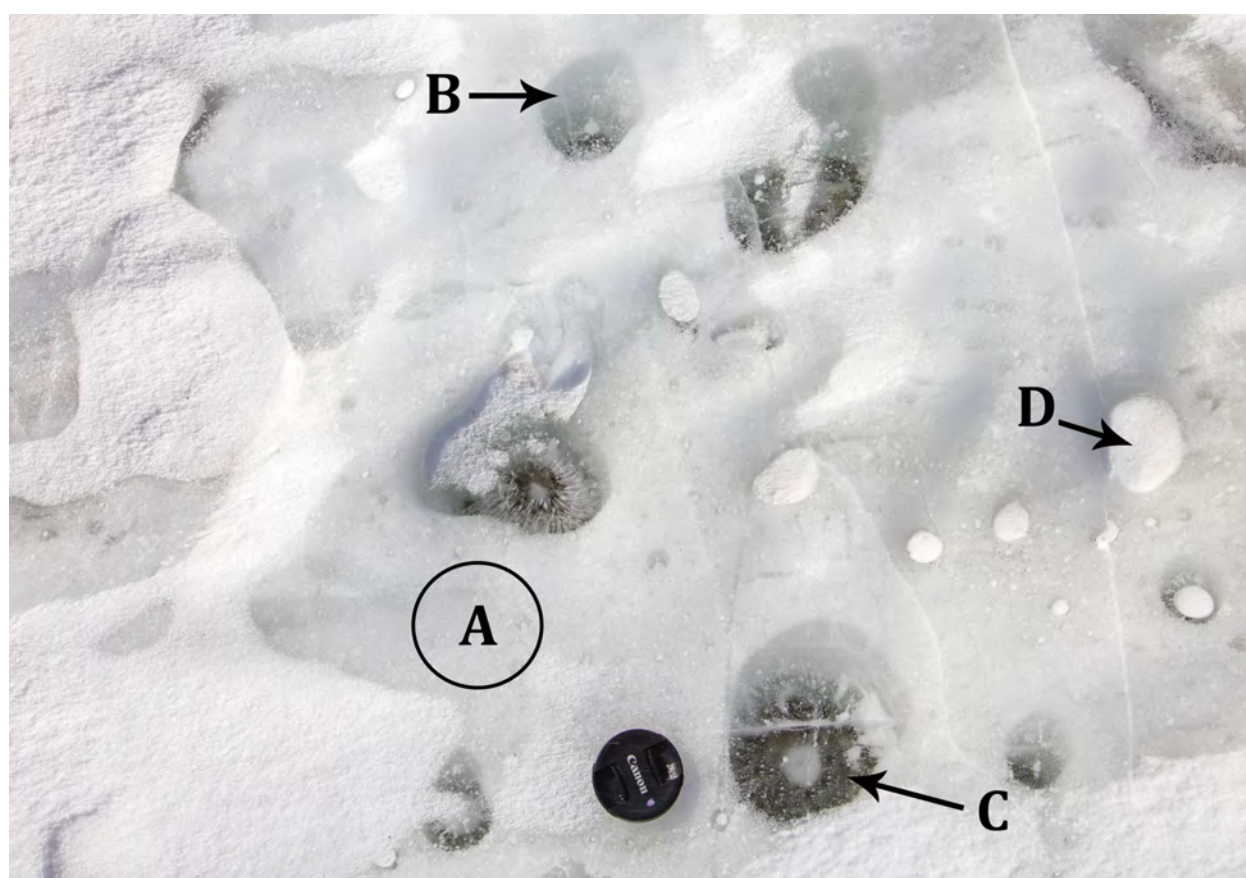


Figure 2.12- Surface ice of Canada Glacier in mid-December. *The glacial ice (A) has a higher albedo of 0.65^{9,15} compared to the denser ice in frozen cryoconite holes (B; ~ 0.53¹⁵). The albedo of sediment at the bottom of the holes is roughly 0.08-0.13.^{35,38} Cryoconite holes that drained during the previous year become filled with snow over the winter. Sublimation and wind dispersal remove snow from the ice surface during the summer, but this snow (0.97)¹⁵ persists longer in these hollow columns and reflects more incoming light.*

Evolution of the dense surface ice observed on the glaciers in mid-December into a porous weathered crust is shown in Figure 2.13.



Figure 2.13- Evolution of Canada Glacier over summer 2014-15. Snow covering the glacier's surface in early December (a) ablates by mid-December (b). Internal melt of dense

ice near the glacial surface (b) is routed off the glacier through a series of drainage channels, leaving a patchy “weathered” crust on the top ~20cm of the glacier with underlying melt channels by early January (c).

Once melting ceases in austral fall, the low-density crust will sublimate and expose the denser ice underneath, returning to the appearance of photos a & b by the following spring. Total surface depletion has been reported at 10-20cm surface loss/year in prior studies,^{32,65} which is offset by downslope gravitational flow and minimal snow accumulation.⁶¹

2.4b Profiles of vertical stratification in cryoconite holes and meltpools

The thickness and depth of ice lids, liquid, air pockets, and sediment are represented in vertical profiles of each melthole below the glacial surface. Samples measured during the 2013-14 and 2014-15 seasons are represented in Figure 2.14 and Figure 2.15 respectively.

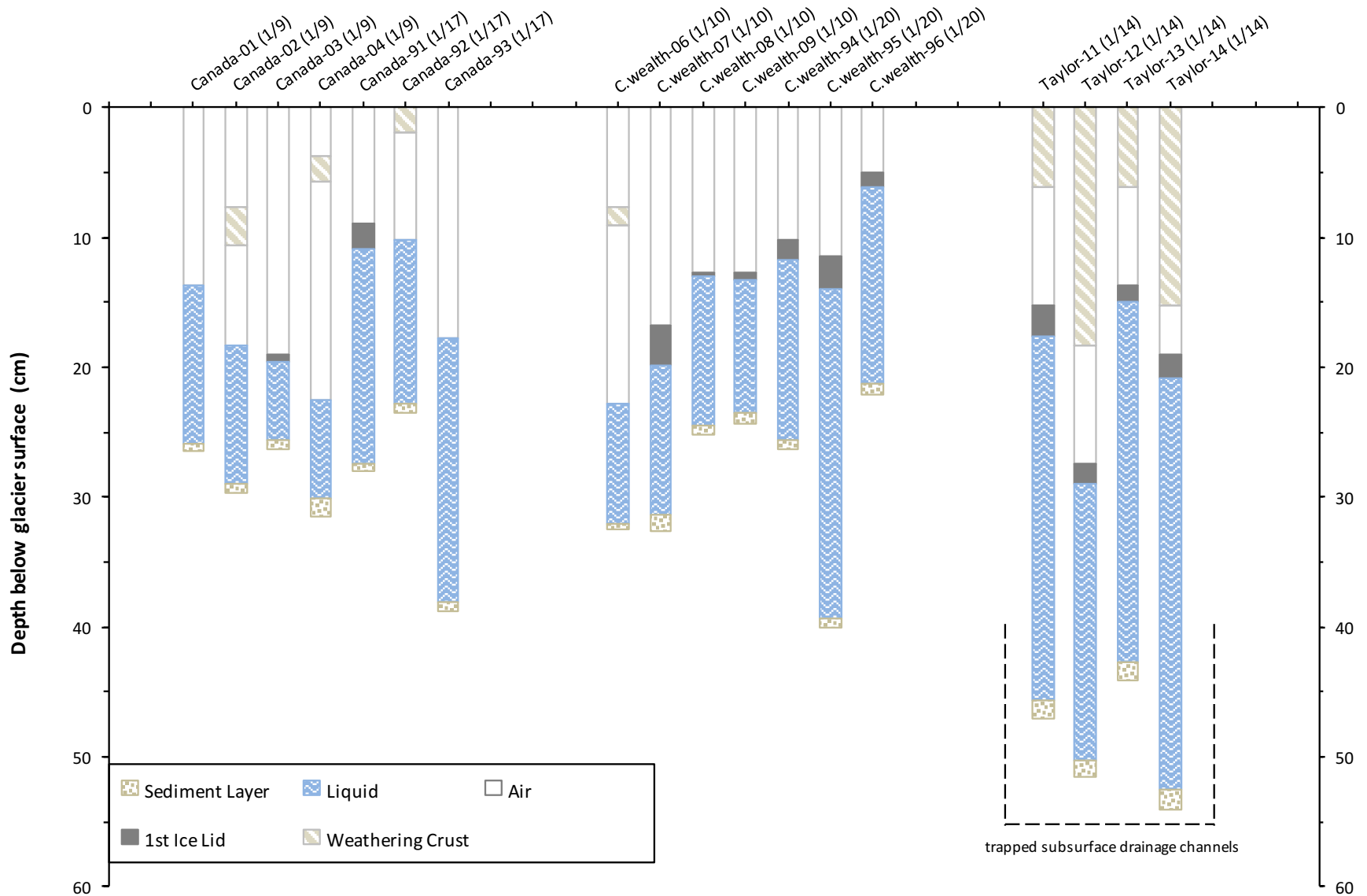


Figure 2.14- Vertical profiles of cryoconite holes and meltpools sampled in 2013-14.

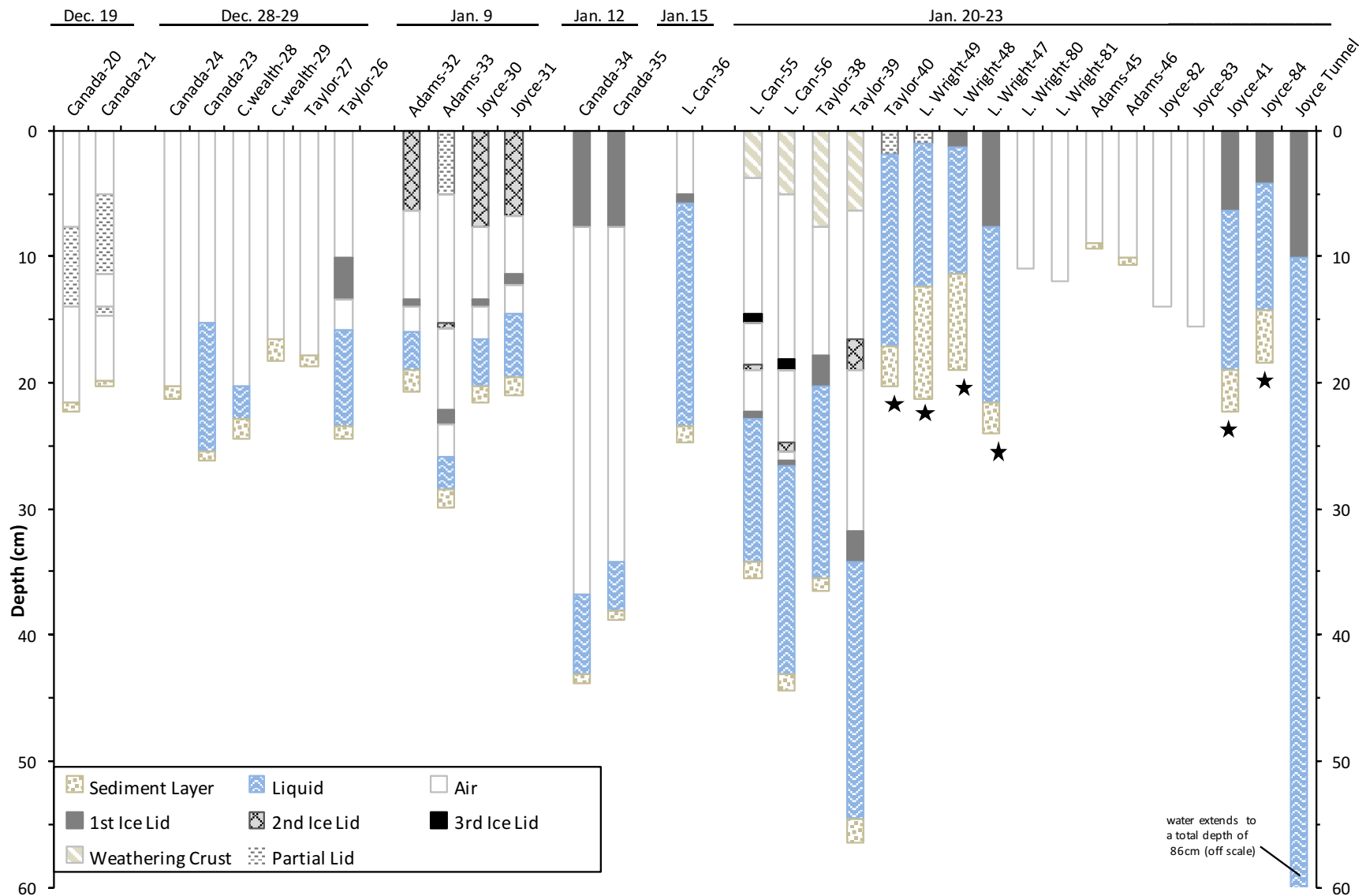


Figure 2.15- Vertical profiles of cryoconite holes and meltpools sampled in 2014-15. Samples subcategorized as 'meltpools' are indicated by a star under the melt column (see section 2.4e). Labels indicate the glacier and sample number (C-#) for each profile. Lower elevations of Canada Glacier are abbreviated as L.Can.

While the distribution of layers varies between samples, three prominent patterns emerged that were used to categorize and compare columns of glacial surface melt. Samples were subsequently designated as cryoconite holes, drainage channels, or melt pools according to characteristics discussed in the following sections. The majority of samples were classified as cryoconite holes. Dry/ drained holes were measured when liquid-filled holes could not be found during a given sampling trip. Thus measurement of liquid pools does not preclude the presence of dry cryoconites during a site visit, but the inclusion of dry holes does indicate that no liquid melt was present on a given date. Field sampling was conducted over a shorter timeframe during peak melt conditions in Season 1 when the vast majority of cryoconites contained liquid, so no dry holes were measured during that time. Dry samples from Season 2 indicate patterns for the onset and drainage of meltwater over the course of the summer.

2.4c The development of ice lids and weathered crusts

The unique feature of lidded cryoconite holes is their isolation from the atmosphere, and thus holes were classified as 'lidded' if a distinct, dense ice layer covered a full horizontal layer of the column. Partially-lidded holes (with a dense lid covering >70% of the surface but containing a chip or crack) were classified as 'open' due to continued gas exchange. Examples of open and lidded holes are shown in Figures 2.16- 2.19 below.



Figure 2.16- An open cryoconite hole on Canada Glacier. *This 24 cm-wide cryoconite hole (C-01) is open to atmospheric exchange. Weathered ice overhangs the perimeter of the hole and makes the column appear narrower than its true diameter. Small ice slivers on the liquid surface suggest that a lid may be forming, but at the time of measurement (1/9/14) it still easily categorized as an unlidded hole.*

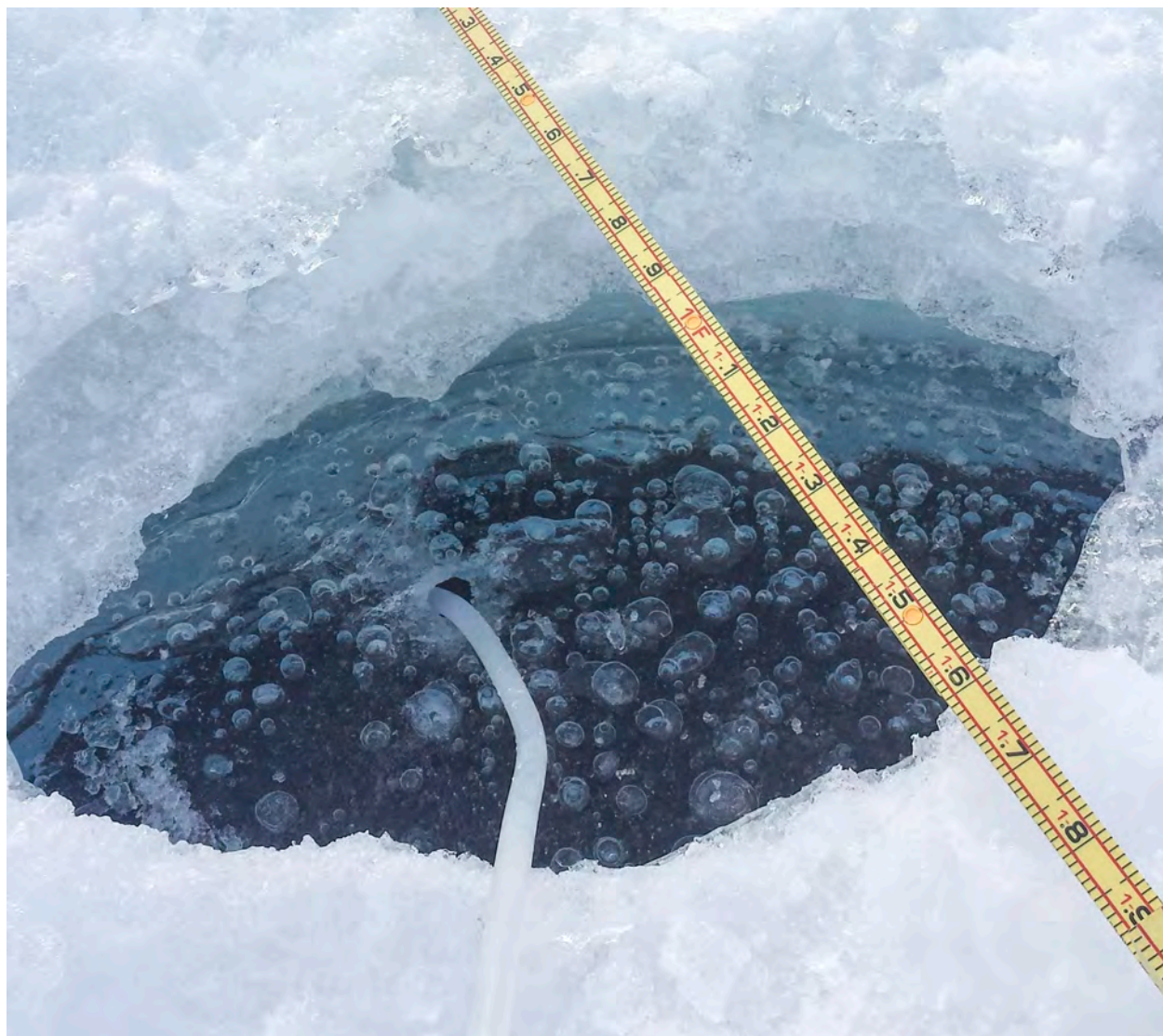


Figure 2.17- A lidded cryoconite hole on Commonwealth Glacier. *This 45 cm-wide hole (C-07) had a full ice lid 3.3 cm thick that was drilled through to extract the liquid inside.*



Figure 2.18- A portion of the ice lid from a cryoconite hole. *This is a $\frac{1}{4}$ section of the ice lid on cryoconite C-07 on Commonwealth Glacier. The lid is 3.3 cm thick, with a complete diameter of 45 cm.*

Prior research³² has confirmed that light penetrating >50 cm through the cryoconite hole column can initiate remelting while keeping the ice lid intact. Internal melt of the surrounding glacial ice is limited to a shallower band 5-15 cm below the surface, which can drain through subsurface channels and leave a low-density 'weathered' crust on the surface. Weathering occurs more rapidly in low-density ice and can become ubiquitous across large swaths of an ablation zone. The process takes comparatively longer to transform the surface of cryoconite lids due to the high density of the refrozen ice, but eventually ice lids can deform into a porous lattice open to surface gas exchange.

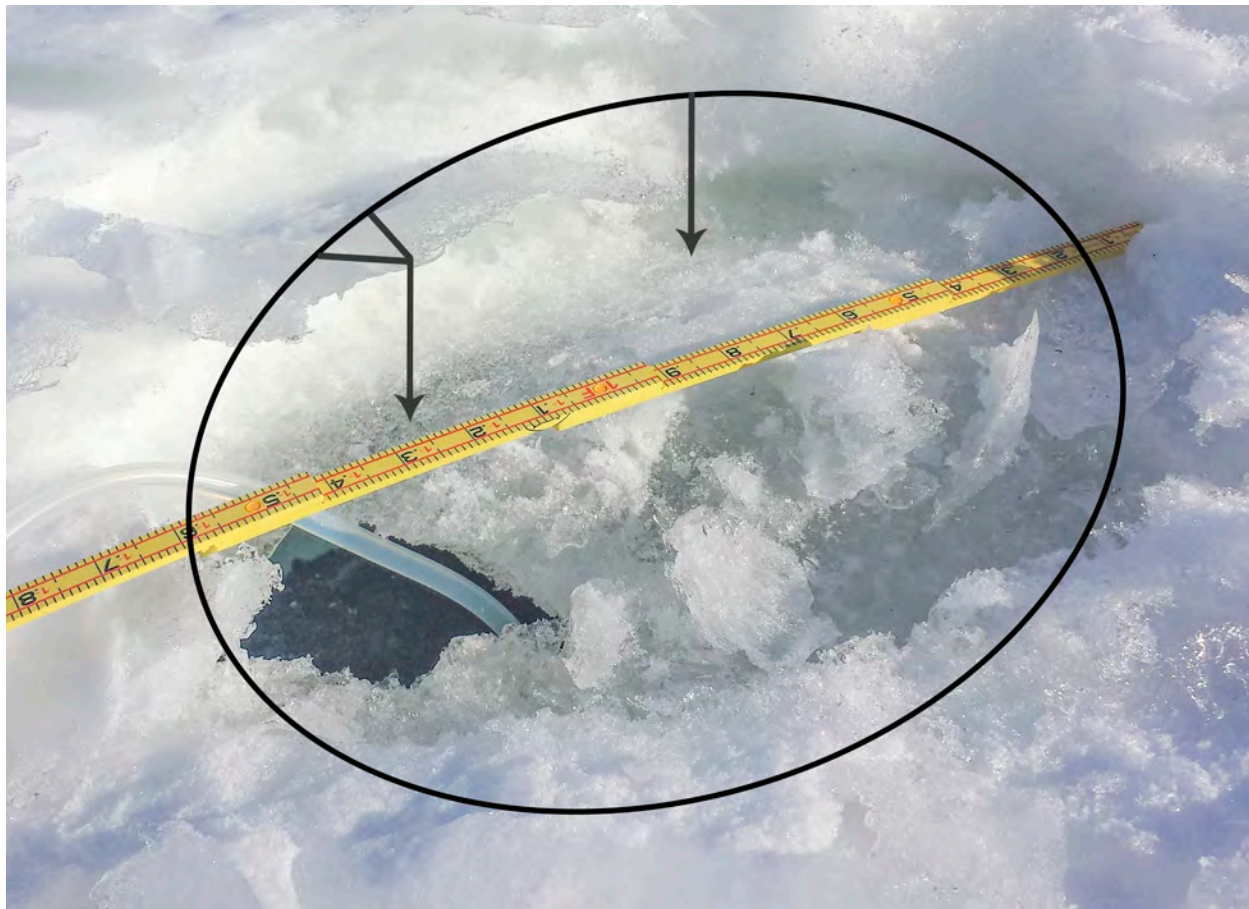


Figure 2.19- A weathered ice lid above a cryoconite hole. *Although mostly covered by ice and wind-blown fragments of the glacier’s weathered crust, this 45 cm-wide cryoconite hole (C-02) was classified as “unlidded” for the purposes of this study— not only is 20% of the lid open, but the lid itself is now part of a porous weathered crust and allows for atmospheric exchange. Note the depression of the lid compared to the surrounding glacial ice and the headspace beneath the lid to the liquid level below. This profile indicates that the column is deepening compared to the rate of surface ablation (see section 2.4e).*

In this study, the distinction between ice lids and weathering crusts refers to porosity and the primary mechanism dominating lid morphology during a given summer. Weathered crusts are the product of a shallow subsurface temperature gradient that warms and melts the ice itself, while melt-deepening of cryoconite holes is driven by warming of low-albedo cryoconite sediment. Freezing at the top of the liquid column produces a dense ice lid with a lower albedo and higher transmissivity than the comparatively white, bubbly glacial ice. It is unlikely for lids formed during a given season

to undergo significant weathering in the same year due to the limited duration of each summer and the lower depth of cryoconite liquid relative to the 15 cm band subject to weathering. In the sense of distinguishing open and lidded holes, weathered lids have essentially 'expired' and are no longer classified as true lids in the profiles outlined above. This difference becomes relevant in the analysis of chemical characteristics and atmospheric equilibrium in the following chapters.

2.4d Static subsurface channels

Four melt features (C-11, 12, 13 and 14) found on Taylor Glacier during Season 1 exhibited an erratic shape, significantly larger diameter, and a weathered crust that was uncharacteristically consistent with the density of the surface ice (Figure 2.20). Although the samples appeared to have distinct walls and no flow could be detected in the pools, these formations were categorized as immobilized segments of subsurface melt channels. These channels exhibited significantly different features from five fast-moving meltwater channels measured on the surface of Canada and Wright LG and will be compared in the following sections. Melt channels may become blocked by the refreezing of a downstream drainage path. Alternately, the water could be subject to hydraulic resistance from the saturation of low-gradient channels during a high-flow event which exceeds the permeability of the existing drainage network. The extremely high flow from Taylor Glacier in 2013-14 and the appearance of the water spread across indistinct "mushy" layers towards the glacial surface (Figure 2.21) suggest that saturation is the likely cause of Taylor's immobilized channels. Each trapped pool included a few distinctly circular sections which suggest that the subsurface network permeated into pre-existing cryoconite holes. The larger width and segmented appearance of the pools could be the result of slow

but pervasive runoff redistributing the sediment content across a basin of interconnected cryoconite holes.



Figure 2.20- A segmented subsurface melt channel on Taylor Glacier. *A red perimeter outlines the rough boundary of this interconnected cryoconite/channel network. Sections with more notable surface depression indicate the location of pre-existing cryoconite holes prior to channelization. Overall the surface of the pool exhibits a similar density and weathering crust to the surrounding ice, supporting the hypothesis that the underlying meltwater originated from other regions of the glacier and is not due to direct melt-deepening through this portion of the surface ice.*



Figure 2.21- Liquid saturation through low-density surface layers in a stagnant melt channel.

2.4e Headspace and the categorization of meltpools

The presence of air pockets either within or above a melt column served as the most visible indicator of a cryoconite hole's ability to melt downwards with respect to surface ablation. Since ice is less dense than water, the total volume/depth of a cryoconite hole should be larger than the depth of liquid produced by the column. New ice lids form directly over the liquid surface, while remelt in a following year can produce headspace between newly-deepening liquid and the remaining ice above. Six samples from Season 2 (C-40, 41, 47, 48, 49, and 84, each denoted by a star in Figure 2.15) did not contain any headspace either within the column or above the frozen lid. This indicates that no melt-deepening occurred within the pool. These samples contained a thicker sediment layer and

the overlying meltwater produced an ice lid that was level with the glacial surface. In essence, these profiles are indicative of columns prevented from further growth which will become shallower over time. Such samples were designated as “melpools”.

This study identifies a boundary in the evolution of cryoconite holes when the continued accumulation of sediment reaches a threshold depth thick enough to insulate the underlying ice. Rather than cryoconite holes at an “equilibrium depth” relative to surface ablation, the vertical profiles in this study indicate that melpools are the product of an absolute limit preventing *any* melt-deepening. As surface ablation continues this will cause melpools to become shallower over time. (In order to maintain this distinction in the following discussion, the combination term “meltholes” is used when referring to both cryoconite holes *and* melpools.) Physical features for each category are outlined in Table 2.2 below.

Table 2.2- Characteristics of meltholes sampled

	Dry Cryo.	All Liquid Cryo.	Open Liquid Cryo.	Lidded Liquid Cryo.	Meltpools	Slow Channels	Fast Channels	Flooded Joyce Tunnel
Sediment depth (cm)	0.5 ± 0.6 ^a	1 ± 0.4	0.9 ± 0.4	1 ± 0.4	5 ± 2.6	0.9 ± 0.1	0.06 ± 0.13	<0.3cm
Liquid depth (cm)	n/a	11.1 ± 5.9	11.5 ± 5.3	10.8 ± 6.4	12.3 ± 2.1	27.2 ± 4.3	2.7 ± 1.6	101.3
Ice lid thickness (cm)	0.5 ± 1.8 ^a	1.4 ± 2	n/a	2.1 ± 2.2 ^b	3.7 ± 2.8	1.8 ± 0.5	0	10.2
Total air layers (cm)	13.2 ± 3.7	15.1 ± 6.1	15.6 ± 5	14.7 ± 6.7	0	7.4 ± 2.5	25.7 ± 31.6	0
Total depth (cm)	14.3 ± 4.6	29.7 ± 8.5	28.1 ± 4.9	30.4 ± 9.8	16 ± 4	47.8 ± 4.5	28.5 ± 31.2	111.5
Diameter (cm)	17 ± 5.2	26.8 ± 8.3	25.7 ± 8.9	27.3 ± 8.3	154.5 ± 58.2	76.2 ± 12.7 ^c	11 ± 4.2 ^c	564
Diametric circularity	0.92 ± 0.05	0.92 ± 0.05	0.93 ± 0.06	0.91 ± 0.08	0.43 ± 0.1	n/a	n/a	0.48
Sample size <i>n</i>	13	28	9	19	6	4	5	1

^aAverage of all dry cryoconite holes, while only 54% contained sediment and 15% of contained lids.

^bAverage of all liquid cryoconite holes, while only 68% contained lids.

^cThese values are the width of channels, since there is no contained diameter to measure.

Interestingly, there were no differences between the air depth of dry and liquid cryoconite holes ($13.2 \pm 3.7 \cong 15 \pm 6.1$ cm). Samples from both types showed signs of multi-year freeze/thaw cycling (based on the presence of prior lids), so the similarity of air content suggests that the difference in total depth is most dependent on melt-deepening during the present season.

2.4f Sediment thickness

Meltpools contained significantly more sediment than liquid-filled cryoconite holes (5.0 ± 2.6 cm \gg 1.0 ± 0.4 cm; $p= 0.014$). The thick layer of sediment in meltpools serves to insulate the bottom of a melt column and prevents melt-deepening of the hole, and supports this study's hypothesis that sediment thickness (Figure 2.22) is the determining factor in this transition from cryoconite holes into static pools shallowed by surface ablation. A threshold between 2-2.4 cm appears to be the boundary sediment thickness inhibiting further melt of cryoconite holes in this region.

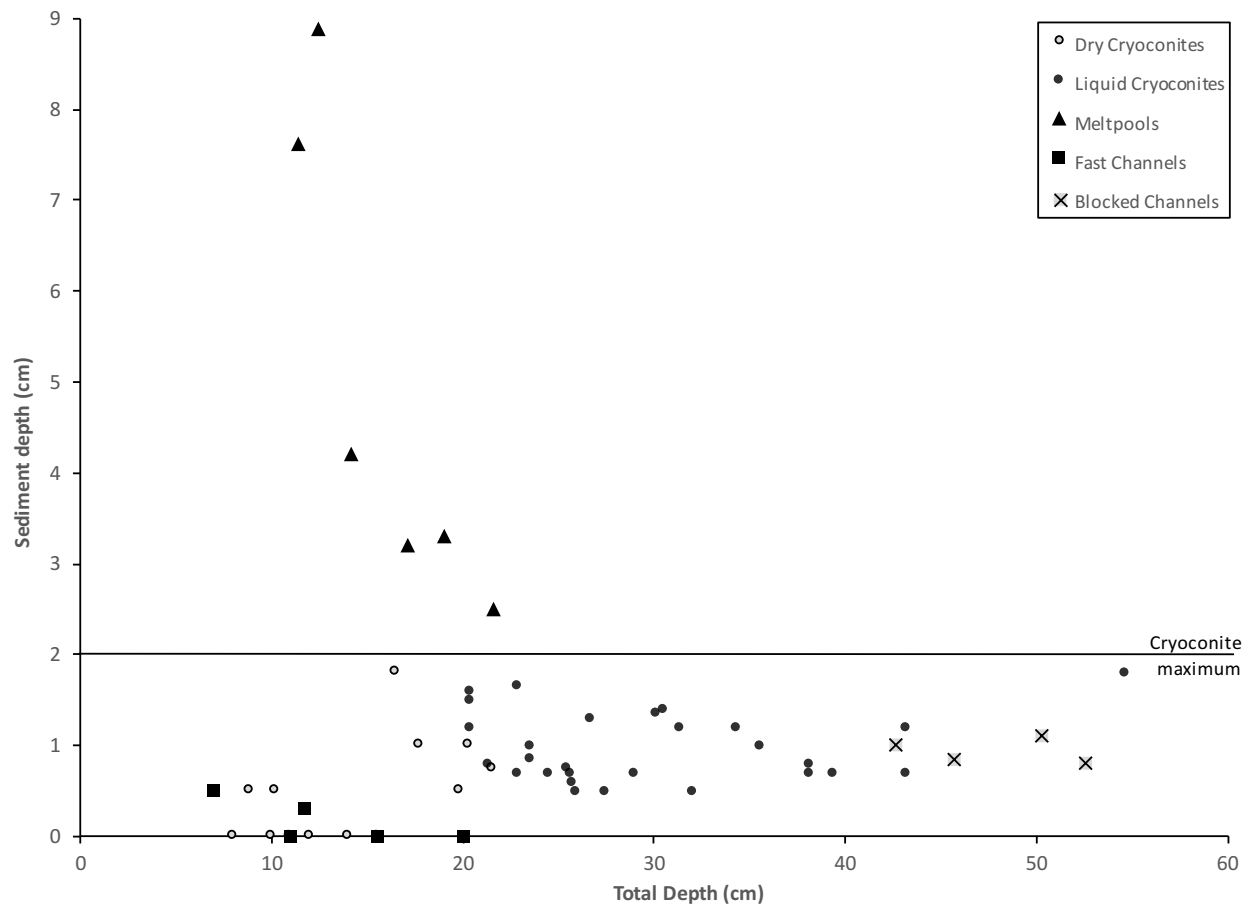


Figure 2.22- Sediment and total depth of meltholes sampled.

Liquid cryoconites contained a sediment layer ranging from 0.5- 1.8 cm. Studies in polar and mid-latitudes found that sediment increased the rate of melt-deepening until a layer ~3-5 mm thick insulated the underlying ice;^{66,67} a limit far below the levels found in this study. However the energy balance is much different in those regions, where cryoconite holes have significantly smaller surface diameters than those in the Dry Valleys and develop in a region subject to surface melt and $>0^{\circ}\text{C}$ ambient air. A previous study by MacDonnell *et al.*⁶⁸ found that a minimum 2mm sediment layer was necessary to initiate cryoconite hole formation in the Dry Valleys, and greater melt efficiency occurred at 4mm (the maximum level used in that study). Of the three cryoconite holes with the thickest sediment layer, one (Taylor C-39; 1.8 cm sediment) was the overall deepest cryoconite and

contained multiple lid layers. The other two were both found close to each other on Commonwealth Glacier and had unusual characteristics. Commonwealth C-29 was a dry hole containing a layer of wet, unusually sticky sediment 1.8 cm thick. The wet sediment may have indicated that the hole was in the early stages of melt-deepening. Sample C-28 on Commonwealth was an unlidded liquid pool within 10 meters of C-29, and had the third largest sediment layer (1.6 cm) with an equally 'sticky' consistency. This sample contained dime- to quarter-sized portions of what appeared to be black algal mat or other black organic matter within the sediment. Both of these cryoconite holes may have been affected by a wind event transporting microbial organisms or organic matter into the holes. C-28 was the only hole where this algal mat material was observed over the two sampling seasons.

Dry cryoconite holes contained less sediment than liquid holes (0.5 ± 0.6 cm \ll 1.0 ± 0.4 cm; $p = 0.007$). This statistic is inclusive of all glaciers, but the pattern is also apparent within each glacier (Figure 2.23). There was no sediment remaining in the dry cryoconite holes sampled after January 18 (2015) on Commonwealth, Joyce, or Wright L. Glaciers. This contributed non-detect values to half of the total data for dry holes. All three glaciers had a deep weathered crust, significant subsurface drainage, and no observable liquid-filled holes towards the end of the summer. The lack of sediment suggests that large-scale drainage flushed both the liquid and underlying cryoconite material out of the holes. Since bottom-layer sediment cannot be removed from a cryoconite column without full drainage of the overlying liquid, liquid-filled holes must inherently still contain sediment. Furthermore, if no sediment remains in a drained cryoconite, there is no way to reinitiate melt of the hole. Out of thirteen data points, seven dry cryoconites had a measurable layer of sediment for

an average 0.86 ± 0.47 cm thickness. There are no statistical differences between this value and liquid-filled holes, but the six non-detect sediment values are important in the overall comparison to liquid-filled pools because they represent events that led to the holes becoming dry.

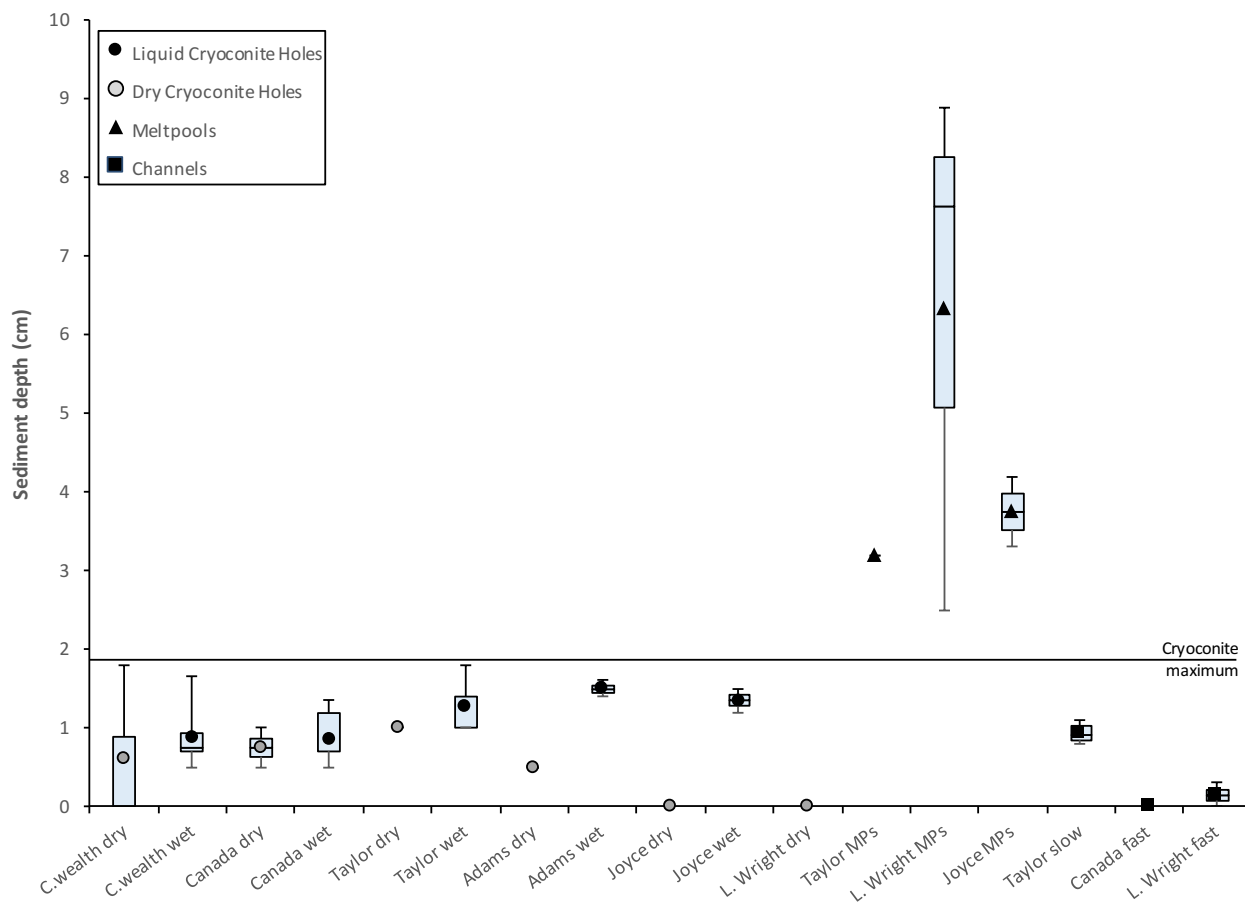


Figure 2.23- Sediment depth of cryoconite holes and meltpools sampled. Vertical bars span the minimum and maximum values in each category, enclosed columns represent the 1st and 3rd quartiles, and each mean is denoted by a central marker. Categories include both seasons of data.

In fast-moving drainage channels the majority of sediment is likely transported with the flow of the meltwater. Only one fast channel contained a measurable amount of sediment in this study (0.3 cm). The majority of meltwater originates from internal melt of the subsurface ice layer where the sediment content is generally low, but connectivity to

cryoconites and melt pools can increase the sediment load in drainage channels. If the water flow decreases significantly the sediment will fall out of suspension. The overall shape of Taylor's immobilized subsurface channels suggests that their paths infiltrated a series of cryoconite holes in a point-to-point pattern travelling down the glacial slope. All four of these channels contained sediment (0.94 ± 0.14 cm) which was evenly distributed throughout the irregular shape of each pool.

2.4g Total depth

Liquid cryoconite holes (29.7 ± 8.5 cm) were significantly deeper than both dry holes (14.3 ± 4.6 cm; $p = 5.4 \times 10^{-9}$) and melt pools (16 ± 4 cm; $p = 0.000015$) as shown in Figure 2.24. However, there was no significant difference in depth between *dry* cryoconite holes and melt pools. Both dry holes and melt pools are shallow columns incapable of melt-deepening at the time of measurement. In the case of dry cryoconites this may be a temporary state; holes measured at the beginning of the season may begin to melt over the course of the summer. On the other hand, holes that are dry due to drainage may be incapable of melt-deepening if there isn't sufficient sediment or adequate insolation (towards the end of summer) to initiate further melting. Both dry holes and melt pools will become shallower over the course of the summer as the glacial surface ablates compared to the depth of the static columns.

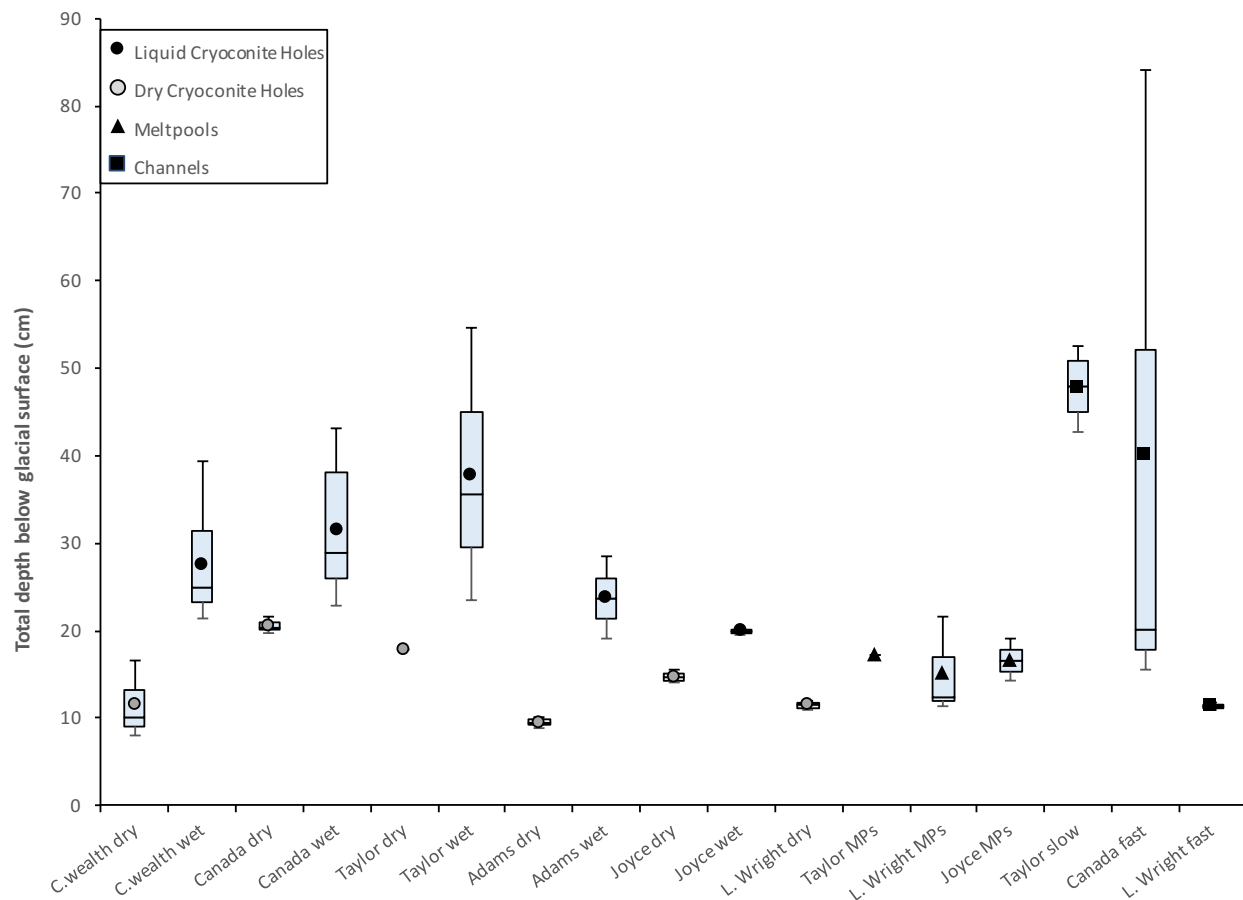


Figure 2.24- Total depth of cryoconite holes and meltpools sampled. Vertical bars span the minimum and maximum values in each category, enclosed columns represent the 1st and 3rd quartiles, and each mean is denoted by a central marker. Categories include both seasons of data.

Melt channels (Figures 2.25 and 2.26) exhibited the largest range of depths. There were no differences in depth between the wide, stationary subsurface drainage channels on Taylor Glacier and the fast-moving surface channels on Wright L. and Canada Glaciers. There were also no statistical differences between the depths of meltwater channels and liquid cryoconites (both capable of melt deepening), although the range of depth was much broader for drainage channels. Like liquid cryoconite depth, channel depth (37.1 ± 24.5 cm) was significantly deeper than both meltpools ($p= 0.033$) and dry cryoconite holes ($p= 0.023$). Channel depth is most likely an indication of slope/velocity, volume, and age. The

removal of shallow surface channels during winter sublimation may cause runoff to form different drainage pathways the following year, but subsurface channels and deeper channels on the glacial surface can both route meltwater into the same paths over multiple seasons. Narrow, high velocity drainage channels of $\geq 0^{\circ}\text{C}$ water can deepen before losing too much heat to the surrounding environment. Slow-moving or immobilized channels lose more heat to the overlying cold air, which can significantly decreasing the rate of channel deepening. This heat loss is evident by the formation of thicker ice lids on the stagnant Taylor channels. Despite this loss, immobile channels can melt-deepen if the meltwater contained a high sediment load that falls out of suspension and melt-deepens the stagnant column. Subsurface drainage that infiltrates cryoconite or meltwater columns can redistribute the existing sediment through a stationary channel segment, which appears to be the case in the subsurface Taylor channels. Prior studies determined that friction between running water and the underlying ice is not a significant source of heat in glacial melt channels.³⁴



Figure 2.25- Deep, narrow drainage channel on Canada Glacier. *CC-87 is a surface melt channel 18 cm wide, 86 cm deep with 1.8 cm of meltwater draining from Canada Glacier. This channel entrance serves as the outlet for a cryolake shown in Figure 2.9.*



Figure 2.26- Shallow surface drainage channel on Canada Glacier. *CC-57 is an overall shallower channel (15 cm deep, 7 cm wide) than Figure 2.25 but contains a deeper 5cm flow of meltwater. This section is located at a lower elevation on the glacier closer to*

the terminus and is therefore subject to a larger drainage basin from upglacial tributary channels.

Liquid depth was not significantly different between wet cryoconites (11 ± 5.9 cm) and melt pools (12.3 ± 2.1 cm), nor was the liquid level different between open and lidded holes. No cryoconite holes contained more than 25 cm of liquid, and liquid depth was independent of total depth across the full range of samples. This study suggests that variation in the liquid: total depth is due to drainage events and the multi-annual age of cryoconite holes. The mean ratio of liquid: total depth was 0.31 in cryoconite holes and 0.71 in melt pools (Figure 2.27). Slow channels had a larger liquid depth than fast-moving channels (27.2 ± 4.3 cm \gg 2.7 ± 1.6 cm; $p= 0.001$).

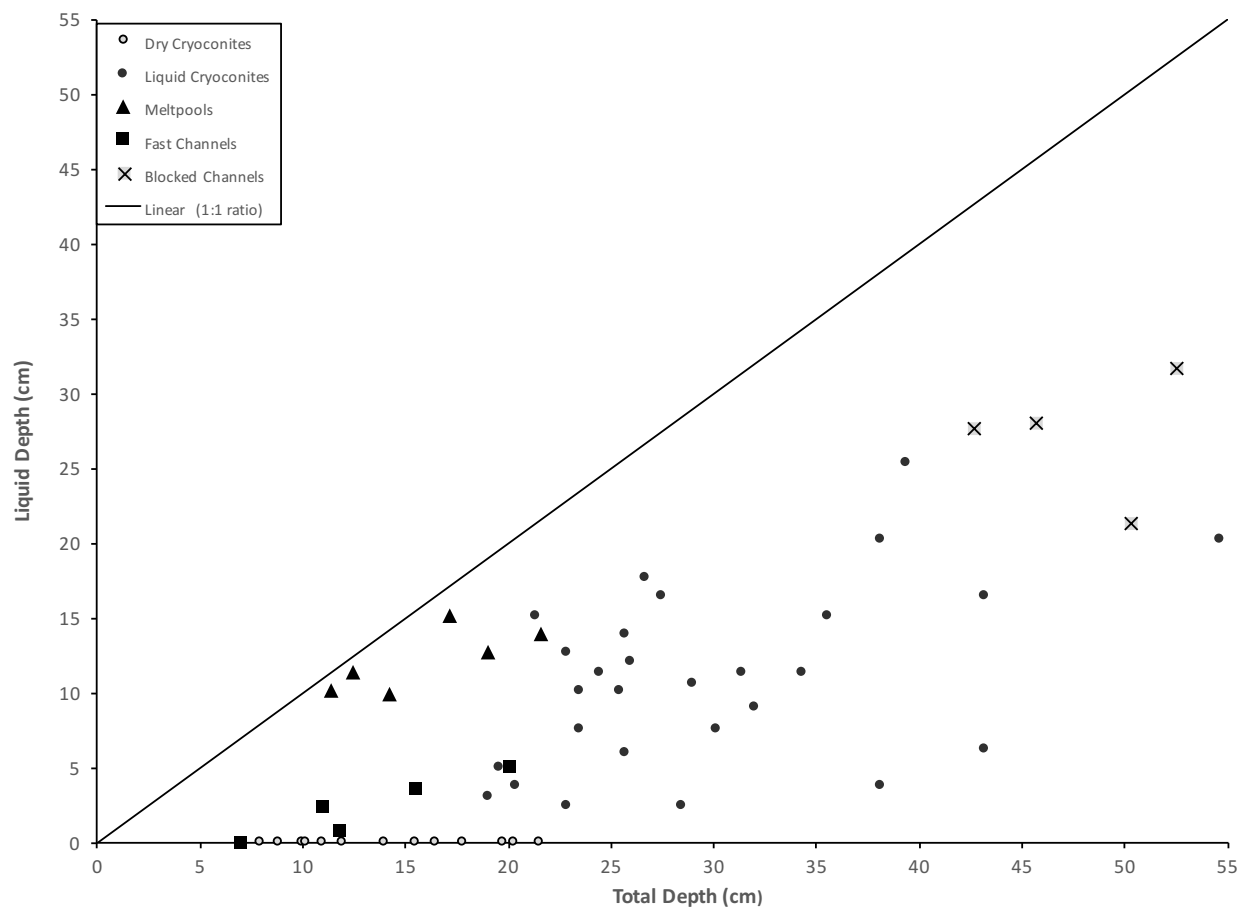


Figure 2.27- Liquid and total depth of cryoconite holes and melt pools sampled.

The profile and lack of remnant ice lids above the current frozen surface of Lower Canada-36 suggest that this cryoconite hole formed during the present season. Although it is plausible that previous ice lids and multi-annual features have ablated away, the ratio of liquid depth: total depth is more characteristic of a new melthole. The density of near-surface glacial ice (~15-100 cm depth) in the Dry Valleys is approximately 870 kg/m^3 . Internal melting of the near-surface layer 7-15 cm deep causes higher variability in ice density (approximated as $\sim 740 \text{ kg/m}^3$), while the top ~3 cm of highly weathered ice contributes little to bulk water equivalence.⁶⁹ If the liquid content of Canada-36 represents the water equivalence of the full cryoconite hole column (excluding sediment depth), this

translates to an ice density of 700-780 kg/m³ depending on how the 3cm surface and internal ice lid are incorporated. These values can be used to represent a 0.7 liquid: total depth in cryoconite holes. The ratio in Canada-36 is 0.67, while no other cryoconite holes contained a ratio above 0.47. Each consecutive season of winter ablation exaggerates the liquid: total depth ratio because the density of ice lids is higher than glacial ice, but both features sublimate equally during the winter. Thus the ~0.7 proportion of liquid:total depth represents a ratio for new melt, while the intermediate density of cryoconite ice lids (less than 1000 kg/m³, but more than ~740 kg/m³) causes a greater amount of refrozen cryoconite liquid to sublimate compared to the water equivalent loss in the surrounding glacial ice.

The comparison of total depth to diameter in Figure 2.28 serves as a good visual representation of the vertical limitation in melt pools even as the accumulation of sediment causes column walls to widen.

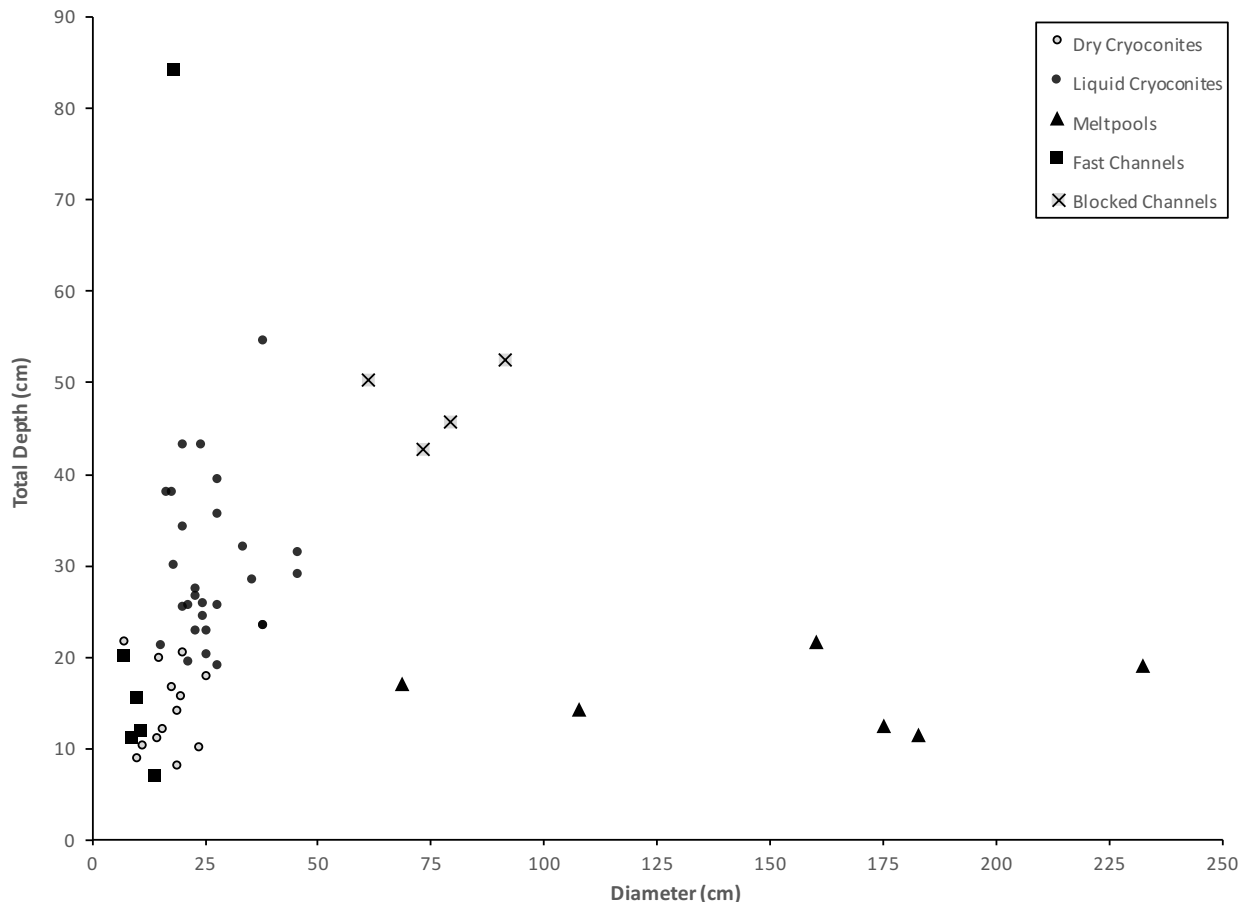


Figure 2.28- Total depth and diameter of cryoconites and melt pools sampled.

2.4h Diameter

Diameter was one of the most prominent characteristics distinguishing cryoconite holes and melt pools beyond their vertical profiles. Surface diameter was significantly smaller for cryoconite holes (26.8 ± 8.3 cm) than melt pools (154.4 ± 58.2 cm; $p = 0.0026$). No cryoconite holes had a diameter larger than 50 cm, while melt pools ranged from 69-232 cm. Patterns for surface diameter also emerged within cryoconites (Figure 2.29); dry holes had smaller diameters than those containing liquid (17 ± 5.2 cm \ll 26.8 ± 8.3 cm; $p = 0.00005$). There were no significant differences between open/lidded liquid holes, nor any differences in diameter between the six study glaciers.

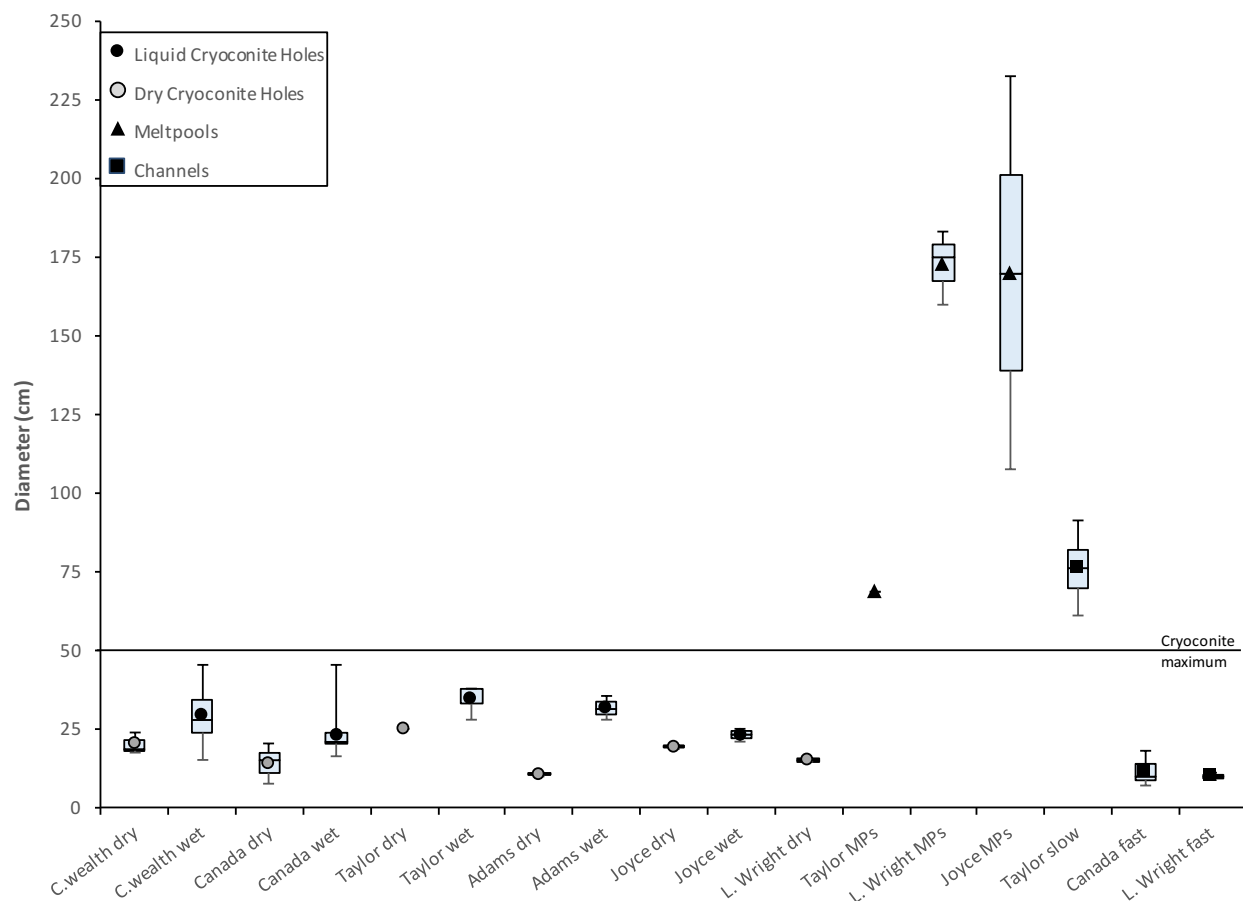


Figure 2.29- Diameter of cryoconite holes and meltpools sampled. Vertical bars span the minimum and maximum values in each category, enclosed columns represent the 1st and 3rd quartiles, and each mean is denoted by a central marker. Categories include both seasons of data. While not technically a diameter, the cross-sectional width of drainage channels was included in this graph for comparison. The flooded Joyce tunnel (diameter 5.64 m) is not included due to scale.

Since pool surfaces were not perfectly round, the diameter of each hole was measured from multiple cross-sectional distances in order to obtain a “general” (average) diameter in every sample. The variability shown in Figure 2.29 represents the distribution of each sample’s general diameter, and does not represent deviation *within* individual samples. Variance from the mean diameter of an individual sample is represented separately as diametric circularity (Figure 2.30 and Table 2.4).

2.4i Circularity

Diametric circularity was used in order to get a quantifiable value for the surface geometry of each pool, and was calculated by dividing the minor/major cross-sectional diameter of each sample. Since this yields a unitless value (in which 1= perfect circle) it can be compared equally across all melthole categories irrespective of the difference between relative cryoconite and meltpool size. (A 5x7cm oval hole has the same circularity as a 5x7 meter hole.) Since the method of reporting surface geometry varies between texts, eccentricity was also calculated for all samples and is included in the Supporting Data section of this chapter.

Cryoconite holes were significantly more circular than meltpools ($0.91 \pm 0.07 \gg 0.43 \pm 0.1$; $p = 3.5 \times 10^{-5}$). There were no statistical differences between open/lidded or dry/liquid cryoconite holes.

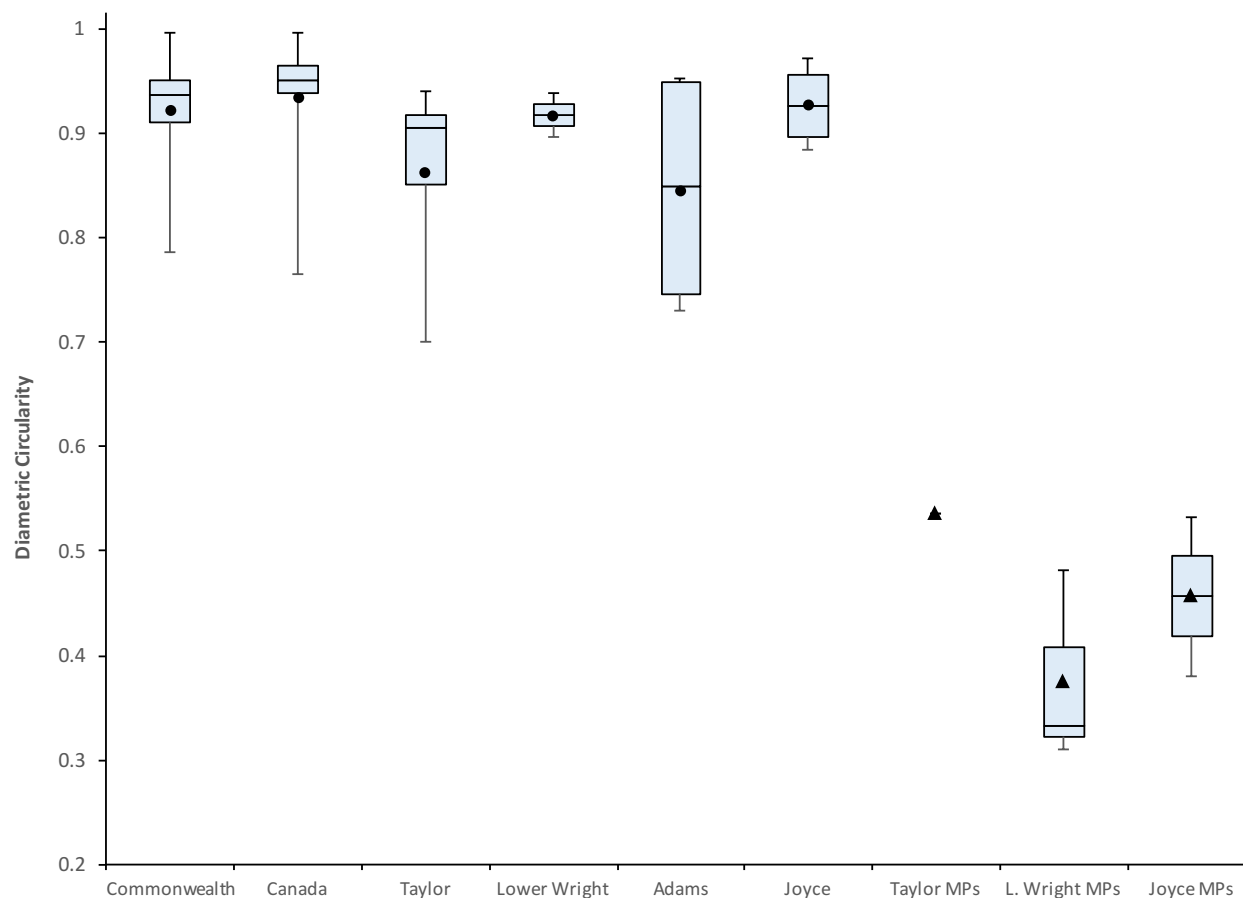


Figure 2.30- Diametric circularity of cryoconite holes and melt pools. Vertical bars span the minimum and maximum values in each category, enclosed columns represent the 1st and 3rd quartiles, and each mean is denoted by a central marker. Categories include both seasons of data.

As cryoconites widen, they begin to lose their circular shape (Figure 2.31). Samples in this study exhibited an exponential loss of circularity with increasing diameter ($R^2=0.86$). Elongation of the major axis is dependent on wind direction and glacial topography which determine the pattern of sediment deposition in each hole.

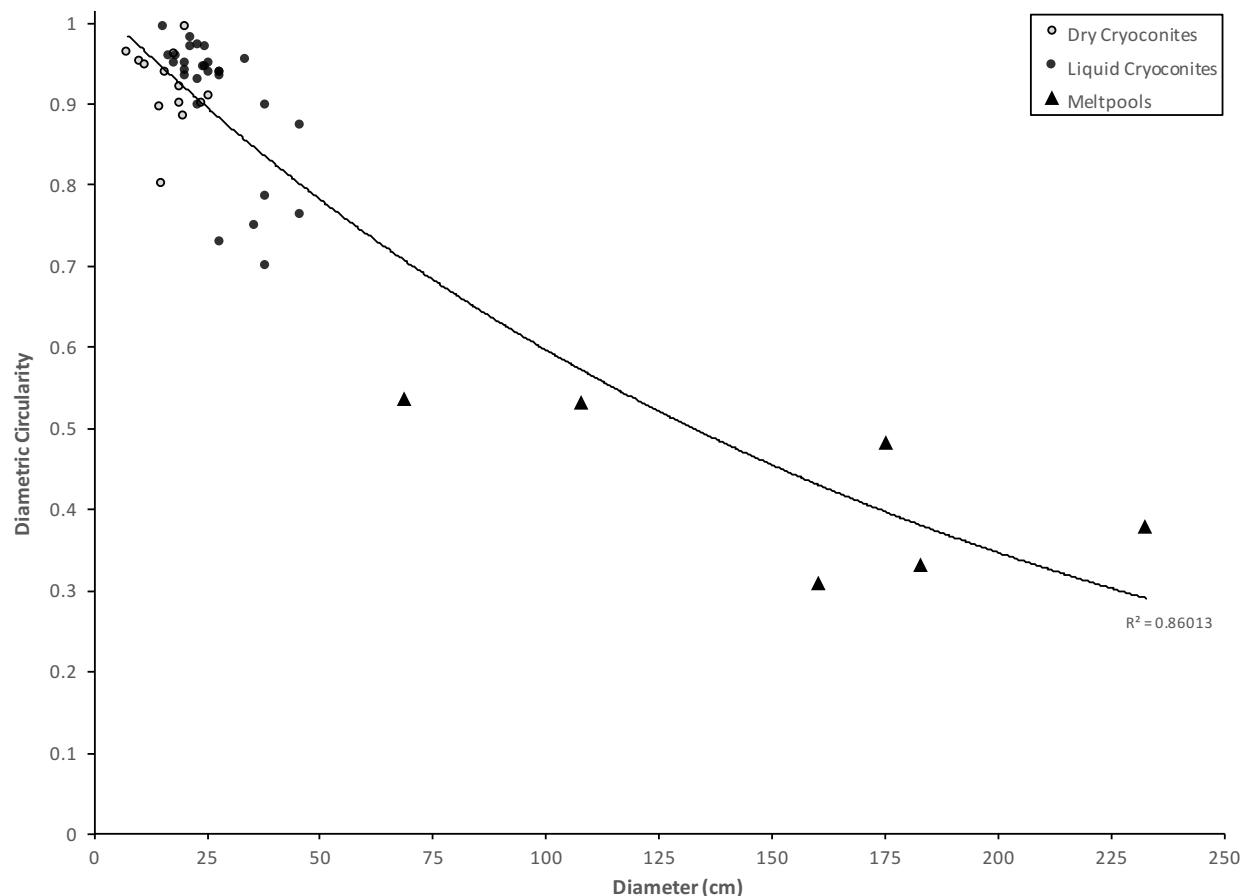


Figure 2.31- Diametric circularity and diameter of melt samples. Reported R^2 is an exponential fit.

2.4j Ice lid thickness

The thickness of a developing ice lid is determined both by the amount of energy absorbed in the bottom sediment and the stability of a convective gradient in the liquid layer above it. Lower insolation during prolonged cloudy weather has a greater impact on downward freezing than shifts in ambient air temperature. While the majority of ice lids resembled a flat disk (Figure 2.32), certain lids had a flat upper surface and an uneven bottom surface that was thicker towards the center of the hole (Figure 2.33). This was particularly evident in samples with a larger surface diameter and a layer of headspace between the lid and underlying meltwater. The pattern exhibited by these samples

suggests that a vapor pressure gradient may cause liquid in the column to accumulate as ice on the central underside of a lid.



Figure 2.32- A flat, disk-like lid on a cryoconite hole. *This portion of the ice lid from cryoconite hole C-07 on Commonwealth Glacier has a consistent thickness of 3.3 cm throughout the lid and was located immediately above the water column in the hole. (The lid is held upside-down to display a thin layer of wind-dispersed sediment encrusted on the lid surface towards the camera.)*



Figure 2.33- Thicker ice towards the center of a large cryoconite hole. *This is a $\frac{1}{4}$ section of the ice lid on cryoconite C-26 on Taylor Glacier. A red outline on the upper lid surface serves as a frame of reference for the cross-section of the lid. Lid thickness ranges from 1.2 cm around the perimeter up to 4.6cm towards the center of the hole (indicated by the medial arrow). A 2.6cm headspace separated the lid from the underlying water. This portion of the lid is 21 cm wide, and the total diameter of the hole is 38 cm.*

Unlidded water should generally serve as an indication of rapid melt-deepening since the generation of heat by cryoconite sediment exceeds longwave radiation loss to the surface. (Prolonged air temperatures $\geq 0^{\circ}\text{C}$ would also support the energy balance for an unlidded pool, but ambient air on the glacial surface rarely rises above freezing.) However, unlidded holes did not have a statistically different liquid- or total depth to lidded cryoconite holes in this study. The contribution of localized factors to individual melt rates and the variability of physical characteristics in multiannual holes contribute too many compounding factors for an accurate comparison in pre-existing cryoconite holes.

There was no significant difference in lid thickness between seasons, (1.5 ± 1.0 cm and 2.5 ± 2.7 cm, respectively) although lids from Season 2 exhibited a wider variety of thicknesses overall. Melpools and lidded cryoconite holes had similar lid thickness (3.7 ± 2.8 cm and 2.1 ± 2.2 cm, respectively). The static melt channels on Taylor Glacier did contain lids although thinner than those on cryoconite holes (1.7 ± 0.5 cm; $p = 0.037$). The velocity of draining water limits the development of frozen lids and none of the fast-moving channels produced overlying ice. Cryoconite holes were the only melt features capable of multiple lids.

Lidded holes comprised 57% of liquid cryoconite holes during Season 1, although the statistic increases to 86% if porous weathered lids are included. None of the lidded holes in Season 1 contained an overlying weathered lid, while four of the six open holes did. These weathered lids protect cryoconite liquid from some of the exposure to cold winds (although still enabling gas exchange) and help to explain the energy balance in these holes.

The presence of multiple lids was observed in cryoconite holes in this study, which has not been reported in previous literature. During Season 2, 86% of liquid cryoconite holes contained at least one lid (lowest lid thickness 2.5 ± 2.7 cm), 57% contained at least two lids (2nd lid thickness 3.6 ± 3.2 cm), and 29% contained three or more lids (3rd lid thickness 2.2 ± 2.5 cm). The oldest lid (farthest from the current liquid surface) was the thickest in all multi-lidded samples. This study proposes a pattern in which a singular, significantly thicker top lid in cryoconite holes represents the remnants of the re-frozen liquid column from the previous season. This will be referred to as the 'annual layer'. The absence of this layer could either indicate that the annual layer has fully ablated away, or that the cryoconite hole has developed within the current season. The presence of a thick

top layer is subsequently used as a frame of reference to identify patterns in each of the smaller underlying lids. The working hypothesis in this study is that each underlying lid indicates a freeze/thaw period in which decreased insolation initiated freezing of the liquid surface during cloudy weather. A subsequent increase in solar radiation in clear conditions could then reinitiate melt-deepening in the hole.

2.4k Cryoconite lid stratification as an indicator of seasonal melt patterns

Melting and refreezing events are influenced by a number of localized factors including sediment thickness, hole diameter, ice density, light scattering, and the uneven distribution of wind-dispersed snow. However, a few patterns in ice lid development and remelting were observed across different glaciers over the course of the summer. The data representing cryoconite holes sampled after melt initiation in Season 2 are isolated in Figure 2.34 in order to visually assess temporal patterns. Accompanying figures for shortwave radiation (Figure 2.35) identify prolonged periods of cloudy weather during the summer.

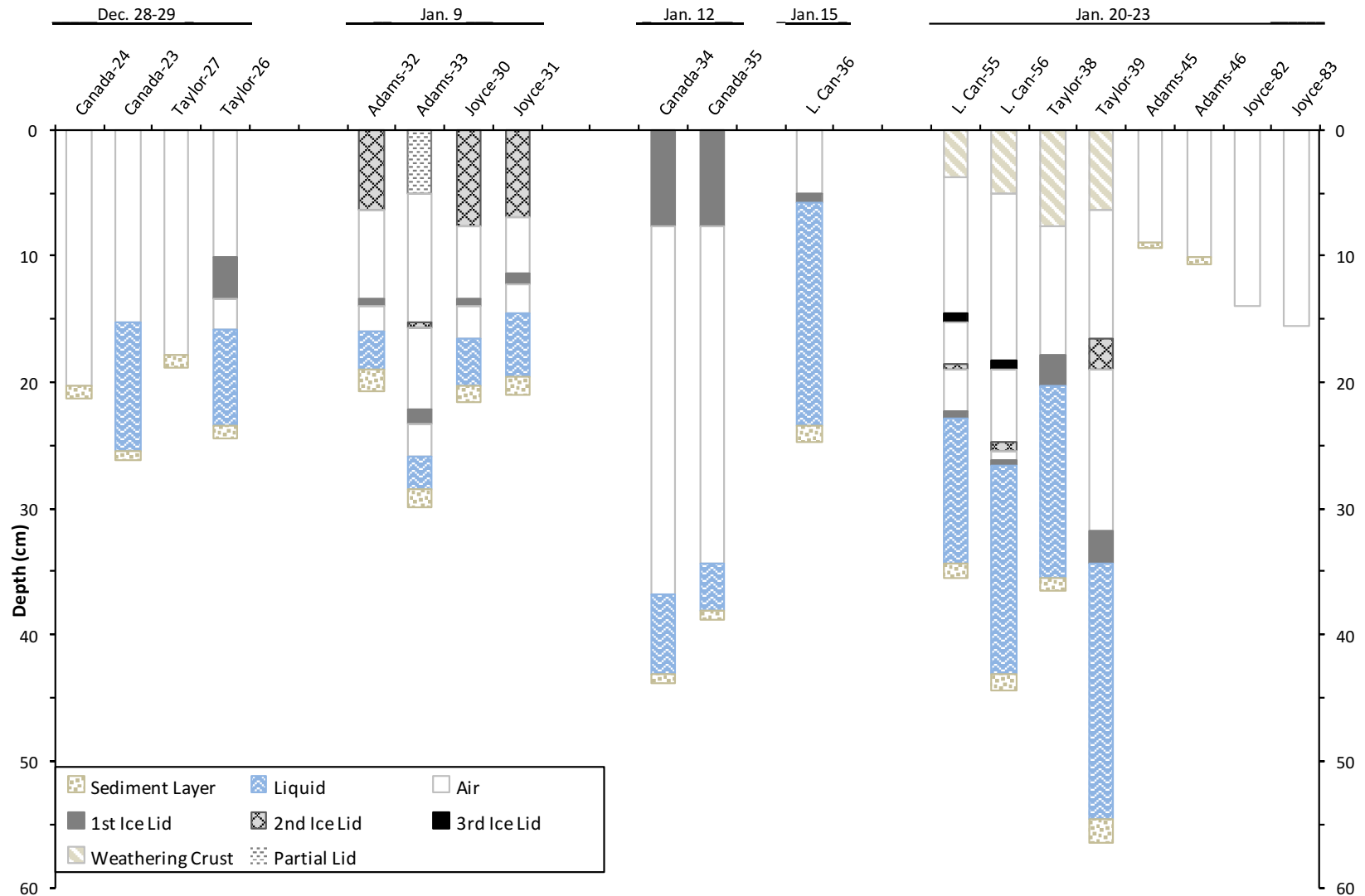


Figure 2.34- Vertical profiles of cryoconite holes from Season 2. Labels indicate the glacier and sample number (C-#) for each profile. Lower elevations of Canada Glacier are abbreviated as L.Can.

The presence of liquid in pre-existing frozen cryoconite holes became apparent across Commonwealth, Canada, and Taylor Glaciers over December 28-29. A proposed pattern of freeze/thaw events is discussed for samples collected after this date. The lack of annual layers on samples measured December 28-29 is due to biased sampling at the beginning of the season because liquid melt could not easily be observed or sampled beneath ~10 cm of ice. The majority of cryoconite holes observed during that time had ice lids >10 cm thick on the glacial surface. Thus the particular cryoconite holes that were measured in late December are not characteristic of the typical ice lid patterns on each glacier. The lack of thick ice lids on these samples is due to partial or full drainage of cryoconite meltwater during the previous year. Partial drainage of meltwater in a cryoconite hole would lead to a thinner liquid layer at the end of the season, and subsequently a thinner column of refrozen ice. Winter sublimation could remove the remnants of a thin annual layer and cause the lack of annual lids in those samples.

The >5 cm top ice lids on Adams, Joyce, and upper Canada Glacier are the remnants of annual layers. The thickness of an annual layer should continue to decrease over the season as the surface ablates away. By the end of the season ~January 21st, the annual lid has developed into a weathered crust on lower Canada and Taylor Glaciers, and has completely ablated from Adams and Joyce. No annual lid was present on Canada-36 because this cryoconite hole sample developed during the present season as discussed earlier.

Taylor Glacier was subjected to two refreezing periods during the summer; one on January 2-8th, and a second on January 12-16th, each indicated by a decreased period of insolation in Figure 2.35.

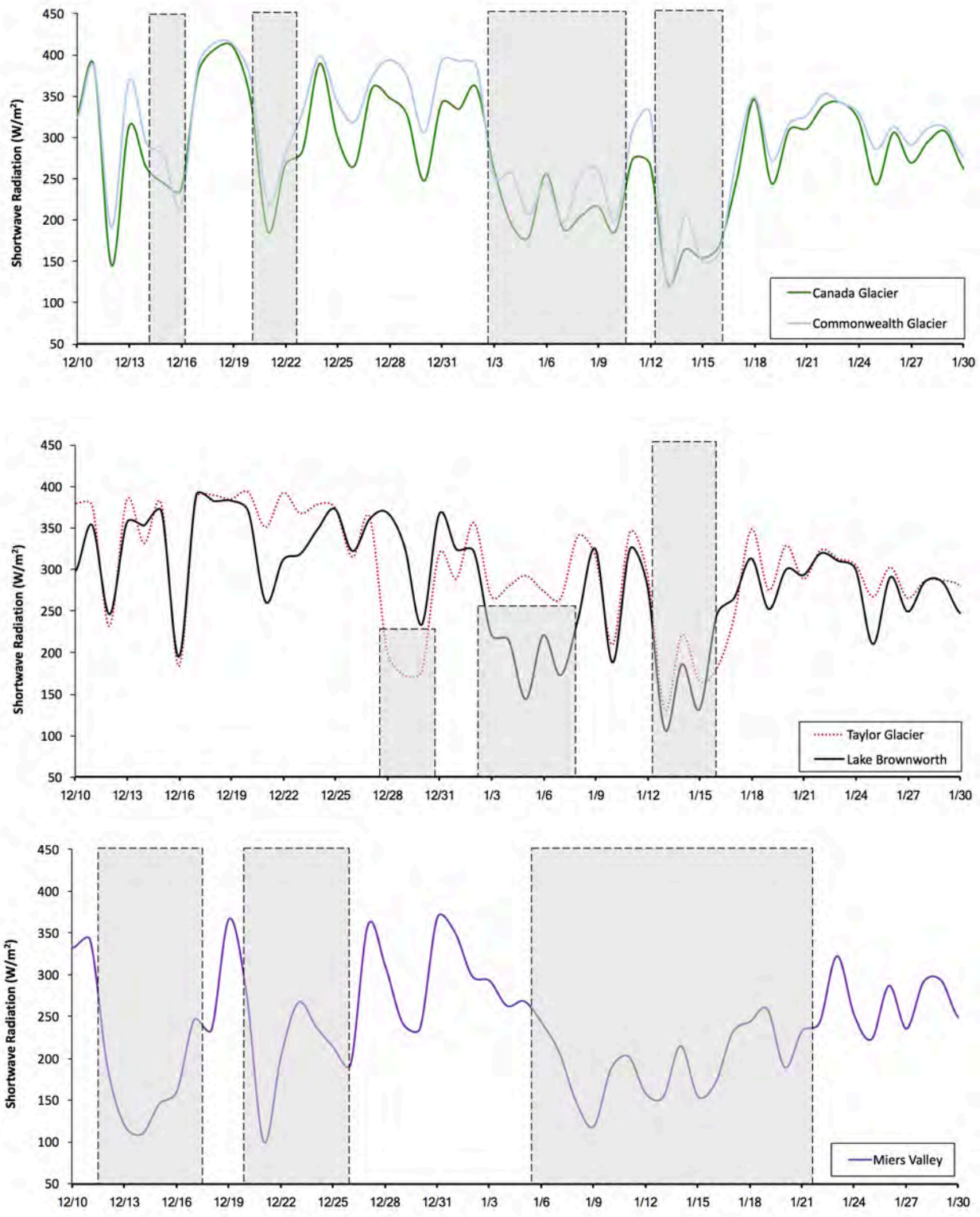


Figure 2.35- Average daily incoming shortwave radiation in summer 2014-15. Prolonged periods (>36hr) of decreased radiation relative to diurnal and seasonal trends are highlighted by grey bands. Glaciers were separated into 3 charts in order to isolate

specific patterns. Meteorological stations are maintained by the MCMLTER on the ablation surface of Canada, Commonwealth, and Taylor Glaciers. Wright LG is represented by a meteorological station situated directly below the glacier's terminus at Lake Brownworth. The Miers Valley meteorological station is located on the valley floor beneath the terminus of Adams Glacier and serves as a general indicator of trends affecting Adams and Joyce Glaciers.

The ice lid beneath the annual layer on Taylor-38 and -39 is due to the January 2-8th freezing event. Increased insolation from January 9-11th enabled melt-deepening in Taylor-39 until the second re-freezing event led to the formation of an additional lid in that sample. Similarity in the headspace layer of each sample indicates that the ice lid on Taylor-38 was formed during the first of the two refreezing events. No melt-deepening occurred after this date because the intermediate spike in insolation was not sufficient to melt the underlying ice in this sample.

The thin primary ice lid on samples from Adams and Joyce Glaciers is due to decreased solar radiation on December 30th. Melt-deepening occurred after this timeframe, but the lower overall insolation on these glaciers led to lower liquid levels in each sample. The sediment in Adams-33 received a higher level of radiation due to the partial opening in the sample's annual layer. This enabled further melt-deepening from January 1- 6th. An additional ice lid developed during cloudy conditions on January 6- 9th. At the time of sampling, the cryoconite hole was melt-deepening in accordance with the temporary increase in insolation from midday January 9- January 12th. Ablation was higher than melting rates on each glacier for the remainder of the season. High subsurface channelization drained the liquid content of most cryoconite holes, producing the dry, shallow columns observed at the end of the season.

Meltwater developed in Canada-34 and -35 until a significant refreezing period January 3-11th fractured each column due to expansion in the surrounding ice, and the majority of liquid drained from each hole. At the time of sampling, each sample was melt-deepening due to the increased radiation during January 10- 12th. Three freeze/thaw cycles on lower Canada Glacier produced ice lids during January 3- 10th, 13- 16th, and 19- 20th.

2.41 Variation in glacial melt features across sampled glaciers

The elevation of cryoconite holes and melt pools observed across the ablation zone of each glacier is displayed in Figure 2.36.

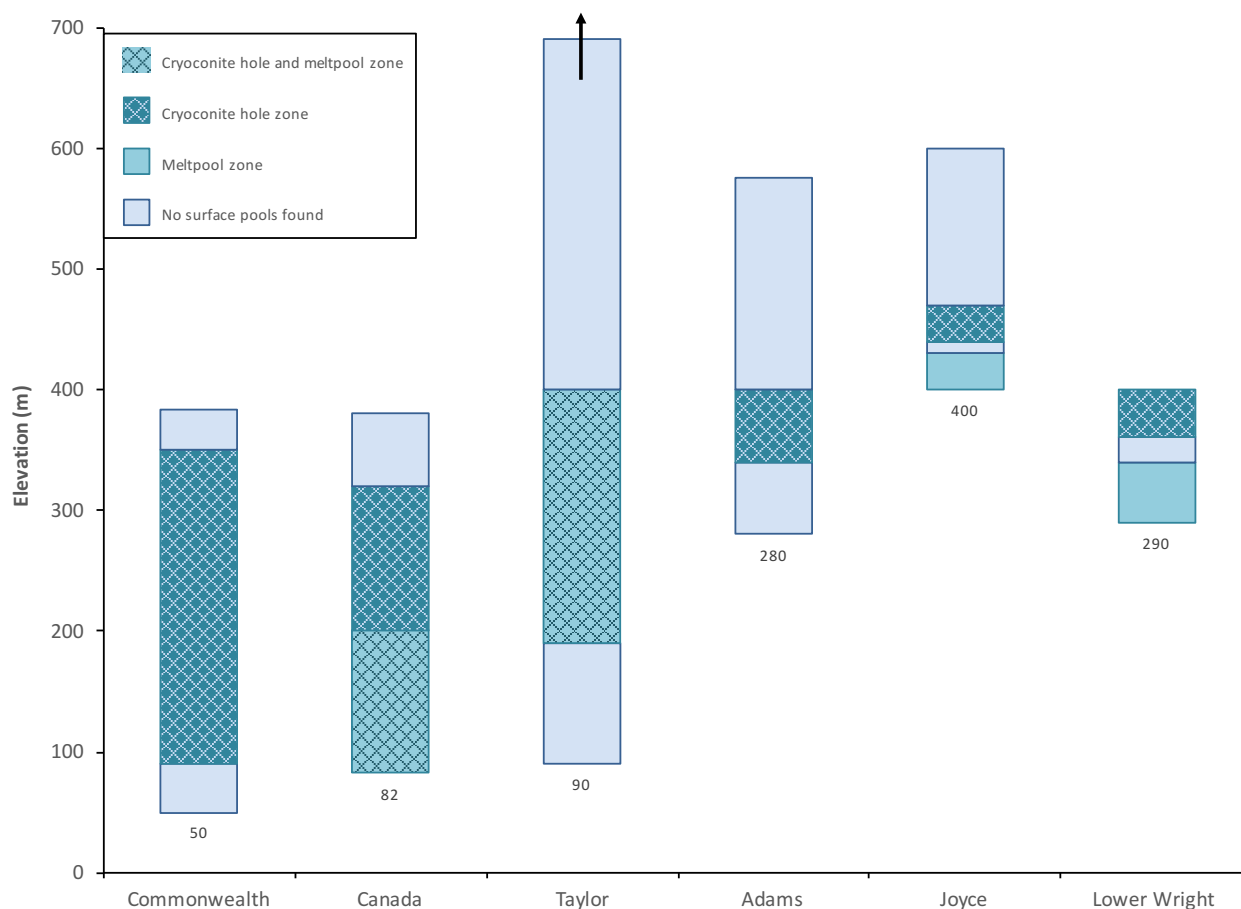


Figure 2.36- Distribution of melt features on the ablation zone of each glacier.

Adams, Joyce, and Wright Lower Glaciers were only sampled during Season 2; the other

glaciers include data from both seasons. The elevation band for each melt type includes observation as well as sampling locations. The ablation zone of Taylor Glacier extends beyond the scale of this graph to 2080m on the East Antarctic Ice Sheet, but all other glaciers are shown from their terminus (denoted with values below each bar) up to their estimated equilibrium line altitude.

The distribution of melthole features appears related to the surface topography and wind direction on each glacier. Liquid melt (in the form of cryoconites, melt pools, or channels) was found on all six study glaciers. However, no liquid could be found on Wright Upper Glacier on the inland side of Wright Valley, nor on higher transects of Taylor Glacier above ~450 m. These regions are both well within the ablation zone of their respective glaciers but consist of smooth surfaces subject to high velocity drainage winds, which may prevent sediment deposition long enough for melt to occur. These dry winds also promote sublimation rather than melting. The surface of Wright Upper Glacier (Figure 2.37) consisted of dense blue ice even at the terminal edge, indicative of high wind erosion of the less-dense white surface ice. In both regions the ablation zones are likely dominated by sublimation rather than the melting processes able to initiate cryoconite hole formation.

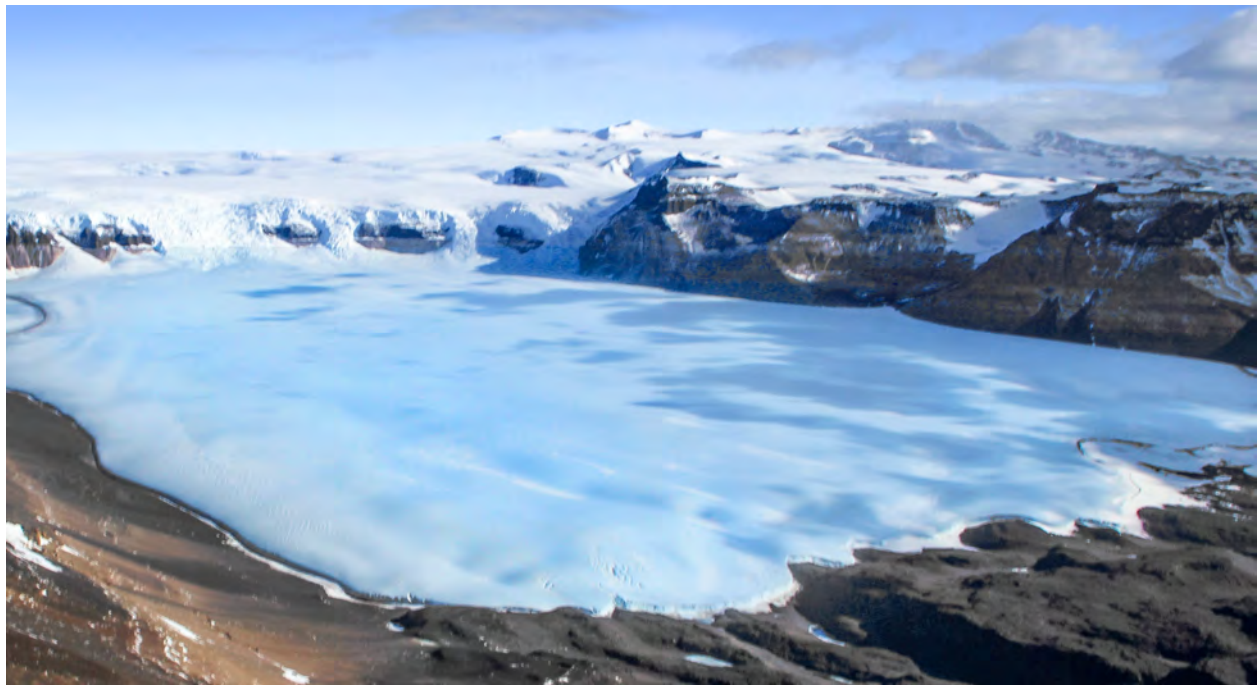


Figure 2.37- The ablation zone of Wright Upper Glacier.



Figure 2.38- Surface and sampling zones on Taylor Glacier. *Arrows indicate the general region for multiple sampling sites. Dense blue ice covers the surface at higher*

*elevations, while the lower terminus of the glacier is dominated by subsurface melt channels. Photo courtesy of NASA.*⁷⁰

Cryoconite holes were present on all six glaciers. Each glacier contained a smoother surface at higher elevations that defined an upper boundary for the sediment deposition necessary to initiate hole formation. The lower boundary for cryoconites was more complex and appears to be related to interaction with other topographic features. The fate of cryoconite holes appears to be influenced by surface topography, ice density, and slope, ultimately favoring the development of melt pools or subsurface channelization on each glacier. The 'scalloped' basins present on Canada Glacier (Figure 2.8) and vertical terracing on Wright LG and sections of Joyce Glacier (Figure 2.7) all promote high sediment deposition expediting cryoconite hole evolution into melt pools.

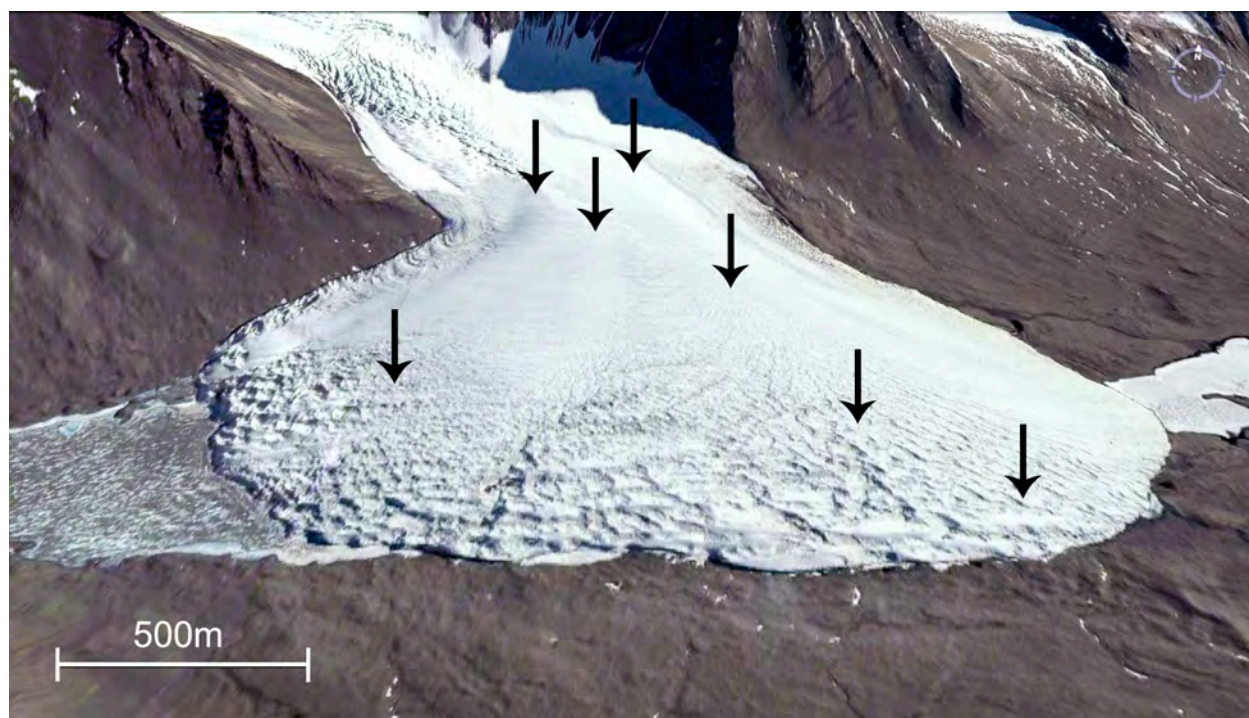


Figure 2.39- Surface and sampling zones on Canada Glacier. *Arrows indicate the general region for multiple sampling sites. Scalloped basins are visible at lower elevations. Satellite imagery from USGS.*³⁰

Comparatively, the relatively level topography and high degree channelization through lower elevations of Taylor (Figure 2.38), Commonwealth (Figure 2.40), and Adams (Figure 2.41) Glaciers may limit cryoconite hole development due to the shallow layer of subsurface drainage. Commonwealth also developed a notably deeper weathered crust than the other glaciers each year, which would also cause increased cryoconite hole drainage.



Figure 2.40- Surface and sampling zones on Commonwealth Glacier. *Arrows indicate the general region for multiple sampling sites. High channelization is visible. Satellite imagery from USGS.³⁰*

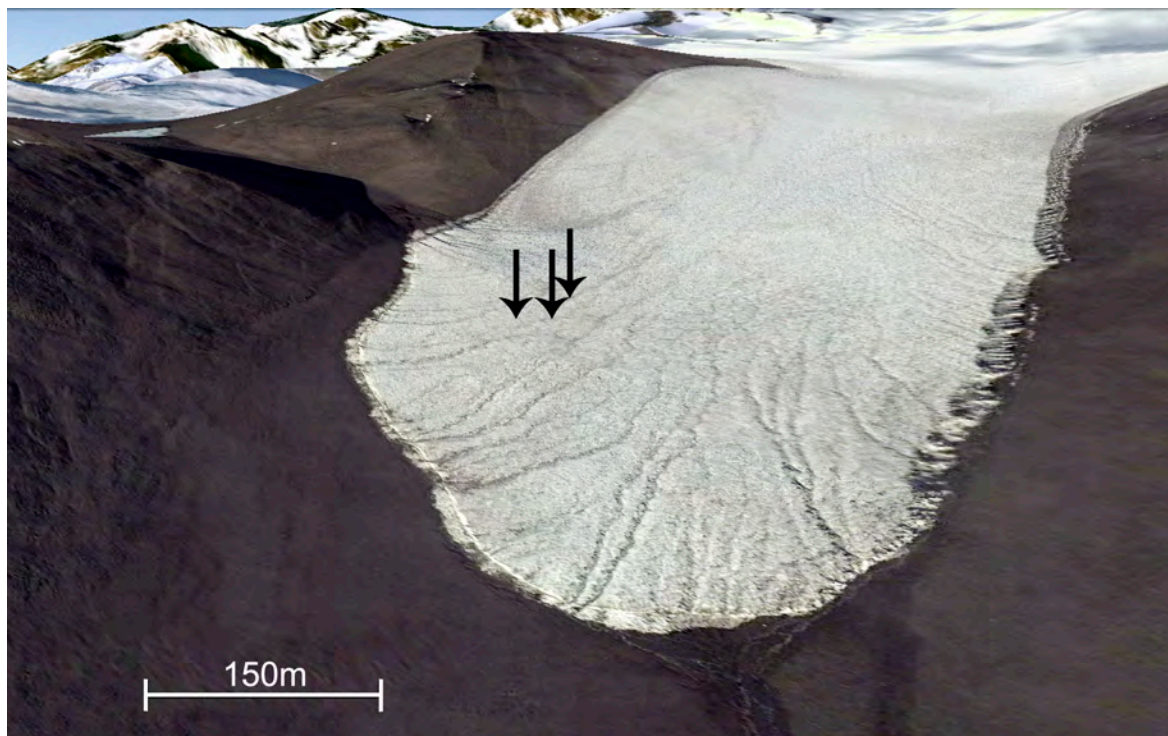


Figure 2.41- Surface and sampling zones on Adams Glacier. *Arrows indicate the general region for multiple sampling sites. The distribution of sampling sites on Adams was confined by an inability to find liquid cryoconite holes towards the highly channelized midline of the glacier. Satellite imagery from USGS.³⁰*

Seasonal refreezing of cryoconites towards austral fall occurred gradually along a spatial gradient towards the coast. Joyce and Adams Glaciers had the shortest melt seasons, followed by Taylor, Canada, Commonwealth, and Wright Glaciers. Liquid also persisted longer at lower elevations on each glacier.

2.5 Conclusions

The physical characteristics measured in this study describe patterns in cryoconite hole evolution into melt pools and ultimately cryolakes on glacial surfaces. The surface depression created by downward melt encourages further sediment deposition into each hole. This leads to a loss of circularity as the major axis of cryoconite holes lengthen

parallel to the predominant wind direction on each glacier. A sediment threshold of ~2.4 cm insulates the underlying ice from further melt-deepening and defines the boundary between cryoconite holes and static melt pools. Rather than cryoconite holes at an “equilibrium depth” relative to surface ablation, the vertical profiles in this study indicate that melt pools are the product of an absolute limit preventing *any* melt-deepening in the column. Continued ablation of the glacial surface will cause melt pools to become shallower over time.

Melting was limited beneath a liquid depth of ~25cm in this study but should not be interpreted as a fixed boundary across cryoconite holes in the Dry Valleys. The amount of incoming solar radiation received by cryoconite sediment decreases as the liquid layer deepens, but insolation is affected by multiple factors including the presence of ice lids and transmissivity of light through the glacial ice surrounding a cryoconite hole. Strong winds and $\leq 0^{\circ}\text{C}$ ambient air lead to the formation of ice lids on the liquid surface of melt holes. Lid thickness increases due to cloudy conditions, snow deposition, or lower irradiance towards the end of summer. This is the first known study to report the presence of multiple ice lids in cryoconite holes. The stratification of ice lids represents fluctuations between melt-deepening and re-freezing events throughout the summer season. These layers may be highly useful to indicate temporal variation in melt flow into ephemeral streams and lakes.

2.6 Supporting Data

2.6a Identification of “extreme subsurface crystal melt” on Joyce Glacier

One sampling site on Joyce Glacier (sample C-44) had an atypical profile including a large 5.6m diameter, 1.2m liquid depth, no underlying sediment, and column walls of extremely dense blue ice. There was no observed aeolian sediment in the column, but a very thin layer of fine, chalk-like material coated the bottom of the hole. The overall morphology suggests that the surface ice is not a ‘lid’ which froze over a liquid layer exposed to ambient air, but rather that a pocket of internal ice that melted without ever opening to the surface. This formation is similar to the description of “extreme cases of subsurface crystal melt” reported by R. Paige (1968)⁷¹, although this sample would be the largest such case ever reported. Subsurface crystal melt refers to the same internal melt process that creates ‘weathered’ surface ice, but “extreme” cases occur at a larger depth and across a much larger area in locations where distinct dark patches of blue ice are exposed on the glacier and absorb solar radiation. Within 20 meters of this site, and adjacent patch of blue ice had a similar ‘internal pocket’ formation, but in this latter case both sides of the pocket were exposed on the slope of the glacier, leading to a tunnel-like path through the ice (Figure 2.42).



Figure 2.42- Englacial tunnel in Joyce Glacier. This horizontal tunnel curves roughly 90° along a 17 meter path from entrance-exit in the side of Joyce Glacier.

The working hypothesis in this study is that the tunnel shown above was once a striated column of blue ice subject to extreme internal melt, which subsequently drained when ablation into the glacial slope exposed the sides of the pocket. Joyce sample C-44 is assumed to have developed from another striated layer of blue ice, in a segment that is still sealed by the surrounding glacial surface and maintains a large internal pool. The following assumptions and observations are relevant to this chapter-

1) Unlike cryoconite holes which form on the glacial surface and melt-deepen due to the low albedo of sediment, this formation is the result of an extreme case of penetrative solar radiation causing a maximum in the temperature profile at a depth beneath the glacial surface. Thus melt occurs from radiative heating of ice crystals, not conductive heat from sediment to ice.

2) While cryoconite holes may become isolated from atmospheric exchange after forming ice lids above the liquid column, the liquid in this column formed without any *initial* exposure to the atmosphere. Gas exchange with ambient air may not have occurred since snow/firn initially compacted the crystals into glacial ice.

3) The lack of sediment transport means it is highly unlikely for a thriving microbial community to exist within the hole.

The term “internal melt” has been used in literature to describe both the melt-deepening of cryoconite sediment beneath ice lids and the distinctly different process of internal melt of ice crystals without conductive heat transfer. The Joyce formation is therefore categorized as “englacial crystalline melt” in order to distinguish the difference in

this study. Characteristics of this sample are included in the 'Supporting Data' section of this chapter below.

2.6b Supporting data tables and figures

Table 2.3- Intraglacial averages of surface diameter

Glacier	Diameter (cm)					
	Dry cryo.	All liquid cryo.	Open liquid cryo.	Lidded liquid cryo.	Meltpools	Channel width
Commonwealth	20.3 ± 3.3 (3)	29.5 ± 9.5 (8)	28.2 ± 7.5 (2)	29.9 ± 10.7 (6)		
Canada	14.4 ± 6.4 (3)	23.1 ± 7.3 (13)	25 ± 9.6 (7)	20.9 ± 2.6 (6)		11.8 ± 5.6 (3 fast)
Taylor	25.4 (1)	34.7 ± 5.9 (3)		34.7 ± 5.9 (3)	68.6 (1)	76.2 ± 12.7 (4 slow)
Wright LG	15.3 ± 1.1 (2)				172.7 ± 11.6 (3)	10 ± 1.4 (2 fast)
Adams	10.8 ± 0.9 (2)	31.8 ± 5.4 (2)		31.8 ± 5.4 (2)		
Joyce	19.5 ± 0.7 (2)	23.3 ± 2.9 (2)		23.3 ± 2.9 (2)	170 ± 88.2 (2)	
All Glaciers	17 ± 5.2 (13)	26.8 ± 8.3 (28)	25.7 ± 8.9 (9)	27.3 ± 8.3 (19)	154.5 ± 58.2 (6)	40 ± 35.3 (9)
<i>(Joyce crystalline melt)</i>					(563.9) (1)	

Each reported average is followed by sampling size (*n*). While not technically a diameter, the cross-sectional width of meltwater drainage channels is included in this table for comparison.

Since pool surfaces were not perfectly round, the diameter of each hole was measured from multiple cross-sectional distances in order to obtain a “general” (average) diameter for every sample used in the table above. Thus the standard deviations listed here are based on deviation from the average “general diameter” in each category, and do not represent deviation *within* individual samples. Variance from the mean diameter of an individual sample is represented separately as diametric circularity (see Figure 2.30 and Table 2.4) and eccentricity (Table 2.5).

Table 2.4- Intraglacial averages of circularity

Glacier	Diametric Circularity				
	Dry cryo.	All Liquid cryo.	Open liquid cryo.	Lidded liquid cryo.	Meltpools
Commonwealth	0.93 ± 0.03 (3)	0.92 ± 0.06 (8)	0.94 ± 0.02 (2)	0.91 ± 0.07 (6)	
Canada	0.92 ± 0.1 (3)	0.94 ± 0.06 (13)	0.92 ± 0.07 (7)	0.96 ± 0.02 (6)	
Taylor	0.91 (1)	0.85 ± 0.13 (3)		0.85 ± 0.13 (3)	0.54 (1)
Wright LG	0.92 ± 0.03 (2)				0.38 ± 0.09 (3)
Adams	0.95 ± 0 (2)	0.74 ± 0.01 (2)		0.74 ± 0.01 (2)	
Joyce	0.89 ± 0.01 (2)	0.96 ± 0.01 (2)		0.96 ± 0.01 (2)	0.46 ± 0.11 (2)
All Glaciers	0.92 ± 0.05 (13)	0.91 ± 0.08 (28)	0.92 ± 0.06 (9)	0.9 ± 0.09 (19)	0.43 ± 0.1 (6)
<i>(Joyce crystalline melt)</i>					<i>(0.48)</i> (1)

Each reported average is followed by sampling size (n).

Circularity was used in order to get a quantifiable value of the surface geometry of each pool, and was calculated by dividing the minor/major cross-sectional diameter of a sample. Since this yields a unitless value (in which 1= perfect circle) it can be compared equally across all melthole categories irrespective of the difference between relative cryoconite and meltpool size. (A 5x7cm oval hole has the same circularity as a 5x7 meter hole.) This table reports the mean circularity for samples within a given glacier and melthole category. Cryoconite holes were significantly more circular than meltpools ($0.91 \pm 0.07 >> 0.43 \pm 0.1$; $p = 3.5 \times 10^{-5}$). There were no statistical differences between open/lidded or dry/liquid cryoconite holes.

Table 2.5- Intraglacial averages of eccentricity

Glacier	Eccentricity (ϵ)				
	Dry cryo.	All Liquid cryo.	Open liquid cryo.	Lidded liquid cryo.	Meltpools
Commonwealth	0.37 ± 0.08 (3)	0.36 ± 0.15 (8)	0.33 ± 0.05 (2)	0.37 ± 0.18 (6)	
Canada	0.32 ± 0.25 (3)	0.33 ± 0.11 (13)	0.37 ± 0.14 (7)	0.29 ± 0.07 (6)	
Taylor	0.42 (1)	0.5 ± 0.19 (3)		0.5 ± 0.19 (3)	0.84 (1)
Wright LG	0.4 ± 0.07 (2)				0.92 ± 0.04 (3)
Adams	0.31 ± 0.01 (2)	0.67 ± 0.02 (2)		0.67 ± 0.02 (2)	
Joyce	0.45 ± 0.02 (2)	0.28 ± 0.05 (2)		0.28 ± 0.05 (2)	0.89 ± 0.06 (2)
All Glaciers	0.37 ± 0.12 (13)	0.38 ± 0.16 (28)	0.36 ± 0.12 (9)	0.38 ± 0.17 (19)	0.9 ± 0.05 (6)
<i>(Joyce crystalline melt)</i>					<i>(0.88)</i> (1)

Each reported average is followed by sampling size (n). Eccentricity was calculated using the semi-major and semi-minor axis from the surface area of each hole.

Although both diametric circularity and eccentricity produce unitless values, the calculation for eccentricity includes a broader range of values from 0 (perfect circle) to ∞ for a straight line. Circular or oval shapes remain $0 \leq \epsilon \leq 1$, but small differences in the aspect ratio of a hole's surface will produce greater differences in eccentricity than diametric circularity. The method used to describe surface shape varies across literature, so both sets of data are included here for reference. Cryoconite holes were significantly less eccentric than meltpools ($0.37 \pm 0.15 \ll 0.9 \pm 0.05$; $p = 1.8 \times 10^{-14}$). There were no statistical differences between open/lidded or dry/liquid cryoconite holes.

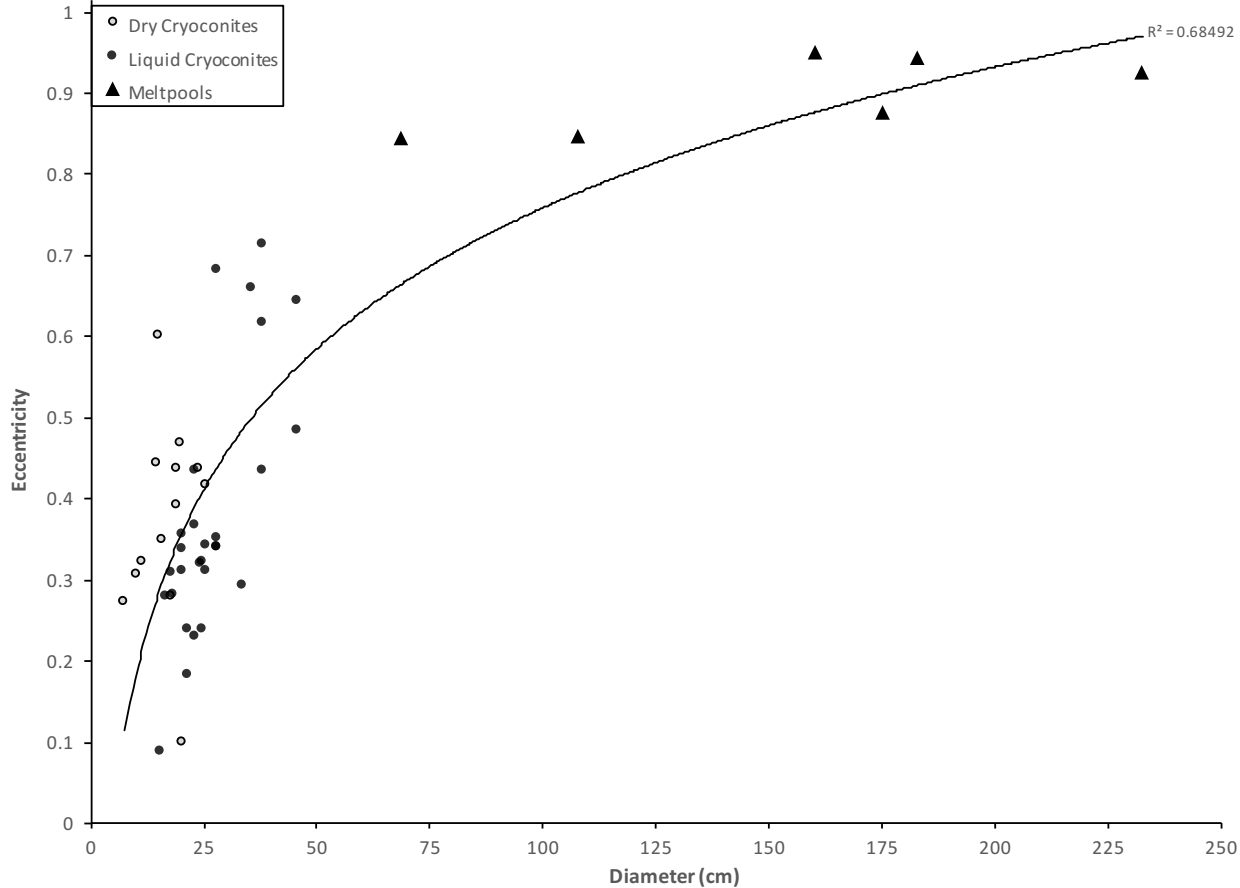


Figure 2.43- Eccentricity and diameter of melt samples. Reported R^2 is an exponential fit. The corresponding graph for diametric circularity is shown in Figure 2.31.

Diameter exhibited a higher R^2 correlation to diametric circularity than eccentricity. This is due to the range of values used in eccentricity calculations; small changes in diameter cause larger changes in eccentricity, and the scale for eccentricity extends beyond 1 for the inclusion of other shapes, such as parabolas, etc.

Table 2.6- Intraglacial averages of total depth

Glacier	Total Depth (cm)					
	Dry cryo.	All liquid cryo.	Open liquid cryo.	Lidded liquid cryo.	Meltpools	Channels
Commonwealth	11.5 ± 4.4 (3)	27.6 ± 6.1 (8)	27.4 ± 6.5 (2)	27.6 ± 6.7 (6)		
Canada	20.6 ± 0.9 (3)	31.5 ± 7 (13)	28.3 ± 4.9 (7)	35.3 ± 7.6 (6)		39.9 ± 38.3 (3 fast)
Taylor	17.8 (1)	37.9 ± 15.7 (3)		37.9 ± 15.7 (3)	17.1 (1)	47.8 ± 4.5 (4 slow)
Wright LG	11.5 ± 0.7 (2)				15.2 ± 5.6 (3)	11.4 ± 0.6 (2 fast)
Adams	9.5 ± 0.9 (2)	23.7 ± 6.6 (2)		23.7 ± 6.6 (2)		
Joyce	14.8 ± 1.1 (2)	19.9 ± 0.5 (2)		19.9 ± 0.5 (2)	16.6 ± 3.4 (2)	
All Glaciers <i>(Joyce crystalline melt)</i>	14.3 ± 4.6 (13)	29.7 ± 8.5 (28)	28.1 ± 4.9 (9)	30.4 ± 9.8 (19)	16 ± 4 (6) <i>(111.5) (1)</i>	37.1 ± 24.5 (9)

Each reported average is followed by sampling size (n). Values represent the total depth of a column from the surrounding glacial surface including all liquid, air pockets, ice lids, or weathered crusts within the column.

Table 2.7- Intraglacial averages of liquid depth

Glacier	Liquid Depth (cm)					
	Dry cryo.	All liquid cryo.	Open liquid cryo.	Lidded liquid cryo.	Meltpools	Channels
Commonwealth	0 ± 0 (3)	12.4 ± 6.5 (8)	5.8 ± 4.7 (2)	14.6 ± 5.6 (6)		
Canada	0 ± 0 (3)	11.7 ± 5 (13)	13.1 ± 4.5 (7)	10.1 ± 5.5 (6)		3.5 ± 1.6 (3 fast)
Taylor	0 (1)	14.4 ± 6.4 (3)		14.4 ± 6.4 (3)	15.2 (1)	27.2 ± 4.3 (4 slow)
Wright LG	0 ± 0 (2)				11.9 ± 1.9 (3)	1.6 ± 1.1 (2 fast)
Adams	0 ± 0 (2)	2.8 ± 0.4 (2)		2.8 ± 0.4 (2)		
Joyce	0 ± 0 (2)	4.4 ± 0.9 (2)		4.4 ± 0.9 (2)	11.4 ± 1.9 (2)	
All Glaciers	0 ± 0 (13)	11 ± 5.9 (28)	11.5 ± 5.3 (9)	10.8 ± 6.4 (19)	12.3 ± 2.1 (6)	13.6 ± 13.2 (9)
<i>(Joyce crystalline melt)</i>					<i>(101.3)</i> (1)	

Each reported average is followed by sampling size (n).

Table 2.8- Intraglacial averages of headspace

Glacier	Total Air Depth (cm)					
	Dry cryo.	All liquid cryo.	Open liquid cryo.	Lidded liquid cryo.	Meltpools	Channels
Commonwealth	11.5 ± 4.4 (3)	13.8 ± 5.4 (8)	20.8 ± 0.7 (2)	11.5 ± 3.8 (6)		
Canada	16.1 ± 3.9 (3)	16.9 ± 6.5 (13)	14.2 ± 4.6 (7)	20.1 ± 7.2 (6)		36.4 ± 39.7 (3 fast)
Taylor	17.8 (1)	15.2 ± 6.7 (3)		15.2 ± 6.7 (3)	0 (1)	7.4 ± 2.5 (4 slow)
Wright LG	11.5 ± 0.7 (2)				0 ± 0 (3)	9.8 ± 1.7 (2 fast)
Adams	9.5 ± 0.9 (2)	14 ± 7.1 (2)		14 ± 7.1 (2)		
Joyce	14.8 ± 1.1 (2)	7.6 ± 1.1 (2)		7.6 ± 1.1 (2)	0 ± 0 (2)	
All Glaciers	13.2 ± 3.7 (13)	15 ± 6.1 (28)	15.6 ± 5 (9)	14.7 ± 6.7 (19)	0 ± 0 (6)	17.6 ± 24.4 (9)
<i>(Joyce crystalline melt)</i>					<i>(0)</i> (1)	

Each reported average is followed by sampling size (*n*). These values represent the amount of total depth not filled by liquid, ice, or sediment.

Table 2.9- Intraglacial averages of sediment depth

Glacier	Sediment Depth (cm)					
	Dry cryo.	All liquid cryo.	Open liquid cryo.	Lidded liquid cryo.	Meltpools	Channels
Commonwealth	0.6 ± 1 (3)	0.9 ± 0.4 (8)	1.1 ± 0.8 (2)	0.8 ± 0.2 (6)		
Canada	0.8 ± 0.3 (3)	0.8 ± 0.3 (13)	0.9 ± 0.3 (7)	0.8 ± 0.3 (6)		0 ± 0 (3 fast)
Taylor	1 (1)	1.3 ± 0.5 (3)		1.3 ± 0.5 (3)	3.2 (1)	0.9 ± 0.1 (4 slow)
Wright LG	0 ± 0 (2)				6.3 ± 3.4 (3)	0.2 ± 0.2 (2 fast)
Adams	0.5 ± 0 (2)	1.5 ± 0.1 (2)		1.5 ± 0.1 (2)		
Joyce	0 ± 0 (2)	1.4 ± 0.2 (2)		1.4 ± 0.2 (2)	3.8 ± 0.6 (2)	
All Glaciers	0.5 ± 0.6 (13)	1 ± 0.4 (28)	0.9 ± 0.4 (9)	1 ± 0.4 (19)	5 ± 2.6 (6)	0.5 ± 0.5 (9)
<i>(Joyce crystalline melt)</i>					(0) (1)	

Each reported average is followed by sampling size (*n*).

Within the channel subcategory, only one fast channel had measurable sediment (0.3cm), leading to a skewed mean 0.06 ± 0.13 cm sediment depth. Slow-moving channels had an average sediment thickness of 0.94 ± 0.14 cm.

Table 2.10- Intraglacial averages of lid thickness

Glacier	Newest Ice Lid Thickness (cm)					
	Dry cryo.	All liquid cryo.	Open liquid cryo.	Lidded liquid cryo.	Meltpools	Channels
Commonwealth	0 ± 0 (3)	1.1 ± 1.2 (8)	0 (2)	1.5 ± 1.1 (6)		
Canada	2.4 ± 3.5 (3)	1.5 ± 2.8 (13)	0 (7)	3.1 ± 3.5 (6)		0 (3 fast)
Taylor	0 (1)	2.8 ± 0.4 (3)		2.8 ± 0.4 (3)	1.9 (1)	1.8 ± 0.5 (4 slow)
Wright LG	0 ± 0 (2)				3.3 ± 3.7 (3)	0 (2 fast)
Adams	0 ± 0 (2)	1 ± 0.4 (2)		1 ± 0.4 (2)		
Joyce	0 ± 0 (2)	0.6 ± 0.2 (2)		0.6 ± 0.2 (2)	5.3 ± 1.5 (2)	
All Glaciers	0.5 ± 1.8 (13)	1.4 ± 2 (28)	0 (9)	2.1 ± 2.2 (19)	3.7 ± 2.8 (6)	0.8 ± 1 (9)
<i>(Joyce crystalline melt)</i>					<i>(10.2)</i> (1)	

Each reported average is followed by sampling size (n). These values refer to the ice lid closest to the liquid surface.

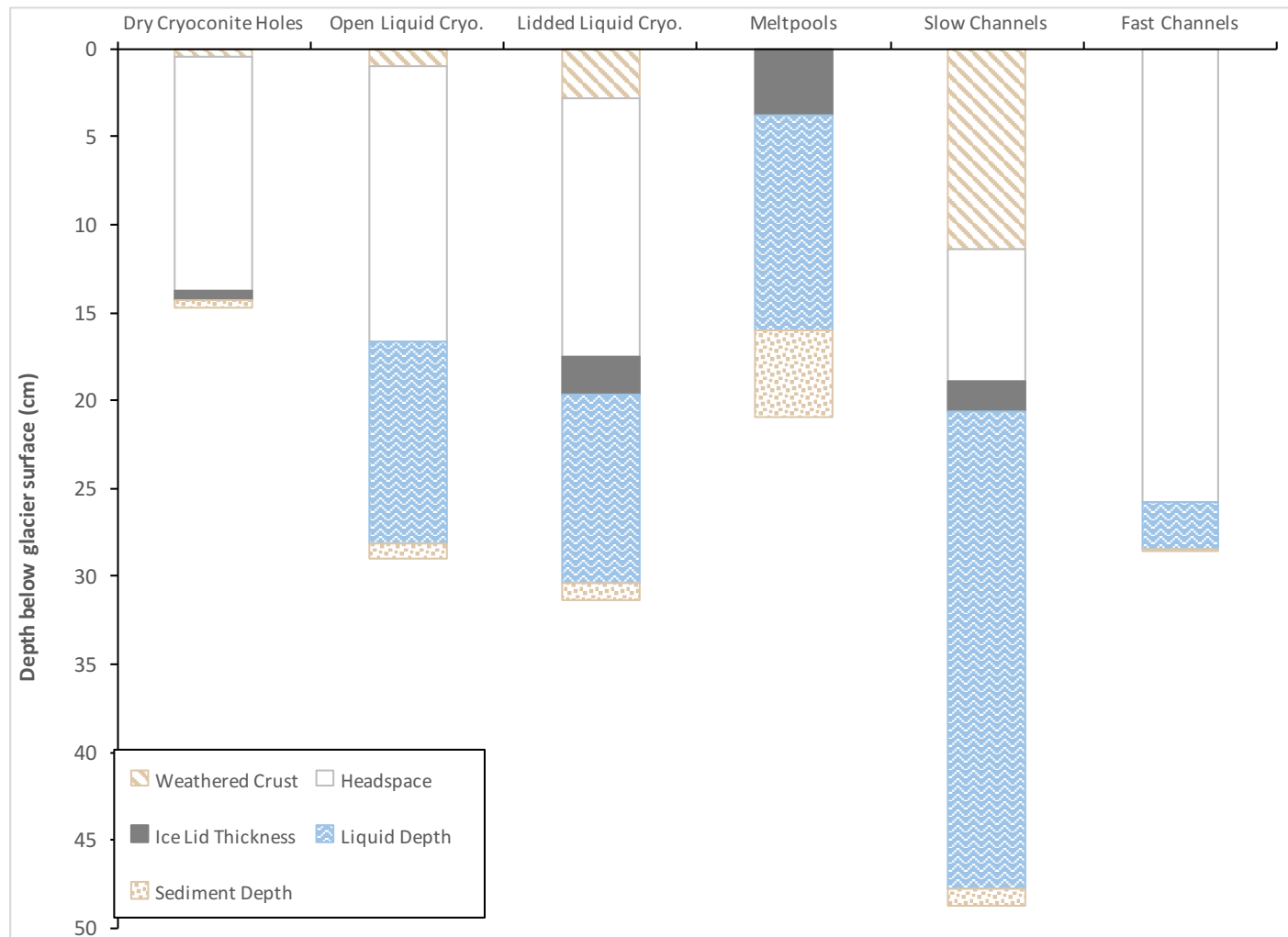


Figure 2.44- Vertical profile for the mean depth of features in each melthole type. *This data is a representative summary of vertical features using the average values in each melthole category. Sediment and liquid were always the lowest layers in each sample. However, this graph represents the absolute (total) values for ice lid and weathering crust thickness rather than their relative locations within the air space of a column due to the variability of stratification across multiple layers.*

Table 2.11- Intraglacial averages of elevation

Glacier	Elevation above sea level (m)					
	Dry cryo.	All liquid cryo.	Open liquid cryo.	Lidded liquid cryo.	Meltpools	Channels
Commonwealth	278.7 ± 11.7 (3)	204.6 ± 75.3 (8)	214.6 ± 109.5 (2)	201.3 ± 74 (6)		
Canada	277.7 ± 6.4 (3)	243.5 ± 86.8 (13)	262 ± 72 (7)	221.8 ± 103.9 (6)		139.6 ± 99.1 (3 fast)
Taylor	323 (1)	338.7 ± 13.7 (3)		338.7 ± 13.7 (3)	345.3 (1)	334.4 ± 8.9 (4 slow)
Wright LG	364 ± 1.4 (2)				319 ± 2.2 (3)	317.4 ± 3.2 (2 fast)
Adams	378.5 ± 0.7 (2)	375 ± 0 (2)		375 ± 0 (2)		
Joyce	463.3 ± 0 (2)	446.2 ± 3.9 (2)		446.2 ± 3.9 (2)	413.3 ± 15.5 (2)	
All Glaciers	338.7 ± 69.6 (13)	266.4 ± 100.3 (28)	251.5 ± 76.3 (9)	273.5 ± 111.1 (19)	354.8 ± 47 (6)	253.1 ± 113.5 (9)
<i>(Joyce crystalline melt)</i>					(410) (1)	

Each reported average is followed by sampling size (*n*).

Meltpools were not found on the surface of Commonwealth or Adams Glaciers. Cryoconites and meltpools overlapped on Taylor but were only found towards the sloped side perimeter where they were more protected from strong surface winds.

Chapter 3

Multi-annual Variability in Cryoconite Hole Distribution on Glaciers in Taylor Valley, Antarctica

3.1 Introduction

Cryoconite holes are columns of liquid melt beneath the surface of glaciers that can accumulate high nutrient and solute content over time. In the McMurdo Dry Valleys these holes can be isolated from hydrologic connectivity on a scale ranging from days to decades, and nearby holes have independent cycles of water storage and release.³⁴ The Dry Valleys are a polar desert in which glacial melt during a narrow 4-10 week melt season is the only significant source of water to ephemeral streams and ice-covered lakes.²⁸ Cryoconite meltwater was estimated to contribute roughly 13% of total runoff on Canada Glacier in 1995-1996³⁴, but this value is likely highly variable each year based on significant fluctuations in hydrologic connectivity and drainage. In this chapter, the spatial distribution of cryoconite holes was measured in transects of Commonwealth and Canada Glaciers in order to obtain an estimate of the glacial surface area populated by cryoconite holes and develop a sense of the scale for the impact these features may have on glacial hydrology. Transect lines were repeated in the same locations on each glacier during two consecutive summers in order to examine changes in the distribution and relative contribution of cryoconite holes to the surface area of these glaciers. A self-similarity matrix-based analysis of cryoconite hole distribution at precise locations between summers was used to estimate the number of cryoconite holes gained, lost, and present on

a multi-annual scale.

3.2 Methods

Sampling sites were established on the ablation zones of Commonwealth and Canada Glaciers; two alpine glaciers descending from mountains of the Asgard range on the northern side of Taylor Valley, Antarctica (Figure 3.1). A thorough description of the Dry Valleys region is available in Chapters 1 and 2.



Figure 3.1- Taylor Valley, Antarctica. Commonwealth (1) and Canada (2) are alpine glaciers on the northern side of Taylor Valley, Antarctica. The namesake Taylor Glacier (3) is an extension of the East Antarctic Ice Sheet, and the dry valley extends 36km east from Taylor Glacier to the coast of McMurdo Sound. Image rendered from multiple composites using USGS³⁰ source data.

Four sampling locations were determined on each glacier in January 2014. Three sites (CW-A, CW-B, and CW-C) on Commonwealth Glacier were located 5-10 meters downslope from a randomly chosen subset of mass-balance stakes installed throughout the ablation zone. The fourth site on Commonwealth (CW-D) was located 200 m upslope from a small meteorological tower. Locations on Canada Glacier were determined by a randomization function for both up/downslope and transverse direction 30-750m from a central reference site on the glacier.

A central post was installed at the determined location for each site and the coordinates were recorded with a Garmin GPS-map 76. A 3-meter rope was clipped to the post and used to determine the circumference and boundaries for a 28.3m² circular sampling area. A reference post was installed at the upslope edge of the sampling radius to indicate the starting point for a series of 1-meter radial transects conducted clockwise around the central post. This uses a modified approach of the method described by Fountain³⁴ for population sampling on glaciers and implements additional protocols to ensure multiannual reproducibility.



Figure 3.2- Ablation stake on Canada Glacier. *This bamboo post was drilled into the glacial surface and protrudes ~1m above the ice.*

Two weight-reinforced 3-meter measuring tapes were clipped to the central post and laid on the glacial surface; one oriented towards the reference post, and one positioned 1 m away from the reference post along the circumference of the sampling area. Consecutive transects were conducted by adjusting both tapes in 1-meter intervals around the central post until the circle was completed. Halfway through measurements an ice screw was drilled into the ice at the 3-meter circumference point for transect #09. Since the location of transect 0 is absolute with respect to the reference post, the ice screw on transect 9 provided a second form of orientation for data recorded the following year. Transects in 2015 were conducted around the central post from the reference post as described, and the distance between the radial edge of transect 9 and the ice screw was recorded.

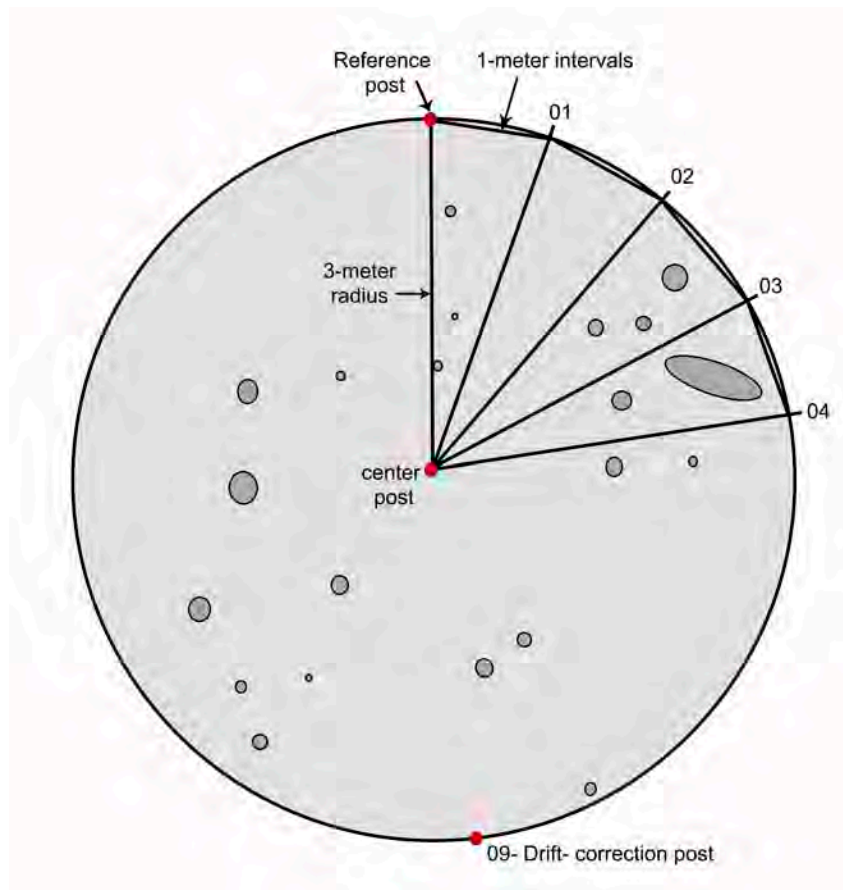


Figure 3.3- Circular transects for cryoconite hole distribution.

Following the measuring tape along the primary transect line (#03 in Figure 3.4), the distance from the center stake to the start (A) and end (B) of each cryoconite hole was recorded. If the cryoconite hole had a visibly eccentric shape, the distance along the transect line closest to the conical point of the hole (C) was also recorded. Using a handheld measuring tape, three additional distances were measured; the perpendicular distance from the transect line to the cryoconite hole (D), the major axis (E), and the minor axis (F). Additional notes characterized each hole as either hollow (dry), liquid-filled, or frozen. Liquid-filled pools were subcategorized as lidded or unlidded columns. Meltwater channels

and other glacial features were also noted. Each site was revisited in January 2015 and new spatial distribution data was recorded.

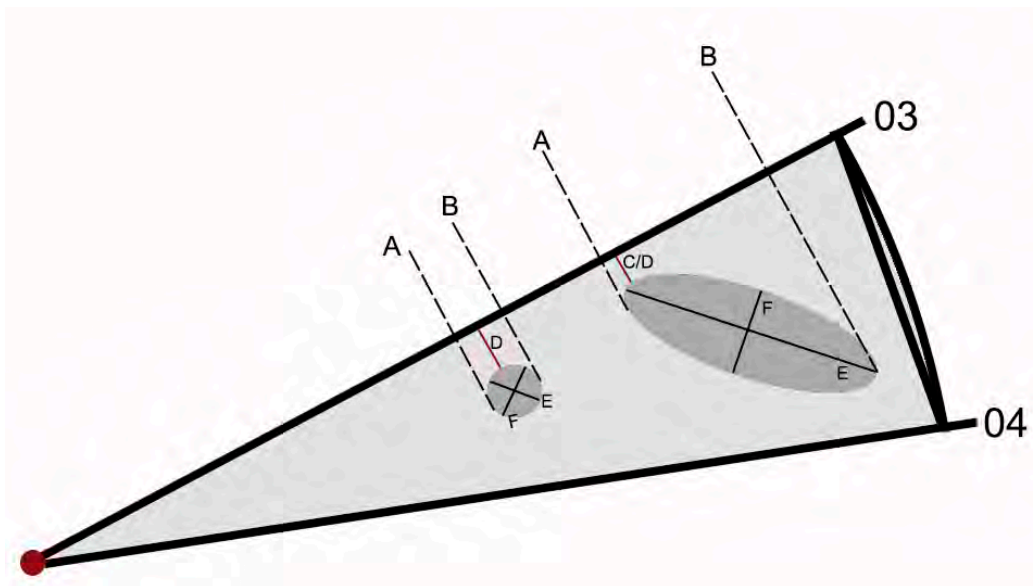


Figure 3.4- Measurements of cryoconite holes along a transect line. *The distance from the central stake to the beginning (A) and end (B) of each cryoconite hole was recorded. The measurement C (proximal conical edge for irregularly shaped holes) is a distance along transect line #03, while measurement D is the perpendicular distance from the transect line to the cryoconite hole. The major and minor axes are measured in E and F.*

The particular location for each sampling site was determined randomly across a large portion of the glacial ablation zone in 2014 in order to prevent sampling bias towards regions with a high number of cryoconite holes. No cryoconite holes were present in the location designated for site D on Commonwealth Glacier but the site was treated equally according to the methods discussed above. The central post and reference post were installed, and empty transect iterations were completed in order to determine the location of the drift-correction stake on transect 09. This ensured that all sites were subjected to the same conditions that may distort the distance between posts (due to internal deformation

of the ice) each year.

3.3 Results

3.3a Meteorological influences on sampling sites

The glacial surface coverage calculated in this study is shown in Table 3.1. These values are significantly lower than prior estimates from Fountain *et al.*³⁴ (4.5% on Canada; 4.8% on Commonwealth), Mueller *et al.*⁷² (3.5% coverage on Canada), and MacDonell & Fitzsimons⁷³ (3.5% on Wright Lower Glacier in the adjacent Wright Valley). However, all three of those studies were focused primarily on other data collection (both MacDonell and Mueller used sites where cryoconites with substantial water volumes could be extracted for other analyses) and the distribution of sampling in those studies may have been inherently skewed towards sites containing cryoconite holes. The 113 m² area covered on each glacier in this study cannot realistically be considered representative of the total ablation surface, but the inclusion of 'empty' transects helps to explain the difference between the values calculated here and those from prior studies. The main purpose of this study, compared to other estimates, was to examine the characteristics and continuity of cryoconite holes in the same location over two consecutive seasons.

Table 3.1- Distribution of cryoconite holes on study glaciers

	Canada 2014	Canada 2015	C.wealth 2014	C.wealth 2015
Holes per m ²	1.09	0.54	0.46	0.22
Mean diameter (cm)	12.39 ± 5.8	15.67 ± 6.03	14.39 ± 9.38	18.72 ± 11.26
Glacial surface coverage (%)	1.6	1.19	1.06	0.82
Total cryoconite holes (113 m ² area)	123	61	52	25
Dry holes	7.3%	4.9%	3.8%	100%
Full frozen columns	0%	75.4%	0%	0%
Wet holes	92.7%	14.8%	96.2%	0%
% of liquid holes with ice lids	53.5%	100%	34%	n/a

The proportion of cryoconite holes in different physical states (dry, liquid, and frozen) in Table 3.1 provides a greater context for the patterns observed in cryoconite distribution over both seasons. The austral summer 2013-14 was a relatively warmer, sunny season with high volumes of streamflow on the valley floor derived from glacial runoff. A significant number of long-duration cloudy periods during the following summer inhibiting meltwater production and produced far less glacial melt overall. The discharge from Canada and Commonwealth streams on the valley floor (each fed by their namesake glaciers) and differences in the shortwave radiation received by each glacier help to illustrate the influence of varying seasonal factors on the condition of the glacial surface each summer.

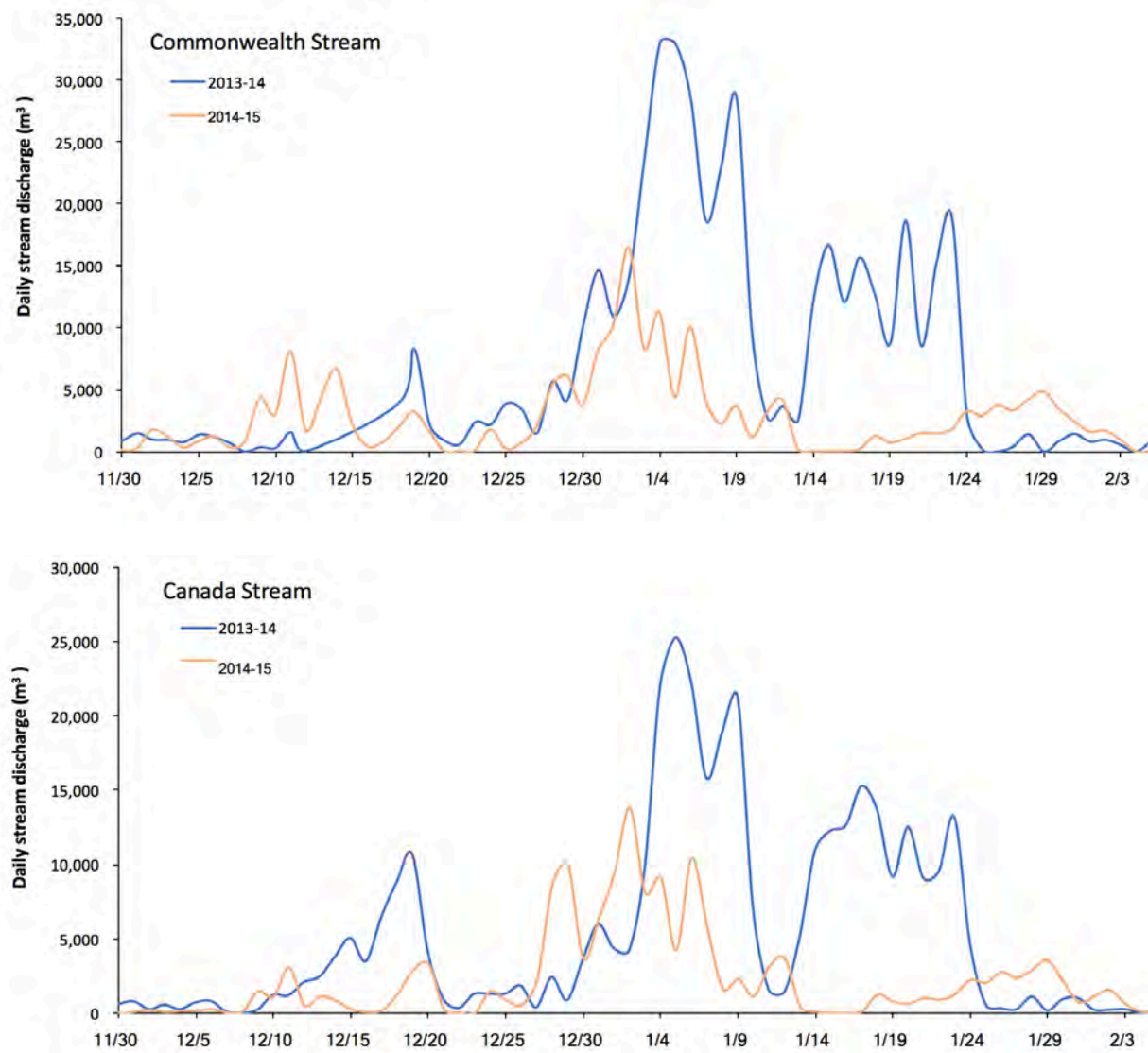


Figure 3.5- Stream discharge derived from glacial melt over two austral summers.

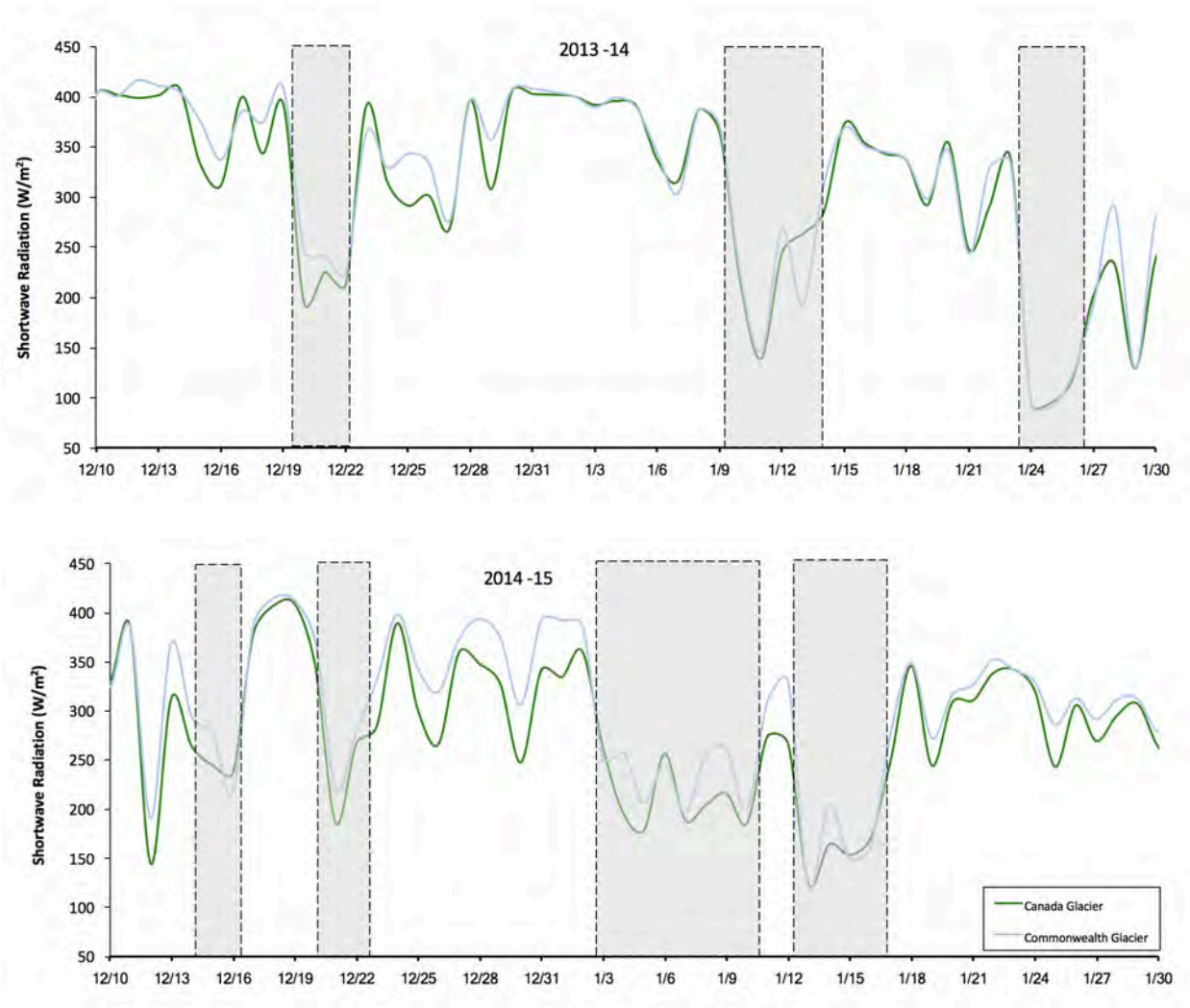


Figure 3.6- Daily average incoming shortwave radiation on glacier surfaces. Meteorological stations maintained by the MCMLTER on the ablation surface of both glaciers measure incoming shortwave radiation in 15-minute intervals. Data was converted into daily averages in order to dampen diurnal fluctuation and highlight prolonged periods (>36hrs) of decreased radiation relative to diurnal and seasonal trends.

While a short period of snowfall on January 11th temporarily decreased melt production on both glaciers in 2014, the snow ablated from the glacial surface and melting resumed at high flow rates towards the end of January. In 2015, the prolonged cloudy

conditions after January 3rd had a significant impact decreasing glacial melt and stream discharge for the remainder of the summer.

Internal melt in cryoconite holes is primarily driven by solar radiation. Melt on the glacial surface is inhibited by a mean summer air temperature below freezing (apprx. -4°C) and perpetual winds averaging $\sim 4\text{m/s}$. Glacial surfaces are colder than the overlying ambient air due to latent heat loss at the ice surface. However, a short period of above-freezing air temperatures (up to 2.2°C) occurred in early January 2014 on Canada Glacier. This helps to explain the presence of the dry surface-melt channels observed on transects of Canada Glacier, which were measured two weeks after the temperature peak. Air temperature $\geq 0^{\circ}\text{C}$ can also support the energy balance for unlidded cryoconite holes, which accounted for 46% and 66% of liquid cryoconite holes on Canada and Commonwealth during the 2014 sampling period.

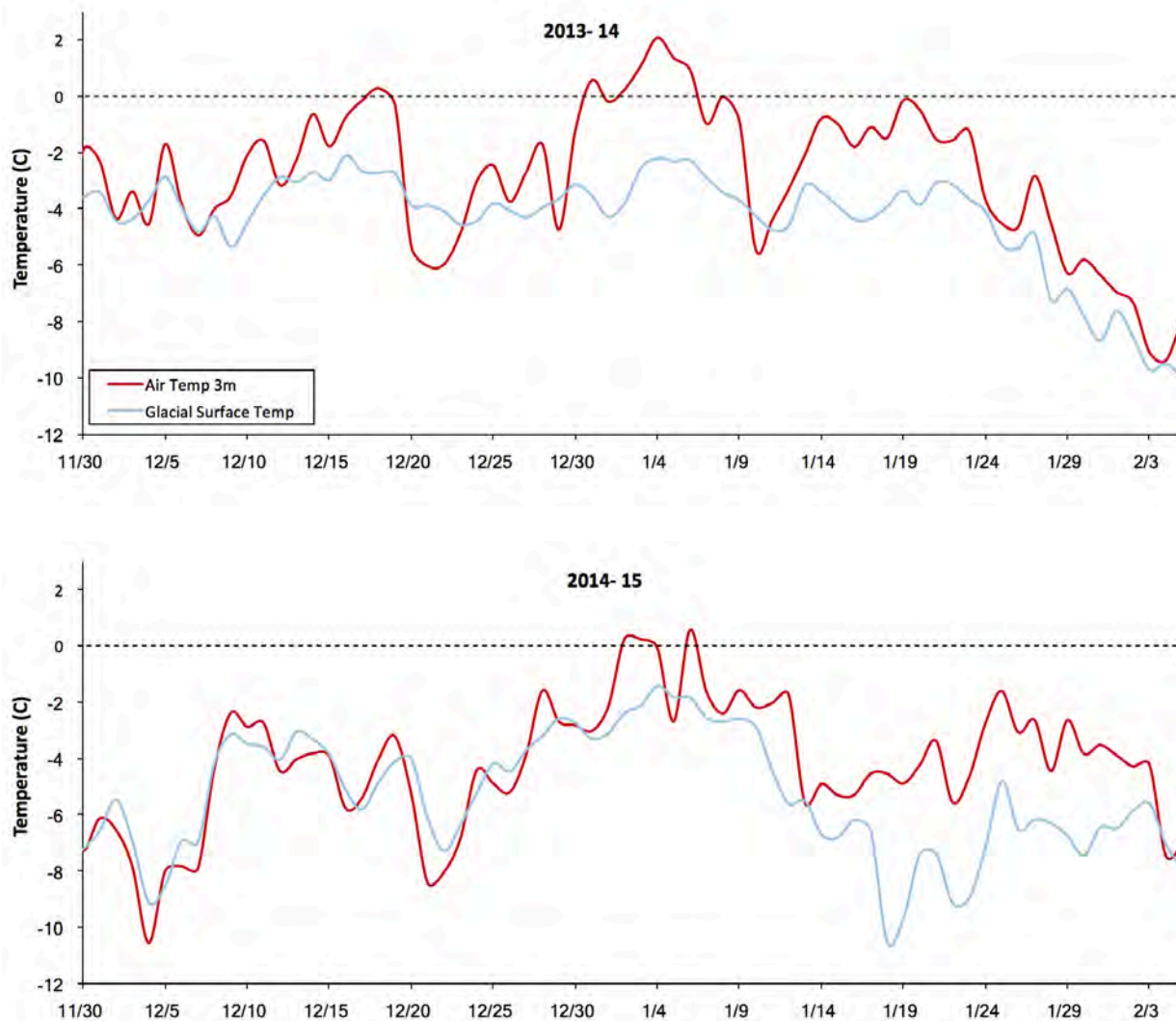


Figure 3.7- Canada Glacier surface temperature. A meteorological station on the ablation zone of Canada Glacier measured the temperature of the ice surface and the ambient air 3 m above the ice.

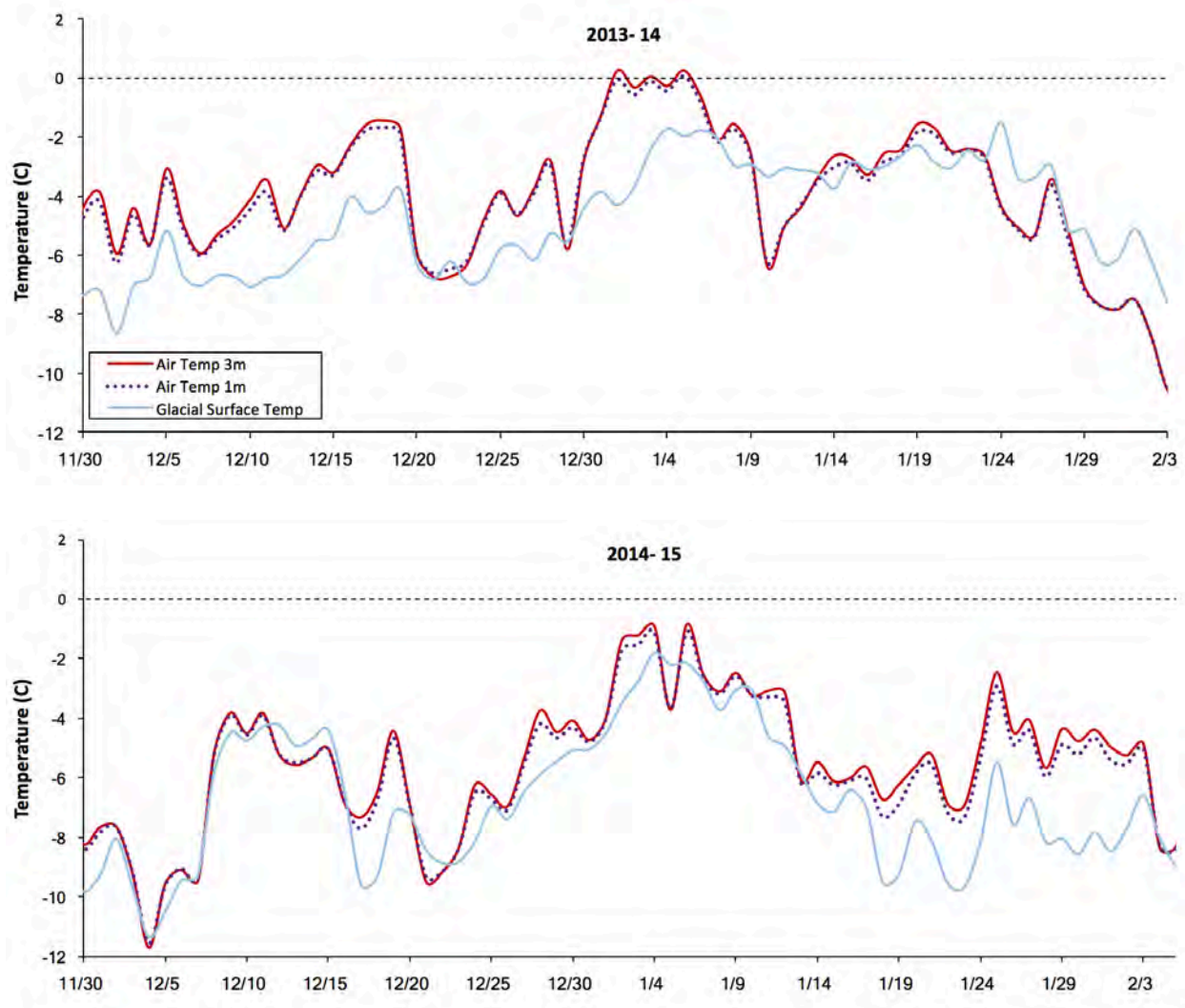


Figure 3.8- Commonwealth Glacier surface temperature. A meteorological station on the ablation zone of Commonwealth Glacier measured the temperature of the surface ice as well as ambient air 1- and 3-meters above the ice surface.

Commonwealth contained a higher number of unlidged holes despite lower ambient air temperature (-2°C). The formation of ice lids is dependent in a number of factors including surface wind, radiation received by cryoconite sediment, and the conductive heat gradient in the liquid column. A large number of the open cryoconite holes on Commonwealth were small and appeared to be immature holes melt-deepening into the ice. New cryoconite holes can form at any time during the summer when sediment absorbs

enough heat to melt the underlying ice but the sudden development of so many new cryoconite holes at the same time late in the summer season is unlikely to be coincidental. The surface ice on Commonwealth was already extremely weathered with a low-porosity surface crust and high flow in subsurface channels by the time spatial transects were conducted on January 20th. Cryoconite holes would have had adequate time to develop before this point. Freshly trapped aggregates of sediment in the otherwise porous surface ice indicate that a recent sediment deposition event brought new cryoconite material onto the surface and served as the basis for these developing holes. Simultaneous deposition across multiple transects of the glacier could be due to cross-valley winds, but no significant wind events were recorded during that time. Ice temperature data suggest that higher elevations of Commonwealth's ablation zone were insulated by snow from January 9- 19th. When the ice surface cleared on January 19/20, remobilization of sediment trapped under, carried within, and agitated by wind-blown snow may have led to sediment deposition onto lower elevations of the glacier.

Late-season cryoconite formation has significant implications on the overall longevity of the holes. If a cryoconite hole is isolated from subsurface drainage, the multiannual longevity of the hole is dependent on the ability to reach a late-summer depth beneath the level that winter sublimation will strip the ice. The ice surface on Commonwealth Glacier was extremely porous due to internal melt 'weathering', and was significantly more weathered than the ice on Canada Glacier. The 'mature' cryoconite holes on Commonwealth had thusfar managed to maintain an equilibrium depth below the increasing depth of the weathered crust. In these conditions newly developing cryoconite holes have a high risk of either melt-deepening into the existing subsurface drainage

network, or not melting down enough (due to decreasing insolation) before freezing and sublimating over the winter.

3.3b Variations in diameter across glaciers and physical states

The mean diameter of cryoconite holes in four different physical states (frozen, hollow, liquid-open, or liquid-lidded) is shown in Table 3.2. Lidded cryoconite holes were significantly larger than open holes on both Canada and Commonwealth Glacier in 2014 ($p < 0.03$). On Commonwealth this is partly due to the large number of small, melt-deepening holes discussed in the previous section. Changes in the proportion of cryoconite holes in each physical state between seasons indicates a shift in the energy balance of these holes. No fully-frozen columns were found on sites in 2014, while no unlidded liquid pools were present in 2015. The vast majority of cryoconite holes on Canada Glacier were fully frozen during sampling in 2015. Canada Glacier was visited multiple times in 2015 for other experiments, but the seasonal timing for transect sampling was kept relatively consistent in order to more accurately represent a 1-year sampling duration. Liquid cryoconite holes were present across broad areas of Canada Glacier until approximately January 4-5. Prolonged cloudy weather (Figure 3.6) and two large snowfall events on January 5 and 10 froze the glacier surface and no melt was observed on upper regions of the ablation zone after transect sampling was conducted on January 18th.

Commonwealth Glacier exhibited drastically different conditions than other glaciers in the Dry Valleys in 2015. The glacier was first visited early that summer on December 29 (2014) at the beginning of the melt season. The surface ice was already extremely weathered and consisted of a brittle series of porous sheets. Only one liquid cryoconite

hole could be found during a 2.5hr exploration of the glacier, and the vast majority of cryoconite columns were hollow rather than frozen. Since cryoconite internal melt had only just begun in Taylor Valley, the ubiquitous distribution of hollow columns suggests that the holes drained in their liquid state at the end of the previous summer. Surface ice is generally extremely dense at the beginning of each summer due to sublimation of the previous 'weathered crust'. The glacial surface remained highly porous throughout the season and no liquid cryoconite holes could be found during transect sampling on January 20 2015. Observations and meteorological data indicate that the near-surface layer of Commonwealth Glacier may have experienced a "stripping" event in late January 2014, in which a large volume of near-surface drainage perforated the upper 30cm of the glacier and all isolated pools were flushed from the glacier. Stripping events were described by Foreman⁷⁴ and Fountain³⁴ during a high-flow melt year in 2001-2. If the deepening weathered crust observed in 2014 was able to penetrate down to existing near-surface drainage channels, the combined depth of both layers could be enough to withstand winter sublimation and present a low-density ice surface early the following summer.

The residual ice on Commonwealth was not conducive to new cryoconite hole formation because there was not a dense enough ice layer for sediment to melt-deepen without immediately draining. All cryoconite holes found in the 4 Commonwealth study sites were hollow in 2015. Ablation should have continued to strip the low-density layer throughout the season and over the following winter. By the following spring in 2016, the underlying surface should have been dense enough to support new cryoconite hole development. This would serve as an excellent study scenario if the vast majority of all cryoconite holes could be identified as new holes. Field sampling during the 2015-16

austral summer was beyond the scope of this research but hopefully this scenario will be examined by future scientists deployed to the Dry Valleys.

Table 3.2- Diameter of cryoconite holes in each physical state on sampling sites

	Canada 2014		Canada 2015		Commonwealth 2014		Commonwealth 2015	
	% n	Diameter	%n	Diameter	%n	Diameter	%n	Diameter
Cryoconites (n)	123	12.39 ± 5.8	61	15.67 ± 6.03	58	14.39 ± 9.38	25	18.72 ± 11.26
Dry holes	7.3%	8.67 ± 2.18	4.9%	12.67 ± 6.66	3.4%	19 ± 2.12	100%	18.72 ± 11.26
Ice columns	0	-	78.7%	14.54 ± 5.29	0	-	0	-
Open liquid holes	49.6%	11.06 ± 5.38	0	-	67.2%	10.5 ± 8.05	0	-
Lidded liquid holes	43.1%	13.87 ± 6.51	16.4%	22 ± 5.68	29.3%	17.71 ± 12.36	0	-

%n refers to the proportion of cryoconite holes in each glacier/season that are present in a given physical state. Enclosed squares denote diameters that are significantly different within a given column. (In Canada 2014, all three enclosed values are significantly different from each other.)

The increase in mean diameter on both glaciers from 2014 to 2015 is somewhat misleading. The change is not due to an overall increase in the diameter of holes but rather a skew in the original distribution due to a loss of smaller holes on each glacier. (Spatial determination of individual cryoconite holes gained/ lost will be discussed later in this chapter.) Shifts in the distribution of cryoconite hole diameters is shown in Figure 3.9.

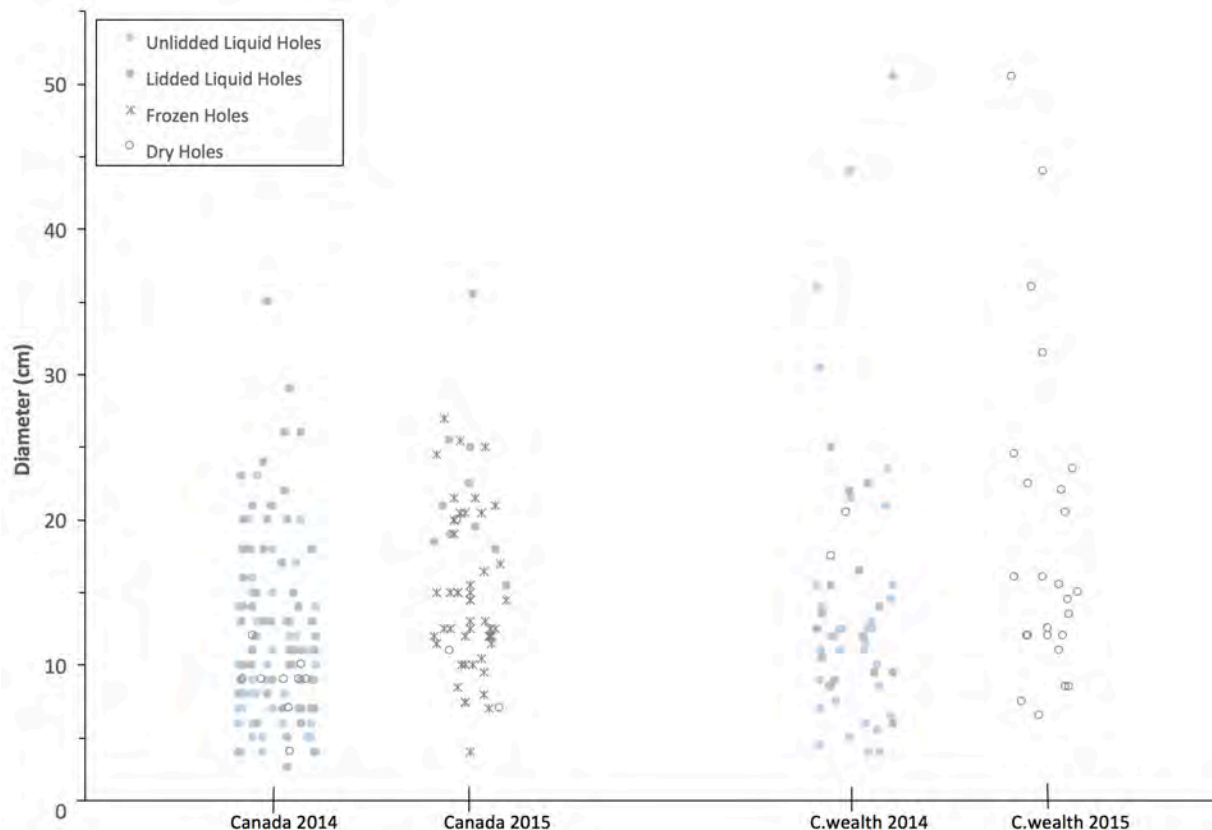


Figure 3.9- Diameter of cryoconite holes measured. *Slight variation along the x-axis within each glacial season is arbitrary in order to enhance visibility; each column represents the total sum of cryoconite holes measured on that glacier/year. Data points indicate the physical state and diameter of each individual cryoconite hole measured.*

These changes led to a significant difference in the total mean diameter of cryoconite holes measured on Canada Glacier between 2014 and 2015 (12.39 ± 5.8 cm << 15.67 ± 6.03 cm; $p = 0.0004$). The difference was also significant on Commonwealth Glacier (14.39 ± 9.38 cm in 2014 << 18.72 ± 11.26 cm in 2015; $p = 0.03$). However, there were no statistically notable differences in diameter between the two study glaciers (ie. comparing Commonwealth and Canada Glacier in 2014) and thus interannual variability was larger than interglacial variability.

3.3c Model-based determination of multiannual cryoconite holes

The relative location of cryoconites measured at each site changed between seasons due to a few factors. Some cryoconites increased in surface area ($\leq 20\%$) and affected the distance of the hole's boundaries parallel and perpendicular to transect lines. Shifts in the ice due to internal deformation of the glacier can distort the original surface distribution and change the angle of the reference post and drift correction post relative to the center of the site. Variability in field-based measurements and drift in the specific location of each transect line are assumed to play a major role in the data recorded. The distance between the ninth transect line conducted in 2015 and the ice screw installed in 2014 varied up to 26cm. (This reflects up to a 1.4% variation along the circumference and does not equate to error in cryoconite hole surface measurements.)

Data from each site was plotted graphically in D3 and Adobe CS6 using vector transformations in a pixel-based matrix to identify spatial similarity between the 2014 and 2015 seasons. A 2-layer spectral gradient was drafted as a background reference layer using hue and shade to define axial and radial distance, respectively. This assigns finite values across the 'negative space' of glacial ice without cryoconite holes and restricts the degree of distortion that can be applied to data sets. Each season was plotted separately using the fixed background layer of the spectral gradient.

A layer-based analysis of each 2015 plot examined the distribution of cryoconite holes relative to each other in contrast to the spatial pattern in 2014. The distance from each cryoconite to all other cryoconites was measured. A drift-correction identified the holes that could be matched back to 2014 plots based on the distribution of 2014 data and

a relative drift of $\leq 5\%$ in the mean distance of each hole to all other holes. Since cryoconite holes can widen over time but should not shrink, proposed matches from the drift-correction were validated if the sum of the major and minor axis did not shrink by more than 2cm in holes ≤ 14 cm, or decrease $>15\%$ in holes >14 cm. The 2cm boundary condition (rather than $>15\%$ decrease) was imposed for smaller holes to account for relative error in human approximation of distances <1 cm.

The matrix of distances between cryoconite holes was adequate to pair sites without applying a more complex simulation for distortion. The gradient layer was a helpful way to review a large data set (a site with 18 cryoconite holes would map similarity from an array of 2,142 distances) and test broader simulations. Cryoconite holes that were identified as unique to a given season in the relative drift model were forced into a best-fit distortion to any of the unmatched holes using Adobe CS6. None of the unique cryoconite holes could be matched without a gross distortion ($>27\%$ drift, or $>22\%$ size reduction with 23% drift). Determinations from the $\leq 5\%$ drift model were therefore deemed appropriate for both the cryoconites matched and unmatched (unique) at each site.

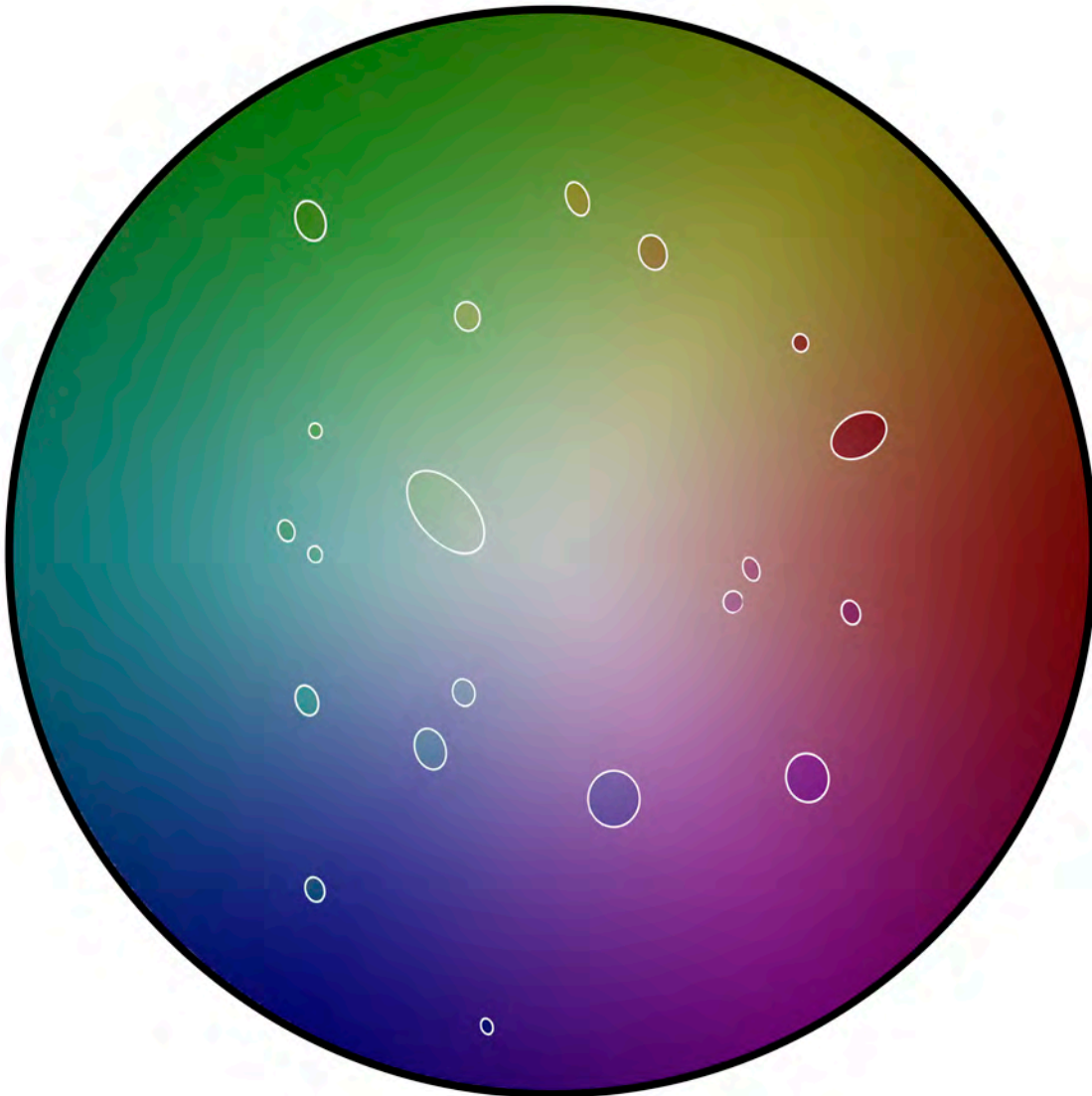


Figure 3.10- Visual representation of drift for matched cryoconite holes. *The shade within the boundary of each cryoconite hole represents the 'absolute' location determined in 2015. Drift correction moves each hole to estimated match sites, and the dissimilarity in spectral gradient illustrates the degree of drift. These holes were exaggerated with a 15% drift for the purposes of this example; actual gradient changes $\leq 5\%$ are not obviously apparent when images are scaled down to small size.*

Simulations of drift correction on Canada Site D indicate that a large hole plotted in 2015 is the result of two smaller holes from 2014 merging together. No other merging

events were observed. Site B did not contain enough cryoconites in 2015 to triangulate relative drift. The determination of cryoconite holes shared/ gained on site B are based on distance within a 5% range of the original cryoconite hole relative to the central post.

3.3d Spatial distribution and net surface change on Canada Glacier

Differences in spatial distribution are more immediately apparent than similarities when comparing consecutive summers on sites A and B on Canada Glacier (Figure 3.11). Each site contained an independent dry, vestigial drainage channel in 2014. These channels are most likely the remnants of a prior subsurface channel that became part of the surface topography when the overlying ice ablated away. Subsurface runoff water continues to route through new paths after old networks rise to the surface, and neither channel on sites A or B contained any flowing water. Ablation of the surface removed the contours defining each channel before sites were re-measured in 2015. Site B experienced a stark net loss of cryoconite holes in 2015. Site C (Figure 3.12) exhibited the most prominent loss of small cryoconite holes. Two cryoconite holes at site D merged into a larger one in 2015.

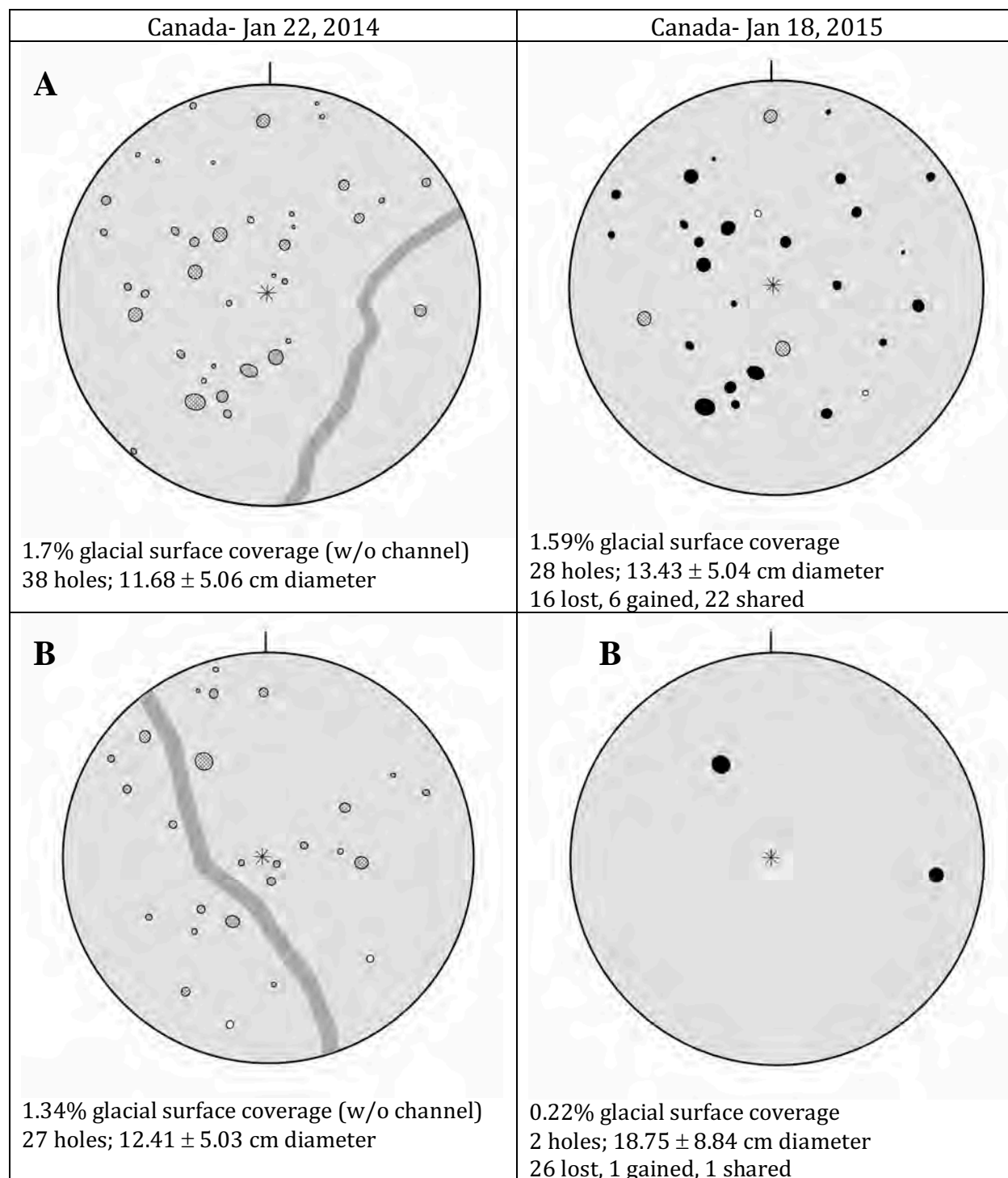


Figure 3.11- Distribution of cryoconite holes on Canada Glacier. Each circle represents a 28.3 m^2 sampling area with a 3-meter radius, oriented respective to an upslope reference stake above each site. Cryoconite holes were displayed as either fully-frozen columns (black), unlidded liquid pools (dark grey), lidded liquid pools (cross-hatched), or dry, hollow columns (white). Two dry surface runoff channels are displayed in dark grey.

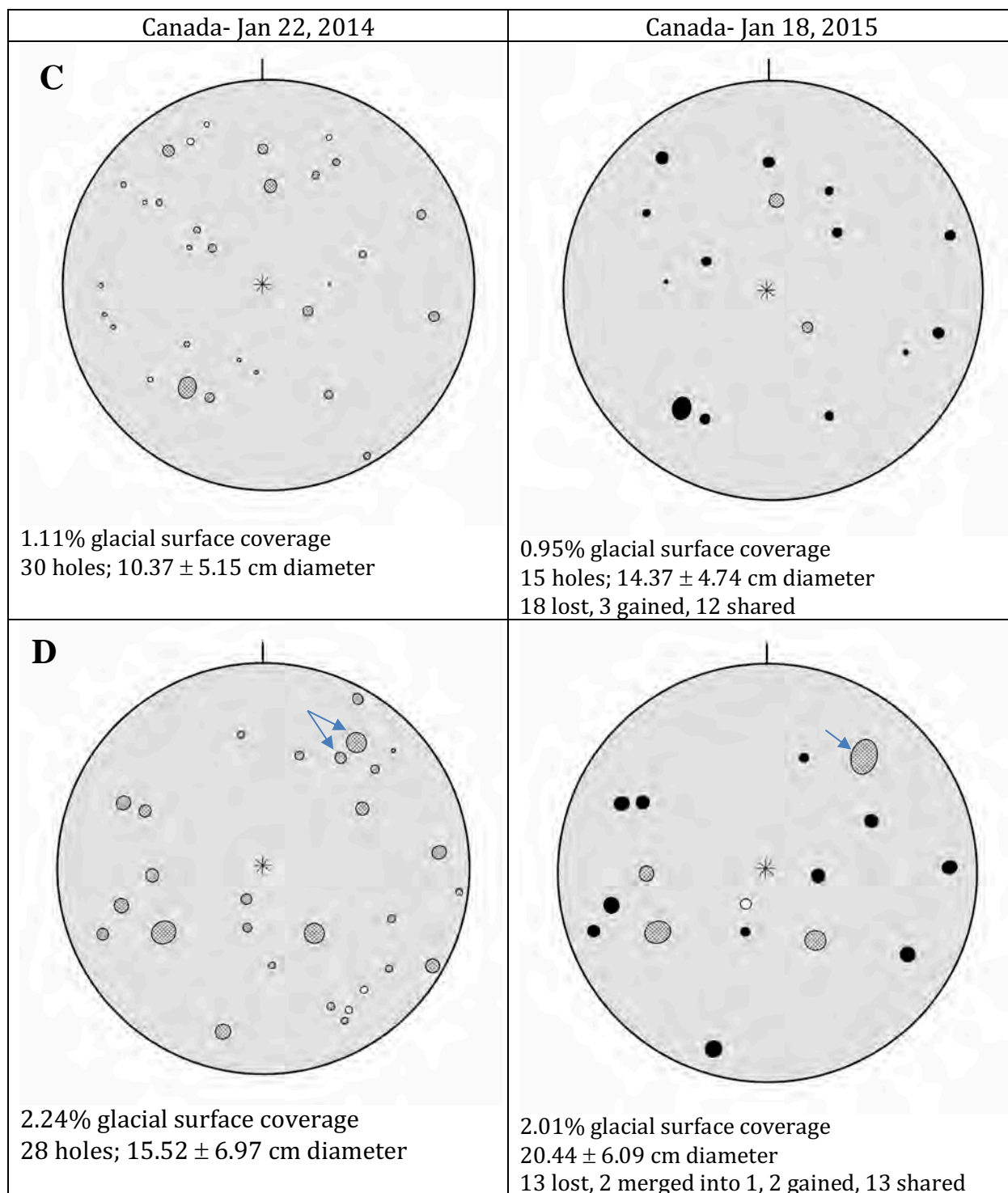


Figure 3.12- Distribution of cryoconite holes on Canada Glacier. Each circle represents a 28.3 m^2 sampling area with a 3-meter radius, oriented respective to an upslope reference stake above each site. Cryoconite holes were displayed as either fully-frozen columns (black), unlidded liquid pools (dark grey), lidded liquid pools (cross-hatched), or dry, hollow columns (white). Merged cryoconite holes are indicated with arrows.

3.3e Spatial distribution and net surface change on Commonwealth Glacier

Site B on Commonwealth Glacier (Figure 3.13) exhibited a total loss of cryoconite holes in 2015. All holes measured at the site in 2014 were smaller, shallower, and more susceptible to total ablation over the course of the year. A vestigial drainage channel on site C ablated in 2015 (Figure 3.14). No cryoconite holes were found on site D in 2014, but two small, dry holes were found in 2015. These were found within the extremely porous surface layer and are more likely the remnants of cryoconite holes that formed in 2014 within the span after the site was measured and before the surface layer was 'stripped' in late summer. Using an estimated 10cm water depth across the total surface area of liquid-filled pools, this indicates 120L discharge across the 113.2 m² area.

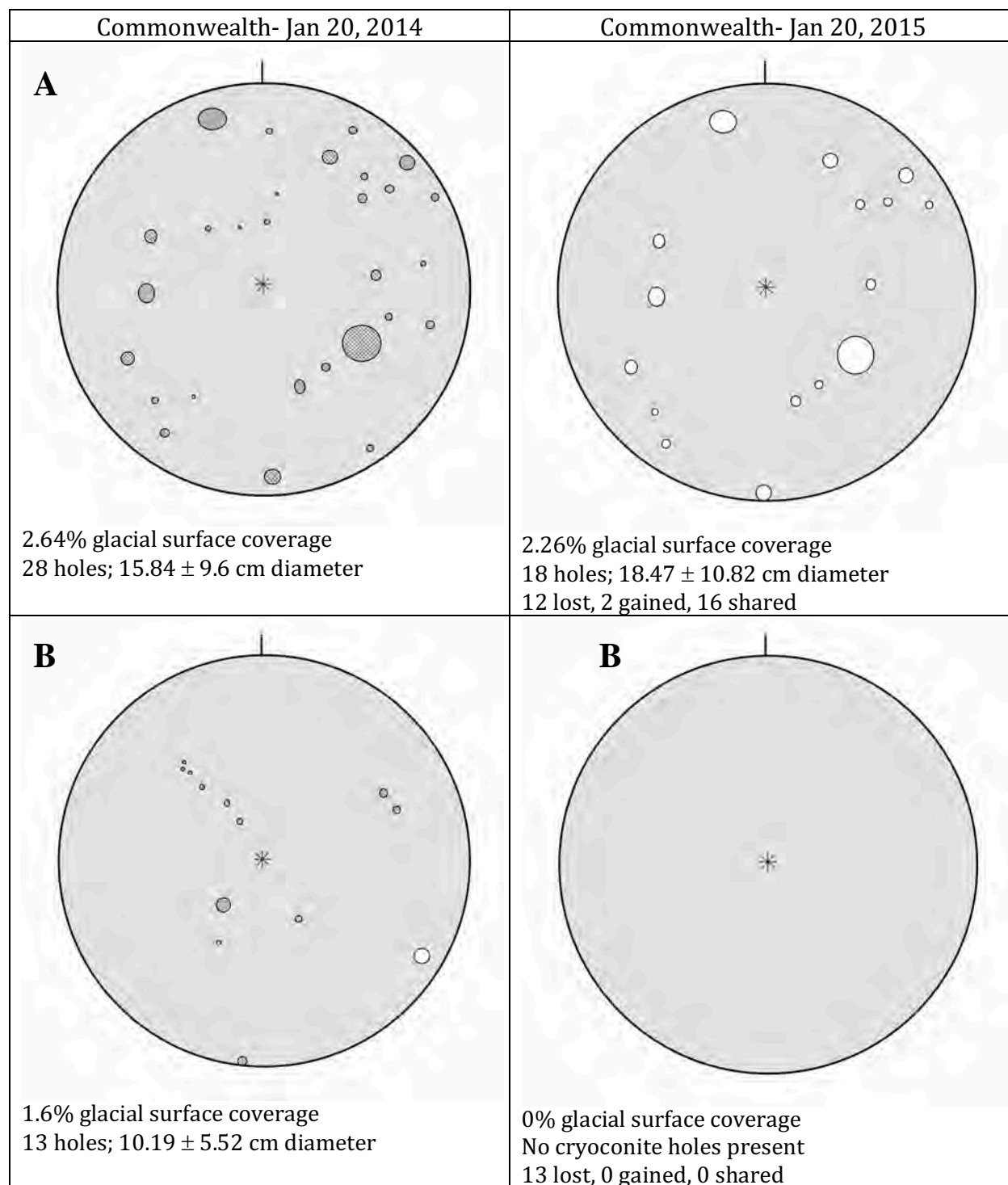


Figure 3.13- Distribution of cryoconite holes on Commonwealth Glacier. Each circle represents a 28.3 m^2 sampling area with a 3-meter radius. Cryoconite holes were displayed as either fully-frozen columns (black), unlidded liquid pools (dark grey), lidded liquid pools (cross-hatched), or dry, hollow columns (white).

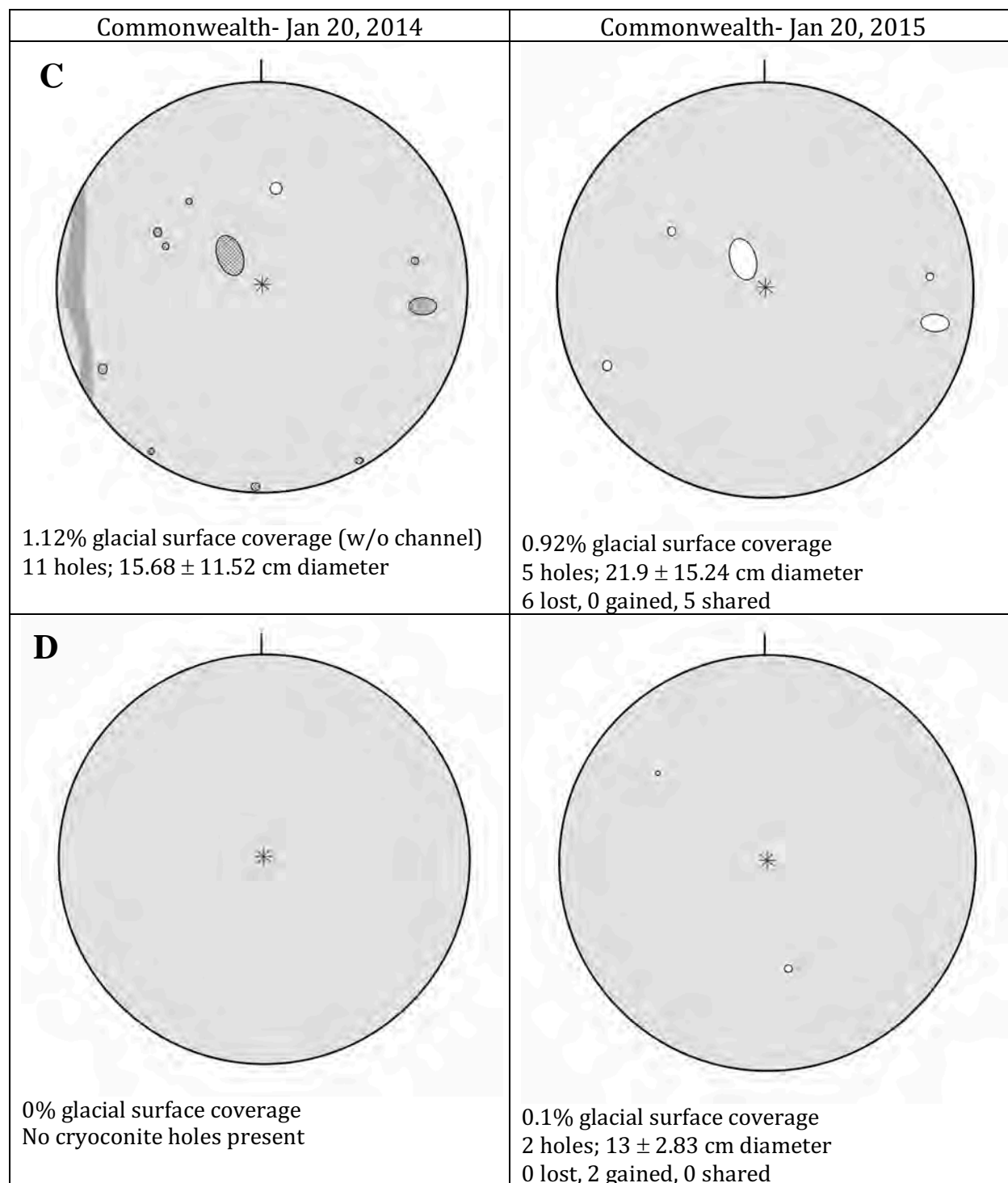


Figure 3.14- Distribution of cryoconite holes on Commonwealth Glacier. Each circle represents a 28.3 m^2 sampling area with a 3-meter radius. Cryoconite holes were displayed as either fully-frozen columns (black), unlidded liquid pools (dark grey), lidded liquid pools (cross-hatched), or dry, hollow columns (white).

3.3f Glacial surface budget

The gains and losses of cryoconite holes at each site is represented in a total surface budget in Table 3.3 and Table 3.4.

Table 3.3- Surface balance of cryoconite hole coverage on Canada Glacier

	Canada Site A		Canada Site B		Canada Site C		Canada Site D	
	#	Glacial coverage						
Cryoconite holes in 2014	38	1.7%	27	1.34%	30	1.11%	28	2.24%
Diameter of holes (cm)	11.68 ± 5.06 cm		12.41 ± 5.03 cm		10.37 ± 5.15 cm		15.52 ± 6.97 cm	
Holes lost before 2015	-16	-0.36%	-26	-1.16%	-18	-0.29%	-13	-0.47%
Diameter of holes lost (cm)	8.41 ± 3.65 cm		11.92 ± 4.45 cm		7.19 ± 2.4 cm		10.54 ± 4.45 cm	
Holes lost to merging events	0		0		0		-2	
Holes shared 2014-15	22	1.34 - 1.43%	1	0.17%	12	0.82 - 0.88%	13	1.77 - 1.91%
Diameter of holes shared			25 cm		14.37 ± 4.74 cm		21.08 ± 6.01 cm	
Holes gained by merging events	0		0		0		+1	
Holes gained in 2015	+6	0.16%	+1	0.04%	+3	0.07%	+2	0.11%
Diameter of holes gained	9.33 ± 3.71 cm		12.5 cm		9 ± 2.65 cm		13.75 ± 1.77 cm	
Cryoconite holes in 2015	28	1.59%	2	0.22%	15	0.95%	16	2.01%
Diameter of holes	13.43 ± 5.04 cm		18.75 ± 8.84 cm		14.37 ± 4.74 cm		20.44 ± 6.09 cm	
Net change		-0.11%		-1.12%		-0.16%		-0.23%

Table 3.4- Surface balance of cryoconite hole coverage on Commonwealth Glacier

	Commonwealth Site A		Commonwealth Site B		Commonwealth Site C		Commonwealth Site D	
	#	Glacial coverage						
Cryoconite holes in 2014	28	2.64%	13	1.6%	11	1.12%	0	0%
Diameter of holes (cm)	15.84 ± 9.6 cm		10.19 ± 5.52 cm		15.68 ± 11.52 cm		n/a	
Holes lost before 2015	-12	0.39%	-13	1.6%	-6	-0.2%	n/a	n/a
Diameter of holes lost (cm)	10.33 ± 3.51 cm		10.19 ± 5.52 cm		11.89 ± 13.42 cm		n/a	
Holes lost to merging events	0		0		0		n/a	
Holes shared 2014-15	16	2.22%	0	0%	5	0.91- 0.92%	0	0%
Diameter of holes shared	19.84 ± 10.7 cm		n/a		21.9 ± 15.24 cm		n/a	
Holes gained by merging events	0		0		0		0	
Holes gained in 2015	+2	0.03%	0	0%	0	0%	+2	0.1%
Diameter of holes gained	7.5 ± 1.41 cm		n/a		n/a		13 ± 2.83 cm	
Cryoconite holes in 2015	18	2.25%	0	0%	5	0.92%	+2	0
Diameter of holes	15.21 ± 9.47 cm		n/a		21.9 ± 15.24 cm		0 cm	
Net change		-0.38%		-1.6%		-0.2%		0.1%

3.4 Conclusions

This study found lower cryoconite hole coverage of glacial surfaces than prior estimates reported in literature. Surface coverage ranged from 0.22- 2.24% on Canada Glacier and 0-2.64% on Commonwealth Glacier. Both glaciers experienced a net loss of holes in 2015. Smaller holes were more susceptible to total ablation between seasons. The physical state of cryoconite holes reflects differences in the meteorological conditions each season. All water-filled cryoconites were in a liquid state during sampling in 2014, and roughly half were unlidded. The following year 85% of water-filled holes were frozen on Canada Glacier, and all columns on Commonwealth had drained. The total drainage of all cryoconite holes on Commonwealth suggests that a 'stripping event' may have flushed all liquid water from the top ~30cm of the glacial surface by the end of summer 2014. Such events have been reported during previous high-flow years in Taylor Valley. Seven out of eight transect sites exhibited a net loss of surface coverage (0.11-1.6%) in 2015. The change was similar between glaciers. Spatial modeling was able to match cryoconite holes over both seasons. This identified a loss of 6-26 individual cryoconite holes per site (/28.3 m² area), a gain of up to 6 new holes, and a range of 0-22 multiannual holes. The relative concentration of cryoconite holes on glacial surfaces is important in order to estimate the contribution of cryoconite drainage to total glacial melt. The 'stripping' from Commonwealth Glacier in 2014 removed approximately 120L of water from a total 113 m² area. This equates to 1.06L of solute-enriched cryoconite liquid drained per m² of the

ablation zone and serves as an extreme example of total hydrologic connectivity for cryoconite holes identified on the glacier in 2014.

Chapter 4

Variations in Meltwater Composition and Nutrient Cycling Between Ice-Lidded and Open System Cryoconite Holes

4.1 Introduction

Cryoconite holes are small melt pools created by the accumulation of wind-transported sediment (known as cryoconite) into grooves on the textured surface of a glacier's ablation zone. This sediment has a low albedo and absorbs more solar radiation than the surrounding glacial surface, preferentially melting the ice below to create a cylindrical water-filled hole. While cryoconite holes in Arctic and mid-latitudes form as pools of water open to the surrounding atmosphere, cryoconites in the McMurdo Dry Valleys of Antarctica are uniquely capable of forming 'lids' of dense blue ice due to advection from cold winds above the liquid surface (Figure 4.1). The entire meltwater column refreezes in the absence of solar radiation during the winter. Melt on the glacial surface is inhibited by a mean summer air temperature below freezing (apprx. -4°C) and perpetual winds averaging ~ 4 m/s. Melting in subsequent summers occurs beneath this frozen column when the underlying sediment resumes downward melting. Lidded cryoconites can therefore be isolated from atmospheric exchange while maintaining subsurface melt in a 'solid state greenhouse'.¹⁵

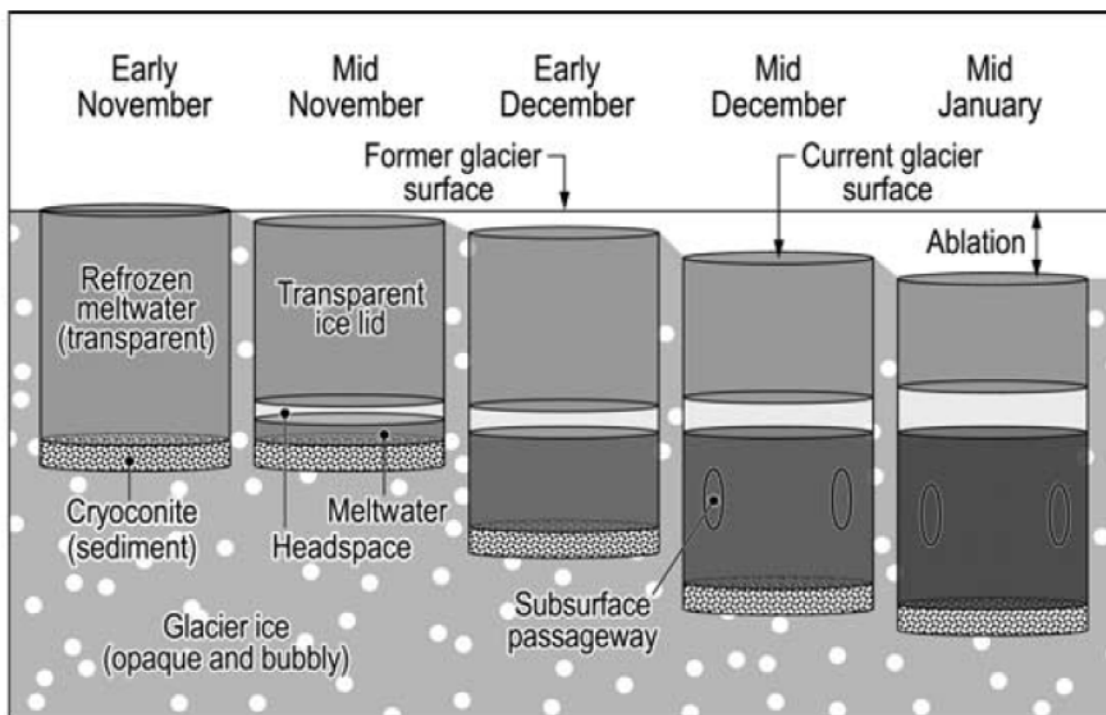


Figure 4.1- Annual melting in a multiannual lidded cryoconite hole. Reprinted from Fountain et al.⁴². Cryoconite sediment absorbs solar radiation and melts the underlying ice. An equilibrium depth is reached when the rate of melt-deepening in the hole matches the ablation rate on the glacial surface. Solutes in the meltwater are excluded from the freeze/formation of new ice lids and will accumulate in the liquid over time. After the liquid freezes in winter, the frozen column becomes shallower due to sublimation. Melt during the following summer occurs beneath the frozen column and continues to deepen the hole.

The wind-dispersed sediment that forms cryoconite holes can also contain algae and other biota capable of surviving the freeze-thaw cycle of ice lids.⁷⁵ Microbial counts in ice cores have been correlated with dust content.⁷⁶ Cryoconite holes are the most biologically active habitat within glaciers and the dominance of either heterotrophs or autotrophs impacts nutrient and carbon cycling. Prior studies have identified an autotrophic dominance in select samples, leading to a higher pH in the liquid column due to algal growth and carbonate depletion.⁴¹ These dynamics are even more complex when ice lids prevent atmospheric exchange. Organic matter produced within a cryoconite can lower the

albedo of cryoconite sediment, increasing ice melt and influencing the mass balance of glaciers.⁷⁷ Flushing events can drain liquid water from the holes or introduce fresh water originating from subsurface drainage channels, while other cryoconite columns can remain hydrologically isolated for decades.⁴⁹ Drainage events lead to the routing of meltwater off glaciers during the summer and provide solute-enriched water to microbial communities thriving in lakes and ephemeral streams.

Lidded cryoconite holes provide a unique scenario to study closed system processes, but no known studies have observed the development and variation of natural cryoconites *in-situ* on glacial surfaces that support the formation of both lidded and unlidded holes. This study measured the chemical characteristics of both lidded and unlidded cryoconite holes across six glaciers of the McMurdo Dry Valleys over two summer seasons in order to gain a better understanding of the biogeochemistry, nutrient cycling, and hydrologic isolation of supraglacial liquid in limited contact with the atmosphere. Inclusion of both open- and lidded pools examines the parameters governing the existence of both in a melt system responsible for up to 15% of glacial surface runoff³⁴ in the Dry Valleys.

4.2 Methods

4.2a Sampling sites

Water was collected from cryoconite holes and other melt features over the November-January austral summers in 2013-14 (Season 1) and 2014-15 (Season 2). The duration of each summer was spent on-site at fieldcamps in Taylor Valley. Season 1 served as a pilot year in which multiple sampling trips were conducted on three glaciers (Canada, Commonwealth, and Taylor) during the peak of the melt season in mid-January. Field

sampling was expanded to six glaciers (adding Joyce, Adams, and Wright Lower Glacier) over the full summer in Season 2. Glaciers were chosen based on the observed presence of liquid-filled cryoconite holes, representation of four different dry valleys, and feasible accessibility from the Lake Hoare research fieldcamp at the base of Canada Glacier.



Figure 4.2- Glacier locations in the McMurdo Dry Valleys. *Commonwealth (1) and Canada (2) Glaciers both reside in Taylor valley, in which the larger Taylor Glacier (3) extends from the East Antarctic Ice Sheet. Taylor Glacier's northeastern tongue faces coastal McMurdo Sound. Joyce Glacier (4) in Garwood Valley and Adams Glacier (5) in Miers Valley are both fed by the larger Blue Glacier. Wright Valley is bookended by Wright Lower Glacier (6) towards the coast. Wright Upper Glacier (7) was not sampled in this study but is included in the figure to illustrate the length of Wright Valley. Image rendered from multiple composites using USGS³⁰ source data.*

Canada Glacier was sampled more frequently due to its proximity to the main camp and the ability to reach the ablation surface by crossing the Asgard mountains on foot. Samples collected from lower elevations of Canada Glacier (82-100m a.s.l.) are

differentiated from those collected higher on the ablation surface (274-304m a.s.l.) in order to compare meltwater composition in the two intraglacial regions. Higher regions of Canada's ablation zone consist of a relatively smooth surface partially shielded by the surrounding Asgard mountains. The lower, terminal lobe of the glacier spreads out in Taylor Valley and is more exposed to strong katabatic winds. Higher sediment deposition in this region contributes to the formation of hills, scalloped basins, and terraced vertical surfaces parallel to the predominant wind direction (Figure 4.3). The high contribution of ice melt from vertical features⁷⁸ on lower elevations of the glacier lead to the dilution of solute-rich meltwater draining from cryoconite holes and melt pools uphill.⁷⁹ Data referring to the total sampling area across Canada Glacier is represented as Canada_T in future discussion.



Figure 4.3- Scalloped basins on lower Canada Glacier.

Since regions of upper and lower Canada Glacier are compared in subsequent sections, it is worth noting that Wright Lower Glacier (LG) is the proper name for the piedmont Glacier on the eastern end of Wright Valley. Field sampling was conducted across a 315-320 m elevation band on Wright LG and the name does not imply any distinct subset of sampling.

4.2b Guidelines for the categorization of melt features

For the purposes of field sampling, “cryoconite holes” were broadly defined as melt holes in glacial surface ice with a contained shape and no visibly apparent connectivity to

surface or subsurface melt channels. Samples needed to exhibit a relatively consistent depth profile; melting downward in a cylindrical shape with perpendicular ice walls and a frozen, level bottom. Additional requirements included a minimum column depth of 6 cm, a diameter less than ~2-3 m, the presence of liquid water, and a bottom layer of sediment in the hole.

The term “melpools” (MPs) is used to describe a unique subset of samples adhering to the guidelines described above which appear to have lost the ability to melt-deepen irrespective of surface ablation rates. This defining boundary was identified during the analysis of physical characteristics discussed in Chapter 2. Since the distinction was not identified until after all fieldwork had been completed, there was no sampling bias towards either type of hole during the course of sampling. Transformation into static melpools in the Dry Valleys occurs when sediment accumulation reaches a thickness above 2-2.4 cm and begins to insulate the underlying ice from further downward melting. These pools can also be identified by distinct patterns in the vertical stratification of the liquid column. The guidelines used to identify cryoconite holes and melpools served as a morphological boundary which prevented sampling from unconfined “cryolake basins”; melt puddles that can develop over large debris catchments tens of meters wide on a glacial surface but lack distinct liquid boundaries in an ice-walled column. Sample selection prioritized cryoconites containing at least 1.5L of liquid for the analyses discussed below, but was randomized beyond these initial parameters.

Cryoconites and melpools were classified as ‘lidded’ if a distinct, dense ice layer covered a full horizontal cross-section of the column. Holes with cracked or porous lids are not isolated from atmospheric exchange and were considered ‘open’ in this study.

Examples of lidded and unlidded holes are shown in Figure 4.4 below.

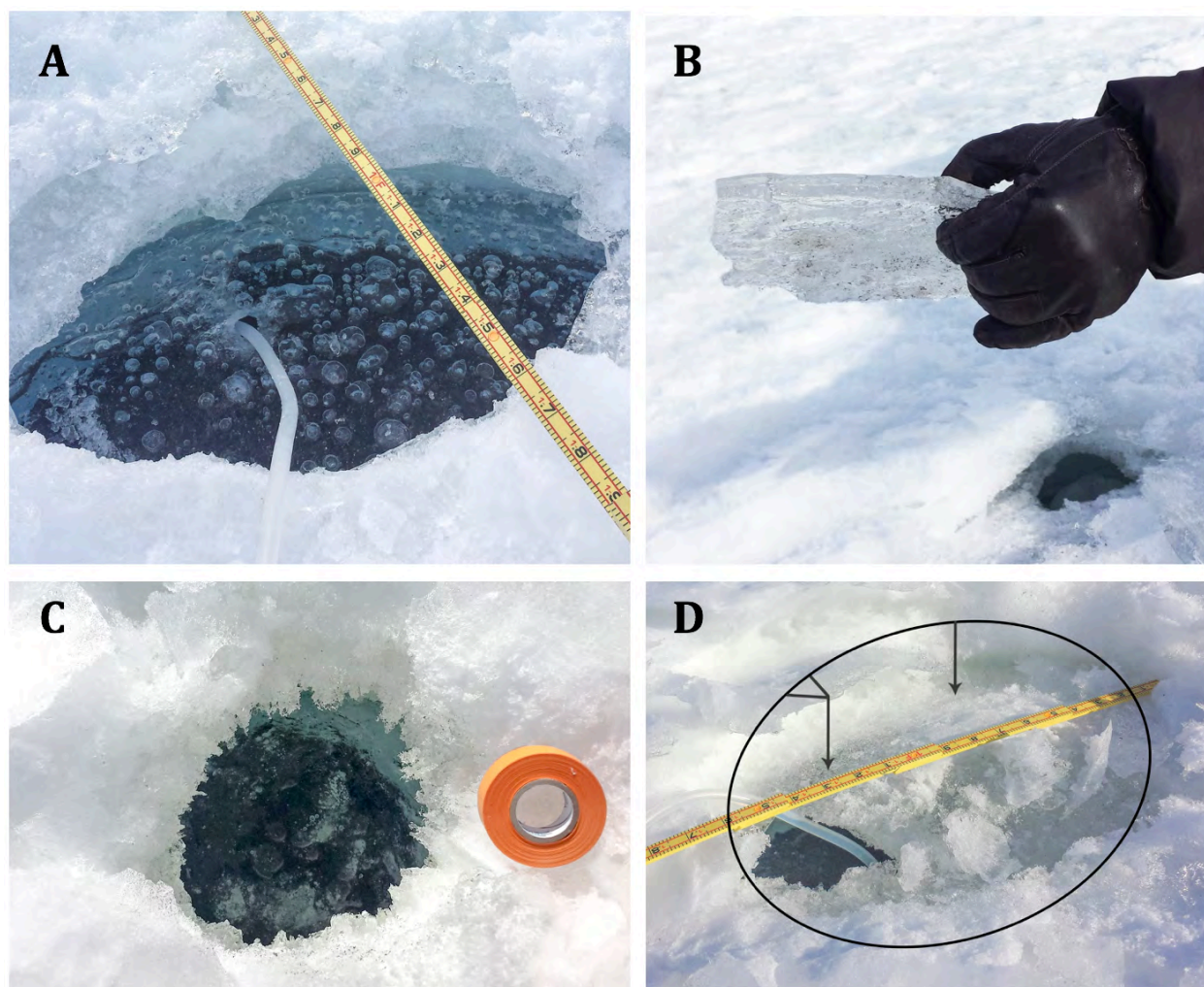


Figure 4.4- Open and Lidded Cryoconite Holes in Taylor Valley. *The 45 cm-wide cryoconite hole in image A had a full ice lid 3.3 cm thick that was drilled through to extract the liquid inside. A portion of the lid is held up in image B. The cryoconite hole in image C contains small slivers of floating ice but is still fully open to the surface. Internal melt ‘weathering’ of the ice lid in image D has transformed the once-thick lid into a low density, porous layer open to gas exchange.*

One sampling site on Joyce Glacier (sample C-44) had an atypical profile including a large 5.6m diameter, 1.2m liquid depth, no underlying sediment, and column walls of extremely dense blue ice. There was no observed aeolian sediment in the column, but a very thin layer of fine, chalk-like material coated the bottom of the hole. The overall

morphology suggests that the surface ice is not a 'lid' which froze over a liquid layer exposed to ambient air, but rather that a pocket of internal ice that melted without ever opening to the surface. This formation is similar to the description of "extreme cases of subsurface crystal melt" reported by R. Paige (1968)⁷¹, although this sample would be the largest such case ever reported. This site is discussed in further detail in the Supporting Data section of Chapter 2. The following assumptions and observations are relevant to this chapter-

1) Unlike cryoconite holes which form on the glacial surface and melt-deepen due to the low albedo of sediment, this formation is the result of an extreme case of penetrative solar radiation causing a maximum in the temperature profile at a depth beneath the glacial surface. Thus melt occurs from radiative heating of ice crystals, not conductive heat from sediment to ice.

2) While cryoconite holes may become isolated from atmospheric exchange after forming ice lids above the liquid column, the liquid in this column formed without any *initial* exposure to the atmosphere. Gas exchange with ambient air may not have occurred since snow/firn initially compacted the crystals into glacial ice.

3) The lack of sediment transport means it is highly unlikely for a thriving microbial community to exist within the hole.

The term "internal melt" has been used in literature to describe both the melt-deepening of cryoconite sediment beneath ice lids and the distinctly different process of internal melt of ice crystals without conductive heat transfer. The Joyce formation is

therefore categorized as “englacial crystalline melt” (abbreviated as ‘crystal melt’ in figures and graphs) in order to distinguish the difference in this study.

4.2c Field methods

Rather than the more common method of removing frozen cryoconite columns with an auger prior to the melt season, this study extracted liquid water from cryoconite holes and other melt features in-situ using a hand-pump manifold. This was done in order to examine the chemistry of meltwater affected by uneven ‘pulse’ melting and multiple freeze/thaw events over the course of the summer. Glaciers were accessed both on-foot and with helicopter assistance. No samples were collected within 100 m of helicopter landing sites and all sampling locations were recorded by handheld GPS (Garmin GPS-map 76). Once an appropriate sampling site was identified on a glacier, 1.5- 2 L of water was removed while taking care not to disturb any underlying sediment.

In Season 1 water was extracted from sampling sites through platinum-cured silicone tubing into an Erlenmeyer flask using indirect suction from a side-arm hand pump. The pump manifold and flask were triple-rinsed with water from each cryoconite hole/melt feature before collecting water for analyses, and subsequently rinsed 3x with DI water after each glacial trip. The water in cryoconite holes remains relatively stable at 0°C due to the energy balance of the holes, but the extracted water was highly susceptible to freezing as soon as it was pumped above the glacial surface due to strong wind exposure. Rapid icing of extraction tubes necessitated the removal of water in <10 minutes, after which bottles were sheathed in multiple layers of insulation. Field sampling began earlier in the summer during Season 2 when ambient air temperatures were colder, and the collection

method was changed due to near-instantaneous freezing of liquid within the extraction tubes. All samples from cryoconite holes and meltpools in 2014-15 were collected with a hand-roller pipette pump using sterile disposable 25 mL polystyrene serological pipettes triple-rinsed in water from the melt feature before collecting water for analyses. During both summers the duration of individual glacier trips was limited to <2.5 hrs to lower the risk of samples freezing and subsequently shattering their respective storage bottles. The extracted water was distributed into two collection bottles on-site; 100 mL into a 125 mL amber borosilicate glass bottle and ~400 mL into a 500 mL high-density polyurethane (HDPE) bottle. The remaining water was filled to the brim of a 1-L amber borosilicate glass bottle for the analysis discussed in Chapter 6.

In most cases the lids on cryoconite holes/ meltpools could be cracked open with a 3x-rinsed sediment spatula. On the rare occasion (<10%) when a metal ice screw was necessary to drill through an ice lid, the screw was rinsed in HPLC water from a pre-furnaced 1 L borosilicate bottle carried onsite. Particular care was taken to prevent the screw from contacting the underlying meltwater in a hole, and use of the screw was included in field notes. Additional samples were collected from drainage channels on/near the glacial surface, waterfalls, and Anderson Creek at the base of Canada Glacier. Meltwater from glacial waterfalls pouring off the terminal face of Canada Glacier was collected directly into bottles held beneath the falls (Figure 4.5).



Figure 4.5- Glacial waterfalls in Taylor Valley. (Left)- A waterfall running down the 14-meter terminal face of a glacier in Taylor Valley. A vertical chain of icicles has formed around the stream of meltwater draining from the ablation surface of the glacier. (Right)- Direct sampling beneath a waterfall on Canada Glacier.

After the necessary 1.5 L of sample water was collected, temperature and pH were measured with a Beckman 0265 meter with a Beckman A57186 probe. The pH probe was stored in a buffer solution and rinsed with excess water extracted from the cryoconite hole prior to measurement in the hole itself. These measurements were conducted after sample extraction in order to minimize possible contamination of collected meltwater by the buffer solution. The pH of nearby cryoconite holes was often also measured. Automatic temperature compensation in the pH probe reported data to the corresponding value at 25°C. The pH probe was calibrated with buffer solutions at pH 4, 7, and 10, compared to each standard after sampling trips, and recalibrated as necessary. No significant recalibration was required during either season. The pH was re-measured from excess sample water at the end of each season at the Crary laboratory at McMurdo Station.

Samples were filtered within 6 hours of collection upon return to one of the Taylor Valley field laboratories. Water from the 125 mL glass collection bottle was filtered through a pre-combusted Whatman GF/C glass microfiber filter into a secondary 125 mL glass amber bottle for the analysis of dissolved organic carbon (DOC). Hydrochloric acid (0.1 mL) was pipetted into the bottle as a biocide, and the bottle was sealed with a Teflon-lined cap. All glass bottles (both pre- and post-filtering) were rinsed with 1% hydrochloric acid, triple-rinsed in DI water, and combusted for at least 4 hours at 475°C prior to use. The remaining procedures were conducted with water from the 500 mL HDPE collection bottle. Two 50 mL samples were each filtered through 0.4 µm Nucleopore membranes and distributed into pre-rinsed 125 mL HDPE bottles for the analysis of major anions and cations, respectively. The bottles for DOC, anions, and cations were stored in a 2°C refrigerator, while the nutrient bottle was frozen at -20°C. The remaining water in the 500 mL collection bottle was stored in the 2°C refrigerator and saved for a secondary determination of pH at McMurdo Station.

Method controls were conducted intermittently throughout each season using high-performance liquid chromatography (HPLC)-grade water subject to one of four different treatments. For each primary control, HPLC water was poured into a new, pre-furnaced borosilicate amber glass bottle which served as a surrogate cryoconite hole. The water was then extracted according to the methods described above, distributed into on-site collection bottles, covered with insulation and stored outside for two hours prior to field laboratory processing. Although all field samples collected during Season 2 were extracted with seriological pipettes, additional controls in 2014-15 were conducted using the original hand-pump manifold in order to compare both methods in the same field conditions at the

same times. Secondary controls used HPLC water poured directly into both the 125 mL glass amber and 500 mL HDPE collection bottles, which were then capped, shaken, and stored for 2hrs before processing. Two tertiary controls consisted of HPLC water poured directly into each storage container. This tiered system was used in order to identify any contamination between the extraction, filtration, and storage of samples in the field. Analytical blanks were also incorporated into each of laboratory analyses conducted at the Crary laboratory at McMurdo Station.

4.2d Laboratory methods

Major ions (F^- , Br^- , Cl^- , NO_3^- , SO_4^{2-} , Li^+ , Na^+ , K^+ , Mg^{2+} , and Ca^{2+}) were analyzed at McMurdo Station with a Dionex DX-120 ion chromatograph with a sample loop of 400 μ L as described by Welch *et al.*⁸⁰ Alkalinity was calculated by subtracting the equivalent sum of cations from anions. DOC was measured with a Shimadzu TOC-V CPN Total Organic Carbon Analyzer. Both major ion and DOC measurements were carried out at the Crary laboratory at McMurdo Station, Antarctica, while nutrients were stored frozen until they could be measured in the United States. NH_4^+ , NO_2^- , NO_3^- , and PO_4^{3-} were measured with a Lachat QuikChem 8000 flow injection autoanalyzer using Omnion 3.0 software at Ohio State University. The long-term monitoring of meteorological and hydrologic data in the Dry Valleys by the McMurdo LTER offered an extensive database of supporting data for this research.

4.2e Critique of current methodology used to estimate isolation age

All Cl⁻ in glacial ice is assumed to derive from marine aerosols.⁸⁰ The magnitude of marine deposition decreases with distance from the coast and increasing elevation on glacial surfaces.⁸¹ However, the *rate* of marine deposition remains constant over large timescales,⁸² and thus Cl⁻ concentrations should be consistent throughout ~1 m depths of ice beneath the surface.³⁴ The majority of solutes in cryoconite meltwater are preferentially excluded from the freezing of new ice lids and will accumulate in the underlying liquid over time.⁴² Since Cl⁻ is non-reactive and not utilized biologically⁸³, there should be no additional means of Cl⁻ gains or loss in an isolated cryoconite hole. This makes Cl⁻ an excellent tracer to estimate the length of time that cryoconite water has been accumulating solutes by comparing the amount of Cl⁻ enrichment in cryoconite holes relative to Cl⁻ in glacial ice.

A series of equations was devised by Fountain *et al.*³⁴ to estimate the 'isolation age' of cryoconite holes. This references hydrologic isolation (the duration of meltwater enrichment before a cryoconite hole drains or is infiltrated by subsurface channels) and should not be confused with atmospheric isolation in lidded cryoconite holes. These equations have been utilized by multiple research teams in subsequent studies.^{47,49,84} Fountain's research in the Dry Valleys is extensive and highly respected, but a minor critique of published methods is addressed below.

The initial quantity Cl⁻ in a hole was described by Fountain *et al.*³⁴ in Equation 4.1.

M₀ = h a i

Equation 4.1- Initial Cl⁻ in new cryoconite holes. (Revised from Fountain³⁴)

M_0 is the initial quantity of Cl^- (μmol), h is the depth of the hole (cm), a is the cross-sectional area of the hole (cm^2) and i is the average concentration of Cl^- in the surrounding ice (stated by Fountain as $\mu\text{mol/L}$). However, since the depth in cm and area in cm^2 are used to calculate mass from initial concentrations, the ice concentration should be represented in $\mu\text{mol}/\text{cm}^3$, not $\mu\text{mol/L}$. This may be a typo in Fountain's paper.

As the hole deepens, the Cl^- mass at time t (M_t) can be calculated with Equation 4.2.

$$M_t = M_0 + ai \left(\frac{dz}{dt} \right) \times \Delta t$$

Equation 4.2 – Cl^- in isolated cryoconite holes at a given time. (Revised from Fountain³⁴)

The rate of downward melting is represented by $\left(\frac{dz}{dt} \right)$ and Δt is the isolation age in years.

This equation was modified from Fountain's published formula in which Δt was added rather than multiplied to the rate of melt-deepening. The change in depth with time $\left(\frac{dz}{dt} \right)$ should be multiplied by time in order to represent the total downward melt over a period of years. Again this discrepancy is assumed to be a typo. The length of time that cryoconite liquid has been isolated from the surrounding hydrologic drainage system can then be estimated by Equation 4.3.

$$\Delta t = \left(\frac{M_t}{ai} - h \right) \left(\frac{dz}{dt} \right)^{-1}$$

Equation 4.3- Isolation age of cryoconite water. (Revised from Fountain³⁴)

This results in an 'isolation age' estimate where $t > 0$ indicates a cryoconite hole isolated from hydrologic exchange, and $t < 0$ suggests that the hole has been infiltrated by fresher water and is connected to the subsurface drainage network in a glacier. This

equation was modified from Fountain's published version in which M_i is used in place of M_t . M_i is not defined in the original literature and substitution of Equation 4.1 into Equation 4.2 leads to the formula above when the total mass at time t (M_t) is used.

Fountain's method substitutes sublimation as the value for downward melting ($\frac{dz}{dt}$) which essentially causes Equation 4.3 to estimate isolation age for cryoconite holes at an equilibrium depth to the surface. On Canada Glacier, the estimated ablation rate is ~ 8 cm w.e./year³⁴, and similar values (~ 6 -10 cm w.e./year) have been reported for glaciers in both Taylor and Wright⁷³ Valleys. Equation 4.3 includes a number of assumptions; primarily that the ablation rate is equal to the rate of melt-deepening in a hole and that all Cl^- is excluded from ice lid. In a study on Canada Glacier, Bagshaw *et al.*⁴¹ identified a small portion of Cl^- in ice lids, indicating that solutes are not entirely rejected from the lids during freezing. Incorporation of ice lid Cl^- based on Bagshaw's equations had a negligible effect on isolation age estimates in this study due to the magnitude of variability from other model assumptions.

Glacial ice Cl^- typically decreases at higher elevations on glacial surfaces and ice core collection was not logistically feasible in this study. A range of glacial surface concentrations reported in published literature on each glacier were used in the calculations in this study. Published values varied depending on the elevation where ice core samples were taken, and individual value of i were chosen for each sample in this study based on similarity to the elevation of ice cores collected in previous studies. A comprehensive list of Cl^- reference concentrations is available in section 4.5 Supporting Data Table 4.10. There were no reported values available for reference on Adams or Joyce Glaciers. Estimates of glacial ice Cl^- were calculated for those glaciers based on ice cores

taken from nearby glaciers and ratios of glacial ice concentrations to meltwater outflow measured by the MCMLTER below each glacier. These estimates are discussed the Supporting Data appendix of this paper.

The morphology of cryoconite holes in the Dry Valleys is described in a similar format across prior literature, generally consisting of a 15-25cm column beneath the ice surface, filled ~50% with water below a small headspace and thick ice lid.^{34,41,42,47-49,68,73,84-87} The presence of unlidded holes is briefly acknowledged in a minority of papers. Chapter 2 in this dissertation is the first known study to report the presence of multiple ice lids and address the complexity of cryoconite hole stratigraphy over multiple freeze/thaw events. Although sublimation may be equal to the rate of melt-deepening in a simplified model of cryoconite holes at an equilibrium depth, the initial development of a hole inherently requires melt-deepening to outpace ablation rates. If a cryoconite hole freezes every winter and new melt occurs beneath the frozen column the following spring, the rate of melt-deepening can be represented by the depth of liquid in a hole. The rate of melt-deepening varies across cryoconite holes due to differences in ice lid thickness, total depth, localized differences in the optical properties of the surrounding ice, etc.. Using liquid depth as a measure of melt-deepening helps to account for these differences during a given sampling season.

The total depth term h used in Equation 4.1 assumes that the mass of Cl^- in a hole can only be explained by one of two scenarios; either complete enrichment from the total column depth, or dilution of cryoconite water by channel infiltration. It does not account for scenarios in which cryoconite holes drain and then continue melt-deepening beneath the fracture site; a pattern observed in multiple samples in Chapter 2. In these cases the

cryoconite hole may remain hydrologically isolated for a period of years after the initial drainage event, but this enrichment will not be representative of the total depth of the column. Chapter 2 determined that liquid depth is independent of total depth in cryoconite holes due to the combination of drainage events, variations in melt rates relative to ablation, etc. Thus liquid depth was used rather than total depth in order to determine isolation age in this study.

Ironically these considerations lead to a vastly simpler equation for isolation age. The depth terms on the right side of Equation 4.3 are equal and produce a value of 1. Multiplying the surface area a by the liquid depth of the hole represents the volume of water. Dividing the mass of Cl^- in cryoconite liquid by the volume of liquid in the column leads back to the concentration of Cl^- in the cryoconite liquid. The final equation is simply the ratio of cryoconite meltwater: glacial ice Cl^- subtracted by 1.

$$\Delta t = \left(\frac{i_{\text{cryo}}}{i_{\text{ice}}} \right) - 1$$

Equation 4.4- Adjusted isolation age of cryoconite water.

Each equation is limited by the assumption that the rate of downward melting (or sublimation) is consistent on an annual basis. Sublimation is more likely to remain relatively constant on a multiannual timescale, but the rate may be different across glaciers or elevations. Using individual liquid depth as a rate of downward melting removes the effect of spatial variance since it uses values inherent to each cryoconite hole at the time of sampling, but it may be more variable on a multiannual scale. Equation 4.4 is preferred in this chapter because it is not biased by variation in column depth, and isolation age can be calculated more accurately for cryoconite holes that have previously drained and have since begun re-melting. The reason these equations are addressed in such detail is because

Fountain's method has been used in many other studies^{47,49,84} and applied to calculations such as nutrient transport from glaciers. The variability in cryoconite depth profiles addressed in Chapter 2 indicates that a simplified equilibrium-state depth profile is unrealistic to the majority of cryoconite holes.

4.3 Results and Discussion

4.3a Estimates of cryoconite hole isolation age

Estimates of cryoconite hole isolation age using Equation 4.4 are shown in Figure 4.6. A logarithmic scale was applied to the x-axis in Figure 4.6 in order to enhance visibility between overlapping data points, but the linear relationship between Cl^- and isolation age is an inherent property of the equation (as long as reliable data for glacial ice Cl^- is used to represent i_{ice}).

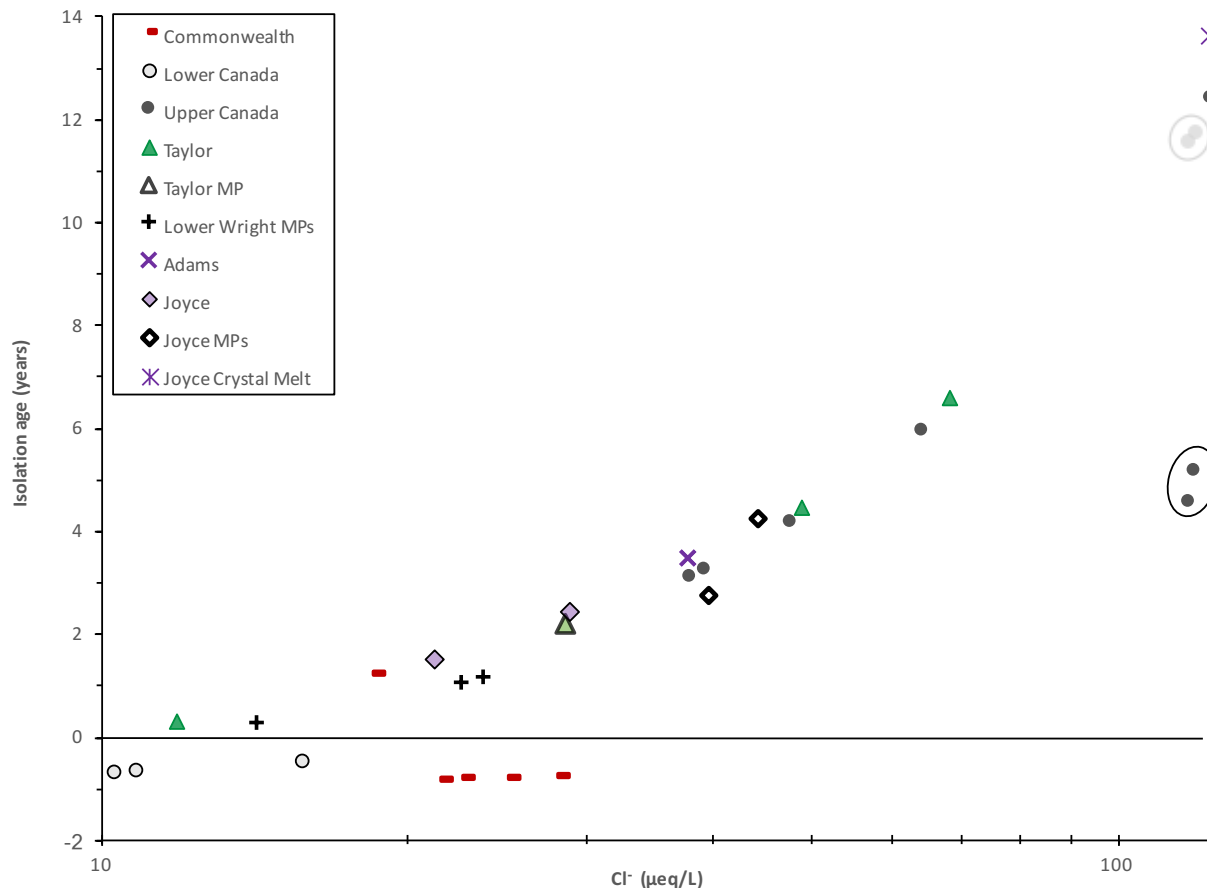


Figure 4.6- Cryoconite hole isolation age. This data uses Equation 4.4 to calculate the length of time cryoconite hole liquid has accumulated solutes within the hole. Two samples impacted by significant freeze/thaw events had disproportionately high Cl^- concentrations leading to overestimated isolation ages (~ 12 years). These overestimated values (encircled in grey) were corrected and represented by new data points (encircled in black). Thus Cl^- is not representative of isolation age in these two cryoconite holes.

80% of cryoconite holes on Commonwealth Glacier were depleted in Cl^- compared to the surrounding glacial ice, which implies that dilute water from internal melt of the glacial surface was able to infiltrate into the cryoconite column through runoff channels at some point during the season. Each of these comparatively dilute samples was collected from lower elevations (~ 140 m a.s.l.) while the one enriched cryoconite hole on Commonwealth was sampled from a much higher surface elevation (292 meters a.s.l.). The

magnitude of subsurface drainage increases closer to the glacial terminus because the catchment area encompasses the majority of the ablation zone. High meltwater flow and a more widespread network of channelization increases the likelihood that cryoconite holes will become hydrologically connected to subsurface drainage.

The extent of glacial surface weathering is also more pronounced at lower elevations due to warmer temperatures, decreased shading from the surrounding mountains, and negligible snow deposition. This increases the porosity of the top ~15 cm of glacial ice and makes cryoconite holes even more susceptible to drainage or channelization. Differences in isolation age with elevation were also observed on Canada Glacier (Table 4.1), where cryoconite holes in the upper sampling region were isolated for a significantly longer period of time than holes on the lower ablation surface (7.52 ± 4.33 >> 0.6 ± 0.1 years; $p= 0.0025$).

Table 4.1- Isolation age calculated by new methods in Equation 4

Glacier	Meltwater isolation age (years)		
	All Cryoconite Holes	Meltpools	Channels
Commonwealth	-0.38 ± 0.9 (5)		
Lower Canada	-0.6 ± 0.1 (3)		n/a (3 fast)
Upper Canada	7.52 ± 4.33 (7)		
Taylor	3.79 ± 3.19 (3)	2.18 (1)	n/a (4 slow)
Wright LG		0.84 ± 0.47 (3)	n/a (2 fast)
Adams	3.48 ± 0 (2)		
Joyce	1.97 ± 0.63 (2)	3.5 ± 1.07 (2)	
All Glaciers	3.24 ± 4.25 (22)	1.95 ± 1.43 (6)	n/a (9)
		Joyce tunnel (1)	Canada Waterfalls (3)
		13.61	n/a

Upper Canada Glacier contained the oldest cryoconite holes out of all glaciers sampled. However, it is worth noting that the three 'oldest' cryoconite samples (indicated by encircled data in Figure 4.6) were all collected during initial melt or significant refreezing periods when the liquid may have had a disproportionately higher solute enrichment. The preferential elution of ions between melting ice crystals causes an 'ionic pulse' of solute-enriched runoff water at the beginning of each melt season. In glacial runoff the magnitude of this pulse wanes over the first ~2 weeks of drainage each summer before runoff water is adequately diluted by the melting of purer 'scavenged' ice. The process is somewhat different in cryoconite holes because melt is directional and absolute; melt deepening occurs evenly throughout the cross-section of the column and does not leave partially-scavenged ice within the liquid pool. In this case the source of the solute pulse is simply the residual 'brine ice' immediately above cryoconite sediment, which represents the degree of enrichment from prior summers that has accumulated in the hole over time.⁴⁷ After cryoconite sediment melts the brine ice it was encased in, it can begin downward melting, and the brine is diluted by the lower Cl^- in underlying ice. Refreezing at the end of the summer will preferentially exclude solutes from the frozen column and the residual brine at the bottom of the hole is now even more enriched another season's accumulation of Cl^- .

Low water volume during extreme freeze/thaw events are occasions when the mass of Cl^- (Equation 4.3) could be a better measure of accumulation than Cl^- concentration. These situations are appropriate when the magnitude of solute-pulse enrichment causes greater overestimation in Equation 4.4 than the degree of underestimation in cryoconite holes deviating from ideal equilibrium state conditions assumed by Fountain et al.³⁴ in

Equation 4.3. Estimates of isolation age calculated by the method of Fountain *et. al.* are included in Table 4.2.

Table 4.2- Isolation age calculated using the method of Fountain *et. al.*³⁴

Glacier	Meltwater isolation age (years)		
	All Cryoconite Holes	Meltpools	Channels
Commonwealth	-2.98 ± 0.67 (5)		
Lower Canada	-3.56 ± 1.29 (3)		n/a (3 fast)
Upper Canada	4.06 ± 4.5 (7)		
Taylor	3.12 ± 4.58 (3)	3.92 (1)	n/a (4 slow)
Wright LG		0.83 ± 0.51 (3)	n/a (2 fast)
Adams	-1.4 ± 1.04 (2)		
Joyce	-0.81 ± 0.75 (2)	4.43 ± 2.16 (2)	
All Glaciers	0.36 ± 4.37 (22)	2.55 ± 2.14 (6)	n/a (9)
		Joyce tunnel (1)	Canada Waterfalls (3)
		171.08	n/a

The estimate calculated by each method was compared to the vertical profiles of cryoconite holes established in Chapter 2. The mean liquid:total depth ratio in cryoconite holes in this study is 0.4, and Fountain's estimates deviate from Table 4.1 the further each hydrologically isolated sample deviates from this ratio. Liquid:total depths above 0.65- 0.7 typically indicate meltpools incapable of melt-deepening, which cannot be estimated by either equation on its own. The hydrologically 'oldest' cryoconite sample in this study (C-23) was collected from Canada Glacier at the very beginning of Season 2 when particularly low water volumes could cause solute-enriched Cl⁻ concentrations in liquid column. However, this cryoconite hole already contained a substantial water depth and a liquid:total depth of precisely 0.4. Fountain's equation produced an estimated age of 13.88 years compared to the 12.43 year age calculated with Equation 4.4. In this case each

equation's assumptions cancelled each other out; the cryoconite melt had already been substantially diluted by a significant degree of melt-deepening and the mass of Cl^- could reasonably be represented by the depth of the total column. Thus the isolation age of that sample was considered a valid estimate and is the longest hydrologically isolated sample in this study.

Two other samples (C-34 and C-35) were collected later in the season after a 13-day period of cloudy weather and snow froze the majority of each cryoconite column. Concentration-based calculations suggest isolation ages of 11.9 and 11.8 years in these samples. The liquid:total depth ratio was 0.1- 0.15, which indicates that the isolation age calculated by Fountain's method (4.8 and 1.3 years) is an underestimation. These samples were compared to cryoconite holes on Canada Glacier that contained similar surface area and total depths. An estimated liquid depth prior to refreezing and comparison of the mass and concentration of Cl^- in each cryoconite hole was used to calculate corrected isolation ages of 5.2 and 4.6 years. These changes are represented by encircled data in Figure 4.6.

No other samples were collected during significant freeze/thaw events. The mean isolation age of cryoconite holes sampled on Canada Glacier during steady weather conditions was 4.13 ± 1.32 years, which is reasonably similar to the estimates discussed above.

Internal melt weathering of the ~15 cm top layer of glacial ice increased ice surface porosity on all glaciers over the season, but the extent of weathering and subsequent late-season drainage was far more extreme on Commonwealth and Wright LG. Cryoconite holes on Canada_T were significantly older than cryoconite holes on Commonwealth ($p= 0.03$) and melt pools on Wright LG ($p= 0.003$), both with or without solute-pulse corrections. There

were no statistical differences between the isolation age of open/ lidded cryoconite holes, cryoconite holes and meltpools, or samples from Season 1/ Season 2.

The englacial ice crystal melt found on Joyce Glacier (C-44) is an anomaly for isolation age estimates. Liquid depth is not an appropriate indicator of total downward melting because the physical characteristics of the pool suggest that the same liquid column is re-melting every year. In cryoconite holes, sediment drives internal melting downwards, but the internal ice temperature gradient determined to drive melting in C-44 would cause radiative heat to spread out in every direction. In this case sublimation of the surface ice would be the primary driver for continued melt and the total liquid depth can be assumed to be 'fixed' based on the penetrative depth of solar radiation. Out of all samples measured, this anomaly is ironically the most representative of the simplified model of cryoconite melting into an equilibrium state proposed by Fountain et. al.³⁴ The isolation age estimated by Equation 4.3 is 171 years. This estimate represents the amount of time it would take for Cl^- to accumulate solely based on exclusion of the solute from the ice layer above the internal pool. However, the dense blue ice exposed on this small region of the glacier's surface is most likely an older layer of glacial ice. This layer could have been left exposed by the uneven movement of younger ice layers sliding over basal layers frozen to the ground. The blue ice layer may have a different Cl^- concentration compared to levels identified in the surface ice on each glacier, so the ice concentration term i cannot accurately represent the content of this unusual layer and the isolation age in this pocket remains unknown.

4.3b Major ions

Br⁻ and Li⁺ were below detection limits in all samples (ND < 1.25 μmol/L and 28.8 μmol/L, respectively). Major ions (F⁻, Cl⁻, NO₃⁻, SO₄²⁻, Na⁺, K⁺, Mg²⁺, and Ca²⁺) are presented in opposing charge balances in Figure 4.7 below. The magnitude of cations was much greater in samples collected from Adams and Joyce Glaciers, so data from those sites were plotted separately in Figure 4.8.

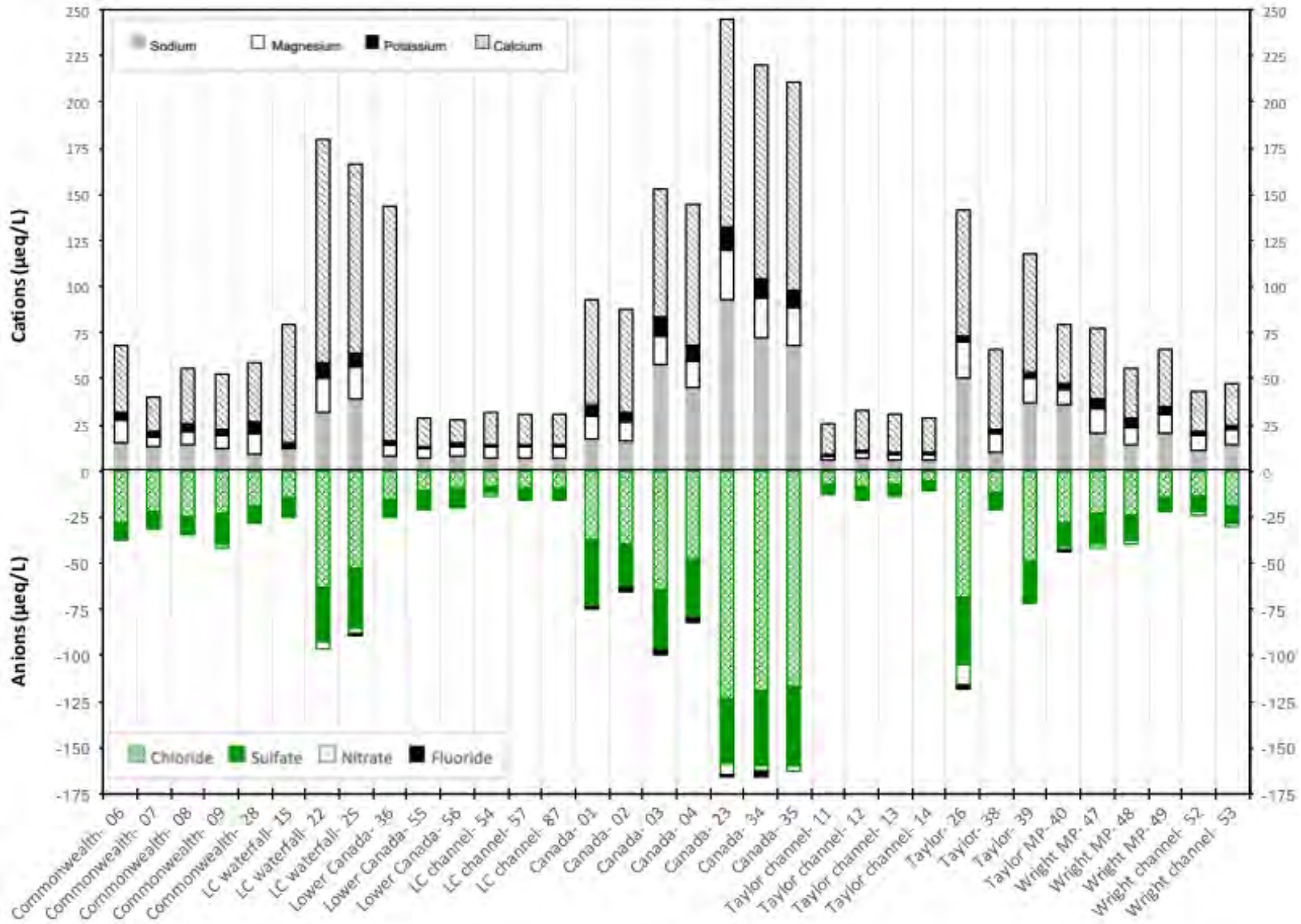


Figure 4.7- Charge balance of subsurface glacial melt in Taylor and Wright valleys.

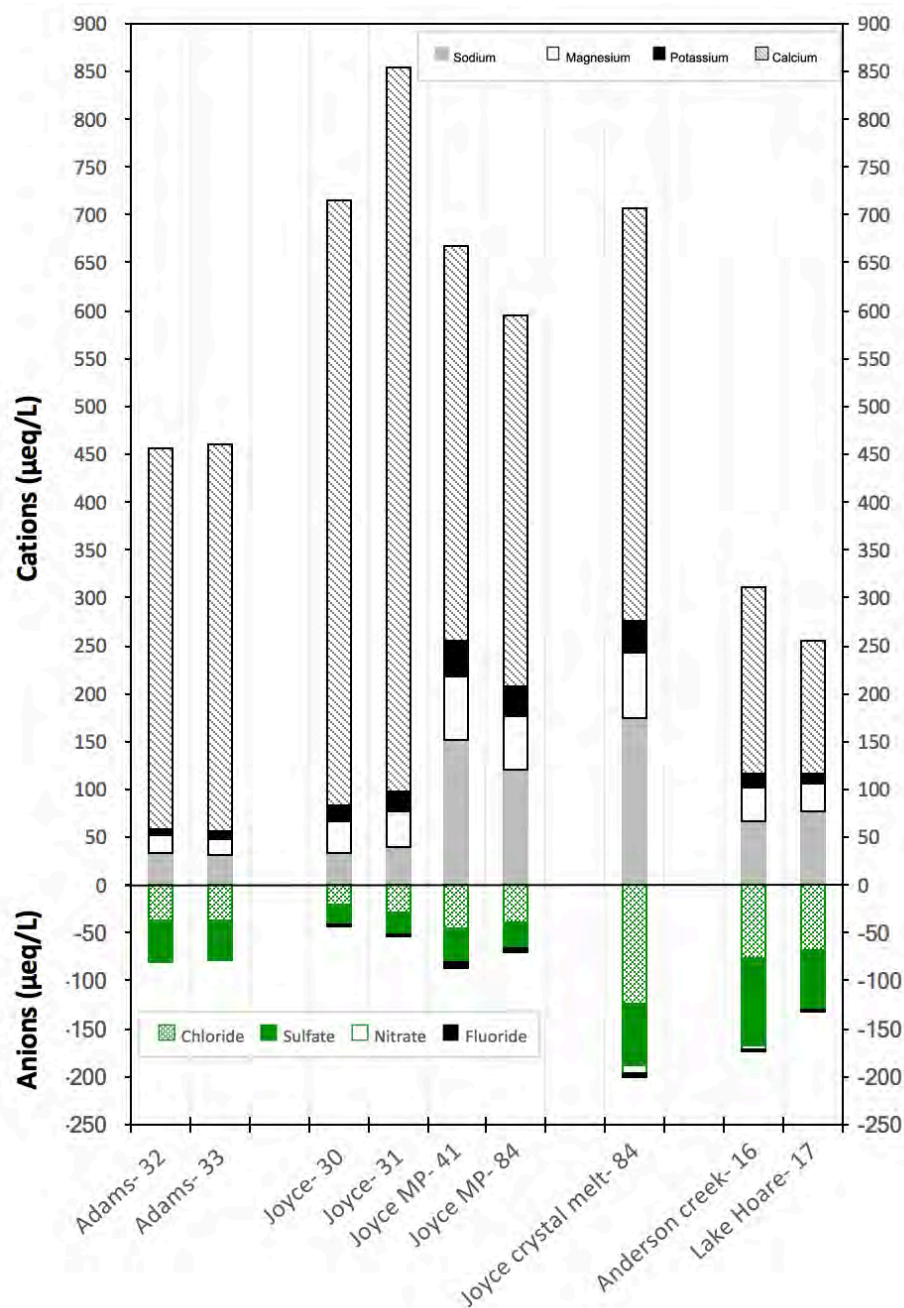


Figure 4.8- Charge balance of subsurface glacial melt in the southern Dry Valleys. Samples from Adams and Joyce Glaciers are contrasted to creek and lake water beneath Canada Glacier, which also exhibited a larger scale than the data in Figure 4.7.

NO_2^- is not displayed in the charge balance graphs above because it represented less than 1% of total anions and was below detection in 61% of samples (ND < 0.057 $\mu\text{mol N-NO}_2^-$). F^- is shown in samples with identified concentrations, but values were below threshold in 66% of samples (ND < 0.54 $\mu\text{mol/L}$).

The charge balance deficit was used to calculate alkalinity in Figure 4.9 below.

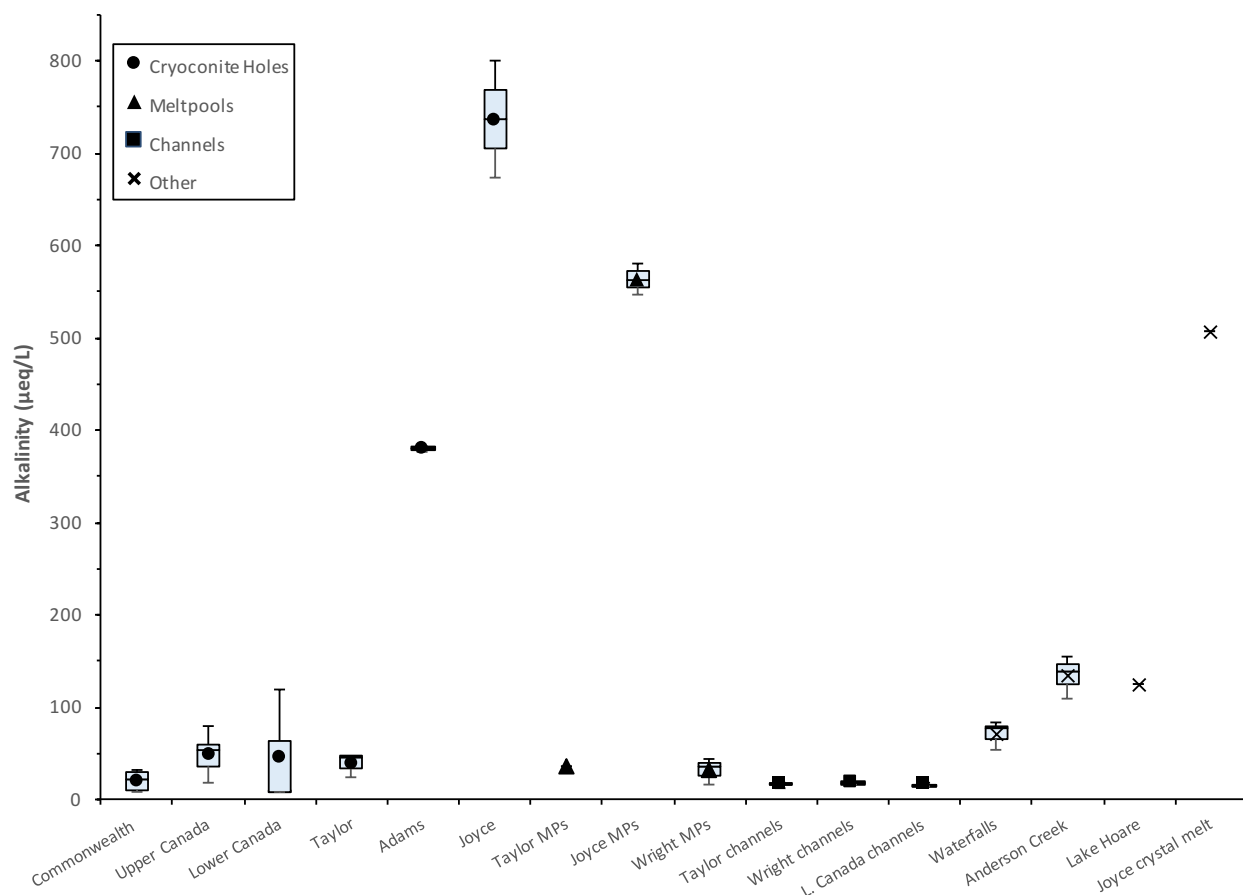


Figure 4.9- Charge balance of subsurface glacial melt in the southern Dry Valleys. Vertical bars span the minimum and maximum values in each category, enclosed columns represent the 1st and 3rd quartiles, and each mean is denoted by a central marker. Categories include both seasons of data.

4.3c The impact of surface elevation on meltwater composition

Cl⁻ was significantly higher in cryoconite holes on upper Canada than the lower ablation surface ($78.41 \pm 39.83 \gg 12.15 \pm 3.18 \mu\text{eq/l}$; $p= 0.004$). This opposes the elevation gradient for marine salt deposition on glaciers and is most likely due to a longer duration of hydrologic isolation in cryoconite holes at higher elevations. However, there was no discernable linear relationship between Cl⁻ and the elevation of individual cryoconite holes. The elevation bands for sampling on lower and upper Canada (80- 122 m and 275- 300 m, respectively) were adequate to compare compositional differences between the two regions, but too narrow to overcome other nuances in Cl⁻ variability between holes in the same elevation band.

Table 4.3- Cl⁻ content of subsurface glacial melt

Glacier	Cl ⁻ (µeq/L)		
	All Cryoconite Holes	Meltpools	Channels
Commonwealth	23.21 ± 3.65 (5)		
Lower Canada	12.15 ± 3.18 (3)		9.06 ± 0.9 (3 fast)
Upper Canada	78.41 ± 39.83 (7)		
Taylor	43.08 ± 28.72 (3)	28.63 (1)	7.21 ± 1.37 (4 slow)
Wright LG		20.19 ± 5.2 (3)	16.61 ± 3.43 (2 fast)
Adams	37.78 ± 0.04 (2)		
Joyce	25.07 ± 5.33 (2)	41.96 ± 3.35 (2)	
All Glaciers	43.47 ± 34.88 (22)	28.85 ± 11.26 (6)	9.91 ± 4.19 (9)
		Joyce crystal melt (1)	Waterfalls (3)
		123.31	43.22 ± 25.63

Glacial ice Cl⁻ decreases with distance from the coast, but cryoconite hole Cl⁻ was higher on Canada than Commonwealth Glacier ($58.53 \pm 45.65 \gg 23.31 \pm 3.65 \mu\text{eq/l}$; $p=0.03$). Commonwealth developed a deeper and more porous weathered crust than Canada Glacier during both seasons. The higher Cl⁻ content on Canada may reflect a longer average isolation age for cryoconite holes on the glacier due to the stability of the surface layer. Taylor Glacier has the lowest glacial ice Cl⁻ but contained cryoconite water concentrations midway between Canada and Commonwealth with no significant differences to either glacier. This suggests that other factors including isolation age may dominate Cl⁻ content on the glacier. There were no differences in Cl⁻ concentration between open and lidded cryoconites, nor cryoconite holes and meltpools. Glacial drainage channels had a significantly lower concentration than cryoconite holes ($9.91 \pm 4.19 \ll 43.47 \pm 34.88 \mu\text{eq/L}$; $p=0.0002$) and meltpools ($9.91 \pm 4.19 \ll 28.85 \pm 11.26 \mu\text{eq/l}$; $p=0.008$) which is

expected since the majority of drainage is derived from near-surface ice that does not accumulate chloride over time.

4.3d Solute enrichment during ionic pulse melt

However, Cl⁻ content was not significantly different for cryoconites or melt pools compared to waterfalls flowing off the side of Canada Glacier. Waterfalls are simply the edge where glacial runoff pours off the terminal face of a glacier and in theory the meltwater chemistry should be the same in both features. The elevated Cl⁻ concentration measured in waterfall runoff can be explained by the seasonal timing of sample collection in this study. Two waterfall samples were collected during the first ten days of glacial melt in Season 2. On December 19th waterfall liquid contained 62.91 µeq/L Cl⁻, which dropped to 52.51 µeq/L by December 28th. During peak flow conditions in mid-summer, waterfall Cl⁻ was 14.24 µeq/L. Surface drainage channels were sampled later in the summer long after the ionic pulse had subsided, and the 9.06 ± 0.9 µeq/l Cl⁻ in Canada Glacier's drainage channels would have closely resembled waterfall concentrations at that time.

The preferential elution of ions between melting ice crystals causes an 'ionic pulse' of solute-enriched runoff water at the beginning of each melt season.⁴⁷ The magnitude of this pulse ebbs over the first ~2 weeks of glacial drainage each summer before runoff water is adequately diluted by the melting of purer 'scavenged' ice. This process is somewhat different in cryoconite holes because melt is both directional and absolute; melt deepening occurs evenly throughout the cross-section of the column and does not leave

partially-scavenged ice within liquid pool. In this case the source of pulse melt is the ice immediately surrounding the cryoconite sediment, which represents the degree of enrichment from prior summers that has accumulated in the hole over time. After cryoconite sediment melts the ice it was encased in, it can begin downward melting and level out to a steady accumulation rate over the rest of the summer.

4.3e Sea-salt adjusted ion concentrations

Prior estimates of chemical composition in glacial ice attribute all chloride and sodium to marine aerosols.⁸⁰ The remaining solutes in meltwater are derived from a combination of marine, atmospheric, lithogenic, and biogenic sources.^{81,82,88} varies on a spatial scale of sea salt on glaciers is relatively constant and a “sea salt corrected concentration” is often used to examine the dynamics of other compounds.⁸⁹ This removes the gradients for marine deposition discussed above (decreasing deposition further from the coast, etc.) in order to examine the influence of non-static factors. Sea salt correction (Equation 4.5) uses the steady ratios of major ions : Cl⁻ in sea water and concentration of Cl⁻ measured in individual melt samples to determine the concentration of each ion that is not derived from marine salts. Sea salt corrected concentrations, also known as non-sea salt (nSS) values, are reported with an asterisk.

$$*X = \left(\frac{[X]_{melt}}{[Cl^-]_{melt}} - \frac{[X]_{marine}}{[Cl^-]_{marine}} \right) \times [Cl^-]_{melt}$$

Equation 4.5- Sea salt correction for major ions in glacial melt

The majority of each ion was derived from non-marine sources (Table 4.4) with the exception of Mg^{2+} , which exhibited a wide variability in nSS-concentration. More than 96% of Ca^{2+} , 98% of F^- and 99% of P-PO_4^{3-} were derived from non-sea salt sources in all samples.

Table 4.4- Mean proportion of each major ion derived from non-marine sources

F^-	SO_4^{2-}	N-NO_3^-	K^+	Mg^{2+}	Ca^{2+}	P-PO_4^{3-}
0.99 ± 0.003	0.82 ± 0.07	0.95 ± 0.06	0.87 ± 0.7	0.48 ± 0.29	0.97 ± 0.01	all >0.99

4.3f Sulfate

* SO_4^{2-} exhibited a linear association with Cl^- with three outlying samples (Figure 4.10). The first outlier is an open cryoconite hole that was the first sample collected during Season 2 when the vast majority of the glacier was frozen. The other two outliers are lidded cryoconites sampled on January 12, two days after heavy snowfall. Again the majority of the glacier was frozen and very little water could be found.

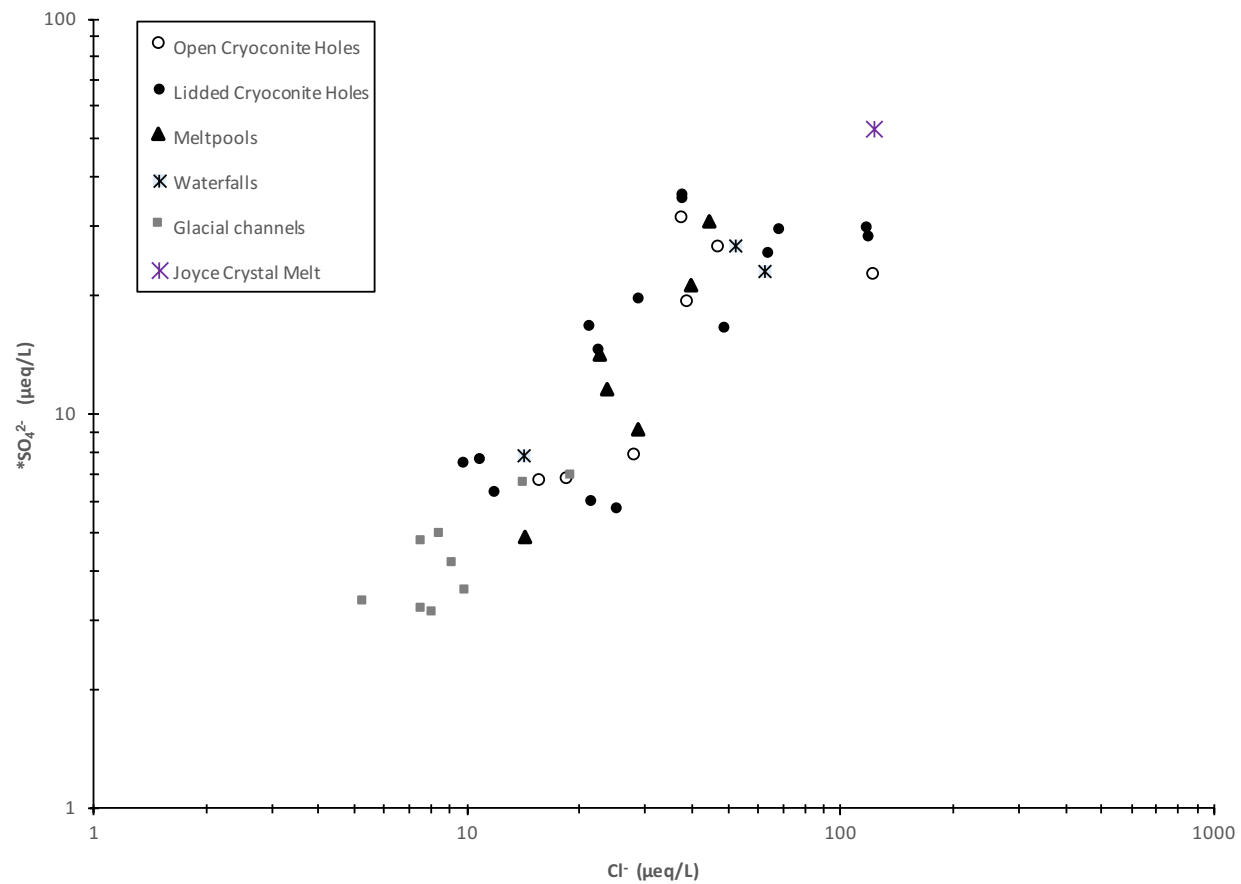


Figure 4.10- Sulfate in subsurface glacial melt. *Sulfate concentrations have been corrected with respect to sea salt.*

4.3g Dissolved Organic Carbon

DOC was extremely low in all samples

4.4 Conclusions

4.5 Supporting Data

Table 4.5- Cl⁻ content of subsurface glacial melt

Glacier	Cl ⁻ (µeq/L)		
	All Cryoconite Holes	Meltpools	Channels
Commonwealth	23.21 ± 3.65 (5)		
Lower Canada	12.15 ± 3.18 (3)		9.06 ± 0.9 (3 fast)
Upper Canada	78.41 ± 39.83 (7)		
Taylor	43.08 ± 28.72 (3)	28.63 (1)	7.21 ± 1.37 (4 slow)
Wright LG		20.19 ± 5.2 (3)	16.61 ± 3.43 (2 fast)
Adams	37.78 ± 0.04 (2)		
Joyce	25.07 ± 5.33 (2)	41.96 ± 3.35 (2)	
All Glaciers	43.47 ± 34.88 (22)	28.85 ± 11.26 (6)	9.91 ± 4.19 (9)
		Joyce crystal melt (1)	Waterfalls (3)
		123.31	43.22 ± 25.63

Upper Canada had significantly higher Cl⁻ than lower regions of the glacier ($p=0.004$). Collectively Canada Glacier contained higher concentrations than Commonwealth Glacier ($p=0.037$) even between similar elevation bands sampled on the glaciers. Both cryoconite holes and meltpools contained higher concentrations than drainage channels ($p<0.008$) but were not significantly different from waterfalls. The explanation for this pattern is discussed in the Cl⁻ results. There were no statistical differences between lidded and unlidded cryoconite holes, cryoconite holes sampled in Season 1 and Season 2, or between cryoconite holes and meltpools. All sampling controls were below detection limits (ND < 0.1 mg/L).

Table 4.6- Sulfate content of subsurface glacial melt

Glacier	<i>*SO₄²⁻</i> (μeq/L)		
	All Cryoconite Holes	Meltpools	Channels
Commonwealth	8.16 ± 3.59 (5)		
Lower Canada	7.29 ± 0.48 (3)		3.62 ± 0.54 (3 fast)
Upper Canada	26 ± 4.15 (7)		
Taylor	17.31 ± 11.49 (3)	9.11 (1)	4.05 ± 0.92 (4 slow)
Wright LG		10.21 ± 4.78 (3)	6.8 ± 0.24 (2 fast)
Adams	35.52 ± 0.61 (2)		
Joyce	18.1 ± 1.98 (2)	25.86 ± 6.72 (2)	
All Glaciers	18.36 ± 10.5 (22)	15.24 ± 9.27 (6)	4.52 ± 1.45 (9)
		Joyce crystal melt (1)	Waterfalls (3)
		52.66	19.13 ± 9.98

SO₄²⁻ is reported in non-sea salt (nSS) concentrations.

Upper Canada had significantly higher **SO₄²⁻* than lower regions of the glacier ($p=0.000015$). Collectively Canada Glacier had higher **SO₄²⁻* than Commonwealth Glacier ($p=0.0038$) even between similar elevation bands sampled on the glaciers. Both cryoconite holes and meltpools contained higher concentrations than drainage channels ($p < 0.036$) but were not significantly different from waterfalls. The explanation for this pattern is discussed in the Cl⁻ results. There were no statistical differences between lidded and unlidded cryoconite holes, cryoconite holes sampled in Season 1 and Season 2, or between cryoconite holes and meltpools. All sampling controls were below detection limits (ND < 0.02 mg/L). **SO₄²⁻* exhibited a linear relationship to Cl⁻ displayed in Figure 4.10.

Table 4.7- Proportion of non-sesalt sulfate

Glacier	*SO ₄ ²⁻ / total SO ₄ ²⁻		
	All Cryoconite Holes	Meltpools	Channels
Commonwealth	0.81 ± 0.12 (5)		
Lower Canada	0.85 ± 0.04 (3)		0.79 ± 0.02 (3 fast)
Upper Canada	0.77 ± 0.09 (7)		
Taylor	0.8 ± 0.04 (3)	0.76 (1)	0.84 ± 0.03 (4 slow)
Wright LG		0.82 ± 0.04 (3)	0.8 ± 0.03 (2 fast)
Adams	0.9 ± 0 (2)		
Joyce	0.88 ± 0.01 (2)	0.85 ± 0.02 (2)	
All Glaciers	0.82 ± 0.09 (22)	0.82 ± 0.05 (6)	0.82 ± 0.03 (9)
		Joyce crystal melt (1)	Waterfalls (3)
		0.81	0.82 ± 0.03

Upper Canada had a lower proportion of nSS-SO₄²⁻ than lower regions of the glacier, although not below $\alpha=0.05$ ($p=0.08$). Collectively the glaciers in Taylor Valley were similar in the proportion of nSS-SO₄²⁻ derived from non-marine sources. Cryoconite holes across Taylor Valley had a lower proportion of nSS-SO₄²⁻ than Adams and Joyce. This indicates a higher influence of [lithogenic and biological] factors on sulfate production/deposition on Adams and Joyce. There were no statistical differences between lidded and unlidded cryoconite holes, cryoconite holes sampled in Season 1 and Season 2, or between cryoconite holes and meltpools.

Table 4.8- *Ca²⁺ content of subsurface glacial melt

Glacier	*Ca ²⁺ (µeq/L)		
	All Cryoconite Holes	Meltpools	Channels
Commonwealth	28.42 ± 6.3 (5)		
Lower Canada	51.12 ± 65.26 (3)		16.64 ± 0.66 (3 fast)
Upper Canada	82.58 ± 26.08 (7)		
Taylor	57.04 ± 12.31 (3)	30.92 (1)	18.78 ± 2.41 (4 slow)
Wright LG		31.22 ± 5.8 (3)	20.8 ± 0.66 (2 fast)
Adams	399.82 ± 5.37 (2)		
Joyce	693.12 ± 87.45 (2)	397.61 ± 17.95 (2)	
All Glaciers	146.84 ± 206.59 (22)	153.3 ± 189.45 (6)	18.52 ± 2.23 (9)
		Joyce crystal melt (1)	Waterfalls (3)
		427.83	94.3 ± 28.28

Ca²⁺ is reported in non-sea salt (nSS) concentrations.

There was no statistical difference in *Ca²⁺ between open/lidded cryoconite holes in Taylor Valley. *Ca²⁺ concentrations were vastly higher in both cryoconite holes and meltpools on Adams and Joyce than all other glaciers ($p < 0.01$). This is most likely an indication of differences in the geologic composition of sediment in Miers and Garwood Valley leading to higher calcium carbonate in cryoconite sediment.

Both Canada and Taylor had higher *Ca²⁺ than Commonwealth Glacier ($p < 0.04$). There was no significant difference in the sediment thickness of cryoconite holes on each glacier, but differences in *Ca²⁺ may indicate differences in the contribution of up-and downvalley winds to the total sediment load in cryoconite holes on each glacier. Upvalley winds will have a stronger influence on sediment deposition on Commonwealth Glacier near the coast than Canada and Taylor towards the west.

Both cryoconite holes and meltpools contained higher concentrations than drainage channels ($p < 0.036$) but were not significantly different from waterfalls. The explanation

for this pattern is discussed in the Cl⁻ results. There were no statistical differences between lidded and unlidded cryoconite holes, cryoconite holes sampled in Season 1 and Season 2 in Taylor Valley, or between cryoconite holes and meltpools. Total Ca²⁺ was used to compare field samples to controls. Sampling controls were all within the range of values recorded for HPLC water and significantly below the mean of the three lowest field samples recorded ($4.17 \pm 1.35 \ll 16.1 \pm 0.03 \mu\text{eq/L}$; $p = < 2.7 \times 10^{-8}$) prior to sea-salt correction of field data.

*Ca²⁺ exhibited a linear relationship to Cl⁻ displayed in Figure 4.10.

Table 4.9- Proportion of non-sesalt sulfate

	*SO₄²⁻ / total SO₄²⁻		
Glacier	All Cryoconite Holes	Meltpools	Channels
Commonwealth	0.81 ± 0.12 (5)		
Lower Canada	0.85 ± 0.04 (3)		0.79 ± 0.02 (3 fast)
Upper Canada	0.77 ± 0.09 (7)		
Taylor	0.8 ± 0.04 (3)	0.76 (1)	0.84 ± 0.03 (4 slow)
Wright LG		0.82 ± 0.04 (3)	0.8 ± 0.03 (2 fast)
Adams	0.9 ± 0 (2)		
Joyce	0.88 ± 0.01 (2)	0.85 ± 0.02 (2)	
All Glaciers	0.82 ± 0.09 (22)	0.82 ± 0.05 (6)	0.82 ± 0.03 (9)
	Canada Waterfalls (3)	Joyce crystal melt (1)	Controls (7)
	0.82 ± 0.03	0.81	n/a

Statistical relationships- Upper Canada had a lower proportion of nSS-SO₄²⁻ than lower regions of the glacier, although not below $\alpha=0.05$ ($p=0.08$). Collectively the glaciers in Taylor Valley were similar in the proportion of nSS-SO₄²⁻ derived from non-marine sources. Cryoconite holes across Taylor Valley had a lower proportion of nSS-SO₄²⁻ than Adams and Joyce. This indicates a higher influence of lithogenic and biological factors on sulfate production/deposition on Adams and Joyce. There were no statistical differences in the proportion of nSS-SO₄²⁻ between open/lidded cryoconite hole or cryoconite holes and meltpools.

Table 4.10- Cl⁻ concentrations in glacial ice in the McMurdo Dry Valleys

Glacier	Cl ⁻ in glacial ice at various surface elevations
Commonwealth	109.8 $\mu\text{mol/L}$ at 126 m ⁸¹ 80.1 $\mu\text{mol/L}$ at 228 m ⁸¹ 35.9 $\mu\text{mol/L}$ at 290 m ⁸¹
Lower Canada (82-100 m a.s.l.)	30.5 $\mu\text{mol/L}$ at 173 m ⁸¹ 50.8 $\mu\text{mol/L}$ for elevations <250 m ⁸¹ Unreported elevations (~82-300m) 9.3 \pm 1.6 $\mu\text{mol/L}$ ⁴⁷ 32 $\mu\text{mol/L}$ ³⁴ 32 \pm 28 $\mu\text{mol/L}$ ⁴⁹
Upper Canada (274-304m)	18.3 $\mu\text{mol/L}$ for elevations 250- 300 m ⁸¹ 9.2 \pm 2.7 $\mu\text{mol/L}$ for elevations 270-295 m ⁴¹
Taylor	1.6 $\mu\text{mol/L}$ average from 198-455 m ⁸¹ 0.96 $\mu\text{mol/L}$ at 324 m ⁸¹
Adams	8.44 $\mu\text{mol/L}$ estimate calculated
Joyce	8.44 $\mu\text{mol/L}$ estimate calculated
Wright LG	11 $\mu\text{mol/L}$ for elevations 315-321 m ⁸⁴

Elevations are reported in meters above sea level (a.s.l.).

No data was available for glacial ice Cl⁻ on Adams or Joyce Glaciers. In order to calculate estimates of Cl⁻ on each glacier, MCMLTER chemistry data from proglacial streams below Adams, Miers, and Garwood Glaciers were compared to samples collected from Anderson Creek and Canada Stream (both below Canada Glacier) on similar sampling dates. The ratio of mean glacial ice Cl⁻ on Canada Glacier to the proglacial streams was 1:14.45. Based on this stream enrichment factor, glacial ice on Adams was estimated to contain 8.44 $\mu\text{mol/L}$ Cl⁻. No streamflow data was available for meltwater beneath Joyce Glacier, but stream chemistry had been analyzed below Garwood Glacier in the same valley. Calculations using the same stream enrichment factor estimate Garwood surface ice to contain roughly 10.17 $\mu\text{mol/L}$ Cl⁻. Joyce Glacier is further inland and at a higher elevation

than Garwood Glacier, so it should contain less Cl^- due to the marine deposition gradients discussed earlier.

Values reported for other glaciers in the same region were examined in order to get a sense of context for the possible accuracy of the stream-enrichment estimate. A study by Williamson et al.⁹⁰ found $4.5 \mu\text{mol/L}$ Cl^- on Blue Glacier, which serves as the high-elevation source glacier for both Adams and Joyce. Additionally, a study by Levy et al.⁹¹ reported Cl^- in the buried ice cliff below Garwood Glacier, with lower bounds $\sim 13.3\text{-}53.3 \mu\text{mol/L}$. Adams and Joyce are beneath Blue Glacier and at a higher elevation more inland than Garwood Glacier, so the boundaries $4.5\text{-}13.3 \mu\text{mol/L}$ are fairly reasonable assumptions. It should be noted that the concentrations reported by Levy et al. are somewhat less comparable than the data for Blue Glacier since Levy examined ice buried beneath sediment layers and not on the ablation surface. However, this value was still useful to form a sense of context for Cl^- values across the valley due to the lack of other data in reported literature. The $8.44 \mu\text{mol/L}$ Cl^- calculated estimate for Adams Glacier surface ice is appropriately within the $4.5\text{-}13.3 \mu\text{mol/L}$ boundaries determined by Blue and Garwood Glaciers. This value is also less than the $10.17 \mu\text{mol/L}$ calculated for Garwood Glacier, so $8.44 \mu\text{mol/L}$ Cl^- was used to represent glacial surface ice concentrations on both Adams and Joyce Glaciers.

Chapter 5

Physical Considerations for the Deposition and Environmental Partitioning of SVOCs in Glacial Meltwater

5.1 Introduction

Antarctica provides a unique environment to study the long-range atmospheric transport of semivolatile organic contaminants (SVOCs) partitioning into liquid in a region far from most anthropogenic sources. Contaminant levels identified in this area are useful in order to gain a better understanding of the reach and magnitude of atmospheric distillation in the Southern hemisphere. SVOCs have been identified in sea water and marine sediments in the Southern Ocean surrounding Antarctica. Biomagnification has been identified in Antarctic food webs, leading to measurable levels of anthropogenic pollutants stored in the lipid layer of penguins, seals, lichens, and other organisms.⁸ Evidence of the long-range transport and deposition of anthropogenic contaminants includes levels of dichlorodiphenyltrichloroethane (DDT), polychlorinated biphenyls (PCBs), and hexachlorobenzene (HCB) identified in Southern Ocean seawater and Antarctic coastal air (Table 5.1) but early studies exhibit wide discrepancies in results, often relied on small sample sizes, and may be affected by a significant degree of analytical error²⁵.

Table 5.1- SVOCs reported in literature

Compound	Env. Medium	Concentration	units	Site	Sampling Period
DDE p,p'	air	0.02- 0.42 ¹⁴	pg/m ³	Norwegian Troll Station	Feb 2007- Dec 2010
DDTs (DDT, DDE & DDD)	air	0.07- 0.4 ²⁰	pg/m ³	Signey Research Station, South Orkney Islands	1994- 1995
DDE p,p'	air	1 ⁹²	pg/m ³	Ross Island	1990
DDT p,p'	air	2 ⁹²	pg/m ³	Ross Island	1990
DDE p,p'	soil	0.03- 3.2 ⁹³	ng/g dry wt	Vostok	1998
DDT p,p'	soil	0.04- 14.9 ⁹³	ng/g dry wt	Vostok	1998
DDTs (DDT, DDE & DDD)	soil	<0.005- 0.02 ⁹⁴	ng/g	James Ross Island	2005
DDTs (DDT, DDE & DDD)	lake/ river sediment	0.1- 1.3 ⁹⁴	ng/g	James Ross Island	2005
HCB	air	10- 80 ¹⁴	pg/m ³	Norwegian Troll Station	Feb 2007- Dec 2010
α- HCH	air	0.2- 0.46 ¹⁴	pg/m ³	Norwegian Troll Station	Feb 2007- Dec 2010
γ- HCH	air	0.1- 0.5 ¹⁴	pg/m ³	Norwegian Troll Station	Feb 2007- Dec 2010
γ- HCH	air	25.8 ⁹²	pg/m ³	Ross Island	1990
α-HCH and γ-HCH	air	3-33 ²⁰	pg/m ³	Signey Research Station, South Orkney Islands	1994- 1995
cis-chlordane	Air	0.02- 0.2 ¹⁴	pg/m ³	Norwegian Troll Station	Feb 2007- Dec 2010
chlordane and nonachlor	air	0.004- 0.9 ²⁰	pg/m ³	Signey Research Station, South Orkney Islands	1994- 1995
PAHs	marine sediment	nd- 11540 ⁹⁵	ng/g	Palmer Station- offshore site of Bahia Paraiso shipwreck	1990
PAHs	soil	800- 86000 ⁹⁵	ng/g	Palmer Station- terrestrial soil (after offshore shipwreck)	1990
PAHs	sediment	nd- 6000 ⁹⁵	ng/g	McMurdo Station	1990-1, 1992-3
PAHs	sediment	up to 13000 ⁹⁵	ng/g	Winter Quarter's Bay (near McMurdo Station)	1990-1, 1992-3
PCB-47	air	0.09- 1.54 ¹⁴	pg/m ³	Norwegian Troll Station	Feb 2007- Dec 2010
PCBs	air	0.02- 17 ²⁰	pg/m ³	Signey Research Station, South Orkney Islands	1994- 1995
PCBs	air	12.1- 92.6 ⁹⁶	pg/m ³	Admiralty Bay	1995- 1996
PCBs	air	15.2 ⁹²	pg/m ³	Ross Island	1990
PCBs	sediment	250- 4300 ⁹⁵	ng/g	McMurdo Station	1991-3
PCBs	sediment	18- 28 ⁹⁵	ng/g	McMurdo Station outskirts; "background" levels	1991-4
PCBs	sediment	2.8- 4.2 ⁹⁵	ng/g	Arthur Harbor, Palmer Station "outskirts"	1991-5
PCBs	limpets	28-76 ⁹⁵	ng/g	Arthur Harbor, Palmer Station	1991-6
PCDDs	air	0.12- 1.8 ⁹⁷	pg/m ³	McMurdo Station	1992- 1994
PCDFs	air	nd- 2.77 ⁹⁷	pg/m ³	McMurdo Station	1992- 1994
PFOA	seawater	15 ⁹⁸	pg/L	Southern Ocean	2010
PFOS	seawater	25- 45 ⁹⁸	pg/L	Southern Ocean	2010

DDT- dichlorodiphenyltrichloroethane, DDE- dichlorodiphenyldichloroethylene, DDD- dichlorodipenyldichloroethane, HCB- hexachlorobenzene, HCH- hexachlorocyclohexane, PAHs- polyaromatic hydrocarbons, PCBs- polychlorinated biphenyls (reported as sum of studied congeners),

*PCDDs- polychlorinated dibenzodioxins, PCDFs- polychlorinated dibenzofurans, PFOA- perfluorooctanoic acid, PFOS- perfluorooctanesulfonic acid. **Many of these reported ranges are biased because only levels above detection were reported, and papers acknowledged a significant number of ND samples. In most cases, it can be assumed that the lower bound is ND.*

The remote conditions on Transantarctic glacial surfaces and relative inaccessibility of advanced laboratory equipment commonly used for trace contaminant measurements (such as solid-phase extraction LC-MS^a) limit the capacity for contaminant analyses conducted in the field. Prior studies have been restricted by data below the detection limit of laboratory instruments. The majority of solid-phase extractions in prior literature were conducted from ship-based measurements of coastal seawater using >20 L of liquid to detect compounds. Comparatively, the liquid volume collected for analysis in Chapter 6 was limited to 1-L samples. No prior data is available to develop a frame of reference for the magnitude or composition of contaminants in Antarctic glacial melt, so values reported in other media were used to estimate the degree of liquid-phase partitioning that may exist in cryoconite holes. It should be stressed that calculated values are *not* assumed to represent actual concentrations in cryoconite liquid. Rather, overall trends are examined because many SVOCs exhibit slow rates of partitioning into liquid layers. Examination of the physical properties of individual contaminants identified in prior literature may provide a sense of scale to determine whether the magnitude of liquid-phase contamination can reasonably be detected by analytical equipment. Many of the calculations used in partitioning models rely on compound characteristics that are highly temperature dependent, so the considerations for model estimates at 0°C are also discussed.

^a LC-MS- liquid chromatography mass spectrometry

5.2 Methods

5.2a Defining cryoconite hole characteristics

Cryoconite holes are small columns of meltwater created by the accumulation of wind-transported sediment on a glacial surface. This sediment has a low albedo and absorbs more solar radiation than the surrounding glacial surface, preferentially melting the ice below to create a cylindrical water-filled hole. Extended periods of high insolation during the summer and elevated ambient air temperatures can provide a narrow seasonal window when the liquid column is open to the atmosphere before refreezing each fall. Other cryoconite holes remain isolated from the atmosphere beneath thick ice lids that do not open during the summer season. The limited timeframe for liquid: air interactions during the ~8-week summer season is an interesting model system to calculate interfacial mass transfer. A two-film gas-liquid passive boundary layer model was used to examine the rate of diffusive flux into fresh meltwater and examine the level of equilibrium obtained before the end of the seasonal timeframe.

Physical data from an unlidded cryoconite hole on Canada Glacier in the McMurdo Dry Valleys was used to represent a 'model' cryoconite hole with defining characteristics outlined in Table 5.2.

Table 5.2- Parameters of a model unlidded cryoconite hole in the Dry Valleys

Cryoconite hole properties	
Water temperature (0°C)	0
Water viscosity (μ in cp) ^a	1.793
Liquid depth (cm)	21.4
Diameter (cm)	24
Surface area (cm ²)	452.4
Liquid volume (cylinder, cm ³)	9681
Interfacial area/liquid volume a_L	0.046731
Vertical dispersion coefficient E_h (cm ² /s) ^b	1.4058
Summer average windspeed (m/s) ^c	3.2
Duration of melt season (days)	56

Mean summer windspeed was determined by a meteorological tower on the ablation surface of Canada Glacier maintained by the MCMLTER. The length of the melt season spans the seasonal timeframe between re-melting of a cryoconite hole in early summer and re-freezing of the liquid column towards austral fall. The presence of ice lids varies each season and is determined by fluctuations in solar radiation and ambient air temperature above the glacial surface. This model limits the analysis to a single melt season and assumes that the cryoconite hole remained open to gas: liquid exchange until refreezing at the end of the season.

There is currently no published data for SVOC concentrations in air or water in the McMurdo Dry Valleys, so compounds and concentrations measured in Antarctic coastal air were used as the baseline for this analysis. Summer concentrations of hexachlorobenzene (HCB), DDT, dichlorodiphenyldichloroethylene (DDE), and polychlorinated biphenyls PCB-31, PCB-52, and PCB-99 were chosen using data from Kallenborn *et al.*¹⁴ in Table 5.3.

Table 5.3- Contaminants in ambient Antarctic air reported by prior studies

Compound	Concentration in coastal air (pg/m ³)	Molec. Weight
HCB	22.9	284.8
PCB-31	0.22	257.55
PCB-52	0.17	291.99
PCB-99	0.04	326.44
DDE	0.44	318.02
DDT	0.42	354.49

Data from coastal air study by Kallenborn et al.¹⁴

This data was chosen due to the critique^{24,99,100} of other data^{22,101,102} reported in literature, particularly regarding the technological feasibility of reporting ppm-ppb levels of contaminants prior to the 21st century. In addition, many 'Antarctic' studies were actually conducted in the sub-Antarctic islands (Auckland, St. George, and South Shetland islands, etc.) far from the continent and with high tourism that may affect contaminant levels.

5.2b Model for diffusive gas-liquid transfer

A two-film model for air-water diffusive transfer was used in this analysis (Figure 5.1).

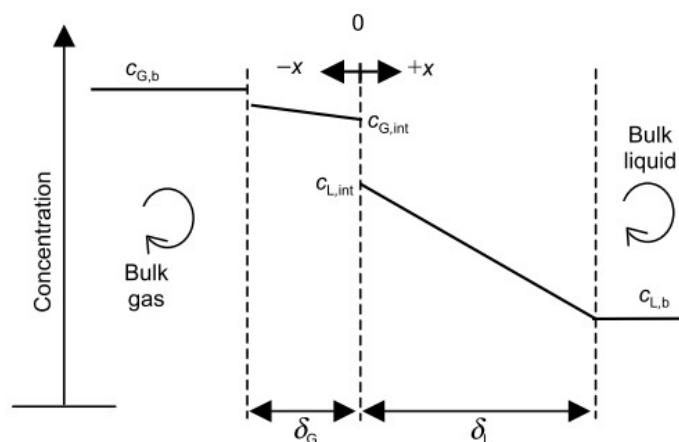


Figure 5.1- Two-film model for interfacial gas-liquid transfer across intermediate boundaries into bulk concentrations. Reprinted from Benjamin and Lawler.¹⁰³

Since this model is designed to estimate diffusive flux into liquid, assumptions and simplifications include ‘pure’ liquid water at the beginning of the melt season and nonreactivity of compounds. The low levels anticipated in these results support use of Henry’s Law estimates for liquid concentration and a lack multiple compound effects on liquid saturation.

5.2c Modification of temperature-dependent calculations for near-freezing conditions

The physical properties of chemicals are most often reported at 20°C or 25°C. Many of these values are temperature-dependent and need to be modified in order to apply to the 0°C liquid temperature in cryoconite holes. Initial values for the diffusivity of HCB, DDT and DDE at 25°C were obtained from EPA values¹⁰⁴ and adjusted to 0°C temperature using Equation 5.1 for air and Equation 5.2 for water. PCB-31,-52, and -99 diffusivities were taken directly from the 0°C levels measured by Hornbuckle et al.¹⁰⁵ and did not need to be temperature-corrected.

$$(1) \quad Dca_{P_2T_2} \cong Dca \left(\frac{P}{P_2} \right) \left(\frac{T_2}{T} \right)^{3/2}$$

Equation 5.1 – Hirschfelder temperature adjustment for diffusion coefficients in air. (Adjusting the diffusion coefficient Dca (cm^2/s) for chemicals in air based on new values of pressure (P_2 , in atm) and temperature (T_2 , in K) compared to initial values.¹⁰⁶)

$$(2) \quad Dcw_{T_2} \cong Dcw \left(\frac{\mu_w}{\mu_{wT_2}} \right) \left(\frac{T_2}{T} \right)$$

Equation 5.2 – Temperature adjustment for diffusion coefficients in water. (Adjusting diffusion coefficient Dcw (cm^2/s) for chemicals in water based on new values of solution viscosity (μ_{wT_2} , in cp) and temperature (T_2 , in K) compared to initial values. Discussed in Logan.¹⁰⁷)

The gas and liquid side mass transfer coefficients were calculated using Equation 5.3 and Equation 5.4.

$$(3) \quad k_g = \left(\frac{Dca}{0.26 \text{ cm}^2 \text{ s}^{-1}} \right)^{\frac{2}{3}} (7U_{10} + 11)$$

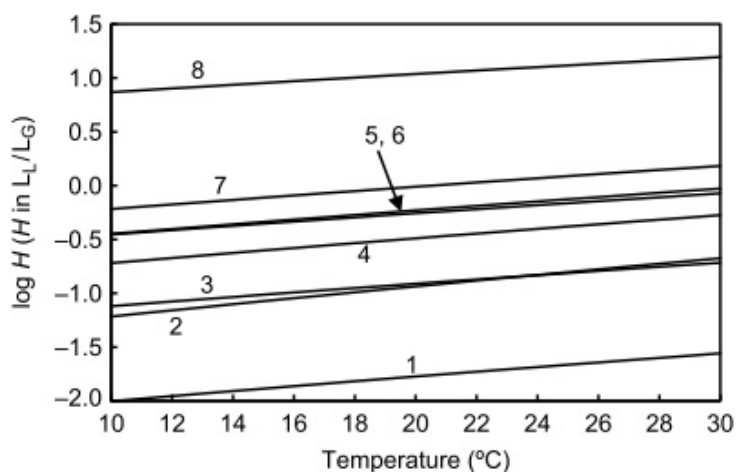
Equation 5.3 – Gas-side mass transfer coefficient estimate for natural water bodies. (k_g in m/hr; See Equation 5.4 for description.)

$$(4) \quad k_l = \left(\frac{Dcw}{2.6 \times 10^{-5} \text{ cm}^2 \text{ s}^{-1}} \right)^{0.57} (0.0014U_{10}^2 + 0.014)$$

Equation 5.4 – Liquid-side mass transfer coefficient estimate for lakes and low-velocity natural waters. (Mass-transfer coefficients for interfacial gas-liquid passive diffusion in environmental conditions, with units k (m/hr), using temperature-corrected diffusion coefficients Dca and Dcw (cm^2/s) and windspeed U_{10} (m/s) 10 m above the water surface. Equations from Schwarzenbach et al.¹⁰⁸ discussed in Nazaroff and Alvarez-Cohen.¹⁰⁹)

Data from a meteorological station on Canada Glacier 2m above the glacial surface was substituted into the traditional U_{10} value in equations 3 and 4, using a reported seasonal average summer wind speed of 3.2m/s.^{34,110}

The Henry's Law constant H for liquid:gas equilibrium varies with temperature (Figure 5.2), and most literature reported H at 25°C. In this paper H is represented as the unitless $H_{l/g}$ unless otherwise noted. Data reported by the EPA¹⁰⁴ and Sander¹¹¹ were adjusted for 0°C conditions with a modified van 't Hoff equation in Equation 5.5.



1: Bromoform; 2: Hexachloroethane; 3: Chloroform; 4: Trichloroethylene; 5: 1,1,1-Trichloroethane; 6: Tetrachloroethylene; 7: Carbon tetrachloride; 8: Dichlorodifluoromethane. *Source:* Based on data in Munz and Roberts (1987).

Figure 5.2- The temperature dependence of Henry's Law constants for several halogenated VOCs. Reprinted from Benjamin and Lawler.¹⁰³

$$(5) \quad H_{T_2} \approx H_{T_1} \times \exp\left[K^* \left(\frac{1}{T_2} - \frac{1}{T_1}\right)\right] \quad \text{where } K = \frac{d \ln(Hcp)}{d \left(\frac{1}{T}\right)}$$

Equation 5.5 – Temperature adjustment to Henry’s Law constants using a modified van’t Hoff equation. Adjusted Henry’s Law constant at a new temperature T_2 (K), using the temperature dependence factor K . H is in units of mol/m³Pa in order to work for appropriate values of K reported in Sander.¹¹¹

The compound-specific values used for temperature dependence factor K were taken from a comprehensive list compiled by Sander.^{17,111} The overall mass transfer coefficient K_L (Equation 5.6) and proportion of liquid-side resistance to gas transfer (Equation 5.7) were then determined.

$$(6) \quad K_L = \frac{k_l k_g H}{k_l + k_g H}$$

Equation 5.6 – Overall gas transfer coefficient. K_L is the combined effect of both sides of transfer across the interfacial boundary represented in m/hr. H is the temperature-corrected unitless Henry’s Law constant $H_{l/g}$.

$$(7) \quad \frac{R_L}{R_{Tot}} = \frac{(k_l)^{-1}}{(k_l)^{-1} + (k_g H)^{-1}}$$

Equation 5.7 – Liquid-side resistance to gas transfer. Liquid-side resistance to gas transfer R_L as a proportion of total resistance R_T . H is the temperature-corrected unitless Henry’s Law constant $H_{l/g}$.

The equilibrium concentration for each compound at 0°C was calculated based on the coastal air concentrations provided by Kallenborn *et al.*¹⁴ in Equation 5.8. This established the concentration gradient necessary to calculate the diffusive flux (Equation 5.9) and rate of diffusive gas transfer (Equation 5.10).

$$(8) \quad c_l^* = c_g^* H_{l/g}$$

Equation 5.8 – Equilibrium liquid concentration. Concentration in liquid c_l in equilibrium with gas (c_g) using Henry's Law constant $H_{l/g}$.

$$(9) \quad J_l = K_L(c_l^* - c_b)$$

Equation 5.9 – Diffusive gas flux into liquid. Flux J (m/hr) uses the overall gas transfer coefficient K_L (m/hr) and calculated equilibrium concentration of gas in the liquid (c_l^* ; $\mu\text{g}/\text{m}^3$).

$$(10) \quad r_{Lgt} = J_l a_l$$

Equation 5.10 – Rate of gas transfer. Rate in ($\mu\text{g}/\text{m}^2/\text{hr}$), using the surface area:volume ratio a_l .

Modifying the overall mass transfer coefficient and surface/volume ratio into a first-order rate constant (Equation 5.11) provided estimates for the liquid concentration of each compound in cryoconite liquid at the end of a 56-day meltwater season. In this case the bulk concentration c_b in water is assumed to be 0 during initial gas transfer.

$$(11) \quad c(t) = c_l^* - c_l^* e^{-K_L a_l t}$$

Equation 5.11 – Concentration in liquid as a function of time. Concentration in liquid ($\mu\text{g}/\text{m}^3$) at time t (hr) using the overall mass transfer coefficient K_L (m/hr) and surface area: volume ratio as a rate constant.

5.3 Results and Discussion

The final concentration of each compound in cryoconite liquid at the end of the 56-day summer melt season is displayed in Table 5.4 below.

Table 5.4- Data for two-film interfacial air: water diffusive transfer model and final summer concentrations

Model results using temperature adjustment parameter K	HCB	PCB-31	PCB-52	PCB-99	DDE	DDT
Formula	C_6Cl_6	$C_{12}H_7Cl_3$	$C_{12}H_6Cl_4$	$C_{12}H_5Cl_5$	$C_{14}H_8Cl_4$	$C_{14}H_9Cl_5$
Diffusivity in Air at 0C (cm^2/s , Eq. 1)	0.048	0.045	0.043	0.041	0.013	0.012
Diffusivity in Water at 0°C (cm^2/s , Eq. 2)	2.70E-06	2.85E-06	2.72E-06	2.60E-06	2.68E-06	2.26E-06
Gas-side mass transfer coef. k_g (m/h, Eq. 3)	10.76	10.33	10.06	9.78	4.45	4.30
Liquid-side mass transfer coef. k_l (m/h, Eq. 4)	0.0079	0.0052	0.0051	0.0050	0.0079	0.0072
Henry's coefficient (Hcc liquid/gas) corrected to 0°C (Eq. 5)	1.6870	0.0712	0.0220	0.0042	0.0342	0.0006
Overall mass transfer coefficient K_L (m/h, Eq. 6)	0.0079	0.0052	0.0050	0.0044	0.0075	0.0018
Portion of resistance in liquid phase; R_l/R_{tot} (Eq. 7)	0.9996	0.9929	0.9774	0.8918	0.9506	0.2512
Concentration in Antarctic coastal air, Kallenborn et al. 2013 (pg/m^3)	22.90	0.22	0.17	0.04	0.44	0.42
Equilibrium concentration in liquid (based on H; pg/m^3 , Eq. 8)	38.6328	1.57E-02	3.73E-03	1.68E-04	1.51E-02	2.35E-04
Flux into liquid J_l ($pg/m/hr$, Eq. 9)	0.3067	8.16E-05	1.86E-05	7.44E-07	1.13E-04	4.24E-07
Rate of diffusive gas transfer ($pg/m^3/hr$, Eq. 10)	0.0143	0.3293	0.0752	0.0030	0.4572	0.0017
Concentration by end of summer season (pg/m^3 after 56 days, Eq. 11)	15.17	4.37E-03	1.00E-03	4.08E-05	5.67E-03	2.52E-05
Percent of equilibrium achieved	39.26	27.88	26.90	24.32	37.65	10.71

The majority of each semivolatile compound remained in ambient air at equilibrium with the exception of HCB. However, the low rate of diffusivity meant that none of the contaminants reached an equilibrium state within the 56-day summer period. DDT exhibited the lowest diffusivity and liquid: gas equilibrium ratio of all compounds. DDE had a similarly low diffusivity, but a liquid: gas equilibrium ratio two orders of magnitude higher than DDT. There is extremely wide variability in the temperature dependence K reported by different sources which affects the estimated Henry's Law constant at 0°C. Calculated estimates were compared to experimentally-derived Henry's Law constants reported for HCB at 0°C,¹¹² PCB congeners at 4°C,¹¹³ and DDT & DDE at 5°C¹¹⁴ from prior literature in Table 5.5.

Table 5.5- Variation in Henry's Law constants

Compound	solubility (mg/L 25°C)	Temp dependence K	H (l/g) at 25°C	H (l/g) calculated with K	H (l/g) reported 0-5°C
HCB	0.0062	6400	0.0269	1.6870	0.0015
PCB-31	0.143	4900	0.0119	0.0712	0.0049
PCB-52	0.0153	3700	0.0126	0.0220	0.0046
PCB-99	0.00366	1900	0.0192	0.0042	0.0061
DDE	0.04	7738	0.0025	0.0342	0.0038
DDT	0.0055	7453	0.0004	0.0006	0.0001

Temperature of reported data for HCB is at 0 °C,¹¹² PCB congeners at 4 °C,¹¹³ and DDT & DDE at 5 °C.¹¹⁴

The difference between final liquid: gas ratios calculated in this model and those reported by experimental studies demonstrates the impact of K on each 0°C estimate. PCB-99 was the only contaminant with a higher liquid: gas ratio in published data compared to model calculations. The calculated Henry's Law constant for HCB was the most dissimilar to experimental values. HCB did not have the largest temperature dependence, but the correction used in Equation 5.5 relies heavily on the magnitude of H at 25°C, and HCB had

one of the broadest ranges of reported values at 25°C to use as a baseline in the model. A second model was run using the experimentally derived 0-5°C ratios in order to test model sensitivity to the variance in each Henry's Law constant. Results of the second model run are shown in Table 5.6.

Table 5.6- Model estimates using low-temperature Henry's Law constants reported in literature

Model results using reported H 0- 5°C	HCB	PCB-31	PCB-52	PCB-99	DDE	DDT
Formula	C ₆ Cl ₆	C ₁₂ H ₇ Cl ₃	C ₁₂ H ₆ Cl ₄	C ₁₂ H ₅ Cl ₅	C ₁₄ H ₈ Cl ₄	C ₁₄ H ₉ Cl ₅
Diffusivity in Air at 0C (cm ² /s, Eq. 1)	0.048	0.045	0.043	0.041	0.013	0.012
Diffusivity in Water at 0°C (cm ² /s, Eq. 2)	2.70E-06	2.85E-06	2.72E-06	2.60E-06	2.68E-06	2.26E-06
Gas-side mass transfer coef. k _g (m/h, Eq. 3)	10.76	10.33	10.06	9.78	4.45	4.30
Liquid-side mass transfer coef. k _l (m/h, Eq. 4)	7.94E-03	5.24E-03	5.10E-03	4.97E-03	7.91E-03	7.18E-03
Henry's coefficient (Hcc liquid/gas) from reported literature	1.49E-03	4.89E-03	4.57E-03	6.05E-03	3.75E-03	7.66E-05
Overall mass transfer coefficient K _l (m/h, Eq. 6)	5.31E-03	4.75E-03	4.59E-03	4.59E-03	5.37E-03	3.15E-04
Portion of resistance in liquid phase; R _l /R _{tot} (Eq. 7)	0.669	0.906	0.900	0.922	0.678	0.044
Concentration in Antarctic coastal air, Kallenborn et al. 2013 (pg/m ³)	22.90	0.22	0.17	0.04	0.44	0.42
Equilibrium concentration in liquid (based on H; pg/m ³ , Eq. 8)	3.42E-02	1.08E-03	7.78E-04	2.42E-04	1.65E-03	3.22E-05
Flux into liquid J _l (pg/m/hr, Eq. 9)	1.82E-04	5.11E-06	3.57E-06	1.11E-06	8.86E-06	1.01E-08
Rate of diffusive gas transfer (pg/m ³ /hr, Eq. 10)	8.49E-06	2.06E-02	1.44E-02	4.48E-03	3.58E-02	4.09E-05
Concentration by end of summer season (pg/m ³ after 56 days, Eq. 11)	9.70E-03	2.77E-04	1.95E-04	6.06E-05	4.72E-04	6.30E-07
Percent of equilibrium achieved	28.38	25.79	25.06	25.04	28.61	1.96

Henry's Law constants were reported for HCB at 0 °C,¹¹² PCB congeners at 4 °C,¹¹³ and DDT & DDE at 5 °C.¹¹⁴

As expected, the concentration of PCB-99 increased in the second model, while all other compounds exhibited lower equilibrium values, lower final concentrations, and a lower rate of equilibrium achieved over the summer season. In other environmental conditions it might be relevant to alter the temperature or surface area data used in a model in order to assess each variable's influence on diffusive transfer, but both the temperature and surface area/volume ratios are relatively constant in cryoconite holes.

5.4 Conclusions

This model was used in order to determine the liquid concentration of atmospheric contaminants in cryoconite holes that could be calculated by diffusive mass transfer. While many assumptions in environmental conditions prevent precise measurement with such a model, the baseline estimates calculated are a useful frame of reference for compounds that may be present above the detection limits of analytical equipment. Air: liquid partitioning is only one route for contaminant transfer into cryoconite liquid and additional sources are likely to contribute to the overall composition in each pool. Snowfall is a major pathway for the transport of organic contaminants in the lower troposphere towards the ground, and snow is a more effective scavenger of hydrophobic contaminants than rain. Many gaseous contaminants can adsorb to the ice interface of snowflakes due to the large surface area of ice crystals and the particular air-ice partition coefficient of individual compounds. In addition, snow scavenges aerosols and aerosol-bound SVOCs.²⁵ Low precipitation (~6-10 cm/year) and high sublimation in the Dry Valleys cause the majority of snow to ablate before reaching the glacial surface, so the impact of snow-scavenging is more difficult to estimate.

There is currently no published data for SVOC concentrations in air or water in the McMurdo Dry Valleys unrelated to localized spill events (which are predominantly analyzed in soil). On both a regional and continental scale it is difficult to assess whether the lack of data is due to a lack of studies or simply a lack of detectable results. Non-detect data is still useful as a frame of reference for the upper boundary concentrations that may exist in samples for the purposes of long-term environmental monitoring. This model estimates extremely low concentrations of semivolatile compounds in cryoconite liquid, but the choice of contaminants used in the model is not ideal. Most contaminant studies conducted in Antarctica are directed towards the detection of specific compounds. Directed analysis is far more feasible from an analytical perspective and a study conducted in coastal air is inherently more likely to test for more volatile compounds. The majority of contaminant studies in Antarctica have been focused on the identification of SVOCs that are particularly prominent in the Arctic. However, the global distillation of semivolatile compounds is a hemispherically divided process and different compounds may dominate the anthropogenic profile in Antarctic media.

A partitioning/ transport model developed by Wania¹¹⁵ assessed the physical changes in four compartments within a snowpack (the interstitial air, liquid water, organic matter, and air-ice interface) to predict the fate of contaminants. As could be expected, the model predicts highly volatile compounds such as chlorobenzenes will quickly evaporate into the atmosphere, more water-soluble compounds such as HCHs will flush out in meltwater, and less volatile hydrophobic chemicals such as DDT will associate with organic matter in the snowpack. Analyses of sea ice melt in both the Arctic¹¹⁶ and Antarctic¹¹⁷ found that while the majority of organic chemicals remained in the dissolved phase of melt

water, compounds with a high soil: water partition coefficient would adsorb to sediment with a substantial fraction of organic carbon. The organic carbon content of cryoconite sediment is likely to vary across spatial scales and varying degrees of biological productivity, and the particular levels are currently unknown. Solid-phase extraction of organic compounds from the liquid and sediment content of cryoconite holes in Chapter 6 may indicate patterns in the compartmental partitioning of contaminants in cryoconite holes.

Chapter 6

Experimental Methods for the Identification of Semivolatile Organic Contaminants in Antarctic Cryoconite Meltwater and Sediment

6.1 Introduction

The long-range atmospheric transport of semivolatile organic contaminants (SVOCs) leads to the preferential deposition and accumulation of many pollutants in the cryosphere. Prior studies have analyzed contaminant levels in Antarctic seawater, marine sediments, and ambient coastal air⁸ in order to determine the magnitude of SVOC transport farther from anthropogenic sources. Glacial meltwater is a particularly relevant substrate to examine the role of glaciers as global contaminant reservoirs and the likelihood of SVOCs to remain in the liquid phase during glacial melting. Despite this, few studies have examined the contamination of meltwater on the Antarctic continent due to logistical limitations, low ambient SVOC concentrations, and the lack of freshwater liquid on most of the continent.

Cryoconite holes are a source of liquid water in the McMurdo Dry Valleys of Antarctica that offer a unique set of environmental conditions to study the extent of anthropogenic distillation in the Southern hemisphere. These holes develop on glacial surfaces when patches of sediment are warmed by solar radiation and melt the underlying ice into small, liquid-filled pools (Figure 6.1).

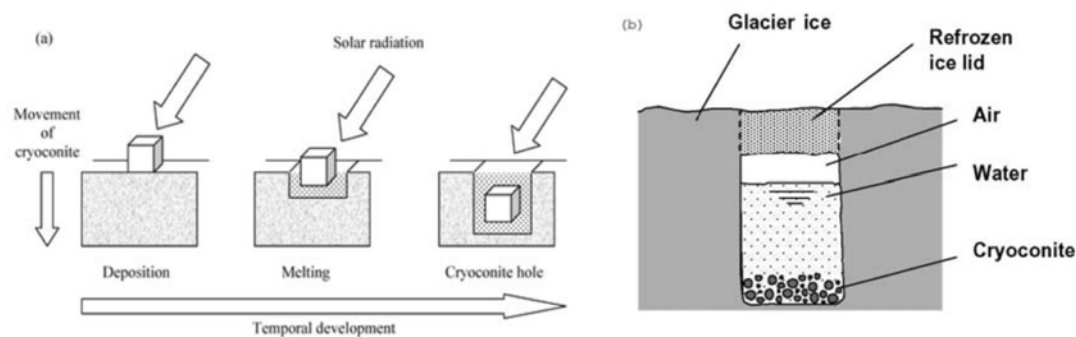


Figure 6.1- Schematic showing (a) the development and (b) the internal structure of a cryoconite hole. Reprinted from (a) Cowan and Tow³³ and (b) Fountain et al..³⁴

Meltwater can only remain in a liquid state during a narrow 6-10 week period of peak solar radiation each summer, after which the column re-freezes in austral fall. Subsequent annual cycles of melting and re-freezing enable cryoconite holes to persist for years. The multi-seasonal age of the meltwater can be estimated by the number of freeze/thaw cycles that preferentially exclude solutes from re-freezing ice. Subzero ambient air temperatures during the melt season cause many cryoconite holes to form ice lids isolating the liquid from gas exchange with overlying ambient air. These conditions could be used to examine differences in anthropogenic contamination as the holes persist over multiple seasons or become increasingly disequibrated with the atmosphere. However, data from coastal ambient air indicates that SVOC deposition on the continent will be extremely low and identification may be constrained by the detection limits of analytical equipment. In this study, cryoconite hole melt was collected and subjected to a series of solid-phase extractions in order to identify persistent organic pollutants and assess the potential role of cryoconite holes as indicators of SVOC deposition in Antarctica.

6.2 Field Methods

6.2a Sample collection

Water was collected from cryoconite holes and other melt features over the November-January austral summers in 2013-14 (Season 1) and 2014-15 (Season 2). The duration of each summer was spent on-site at fieldcamps in Taylor Valley. Season 1 served as a pilot year in which multiple sampling trips were conducted on three glaciers (Canada, Commonwealth, and Taylor) during the peak of the melt season in mid-January. Field sampling was expanded to six glaciers (adding Joyce, Adams, and Wright Lower Glacier) over the full summer in Season 2. Glaciers were chosen based on the observed presence of liquid-filled cryoconite holes, representation of four different dry valleys, and feasible accessibility from the Lake Hoare research fieldcamp at the base of Canada Glacier.



Figure 6.2- Glacier locations in the McMurdo Dry Valleys. *Commonwealth (1) and Canada (2) Glaciers both reside in Taylor valley, in which the larger Taylor Glacier (3) extends from the East Antarctic Ice Sheet. Taylor Glacier's northeastern tongue faces coastal McMurdo Sound. Joyce Glacier (4) in Garwood Valley and Adams Glacier (5) in Miers Valley are both fed by the larger Blue Glacier. Wright Valley is bookended by Wright Lower Glacier (6) towards the coast. Wright Upper Glacier (7) was not sampled in this study but is included in the figure to illustrate the length of Wright Valley. Image rendered from multiple composites using USGS³⁰ source data.*

For the purposes of field sampling, “cryoconite holes” were broadly defined as melt holes in glacial surface ice with a contained shape and no visibly apparent connectivity to surface or subsurface melt channels. Samples needed to exhibit a relatively consistent depth profile; melting downward in a cylindrical shape with perpendicular ice walls and a frozen, level bottom. Additional requirements included a minimum column depth of 6 cm, a diameter less than ~2-3 m, the presence of liquid water, and a bottom layer of sediment in the hole. The term “melpools” (MPs) is used to describe a unique subset of cryoconite holes which appear to have lost the ability to melt-deepen irrespective of surface ablation

rates. Transformation into static melt pools in the Dry Valleys occurs when sediment accumulation reaches a thickness above 2-2.4 cm and begins to insulate the underlying ice from further downward melting. Cryoconites and melt pools were classified as 'lidded' if a distinct, dense ice layer covered a full horizontal cross-section of the column. Holes with cracked or porous lids are not isolated from atmospheric exchange and were considered 'open' in this study. Examples of lidded and unlidded holes are shown in Figure 6.3 below.

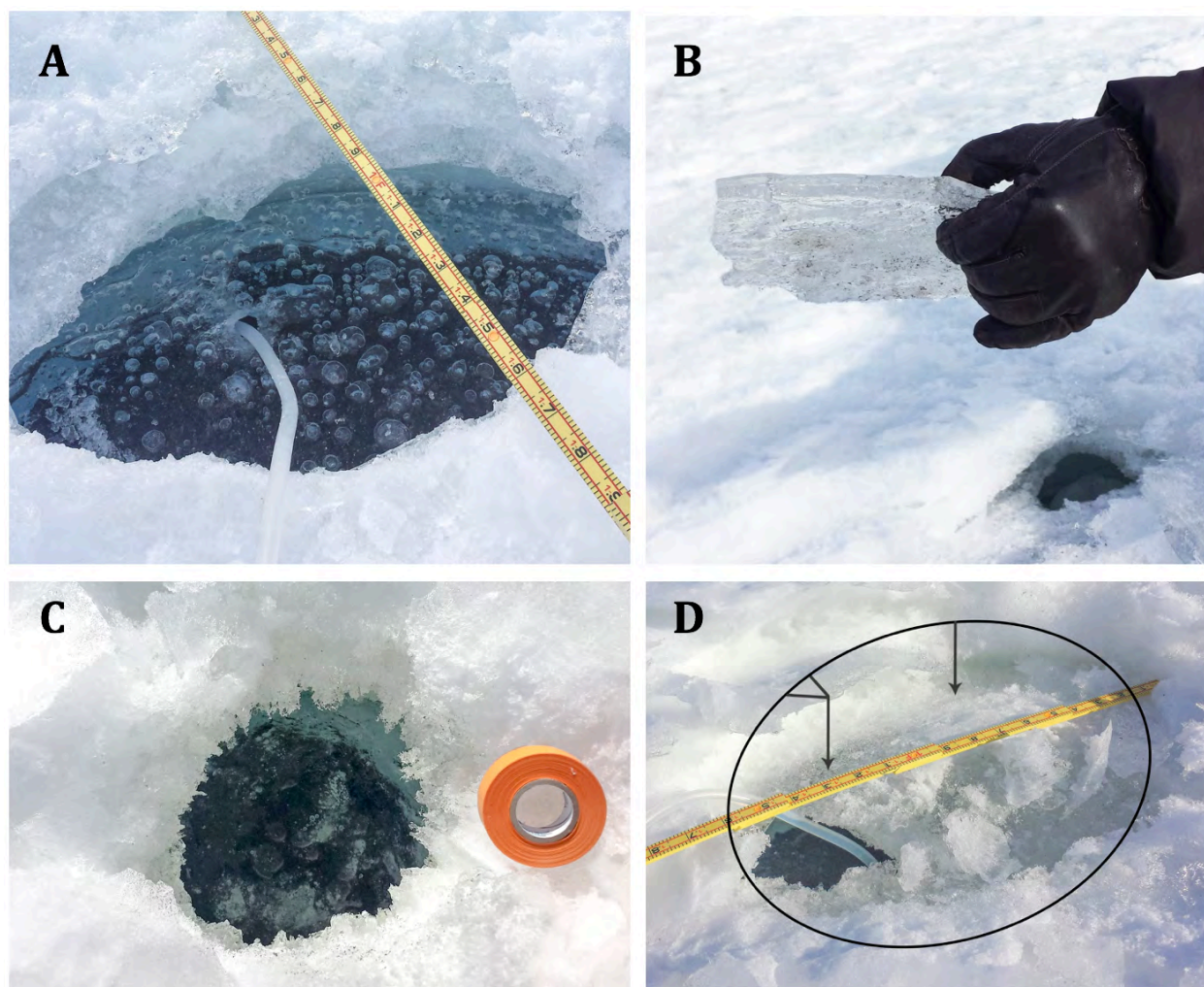


Figure 6.3- Open and lidded cryoconite holes in Taylor Valley. The 45 cm-wide cryoconite hole in image A had a full ice lid 3.3 cm thick that was drilled through to extract the liquid inside. A portion of the lid is held up in image B. The cryoconite hole in image C contains small slivers of floating ice but is still fully open to the surface. Internal melt 'weathering' of the ice lid in image D has transformed the once-thick lid into a low density, porous layer open to gas exchange.

Glaciers were accessed both on-foot and with helicopter assistance. No samples were collected within 100 m of helicopter landing sites and all sampling locations were recorded by handheld GPS (Garmin GPS-map 76). The water analyzed in this study is a subset of the liquid volume collected from cryoconite holes in Chapter 4. Sample selection prioritized meltholes containing at least 1.5L of water for analysis but was randomized beyond these parameters. Additional samples were collected from meltwater runoff channels on glacier surfaces, waterfalls flowing off the side of Canada Glacier, and water from Anderson Creek and Lake Hoare beneath Canada Glacier. These characteristics of features are described in greater detail in Chapter 2 and 4.

Once an appropriate cryoconite hole was identified on a glacier, 1.5- 2L of water was removed using indirect suction from a hand-pump device while taking care not to disturb the cryoconite sediment at the bottom of each hole. Water was 'overpoured' to the upper brim of a brand new, pre-furnaced 1-L amber borosilicate glass bottle and capped in order to avoid the presence of air bubbles and volatilization of compounds into bottle headspace. All glass collection bottles used in field sampling were new Wheaton 1-L amber borosilicate glass bottles that were pre-furnaced at 500°C for 5 hours and sealed with new polypropylene caps. During Season 1, meltwater was collected through platinum-cured silicone tubing into an Erlenmeyer flask using indirect suction from a side-arm hand pump. The pump manifold and flask were triple-rinsed with water from each cryoconite hole/melt feature before collecting water for analyses, and subsequently rinsed 3x with DI water after each glacial trip. Field sampling began earlier in the summer during Season 2 when ambient air temperatures were colder, and the collection method was changed due to near-

instantaneous freezing of liquid in the silicone tubes. All samples from cryoconite holes and meltpools in 2014-15 were collected with a hand-roller pipette pump using sterile disposable 25 mL polystyrene serological pipettes triple-rinsed in water from the melthole before collecting water for analyses.

In most cases the ice lids on meltholes could be cracked open with a 3x-rinsed sediment spatula in order to collect the underlying water. On the rare occasion (<10%) when a metal ice screw was necessary to drill through an ice lid, the screw was pre-rinsed with high-performance liquid chromatography (HPLC)-grade water carried onsite in a pre-furnished amber borosilicate bottle. Particular care was taken to prevent the screw from contacting the underlying meltwater in a hole, and use of the screw was included in field notes.

Cryoconite sediment was collected into sterile polyethylene whirlpack bags using a metal spatula triple-rinsed in cryoconite water. If the remaining water in the cryoconite hole was too deep to collect sediment without submerging a hand into the water, the hand was covered by an additional sterile whirlpak bag turned inside-out (so the sterile side was on the outside) and used as 'sterile glove' reaching into the water to avoid contaminating the water and sediment. Sediment sampling was always conducted after the water sample was collected to minimize the influence of these additional factors on water collection.

Once cryoconite water was collected on a glacier, the physical characteristics (cryoconite hole dimensions/depth, water volume, site elevation, thickness of ice lids present, etc.) and chemical properties (pH, conductivity, and temperature of the water) were measured. Upon return to the field laboratory, all water samples were stored in a 2-4°C refrigerator, and sediment samples were frozen at -20°C. Samples remained in

temperature controlled conditions throughout transport from Antarctica until analyses were conducted in the United States.

6.2b Field sampling controls

Method controls were conducted intermittently throughout each season using high-performance liquid chromatography (HPLC)-grade water. For each primary control, HPLC water was poured into a new, pre-furnaced borosilicate amber glass bottle which served as a surrogate cryoconite hole. The water was then syphoned out of the surrogate melthole according to the methods described above and poured into a new collection bottle.

Although all field samples in Season 2 were extracted with seriological pipettes, additional controls in 2014-15 were conducted using the original hand-pump manifold to compare both methods in the same field conditions at the same times. An additional set of controls used HPLC water poured directly into 1-L pre-furnaced bottles to compare each control set and identify possible contamination from sampling methods.

6.2c Analytical strategies

While one of the primary objectives of this study was to determine possible contaminant deposition in glacial cryoconite meltwater in Antarctica, the low concentration of semivolatile contaminants identified in coastal studies suggest that levels of deposition on glaciers may be below the detection limit of analytical equipment. Ship-based measurements of contaminants in seawater often used >20L of water for each sample^{14,99,118} followed by various methods of solid-phase extraction (SPE) for detection of trace contaminants. Since the volume of water in cryoconite holes is often limited to <2L, a strategy of 1-L sample collection followed by subsequent solid-phase extraction and

detection via gas/liquid chromatography with mass spectrometry back in the United States was determined based on the advice of Dr. Mike Thurman at the University of Colorado and Dr. Shane Snyder at the University of Arizona Lab for Emerging Contaminants (ALEC). Although a time delay between sample collection in Antarctica and analysis in the US could possibly result in further transformation/degradation of contaminants in each sample, laboratory conditions available at McMurdo Station are not suited for trace contaminant studies. Collaborators supported the decision to analyze cryoconite samples in a US laboratory designed for trace contaminant studies, assuming that the relatively persistent nature of contaminants reaching Antarctica and consistent storage in 2-4°C/ -20°C would permit for a short delay before analysis.

The major use of analytical equipment was carried out with the support of three collaborations vital to this project. These consisted of the measurement of basic water chemistry characteristics carried out by the MCMLTER as discussed in Chapter 4, three weeks of on-site training and equipment access granted by Dr. Shane Snyder and the Arizona Lab for Emerging Contaminants (ALEC) in 2014, and a research collaboration with Dr. Craig Marvin, Dr. Tarun Anumol, and the Environmental Methods Development group at Agilent Technologies in Wilmington, Delaware 2015-17. Methodological training and use of both gas and liquid chromatography-mass spectrometry for the analysis of glacial melt and sediment samples were completed during two 3-week trips to Agilent's facilities in 2015 (water) and 2017 (frozen sediment). Furthermore, the long-term monitoring of meteorological and hydrologic data by the McMurdo Long Term Ecological Research program offered an extensive database of supporting data for this research.

6.3 Cryoconite Water Extractions

6.3a Solid-phase extractions after Season 1

15 samples collected during the 2013-14 season were analyzed at the Arizona Lab for Emerging Contaminants. Water was separated into two analyses; 250 mL was used in a broad analysis for organic contaminants using liquid chromatography with an Agilent 1290 Infinity and 6550 QTOF-MS^b. The other 250 mL was used in a targeted analysis for PFCs (perfluorinated compounds) by liquid chromatography- tandem mass spectrometry (LC MS/MS) with a an Agilent 6460 triple quadrupole mass spectrometer.

Samples in the general organics analysis were spiked with a solution of 19 isotopically labeled organic contaminants at 50 ng/L as internal standards, using the trace organic contaminants IS solution outlined by Anumol *et al.*¹¹⁹ Solid-phase extraction was conducted with a Dionex Autotrace 280 using methanol and methyl tertiary butyl ether (MTBE) as solvents. Oasis 6-cc 150mg hydrophilic-lipophilic bonding cartridges were preconditioned with 5 mL MTBE^c, followed by 5mL methanol and then 5 mL ultrapure water. The 250mL aliquots of meltwater were filtered through the cartridges at 15mL/min and discarded. Cartridges were rinsed in ultrapure water and dried under low-flow nitrogen for 30 minutes, then eluted with 5 mL methanol followed by a 5 mL solution of 10/90 v/v methanol/MTBE. Extracts were evaporated down to 0.5mL with a TurboVap LV evaporator in a 25°C water bath under 10psi nitrogen flow with an LC/MS-grade nitrogen purifier. At ~0.5mL the inside of the glass vials were rinsed in methanol (bringing the volume back to ~3mL), then evaporated back down to 0.5mL and transferred to 2mL glass

^b QTOF-MS- quadrupole time of flight mass spectrometer

^cMTBE- methyl tert-butyl ether, PFOA- perfluorooctanoic acid, PFOS- perfluorooctanesulfonic acid, PFBA- perfluorobutanoic acid

amber scintillation vials. Each extraction run was accompanied by a method blank using DI water for quality control, and all vials were stored at 4°C until analysis.

The 250 mL water samples for targeted PFC analysis were spiked with 25 µL of a 0.1 ppb solution of nine isotopically labeled PFCs, outlined in Table 6.1.

Table 6.1- Isotopically labeled PFCs used as internal standards

Isotopically labeled PFCs
18O2-Perfluorohexylsulfonate (PFHxS*)
13C4-Perfluorooctylsulfonate (PFOS*)
13C4-Perfluorobutanoate (PFBA*)
13C2-Perfluorohexanoate (PFHxA*)
13C4-Perfluorooctanoate (PFOA*)
13C5-Perfluorononanoate (PFNA*)
13C2-Perfluorodecanoate (PFDA*)
13C2-Perfluoroundecanoate (PFUnA*)
13C2-Perfluorododecanoate (PFDoA*)

Samples were then extracted to a 500x concentration factor using a Dionex AutoTrace 280 as described above with Oasis 500 mg WAX cartridges. Cartridges were preconditioned with 4 mL methanol solution with 0.1% ammonium hydroxide, followed by 4 mL methanol and 4 mL ultrapure water. followed by 5 mL methanol and 5 mL ultrapure water. Samples were filtered through the cartridges at 15 mL/min, after which the cartridges were rinsed with 4 mL of a pH 4 buffer (1.27 g glacial acetic acid and 0.51 g sodium acetate/ L DI water) followed by 4 mL methanol. Cartridges were eluted with 4 mL methanol- 0.1% ammonium hydroxide solution and evaporated using the methods described above. A 250 mL method blank was included in each extraction procedure (including the internal standards) in order to assess measurement efficiency. A 10-pt

calibration curve for PFCs was made using 0.1- 100 ppb concentrations of a native PFC stock in methanol and spiked with the internal standards.

6.3b Solid-phase extractions after Season 2

Analysis after the 2014-15 season was carried out at Agilent Technologies in Wilmington, Delaware. The SPE extracts from ALEC were also shipped to Agilent for further analysis. The Season 1 extracts had been stored in a -4°C freezer (in methanol solution) and were transferred to -4°C freezers at Agilent. Solid-phase extraction of the Season 2 samples was carried out manually with a vacuum pump at 15 mL/min. Extraction followed the same procedures as during Season 1 (same solvents, cartridges, etc.) but without the automated Dionex system. Water was separated out for 250mL general organics analysis and 250 mL PFCs analysis and the same internal standards were used. The only methodological difference is that cartridges were dried by pulling air through the vacuum pump for ~30 minutes under a fume hood rather than drying with nitrogen in the Dionex. Nitrogen evaporation of eluents was performed with the same methods described for Season 1.

6.4 Sediment Extractions

All sediment samples (both seasons; 43 samples total) were stored frozen at -20°C to limit any microbial activity before analysis. The sediment whirlpaks were thawed gently in a 2C° refrigerator over 48 hours at the University of Colorado in 2016. An ethanol/flammesterilized scoopula was used to transfer 2g of thawed sediment into DNA vials for a separate microbiological analysis in collaboration with Pacifica Sommers and the Schmidt laboratory at the University of Colorado. The remaining sediment was then divided

between two 40mL glass amber vials for each sample, dried at 30-35°C in a dehydration oven, and capped with polypropylene lids.

Soil extraction and analysis was conducted at Agilent Technologies in early 2017. Small 2.5g samples were measured out into 15 mL polypropylene centrifuge tubes. The exact sediment weight of these 2.5g portions were recorded to the μg level in order to adjust final analyses accordingly. Each sample was spiked with the internal standards (IS) outlined in Table 6.1, but in this case the concentration of each IS was 400 ng/kg of sediment. This was back-calculated for the actual ng/kg sediment after LC-MS/MS using the sediment weights recorded. Of the 43 samples, 10 were used for duplicates and another 10 were conducted in triplicate. Eight control samples were created using sterilized Ottawa sand (BDH Analytical fine granular silicon dioxide, calcined for analysis) as the sediment substrate and subjected to the same methods discussed above. A set of PFC standards (non-isotopically labeled target compounds) were added to select samples and are listed in Table 6.2. One of each triplicate sample was spiked with a mid-range level of target PFCs (0.1 ng/g each compound), and one of each triplicate was spiked with a higher level of the target PFCs (5 ng/g) based on ranges used in the calibration curve discussed below. Four of the Ottawa sand samples were used for low- and high spikes. All of these samples included an internal isotopically labeled spike.

Table 6.2- PFC standards

Target PFC Standards
Perfluorobutylsulfonate (PFBS)
Perfluorohexanoate (PFHxA)
Perfluorohexylsulfonate (PFHxS)
Perfluorooctanoate (PFOA)
Perfluorooctylsulfonate (PFOS)
Perfluorononanoate (PFNA)
Perfluorodecanoate (PFDA)
Perfluorododecanoate (PFDoA)
Perfluorobutanoate (PFBA)
Perfluoropentanoate (PFPeA)
Perfluoroheptanoate (PFHpA)
N-Methyl-perfluorooctane sulfonamido acetic acid (N Me-FOSAA)
Perfluorotridecanoate (PFTrDA)

After separating the sediment, 10 mL of methanol:water (50:50) was added and vortexed for 1 minute. After vortexing, the pH of the samples was adjusted pH ~ 9-10 with 20 μ L ammonium hydroxide and vortexed again for 1 minute. The sample tubes were tumbled on a rotator for 1 hour, then centrifuged at 1900 rpm for 20 min. The supernatant was then separated out carefully so as not to extract the centrifuged sediment; 500 μ L was pipetted into 2 mL amber vials for storage, and 7 mL was evaporated down to 0.5mL using the nitrogen evaporation methods described above and transferred into 2 mL vials. The remaining sediment and soil in each tube was discarded. Eight lab blanks; 4 of ultrapure water and 4 in methanol:water, were included in analysis after the extraction step. Out of

each set of four, the PFC standards and internal (isotopic) standards were added to one sample, the second sample was only spiked with the isotopic standard, and the remaining two did not have any additions. The PFC standards were also used to create an eight-point calibration curve from 0.05 ppb to 10 ppb.

6.5 Liquid Chromatography

Liquid chromatography of the general organics samples was performed with an Agilent 1290 Infinity and 6550 QTOF-MS. Initial examination from ALEC after Season 1 was inconclusive, so these extracts were included with the Season 2 analysis at Agilent, adhering to the LC-QTOF instrument guidelines of Moschet *et al.*¹²⁰ Subsequent analysis of chromatograms was performed using the “unknown trace micropollutants” method in MassHunter Qualitative Analysis software described by Moschet *et al.*¹²¹

Liquid chromatography for the PFC extracts was performed with an Agilent 1290 LC and Agilent 6460 triple quadrupole mass spectrometer using the method described in Anumol *et al.*¹¹⁹ and the ASTM standard method for PFCs in water (D7979-15).¹²² Sediment analysis for PFCs the following year was conducted following the analytical guidelines outlined in the ASTM standard method for PFCs in sediment (D7968-14).¹²³

6.6 Results

The original analysis at ALEC was inconclusive; no data could be teased from the general organics method, but there were peaks within the noise of the PFC chromatograms that suggested there may be trace, unquantifiable PFCs in the water. The water analysis on all extracts at Agilent the following year was more sensitive, but still unquantifiable. The LC-QTOF is better suited for analysis of “unknowns”, but compound identification is still

much more difficult without very defined search parameters. Targeted analyses for specific compounds is the most efficient way to identify contaminants, followed by a broader “suspect screening”, while unknown compound identification is the least sensitive. This is why the vast majority of Antarctic contaminant studies (100% of the studies found in the research for this thesis) used a targeted analysis as discussed in Chapter 5. Data from the LC-QTOF was run through the available contaminant libraries with no conclusive results. The chromatogram for sample 36 is shown in Figure 6.4.

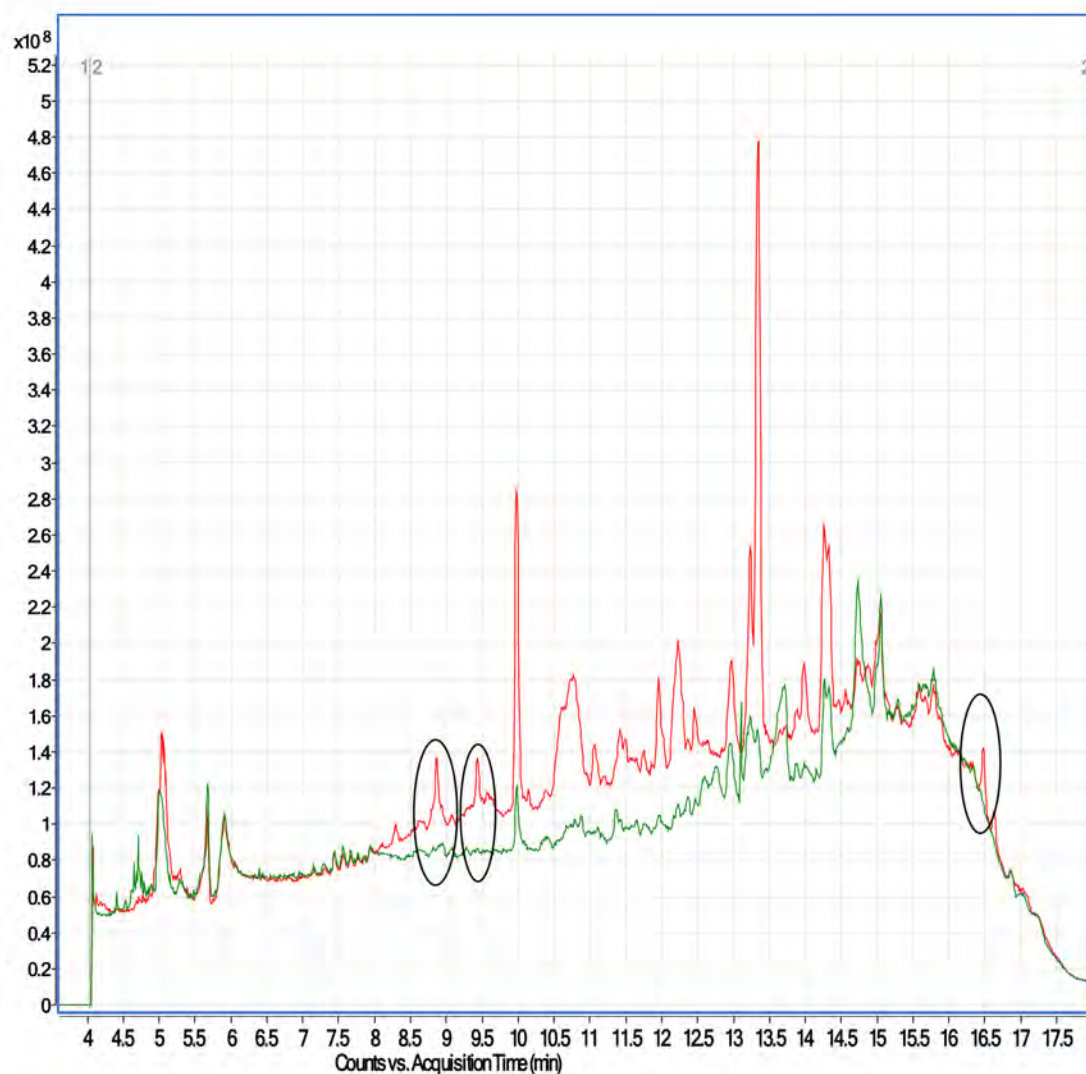


Figure 6.4- Total ion chromatograms for Canada Glacier cryoconite hole 36. *Sample 36 is indicated by the red line, while the green line represents one of the field sampling controls collected through the meltwater pump in Antarctica. The three circled areas represent potential peaks of interest that have no corresponding peak in the field control. These fragments are most likely to be one of a variety of different hydrocarbon chains, but the data is not distinct enough to determine the particular compounds.*

Water data for the PFCs was likewise inconclusive, but did show more distinct differences. The soils analysis was targeted for PFCs in order to provide a better sense of accuracy to results, and with the working hypothesis that these compounds may sorb to cryoconite sediment at the bottom of the water column due to their relative

hydrophobicity. A few example chromatograms are shown in the following pages; displaying the results of eight targeted PFC analyses both before and after each data set was corrected from method blanks and field sampling controls.

Field sampling controls are displayed on the first row, followed by the lowest concentration of each PFC standard (0.05ppb) used to create the 8-point calibration curve. Four cryoconite samples are then included for comparison. Cryoconite sample 36 was an unlidded cryoconite hole on lower Canada Glacier sampled mid-season during Season 2 with an average depth and diameter among samples and a 1.3 cm sediment layer. Samples 49 and 48 were both lidded melt pools collected from Wright Lower Glacier with a thick, 3 cm sediment layer. When sediment was collected from these larger, ovular shallow pools, a significant amount of bubbles were released from the layer, which may be due to microbial activity. These two samples had the lowest pH values recorded in cryoconite water onsite (5.2-5.3), which equilibrated to pH 6.4 a week later when they were re-measured at McMurdo Station. These details are discussed in more depth in Chapter 4. Sample 28 was a cryoconite hole on Commonwealth Glacier which contained an unusually glutinous/ sticky sediment layer and quarter- to dime-sized portions of what appeared to be black algal mat or other black organic matter. It was the only cryoconite hole sampled during either season where this material was observed. The last row shows one of the other triplicate samples from C-28, in which 0.1ppb of each target PFC standard was added to the sample. This provided a frame of reference for where the peaks should be in a chromatogram, along with any additive effects between the field sample itself and the target standard in it.

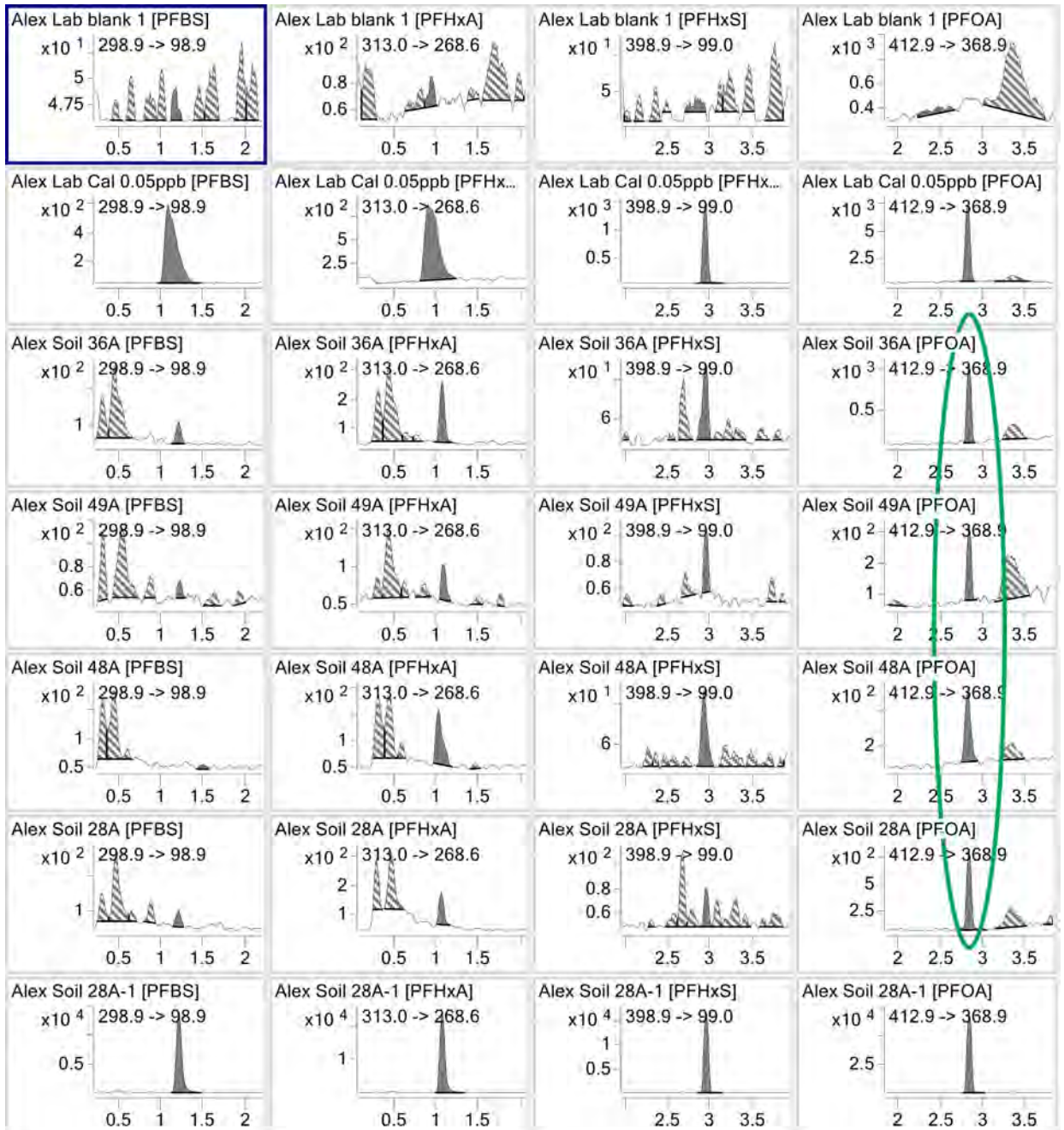


Figure 6.5- PFCs in sediment before correcting for field, method, and target controls, part 1. The top row of this chart represents field sampling controls conducted in Antarctica, followed by 0.05 ppb calibration standards and four cryoconite hole sediment samples described above. The final row displays a cryoconite sample in which a 0.1ppb standard of each PFC was spiked into samples in order to identify similarities between peaks in in un-spiked (28A) and spiked (28A-1) samples.

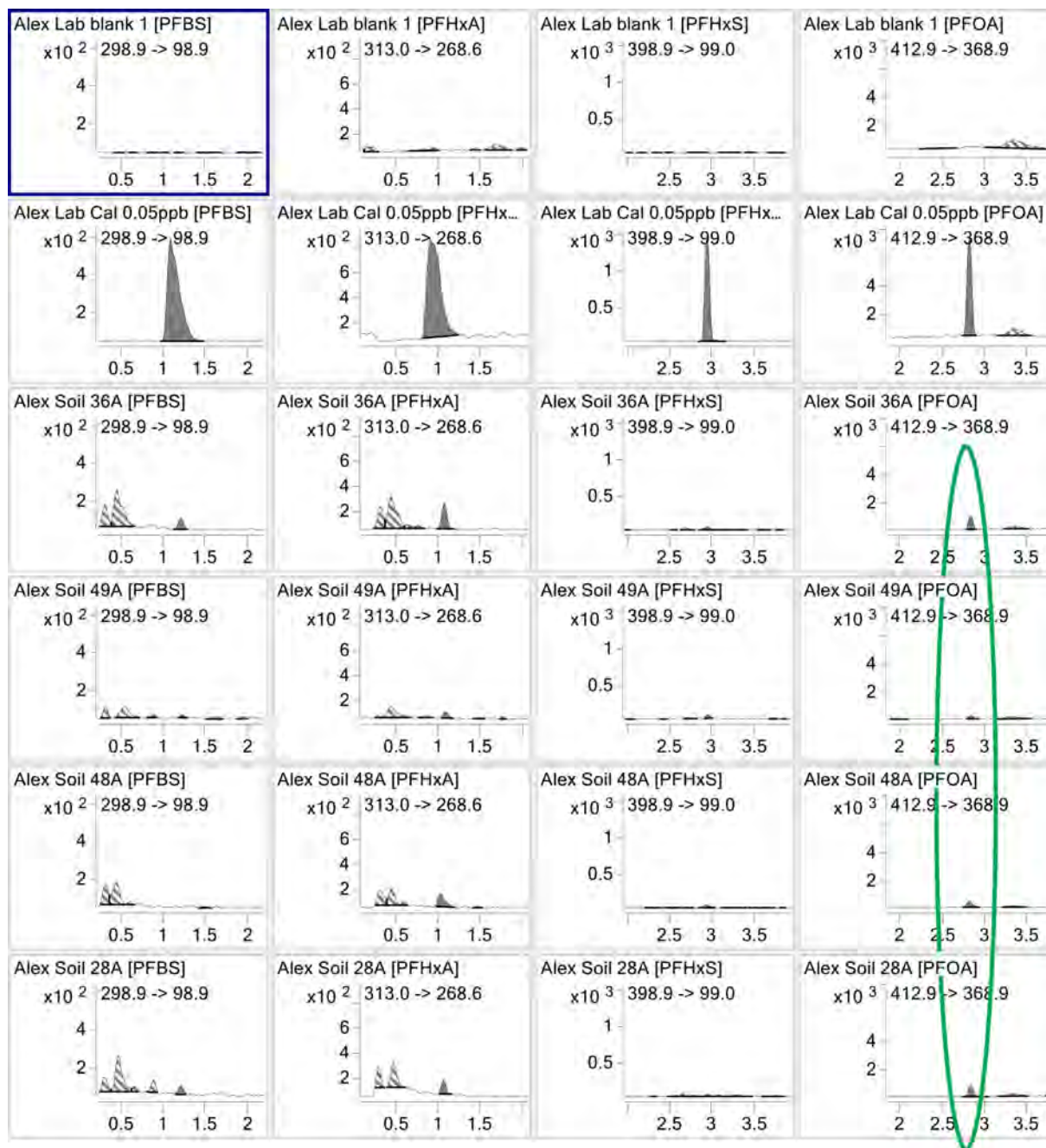


Figure 6.6- PFCs in sediment after correcting for field, target, and method controls, part 1. The top row of this chart represents field sampling controls conducted in Antarctica, followed by 0.05 ppb calibration standards and four cryoconite hole sediment samples described above. The final row from Figure 6.5 is not included in this figure due to scale for corrected samples.

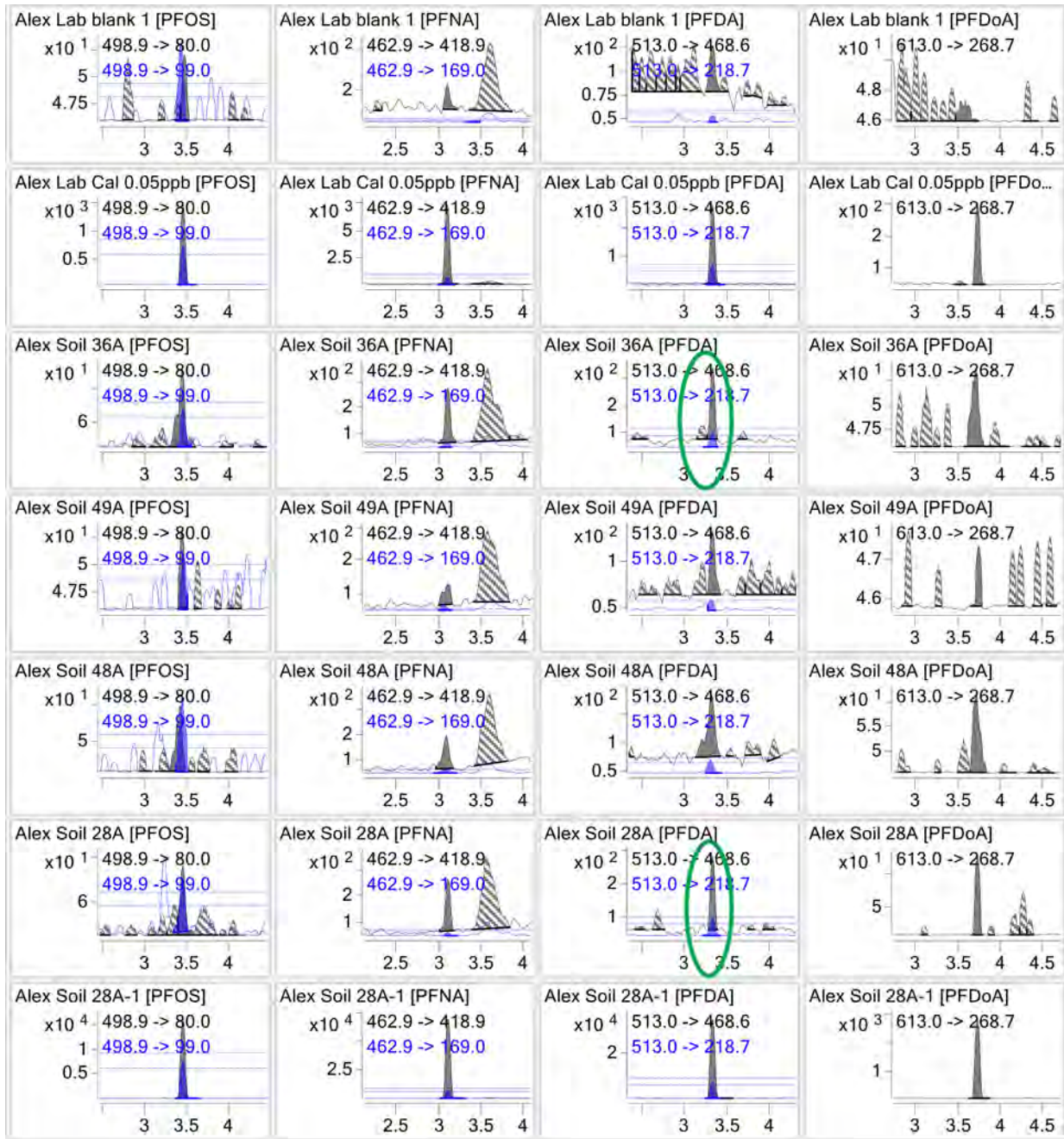


Figure 6.7- PFCs in sediment before correcting for field, method, and target controls, part 2. The top row of this chart represents field sampling controls conducted in Antarctica, followed by 0.05 ppb calibration standards and four cryoconite hole sediment samples described above. The final row displays a cryoconite sample in which a 0.1ppb standard of each PFC was spiked into samples in order to identify similarities between peaks in in un-spiked (28A) and spiked (28A-1) samples.

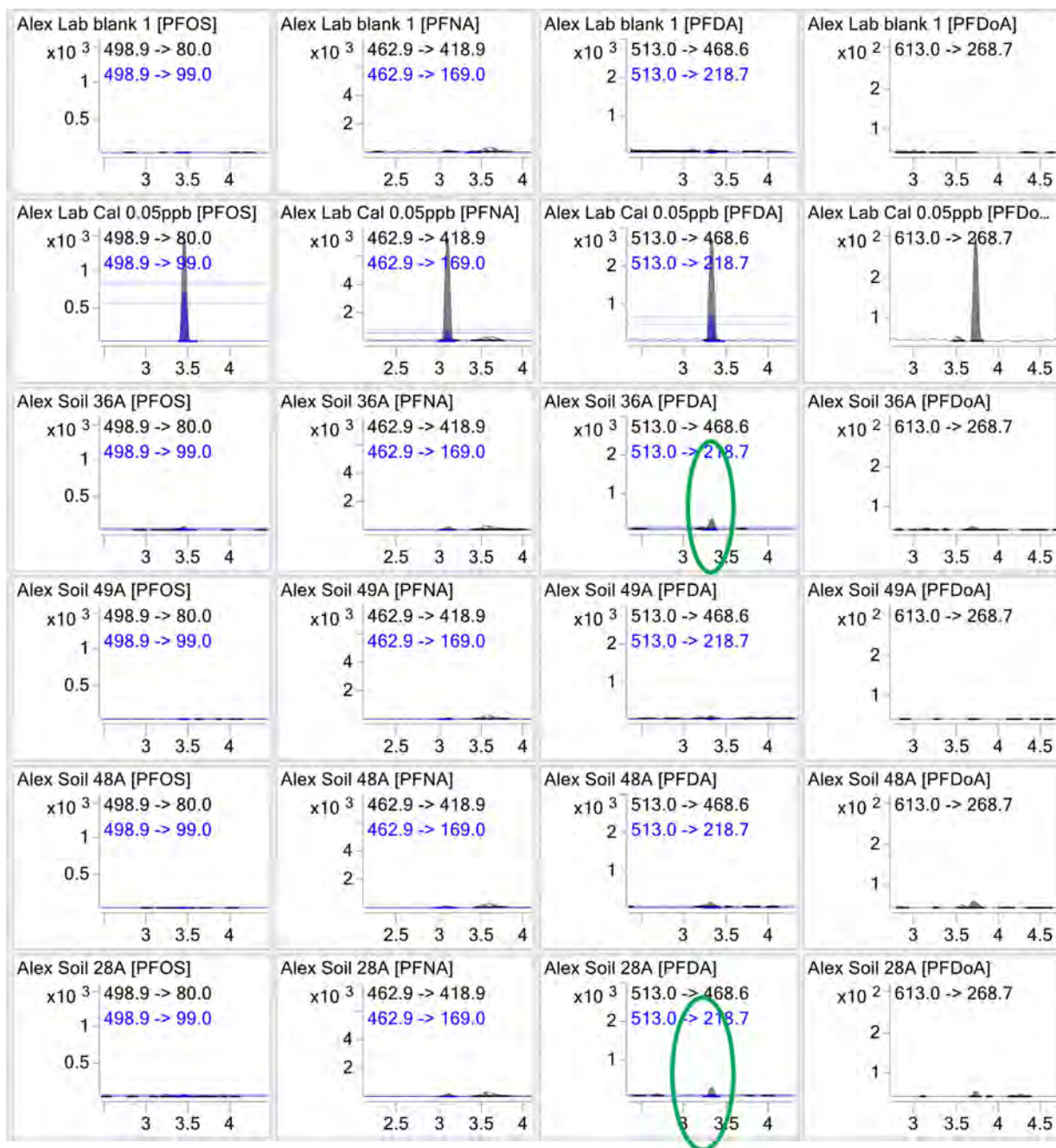


Figure 6.8- PFCs in sediment after correcting for field, method, and target controls, part 2. The top row of this chart represents field sampling controls conducted in Antarctica, followed by 0.05 ppb calibration standards and four cryoconite hole sediment samples described above. The final row from Figure 6.7 is not included in this figure due to scale for corrected samples.

The top row of Figure 6.5 shows the compounds present in the field sampling controls, which cannot be excused from the rest of the samples. However, the most noticeable difference in that graph is the lack of a defined peak for PFOA in the controls, which is present in the four cryoconite samples. The following graphs in Figure 6.6 show each sample after correcting the graphs to remove the signal of background controls for each particular compound. There is a higher degree of uncertainty in the detection of PFBS and PFHxA because of the wide area covered by the 0.05ppb calibration peak. PFHxS does not appear to have peaks in any of the adjusted samples. However, PFOA has a well-defined calibration peak, a lack of detection in the field sampling control, and small peaks in each of the four study compounds. The same trend can be observed for PFDA in the following graphs. This data shows that PFOA and PFDA are present in some of the samples above detection limits, but below reporting limits (quantification limits). So the presence of these compounds can be noted, but not the concentrations. The method detection limit for this sediment analysis is included in Table 6.3.

Table 6.3- Method detection limits and reporting limits for soil/ PFC extraction**TABLE 1 Method Detection Limit and Reporting Range^A**

Analyte	MDL (ng/kg)	Reporting Limit (ng/kg)
PFTreA	6.76	25–1000
PFTriA	5.26	25–1000
PFDoA	3.56	25–1000
PFUnA	2.45	25–1000
PFDA	5.54	25–1000
PFOS	18.83	50–1000
PFNA	2.82	25–1000
PFecHS	2.41	25–1000
PFOA	6.24	25–1000
PFHxS	7.75	25–1000
PFHpA	5.80	25–1000
PFHxA	15.44	50–1000
PFBS	6.49	25–1000
PFPeA	20.93	125–5000
PFBA	22.01	125–5000
FHEA	199.04	600–20 000
FOEA	258.37	750–20 000
FDEA	137.46	500–20 000
FOUEA	4.85	25–1000
FhpPa	5.09	25–1000
FHUEA	3.50	25–1000

Based off of the ASTM standard method for PFCs in sediment (D7968-14)¹²³ with the sediment content and calibration curves used in this analysis.

Across all samples, PFOA was detected in 71% of samples, PFDA in 30%, and PFDoA in 14%. These compounds were more likely to be found in melt pools than cryoconite holes, which makes sense since melt pools have a larger amount of sediment that has accumulated over a longer period of time. While point-source contamination from helicopters traffic or research teams cannot be ruled out with complete certainty, the two glaciers that exhibited the most frequent presence of each compound were Wright Lower Glacier and Joyce Glacier; both in different valleys from the location of fieldcamps and major helicopter traffic. Joyce Glacier in particular is very rarely sampled. These also happened to be glaciers with some of the highest sediment loads. With these patterns, it is less certain if detectable PFCs preferentially sorbed to organic matter after depositing in cryoconite liquid, or if the compounds were already sorbed to sediment when the cryoconite hole originally formed.

The half life of PFCs in air or surface sediment ranges ~20- 90 days according to the EPA,³ yet up to 90 years in water. This may give slight weight to the theory of atmospheric deposition into water and subsequent adsorption to soil.

The low levels of compounds identified in these analyses do not provide enough data to compare lidded/ unlidded pools, or make particular determinations based on isolation age. The limited results do, however, identify the presence of anthropogenic compounds corrected for field controls in an environment that supports the chemical behavior of PFCs, which exhibit slightly hydrophobic tendencies yet are still relatively water soluble. As analytical methods continue to decrease the detection limits of equipment, other compounds with similar deposition and phase-partitioning characteristics may be found in the same environment. In addition, the lack of detection in other analyses in this chapter is useful for environmental monitoring in order to examine changes in contaminant concentrations that may occur over time.

References

- (1) UNEP. *Stockholm Convention on Persistent Organic Pollutants as Amended in 2013*; United Nations Environmental Programme, 2013.
- (2) Grannas, A. M.; Bogdal, C.; Hageman, K. J.; Halsall, C.; Harner, T.; Hung, H.; Kallenborn, R.; Klán, P.; Klánová, J.; MacDonald, R. W.; Meyer, T.; Wania, F. The Role of the Global Cryosphere in the Fate of Organic Contaminants. *Atmos. Chem. Phys.* **2013**, *13* (6), 3271–3305.
- (3) US EPA. Persistent Bioaccumulative Toxic (PBT) Chemicals Covered by the Toxic Release Inventory Program <https://www.epa.gov/toxics-release-inventory-tri-program/persistent-bioaccumulative-toxic-pbt-chemicals-covered-tri> (accessed Jun 2, 2017).
- (4) International Agency for Research on Cancer. Classifications of Carcinogenicity http://monographs.iarc.fr/ENG/Classification/latest_classif.php.
- (5) UNEP. *Success Stories, Stockholm Convention 2001–2011*; United Nations Environmental Programme, 2012.
- (6) Wania, F. I.; Mackay, D. H. Global Fractionation and Cold Condensation of Low Volatility Organochlorine Compounds in Polar Regions. *Ambio* **2013**, *22* (1), 10–18.
- (7) AMAP. *Arctic Monitoring and Assessment Program Report: Arctic Pollution Issues*; Arctic Monitoring and Assessment Programme (AMAP), 1998.
- (8) UNEP. *Regionally Based Assessment of Persistent Toxic Substances: Antarctica Regional Report*; United Nations Environmental Programme, 2002.
- (9) UNEP- United Nations Environmental Programme. *Global Outlook for Ice & Snow*; 2007.
- (10) Wania, F. Assessing the Potential of Persistent Organic Chemicals for Long-Range Transport and Accumulation in Polar Regions. **2003**, *37* (7), 1344–1351.
- (11) Gouin, T.; MacKay, D.; Jones, K. C.; Harner, T.; Meijer, S. N. Evidence for The “grasshopper” effect and Fractionation during Long-Range Atmospheric Transport of Organic Contaminants. *Environ. Pollut.* **2004**, *128* (1–2), 139–148.
- (12) AMAP; Symon, C.; Wilson, S. J. *AMAP Assessment 2009: Human Health in the Arctic*; Arctic Monitoring and Assessment Programme (AMAP): Oslo, Norway, 2009.
- (13) Kallenborn, R.; Berg, T. Long-Term Atmospheric Contaminant Monitoring for the Elucidation of Airborne Transport Processes into Polar Regions. In *Arctic Alpine Ecosystems and People in a Changing Environment*; Springer, 2007; pp 351–376.

- (14) Kallenborn, R.; Breivik, K.; Eckhardt, S.; Lunder, C. R.; Manø, S.; Schlabach, M.; Stohl, A. Long-Term Monitoring of Persistent Organic Pollutants (POPs) at the Norwegian Troll Station in Dronning Maud Land, Antarctica. *Atmos. Chem. Phys.* **2013**, *13* (14), 6983–6992.
- (15) Lewis, K. J. Solar-Forced Roughening of Antarctic Glaciers and the Martian Icecaps: How Surficial Debris and Roughness Affect Glacial Melting in Taylor Valley, Antarctica and How This Can Be Applied to the Martian Icecaps, University of Colorado- Boulder, 2001.
- (16) NSIDC- National Snow and Ice Data Center. Facts about glaciers <https://nsidc.org/cryosphere/glaciers/quickfacts.html> (accessed Feb 6, 2017).
- (17) Sander, R. Compilation of Henry's Law Constants for Inorganic and Organic Species of Potential Importance in Environmental Chemistry, Max-Planck Institute of Chemistry: Mainz, Germany, 1999.
- (18) Nash, S. B. Persistent Organic Pollutants in Antarctica: Current and Future Research Priorities. *J. Environ. Monit.* **2011**, *13* (3), 497–504.
- (19) Rankin, B. Population Histograms By Latitude, Based on NASA's Global Rural-Urban Mapping Program.
- (20) Kallenborn, R.; Oehme, M.; Wynn-Williams, D. D.; Schlabach, M.; Harris, J. Ambient Air Levels and Atmospheric Long-Range Transport of Persistent Organochlorines to Signy Island, Antarctica. *Sci. Total Environ.* **1998**, *220* (2–3), 167–180.
- (21) Bargagli, R. *Antarctic Ecosystems: Environmental Contamination, Climate Change, and Human Impact*; Springer Science & Business Media, 2006; Vol. 175.
- (22) Geisz, H. N.; Dickhut, R. M.; Cochran, M. a; Fraser, W. R.; Ducklow, H. W. Melting Glaciers: A Probably Source of DDT to the Antarctic Marine Ecosystem. *Environ. Sci. Technol.* **2008**, *42* (11), 3958–3962.
- (23) Geisz, H. N.; Dickhut, R. M.; Cochran, M. a; Fraser, W. R.; Ducklow, H. W. Response to Comment on "Melting Glaciers: A Probably Source of DDT to the Antarctic Marine Ecosystem." *Environ. Sci. Technol.* **2009**, *43*, 3974–3975.
- (24) Van Den Brink, N.; Riddle, M.; Van Den Heuvel-Greve, M.; Allison, I.; Snape, I.; Van Franeker, J. A. Correspondence on Geisz et Al. Melting Glaciers: A Probable Source of DDT to the Antarctic Marine Ecosystem. *Environ. Sci. Technol.* **2009**, *43* (10), 3976–3977.
- (25) Wania, F.; Hoff, J. T.; Jia, C. Q.; Mackay, D. The Effects of Snow and Ice on the Environmental Behaviour of Hydrophobic Organic Chemicals. *Environ. Pollut.* **1998**, *102*, 25–41.

- (26) Wang, X. ping; Yao, T. dong; Wang, P. ling; Wei-Yang; Tian, L. de. The Recent Deposition of Persistent Organic Pollutants and Mercury to the Dasuopu Glacier, Mt. Xixiabangma, Central Himalayas. *Sci. Total Environ.* **2008**, *394* (1), 134–143.
- (27) Fretwell, P. T. An Automated Methodology for Differentiating Rock from Snow, Clouds and Sea in Antarctica from Landsat 8 Imagery: A New Rock Outcrop Map and Area Estimation for the Entire Antarctic Continent. *Cryosph.* **2016**, *10* (4), 1665.
- (28) McKnight, D. M.; Niyogi, D. K.; Alger, A. S.; Bomblies, A.; Conovitz, P. A.; Tate, C. M. Dry Valley Streams in Antarctica: Ecosystems Waiting for Water. *Bioscience* **1999**, *49* (12), 985–995.
- (29) Bindschadler, R.; Vornberger, P.; Fleming, A.; Fox, A.; Mullins, J.; Binnie, D.; Paulsen, S. J.; Granneman, B.; Gorodetzky, D. The Landsat Image Mosaic of Antarctica. *Remote Sens. Environ.* **2008**, *112* (12), 4214–4226.
- (30) Google Earth. McMurdo Dry Valleys (USGS and Digital Globe 2016 Satellite Imagery). Version 7.1.8.3036, 2017.
- (31) Fuoco, R.; Capodaglio, G.; Muscatello, B.; Radaelli, M. *Persistent Organic Pollutants (POPs) in the Antarctic Environment. A Review of Findings*; 2009.
- (32) Hoffman, M. J.; Fountain, A. G.; Liston, G. E. Near-Surface Internal Melting: A Substantial Mass Loss on Antarctic Dry Valley Glaciers. *J. Glaciol.* **2014**, *60* (220), 361–374.
- (33) Cowan, D. A.; Tow, L. A. Endangered Antarctic Environments. *Annu. Rev. Microbiol.* **2004**, *58*, 649–690.
- (34) Fountain, A. G.; Tranter, M.; Nysten, T. H.; Lewis, K. J.; Mueller, D. R. Evolution of Cryoconite Holes and Their Contribution to Meltwater Runoff from Glaciers in the McMurdo Dry Valleys, Antarctica. *J. Glaciol.* **2004**, *50* (168).
- (35) Bøggild, C. E.; Brandt, R. E.; Brown, K. J.; Warren, S. G. The Ablation Zone in Northeast Greenland: Ice Types, Albedos and Impurities. *J. Glaciol.* **2010**, *56* (195), 101–113.
- (36) Warren, S. G. Snowball Earth: Ice Thickness on the Tropical Ocean. *J. Geophys. Res.* **2002**, *107* (C10), 1–18.
- (37) NSIDC- National Snow and Ice Data Center. Thermodynamics: Albedo <https://nsidc.org/cryosphere/seaice/processes/albedo.html>.
- (38) Takeuchi, N. Optical Characteristics of Cryoconite (Surface Dust) on Glaciers: The Relationship between Light Absorbency and the Property of Organic Matter Contained in the Cryoconite. *Ann. Glaciol.* **2002**, *34* (1), 409–414.

- (39) Wharton, R. A.; McKay, C. P.; Simmons, G. M.; Parker, B. C. Cryoconite Holes on Glaciers. *Bioscience* **1985**, *35* (8), 499–503.
- (40) Hodson, A.; Anesio, A. M.; Ng, F.; Watson, R.; Quirk, J.; Irvine-Fynn, T.; Dye, A.; Clark, C.; McCloy, P.; Kohler, J. A Glacier Respires: Quantifying the Distribution and Respiration CO₂ Flux of Cryoconite across an Entire Arctic Supraglacial Ecosystem. *J. Geophys. Res. Biogeosciences* **2007**, *112* (G4).
- (41) Bagshaw, E. A.; Tranter, M.; Fountain, A. G.; Welch, K. A.; Basagic, H.; Lyons, W. B. Biogeochemical Evolution of Cryoconite Holes on Canada Glacier, Taylor Valley, Antarctica. *J. Geophys. Res. Biogeosciences* **2007**, *112* (4), 1–8.
- (42) Fountain, A. G.; Nylén, T. H.; Tranter, M.; Bagshaw, E. Temporal Variations in Physical and Chemical Features of Cryoconite Holes on Canada Glacier, McMurdo Dry Valleys, Antarctica. *J. Geophys. Res. Biogeosciences* **2008**, *113* (1), 1–11.
- (43) Dong, Z.; Kang, S.; Qin, D.; Li, Y.; Wang, X.; Ren, J.; Li, X.; Yang, J.; Qin, X. Provenance of Cryoconite Deposited on the Glaciers of the Tibetan Plateau: New Insights from Nd-Sr Isotopic Composition and Size Distribution. *J. Geophys. Res. Atmos.* **2016**, *121* (12), 7371–7382.
- (44) Cook, J.; Edwards, A.; Takeuchi, N.; Irvine-Fynn, T. Cryoconite: The Dark Biological Secret of the Cryosphere. *Prog. Phys. Geogr.* **2016**, *40* (1), 66–111.
- (45) Marshak, S. *Earth: Portrait of a Planet*, 2nd ed.; W.W. Norton, 2005.
- (46) Fountain, A. G.; Tranter, M. Introduction to Special Section on Microcosms in Ice: The Biogeochemistry of Cryoconite Holes. *J. Geophys. Res. Biogeosciences* **2008**, *113* (2), 1–2.
- (47) Telling, J.; Anesio, A. M.; Tranter, M.; Fountain, A. G.; Nylén, T.; Hawkings, J.; Singh, V. B.; Kaur, P.; Musilova, M.; Wadham, J. L. Spring Thaw Ionic Pulses Boost Nutrient Availability and Microbial Growth in Entombed Antarctic Dry Valley Cryoconite Holes. *Front. Microbiol.* **2014**, *5*.
- (48) Bagshaw, E. A.; Tranter, M.; Fountain, A. G.; Basagic, H.; Welch, K. A.; Lyons, W. B. The Hydrology and Biogeochemistry of Cryoconite Holes in Taylor Valley, Antarctica: Evolution Over an Ablation Season. In *AGU Fall Meeting Abstracts*; 2006.
- (49) Tranter, M.; Fountain, A. G.; Fritsen, C. H.; Lyons, W. B.; Priscu, J. C.; Statham, P. J.; Welch, K. A. Extreme Hydrochemical Conditions in Natural Microcosms Entombed within Antarctic Ice. *Hydrol. Process.* **2004**, *18* (2), 379–387.
- (50) NASA. NASA Earth Observatory- Taylor Glacier
<https://earthobservatory.nasa.gov/IOTD/view.php?id=82524&src=eoaiotd>.

- (51) Levy, J. How Big Are the McMurdo Dry Valleys? Estimating Ice-Free Area Using Landsat Image Data. *Antarct. Sci.* **2013**, *25* (1), 119.
- (52) Bromley, A. M. Weather Observations in Wright Valley, Antarctica. *New Zeal. Antarct. Res. Program. Vanda Stn.* **1985**.
- (53) Fountain, A. G.; Lyons, W. B.; Burkins, M. B.; Dana, G. L.; Doran, P. T.; Lewis, K. J.; McKnight, D. M.; Moorhead, D. L.; Parsons, A. N.; Priscu, J. C.; Wall, D. H.; Wharton, R. A.; Virginia, R. A. Physical Controls on the Taylor Valley Ecosystem, Antarctica. *Bioscience* **1999**, *49* (12), 961.
- (54) United States Antarctic Program. *Down in the Valleys: The Complexities of a Simple Ecosystem (Interview with Andrew Fountain)*; McMurdo Station, Antarctica, 2003.
- (55) Nylén, T. H.; Fountain, A. G.; Doran, P. T. Climatology of Katabatic Winds in the McMurdo Dry Valleys, Southern Victoria Land, Antarctica. *J. Geophys. Res.* **2004**, *109* (D3), D03114.
- (56) Fountain, A. G.; Nylén, T. H.; Monaghan, A.; Basagic, H. J.; Bromwich, D. Snow in the McMurdo Dry Valleys, Antarctica. *Int. J. Climatol.* **2010**, *30* (5), 633–642.
- (57) Dana, G. L.; Wharton, R. A.; Dubayah, R. A. Solar Radiation in the McMurdo Dry Valleys, Antarctica. In *Ecosystem dynamics in a polar desert: the McMurdo Dry Valleys, Antarctica*; Priscu, J. C., Ed.; American Geophysical Union, 1998; pp 39–64.
- (58) Fountain, A. G.; Lewis, K. J.; Doran, P. T. Spatial Climatic Variation and Its Control on Glacier Equilibrium Line Altitude in Taylor Valley, Antarctica. *Glob. Planet. Change* **1999**, *22* (1), 1–10.
- (59) Lewis, K. J.; Fountain, A. G.; Dana, G. L. How Important Is Terminus Cliff Melt?: A Study of the Canada Glacier Terminus, Taylor Valley, Antarctica. *Glob. Planet. Change* **1999**, *22* (1–4), 105–115.
- (60) Fountain, A. G.; Basagic, H. J.; Niebuhr, S. Glaciers in Equilibrium, McMurdo Dry Valleys, Antarctica. *J. Glaciol.* **2016**, *62* (235), 976–989.
- (61) Fountain, A. G.; Nylén, T. H.; MacClune, K. L.; Dana, G. L. Glacier Mass Balances (1993–2001), Taylor Valley, McMurdo Dry Valleys, Antarctica. *J. Glaciol.* **2006**, *52* (178), 451–462.
- (62) Robinson, P. H. Ice Dynamics and Thermal Regime of Taylor Glacier, South Victoria Land, Antarctica. *J. Glaciol.* **1984**, *30* (105), 153–160.
- (63) United States Geological Survey. Joyce Glacier. Land Information New Zealand Topographic Map (1:50,000), PGC Map ID 592. 1997.

- (64) Polar Geospatial Center. T-902 Field Planning 2012: Blue Glacier, Southern Dry Valleys. Topographic Map (1:140,000), PGC Map ID 135. 2012.
- (65) Fountain, A. G.; Dana, G. L.; Lewis, K. J.; Vaughn, B. H.; Mcknight, D. H. Glaciers of the McMurdo Dry Valleys, Southern Victoria Land, Antarctica. In *Ecosystem dynamics in a polar desert: the McMurdo Dry Valleys, Antarctica*; Priscu, J. C., Ed.; American Geophysical Union: Washington D.C., 1998; pp 65–77.
- (66) Östrem, G. Ice Melting under a Thin Layer of Moraine, and the Existence of Ice Cores in Moraine Ridges. *Geogr. Ann.* **1959**, *41* (4), 228–230.
- (67) Kayastha, R. B.; Takeuchi, Y.; Nakawo, M.; Ageta, Y. Practical Prediction of Ice Melting beneath Various Thickness of Debris Cover on Khumbu Glacier, Nepal, Using a Positive Degree-Day Factor. *IAHS Publ.* **2000**, 7182.
- (68) MacDonell, S.; Fitzsimons, S. The Formation and Hydrological Significance of Cryoconite Holes. *Prog. Phys. Geogr.* **2008**, *32* (6), 595–610.
- (69) Hoffman, M. J. Spatial and Temporal Variability of Glacier Melt in the McMurdo Dry Valleys, Antarctica, Portland State University, 2011.
- (70) Simmon, R. Landsat 8 Image- Taylor Glacier. NASA Earth Observatory 2013.
- (71) Paige, R. A. Sub-Surface Melt Pools in the McMurdo Ice Shelf, Antarctica. *J. Glaciol.* **1968**, *7* (51), 511–516.
- (72) Mueller, D. R.; Vincent, W. F.; Pollard, W. H.; Fritsen, C. H. Glacial Cryoconite Ecosystems: A Bipolar Comparison of Algal Communities and Habitats. *Nov. Hedwigia Beih.* **2001**, *123*, 173–198.
- (73) Macdonell, S. A.; Fitzsimons, S. J. Observations of Cryoconite Hole System Processes on an Antarctic Glacier. *Rev. Chil. Hist. Nat.* **2012**, *85* (4).
- (74) Foreman, C. M.; Wolf, C. F.; Priscu, J. C. Impact of Episodic Warming Events. *Aquat. Geochemistry* **2004**, *10* (3), 239–268.
- (75) Nkem, J. N.; Wall, D. H.; Virginia, R. A.; Barrett, J. E.; Broos, E. J.; Porazinska, D. L.; Adams, B. J. Wind Dispersal of Soil Invertebrates in the McMurdo Dry Valleys, Antarctica. *Polar Biol.* **2006**, *29* (4), 346–352.
- (76) Price, P. B. A Habitat for Psychrophiles in Deep Antarctic Ice. *Proc. Natl. Acad. Sci.* **2000**, *97* (3), 1247–1251.
- (77) Takeuchi, N.; Kohshima, S.; Goto-Azuma, K.; Koerner, R. M. Biological Characteristics of Dark Colored Material (Cryoconite) on Canadian Arctic Glaciers (Devon and Penny Ice Cap). In *Proceeding of the Memoirs of National Institute of Polar Research*; 2001; pp 495–505.

- (78) Lewis, K. J.; Fountain, A. G.; Dana, G. L. Surface Energy Balance and Meltwater Production for a Dry Valley Glacier, Taylor Valley, Antarctica. *Ann. Glaciol.* **1998**, *27*, 603–609.
- (79) Tranter, M.; Fountain, A. G.; Lyons, W. B.; Nylén, T. H.; Welch, K. A. The Chemical Composition of Runoff from Canada Glacier, Antarctica: Implications for Glacier Hydrology during a Cool Summer. *Ann. Glaciol.* **2005**, *40* (1), 15–19.
- (80) Welch, K. a.; Lyons, W. B.; Whisner, C.; Gardner, C. B.; Gooseff, M. N.; McKnight, D. M.; Priscu, J. C. Spatial Variations in the Geochemistry of Glacial Meltwater Streams in the Taylor Valley, Antarctica. *Antarct. Sci.* **2010**, *22* (6), 662–672.
- (81) Lyons, W. B.; Welch, K. A.; Fountain, A. G.; Dana, G. L.; Vaughn, B. H.; McKnight, D. M. Surface Glaciochemistry of Taylor Valley, Southern Victoria Land, Antarctica and Its Relationship to Stream Chemistry. *Hydrol. Process.* **2003**, *17* (1), 115–130.
- (82) Legrand, M.; Mayewski, P. Glaciochemistry of Polar Ice Cores: A Review. *Rev. Geophys.* **1997**, *35* (3), 219–243.
- (83) Gooseff, M.; Mcknight, D.; Runkel, R. *Reach-Scale Cation Exchange Controls on Major Ion Chemistry of an Antarctic Glacial Meltwater Stream*; 2004; Vol. 10.
- (84) MacDonell, S.; Sharp, M.; Fitzsimons, S. Cryoconite Hole Connectivity on the Wright Lower Glacier, McMurdo Dry Valleys, Antarctica. *J. Glaciol.* **2016**, *62* (234), 714–724.
- (85) Porazinska, D. L.; Fountain, A. G.; Nylén, T. H.; Tranter, M.; Virginia, R. a.; Wall, D. H. The Biodiversity and Biogeochemistry of Cryoconite Holes from McMurdo Dry Valley Glaciers, Antarctica. *Arctic, Antarct. Alp. Res.* **2004**, *36* (1), 84–91.
- (86) Bagshaw, E. A.; Tranter, M.; Wadham, J. L.; Fountain, A. G.; Dubnick, A.; Fitzsimons, S. Processes Controlling Carbon Cycling in Antarctic Glacier Surface Ecosystems. *Geochemical Perspect. Lett.* **2016**.
- (87) Bagshaw, E. a.; Tranter, M.; Fountain, A. G.; Welch, K.; Basagic, H. J.; Lyons, W. B. Do Cryoconite Holes Have the Potential to Be Significant Sources of C, N, and P to Downstream Depauperate Ecosystems of Taylor Valley, Antarctica? *Arctic, Antarct. Alp. Res.* **2013**, *45* (4), 440–454.
- (88) Fortner, S. K. *The Geochemistry of Glacier Snow and Melt: The Oregon Cascades and the Taylor Valley, Antarctica*, The Ohio State University, 2008.
- (89) Lyons, W. B.; Welch, K. A.; Neumann, K.; Toxey, J. K.; McArthur, R.; Williams, C.; McKnight, D. M.; Moorhead, D. Geochemical Linkages Among Glaciers, Streams And Lakes Within The Taylor Valley, Antartica. In *Ecosystem dynamics in a polar desert: the McMurdo Dry Valleys, Antarctica*; Priscu, J. C., Ed.; American Geophysical Union, 1998; pp 77–92.

- (90) Williamson, B. R.; Kreutz, K. J.; Mayewski, P. A.; Bertler, N. A. N.; Sneed, S.; Handley, M.; Introne, D. A Coastal Transect of McMurdo Dry Valleys (Antarctica) Snow and Firn: Marine and Terrestrial Influences on Glaciochemistry. *J. Glaciol.* **2007**, *53* (183), 681–693.
- (91) Levy, J. S.; Fountain, A. G.; O'Connor, J. E.; Welch, K. A.; Lyons, W. B. Garwood Valley, Antarctica: A New Record of Last Glacial Maximum to Holocene Glaciofluvial Processes in the McMurdo Dry Valleys. *Geol. Soc. Am. Bull.* **2013**, *125* (9–10), 1484–1502.
- (92) Larsson, P.; Järnmark, C.; Södergren, A. PCBs and Chlorinated Pesticides in the Atmosphere and Aquatic Organisms of Ross Island, Antarctica. *Mar. Pollut. Bull.* **1992**, *25* (9–12), 281–287.
- (93) Negoita, T. G.; Covaci, A.; Gheorghe, A.; Schepens, P. Distribution of Polychlorinated Biphenyls (PCBs) and Organochlorine Pesticides in Soils from the East Antarctic Coast. *J. Environ. Monit.* **2003**, *5* (2), 281–286.
- (94) Klánová, J.; Matykiewiczová, N.; Máčka, Z.; Prošek, P.; Láska, K.; Klán, P. Persistent Organic Pollutants in Soils and Sediments from James Ross Island, Antarctica. *Environ. Pollut.* **2008**, *152* (2), 416–423.
- (95) Kennicutt, M. C.; McDonald, S. J.; Sericano, J. L.; Boothe, P.; Oliver, J.; Safe, S.; Presley, B. J.; Liu, H.; Wolfe, D.; Wade, T. L.; Crockett, A.; Bockus, D. Human Contamination of the Marine Environment - Arthur Harbor and McMurdo Sound, Antarctica. *Environ. Sci. Technol.* **1995**, *29* (5), 1279–1287.
- (96) Montone, R. C.; Taniguchi, S.; Weber, R. R. PCBs in the Atmosphere of King George Island, Antarctica. *Sci. Total Environ.* **2003**, *308* (1–3), 167–173.
- (97) Lugar, R. M.; Harless, R. L.; Dupuy, A. E.; McDaniel, D. D. Results of Monitoring for Polychlorinated Dibenzo-P-Dioxins and Dibenzofurans in Ambient Air at McMurdo Station, Antarctica. *Environ. Sci. Technol.* **1996**, *30* (2), 555–561.
- (98) Zhao, Z.; Xie, Z.; Möller, A.; Sturm, R.; Tang, J.; Zhang, G.; Ebinghaus, R. Distribution and Long-Range Transport of Polyfluoroalkyl Substances in the Arctic, Atlantic Ocean and Antarctic Coast. *Environ. Pollut.* **2012**, *170*, 71–77.
- (99) Connell, D. W.; Miller, G. J.; Mortimer, M. R.; Shaw, G. R.; Anderson, S. M. Persistent Lipophilic Contaminants and Other Chemical Residues in the Southern Hemisphere. *Crit. Rev. Environ. Sci. Technol.* **1999**, *29*, 47–82.
- (100) Van Leeuwen, S. P. J.; De Boer, J.; Van Leeuwen, S. P. J.; Van Bavel, B. First Worldwide UNEP Interlaboratory Study on Persistent Organic Pollutants (POPs), with Data on Polychlorinated Biphenyls and Organochlorine Pesticides. *TrAC - Trends in Analytical Chemistry*. 2013, pp 110–117.

- (101) Peterle, T. J. DDT in Antarctic Snow. *Nature* **1969**, 224 (5219), 620.
- (102) Tanabe, S.; Hidaka, H.; Tatsukawa, R. PCBs and Chlorinated Hydrocarbon Pesticides in Antarctic Atmosphere and Hydrosphere. *Chemosphere* **1983**, 12 (2), 277–288.
- (103) Benjamin, M. M.; Lawler, D. F. *Water Quality Engineering: Physical/chemical Treatment Processes*; John Wiley & Sons: New York, 2013.
- (104) EPA. *Soil Screening Guidance: Chemical Properties for SSL Development*; Environmental Protection Agency Office of Emergency and Remedial Response: Washington D.C., 1996.
- (105) Hornbuckle, K. C.; Jeremiason, J. D.; Sweet, C. W.; Eisenreich, S. J. Seasonal Variations in Air Water Exchange of Polychlorinated Biphenyls in Lake Superior. *Environ. Sci. Technol.* **1994**, 28 (8), 1491–1501.
- (106) Hirschfelder, J.; Bird, R. B.; Spotz, E. L. The Transport Properties of Gases and Gaseous Mixtures. *Chem. Rev.* **1949**, 44 (1), 205–231.
- (107) Logan, B. E. *Environmental Transport Processes*; John Wiley & Sons: New York, 2012.
- (108) Schwarzenbach, R. P.; Gschwend, P. M.; Imboden, D. M. *Environmental Organic Chemistry*; John Wiley & Sons: New York, 1993.
- (109) Nazaroff, W. W.; Alvarez-Cohen, L. *Environmental Engineering Science*; John Wiley & Sons: New York, 2001.
- (110) Doran, P. T.; McKay, C. P.; Clow, G. D.; Dana, G. L.; Fountain, A. G.; Nylén, T.; Lyons, W. B. Valley Floor Climate Observations from the McMurdo Dry Valleys, Antarctica, 1986-2000. *J. Geophys. Res. Atmos.* **2002**, 107 (24), 1–12.
- (111) Sander, R. Compilation of Henry's Law Constants (Version 4.0) for Water as Solvent. *Atmos. Chem. Phys.* **2015**, 15 (8), 4399–4981.
- (112) Su, Y.; Hung, H.; Blanchard, P.; Patton, G. W.; Kallenborn, R.; Konoplev, A.; Fellin, P.; Li, H.; Geen, C.; Stern, G.; Rosenberg, B.; Barrie, L. A. Spatial and Seasonal Variations of Hexachlorocyclohexanes (HCHs) and Hexachlorobenzene (HCB) in the Arctic Atmosphere. *Environ. Sci. Technol.* **2006**, 40 (21), 6601–6607.
- (113) Bamford, H. A.; Poster, D. L.; Baker, J. E. Henry's Law Constants of Polychlorinated Biphenyl Congeners and Their Variation with Temperature. *J. Chem. Eng. Data* **2000**, 45 (6), 1069–1074.
- (114) Cetin, B.; Ozer, S.; Sofuoglu, A.; Odabasi, M. Determination of Henry's Law Constants of Organochlorine Pesticides in Deionized and Saline Water as a Function of Temperature. *Atmos. Environ.* **2006**, 40 (24), 4538–4546.

- (115) Wania, F. Modelling the Fate of Non-Polar Organic Chemicals in an Ageing Snow Pack. *Chemosphere* **1997**, 35 (10), 2345–2363.
- (116) Hargrave, B. T.; Vass, W. P.; Erickson, P. E.; Fowler, B. R. Distribution of Chlorinated Hydrocarbon Pesticides and PCBs in the Arctic Ocean. *Can. Tech. Rep. Fish. Aquat. Sci.* **1989**, No. 1644, 1644.
- (117) Desideri, P.; Lepri, L.; Santianni, D.; Checchini, L. Chlorinated Pesticides in Sea-Water and Pack Ice in Terra-Nova Bay (Antarctica). *Ann. Chim.* **1991**, 81 (9–10), 533–540.
- (118) Dickhut, R.; Cincinelli, A.; Cochran, M.; Ducklow, H. Atmospheric Concentrations and Air - Water Flux of Organochlorine Pesticides along the Western Antarctic Peninsula. *Environ. Sci. Technol.* **2005**, 39, 465–470.
- (119) Anumol, T.; Merel, S.; Clarke, B. O.; Snyder, S. A. Ultra High Performance Liquid Chromatography Tandem Mass Spectrometry for Rapid Analysis of Trace Organic Contaminants in Water. *Chem. Cent. J.* **2013**, 7 (1), 104.
- (120) Moschet, C.; Lew, B. M.; Hasenbein, S.; Anumol, T.; Young, T. M. LC-and GC-QTOF-MS as Complementary Tools for a Comprehensive Micropollutant Analysis in Aquatic Systems. *Environ. Sci. Technol.* **2017**, 51 (3), 1553–1561.
- (121) Moschet, C.; Young, T.; Anumol, T. *LC/QTOF Workflows for Comprehensive Micropollutant Analysis*; 2017.
- (122) ASTM International. ASTM D7979- Standard Test Method for Determination of Per- and Polyfluoroalkyl Substances in Water, Sludge, Influent, Effluent and Wastewater by Liquid Chromatography Tandem Mass Spectrometry (LC/MS/MS). 2016.
- (123) ATSDM-D7968-14. Standard Test Method for Determination of Perfluorinated Compounds in Soil by Liquid Chromatography Tandem Mass Spectrometry (LC/MS/MS). ASTM International: West Conshohocken, PA 2014.